Improving Parton Showers with Fixed Order Matrix Elements

Prestel, Stefan

2013

Improving Parton Showers with Fixed Order Matrix Elements

Stefan Prestel

Department of Astronomy and Theoretical Physics
Lund University

Thesis for the degree of Doctor of Philosophy

Thesis Advisor: *Leif Lönnblad*
Faculty Opponent: *Frank Krauss*

To be presented, with the permission of the Faculty of Science of Lund University, for public criticism in Lundmarksalen lecture hall of the Department of Astronomy and Theoretical Physics on Friday, the 22th of March 2013, at 10.15.

Organization

LUND UNIVERSITY
Department of Astronomy and Theoretical Physics
Sölvegatan 14A
SE–223 62 Lund
Sweden

Document name
DOCTORAL DISSERTATION

Date of issue
March 2013

Sponsoring organization

Author(s)
Stefan Prestel

Title and subtitle
Improving Parton Showers with Fixed Order Matrix Elements

Abstract
This thesis considers numerical simulations of high energy particle collisions, and improvements in the description of multiple collimated jets of hadrons in collision events in particular. In the event simulation software called event generators, the structure of multi-jet events is determined through an interplay of the input calculation, parton showers and phenomenological hadronisation models. Prescriptions to imbue existing event generator simulations with more complex input calculations are presented, and public implementations of the proposed methods provided.
Paper I describes the implementation of an earlier algorithm to include regularised tree-level multi-jet configurations into event generators. The implementation is applied to collisions at LEP, Tevatron and LHC.
Paper II proposes a method to amend cross section changes in traditional multi-jet merging schemes. The implementation of the new scheme is tested for W-boson + jets and QCD Dijet production at the LHC.
Paper III presents extentions of the algorithms of Papers I and II to allow the inclusion of virtual corrections to the scattering processes. The resulting NLO merging methods are applied to W-boson + jets and Higgs-boson + jets at the LHC.

Key words:
QCD, Phenomenology, Parton Shower, Matrix Element Merging

Classification system and/or index terms (if any):

Supplementary bibliographical information:

Language
English

ISSN and key title:

ISBN
978-91-7473-473-7

Recipient's notes

Number of pages
235

Price

Security classification

Distributor
Stefan Prestel
Department of Theoretical Physics, Sölvegatan 14A, SE–223 62 Lund, Sweden

Signature S. Prestel Date 2013-02-11

Improving Parton Showers with Fixed Order Matrix Elements

Stefan Prestel

Department of Astronomy and Theoretical Physics
Lund University

Thesis for the degree of Doctor of Philosophy

Thesis Advisor: *Leif Lönnblad*
Faculty Opponent: *Frank Krauss*

To be presented, with the permission of the Faculty of Science of Lund University, for public criticism in Lundmarksalen lecture hall of the Department of Astronomy and Theoretical Physics on Friday, the 22th of March 2013, at 10.15.

Department of Astronomy and Theoretical Physics, Lund University
ISBN 978-91-7473-473-7

Printed in Sweden by Media-Tryck, Lund University
Lund 2013

Sammanfattning

Fysik försöker förklara naturfenomen med matematiska beskrivningar som beror på systemet som studeras. Även om vi till exempel vet hur man beskriver rörelsen av ett fallande äpple, blir övervägandet av detaljer som ett fallande äpple knappast relevant när man försöker beräkna jordens rörelse runt solen. Å andra sidan spelar partikelfysik ingen roll i beskrivandet av äpplen. Målet med fysik är att finna en grundläggande teori, och väldefinierade sätt att ta bort alla onödiga detaljer, om vi vill på ett effektivt sätt beskriva ett "större" system. Idag, hittar vi – åtminstone i princip – progressionen

$$
\begin{aligned}
? \longrightarrow\ & \text{Kärnsönderfall på subatomära avstånd} \\
& \quad \text{beskrivs av partikelfysik} \\
\longrightarrow\ & \text{Atomer, molekyler, kemi på atomära avstånd} \\
& \quad \text{beskrivs av kvantmekanik} \\
\longrightarrow\ & \text{Vardagsliv, biologi vid mellanliggande avstånd} \\
& \quad \text{beskrivs med klassisk mekanik} \\
\longrightarrow\ & \text{Gravitation på astronomiska avstånd} \\
& \quad \text{beskrivs av den allmänna relativitetsteorin} \\
\longrightarrow\ & ?
\end{aligned}
$$

Beskrivningen av den naturliga världen kräver fyra grundläggande krafter: gravitation, elektromagnetism och "svaga" och "starka" kärnkrafter. De svaga och starka krafterna blir relevanta vid väldigt små avstånd, som bara kan lösas upp med högenergetiska prober, dvs. genom att kollidera protoner med varandra med energier som är jämförbara med de som fanns i ögonblicket efter big bang.

Standardmodellen (SM) för partikelfysik kan, än så länge, förklara resultaten av sådana kollisionsexperiment genom att inkludera de tre grundläggande krafter som kan beskrivas med kvantmekaniskt utbyte av kraftbärande partiklar — så kallade *gauge bosoner*. Elektromagnetism beskrivs av emission och absorption av *fotoner*. Den svaga kärnkraften, som t.ex. är ansvarig för omvandlingen av guld till bly, förmedlas av partiklar som kallas *W*- och *Z-bosoner*. Den starka kärnkraften motverkar den elektriska repulsionen i atomkärnan, vilket gör kärnan av helium stabil. Denna interaktion är en kvarleva av den kraft som kallas kvantkromodynamik (Quantum Chromodynamics — QCD), som förmedlas av partiklar som kallas *gluoner* och buntar ihop grundläggande *kvarkar* till protoner och neutroner.

Eftersom SM inte innefattar gravitationen är det i slutändan en ofullständig teori. Högenergipartikelkollisionsexperiment som Large

Hadron Collider (LHC) hoppas att avslöja nya grundläggande partiklar och nya fundamentala krafter, som inte ingår i SM. Denna uppgift kräver allt högre energier för öka sannolikheten att producera och upptäcka tidigare okända partiklar. Uppgiften kräver också mycket noggranna beskrivningar av förväntade SM resultat för att kunna särskilja spår av sällsynta nya företeelser från "vanliga" kollisioner i experimentell data.

LHC är utformad för att kollidera protoner, eftersom protoner enklare kan accelereras till stora kinetiska energier än lättare partiklar, såsom elektroner. Att kollidera protoner är dock en rörig historia, och en mycket detaljerad förståelse av det sammansatta initialtillståndet och de överblivna protonrester är nödvändig. För att beskriva SM-strukturen, konstrueras datorprogram för att simulera partikelspridningarna i kollisionerna i detalj. Dessa så-kallade händelsegeneratorer bryter ner beskrivningen av kollisionsförloppet i följande steg:

- ◇ Välj en beståndsdel (en kvark eller gluon, som gemensamt benämns *partoner*) ur varje kolliderande proton och forma ett nytt "sluttillstånd". Detta steget kan repeteras flera gånger för ett par protoner, vilket producerar en händelse med flera sub-kollisioner av protonbeståndsdelar. Den primära spridningen som tar i anspråk den största andelen av de inkommande protonernas energi, är ofta en bakgrundskandidat för oväntade signaler.
- ◇ Spridningsprocessen som simuleras på detta sätt initierar sedan en strålningskaskad där ett stort antal nya partoner produceras i en process vanligen kallad *partonskur*.
- ◇ I slutet av kaskaden kombineras de producerade partonerna med varandra och med protonresterna till detekterbara partiklar såsom protoner och pioner.

En detaljerade beskrivning av mer komplexa konfigurationer i mycket energetiska primära spridningar kräver specialiserade program som kallas matriselementgeneratorer, och resultaten från dessa måste på ett konsekvent sätt jämkas samman med genereringen av partonskurarna.

Denna avhandling handlar om att förbättra av beskrivningen av primära spridningar i kollisionshändelser genom att utveckla och förfina denna sammanjämkning av matriselement- och partonskursprogram. Resultaten har implementerats som en del i en händelsegenerator kallad PYTHIA8 som utvecklats i Lund men som används värden över av både teoretiker och experimentalister.

This thesis contains the following publications:

I L. Lönnblad and S. Prestel, "Matching Matrix Elements and Interleaved Showers", JHEP 1203 (2012) 019

II L. Lönnblad and S. Prestel, "Unitarising Matrix Element + Parton Shower merging",
arXiv:1211.4827 [hep-ph], accepted for publication in JHEP

III L. Lönnblad and S. Prestel, "Merging Multi-leg NLO Matrix Elements with Parton Showers",
arXiv:1211.7278 [hep-ph], submitted to JHEP

Contents

i

Introduction

The topic of this thesis is high energy particle physics, and event simulations for particle colliders in particular. As particle physics is a rather mature field of science, finding a moderate tone for this introduction – which appeals to friends, family and the thesis committee – seems a difficult endeavour. Thus, I will not attempt to be comprehensive and lucid at the same time, but rather divide this introduction into a general, and a more mathematical section, hoping that each person will find some interesting pieces.

The general introduction begins by giving a brief historical introduction on how particle physics developed. Then, the Standard Model (SM) of particle physics is outlined, and Quantum Chromodynamics (QCD) is touched upon. The general introduction concludes by addressing measurements at particle colliders.

The subsequent sections expand the discussion. First, the SM is introduced in the language of gauge theory, and comments on QCD are made. Then, calculations of scattering probabilities are illustrated with the help of Feynman diagrams, and the collinear approximation is discussed. This leads to an introduction to parton showers and resummation. To conclude, the work of this thesis is put into perspective by outlining ways to improve the precision of parton showers.

The introductory sections are supplemented by a short description of the publications that form the basis of this doctoral thesis. The reproduction of the actual articles, as published in (or submitted to) the Journal of High Energy Physics, forms the main body of the thesis.

i.1 Origins of particle physics

The aim of this section is to introduce some concepts of particle physics for non-specialists. To remain as pedagogical as possible, we will spend some words on physics in general, before describing measurements that

led to the construction of the SM of particle physics. We then try to motivate QCD (the model explaining the strong nuclear force) and end this section by discussing measurements at particle colliders.

i.1.1 The story so far

Modern physics views the description of the universe as a problem of resolution. It is useful to think of this "resolution" as the minimal (spatial) distance at which the structure of the monitored system can be investigated. A keen-eyed person for example might be able to discern precisely two trees at the horizon, whereas a short sighted person might only be able to assert that there are trees, but not how many. In this example, the characteristic size at which the short sighted person's eyes resolve objects is larger than the distance between the two trees. All measurement devices have a certain range of resolution: microscopes help to investigate small distance phenomena but fail at large scales, while telescopes enable us to form a picture of our surroundings at a large scale, but remain oblivious to small details. At the same time, the relevant input to describe observations depends on the distance scales (or resolution). It is not necessary to know the inner workings of a bacterium when measuring the rotation of Jupiter around the Sun, and the precise position of Jupiter is conversely irrelevant for the description of a bacterium. The laws governing the movements of planets are independent of biological laws. We polemically generalise this by stating that at each characteristic resolution, characteristic equations govern the system. Natural science tries to assemble a unique sequence of such specialised equations in order to describe the universe. If there was a "complete" theory of natural sciences, such a sequence of physical laws should ideally be obtained by gradually (and in a well-defined way) removing unnecessary details of a small-distance theory when investigating large-scale structures.

Particle physics aims to formulate a theory from which, at least in principle, most other physical laws can be derived. Let us acclimatise to the unfamiliar concepts of particle physics by describing its history, again bearing in mind that every physical law is valid only in a particular region of resolution.

The physics that we experience with our senses is almost exclusively described by classical mechanics (as introduced by Newton). Classical mechanics (CM) postulates that objects interact through forces, and allows to describe the motion of objects if the mathematical form of the forces is known. However, CM gives no explanation to what forces are

and how the interaction takes place: the "force" is defined through the object's change in momentum[1] over an infinitesimally short time span, i.e. the force concept simply states that if an object (of fixed mass) experiences a change in speed, some "force" must have acted on the object to compel this change. Thus, CM is in some sense a meta-theory: the mathematical apparatus of CM allows us to, from simple principles, build models for how a system of objects changes by the action of forces. These changes are encoded into the equations of motion, which allow to calculate the state[2] of an object. These equations can be derived by the following prescription:

1. Write down the difference between kinetic energy (i.e. the energy stored by motion) and potential energy (i.e. the energy stored in the force field). This difference is called Lagrange function.
2. Insert the Lagrange function into a set of equations called the Euler-Lagrange equations.
3. Read off the equations of motion.

The paramount lesson of CM lies in the importance of the concept of symmetry. Mathematically, a symmetry is defined by a variable transformation that leaves a certain function unchanged. For example, imagine a person standing at the centre of a circle, looking at a point on the circle. Every point on the circle will be equally far away, wherever the person turns: the radius of the circle is constant, irrespectively where the person looks. Put mathematically, the radius has a (continuous) symmetry under rotations around the centre. In physics, a symmetry is defined as a transformation that does not change the Lagrange function. Assume e.g. that an object at rest will always be at rest if no force applies. Then the Lagrange function should not change when increasing the time by a small step. This invariance, when cast into a differential equation, directly leads to the prediction that the total energy is conserved. Thus, an extremely simple idea leads to a symmetry, which in turn leads to one of the most fundamental predictions of physics – that energy cannot be created or destroyed. The realisation that continuous symmetries lead to conserved quantities is not only limited to CM, put is a general feature of theories that describe the the motion of objects in position-dependent force fields (field theories). Symmetry consider-

[1] The momentum is a linear function of the the velocity (or speed) of the object.

[2] A state is a set of statements that define the whole system. To describe the movement of a falling ball, it is for example enough to know its x-, y- and z-coordinates, and its velocities v_x, v_y and v_z along x, y and z-direction.

ations are, because of this generality, omnipresent in modern physics, and form the basis of particle physics.

Classical mechanics reaches its limitations at very small scales, when details of mechanisms generating the forces become important. The first description of a mechanism that produces a force was given in electromagnetism, which explains the interaction of electric charges by "electromagnetic waves". Such waves transport energy and momentum from one electrically charged object to another, and thus act as an electric force. Electromagnetic interactions are significantly stronger than gravitational forces. Electric charges can, however, be shielded at the microscopic level: the attraction between positive and a negative charges leads to the formation of objects that consist of equal numbers of positive and negative charges. Since the electric force fields of positive and negative charges cancel out, this leads to a vanishing electromagnetic force at larger distances. Mass on the other hand is additive, so that when combining two heavy objects, the gravitational force will always increase. At small scales, when the electrical charges of light objects are separately visible, the strength of electromagnetism dwarfs gravitational attraction.

One crucial experimental observation is that an electric charge cannot be infinitely small, but rather comes in in small portions, called quanta. Experiments also show that at small distances, matter is not distributed evenly, but that mass is collected in small entities called atoms. Atoms in turn consist of a very small, positively charged, heavy core, shielded by a negatively charged cloud. These atoms cannot be described with CM. The photoelectric effect shows that negatively charged quanta can be liberated from an atom by using ultraviolet light. The negatively charged "cloud", that shields the positive charge of the atomic core, thus rather consists of quanta. These are called *electrons*. However, this effect only occurs above certain frequencies of light. For frequencies below this threshold, even prolonged exposure does not produce free electrons. This means that the binding energy of electrons in the atom can only take particular values, and that light itself is quantised to transfer these particular energies to an electron in one portion. The quanta of light are called *photons*. Light has corpuscular properties as well as characteristics of an electromagnetic wave – a dichotomy that cannot be reconciled within CM. The physical theory at such small scales is called quantum mechanics.

Quantum mechanics (QM) postulates that at the heart of everything lie simple, indivisible quanta or *particles*, which intrinsically are a mix-

ture of different states. Whenever we make a measurement, we detect the value of an observable in one of these states, but it is not possible to exactly predict which value will be measured. This makes the measurement itself non-deterministic. Take as an analogy a machine that shoots balls in two "states": Red ball or yellow ball. Whenever we see a ball, it is either red or yellow, and never green. If we do not know the inner workings of the machine, we cannot predict the colour of the next ball. However, assume that after 100 shots, we find the value "red" 90 times, and "yellow" 10 times, then it seems as if the machine draws balls from a reservoir that is to 90% filled with red balls, and contains 10% yellow balls. From this observation we can deduce that the 101st ball will be a yellow ball with probability $p_{\text{yellow}} = 0.1$, and a red ball with probability $p_{\text{red}} = 0.9$. As long as we do not know the intricate details of the ball-shooting machine, we will only ever be able to make probabilistic statements. QM is a probabilistic theory, since it, in Dirac's words, assumes that there is "a limit which is inherent in the nature of things and can never be surpassed by improved technique or increased skill on part of the observer" [1]. Applied to the ball-colour problem, QM postulates that before the observation, the state ball was *in a mixture* of red and yellow states, and that the outcome of the measurement depends on the proportions at which red and yellow contribute. Another famous two-state system is the electron, which is a mixture of two states with intrinsic angular momentum "spin up" and "spin down". The electron is an example of a spin-$\frac{1}{2}$ particle[3].

An observation measures the properties of one particular component of the mixture (or superposition) of states. Conversely, all possible states contribute to the superposition called "particle wave function". If measurements of the position of the particle give the values $x_1, \ldots, x_n$, then each of these measurements corresponds to a component in the wave function. Some measurement are however incompatible. It is for example not possible to determine the position and the velocity of a particle simultaneously to infinite precision. The situation is even more drastic, since an infinitely precise measurement of the position leaves the velocity completely undetermined[4].

For very precisely measured positions, meaning small resolution

[3] Quanta with non-integer spin are called *fermions*, while *bosons* have integer spin.

[4] You can liken this effect to a photography of a moving car. It is not possible to deduce the speed of the car from a sharp picture. Thus, if the position of the car is well-known from an accurate picture, the car could have any velocity. From a blurry picture taken with a long shutter time, it is possible to deduce at least of a range of possible speeds, whereas the precise position is unknown.

scales, very high velocities are possible. If a measurement would indeed detect a high velocity, we have to supplement QM with a description that is reliable for fast particles. The theory that describes fast objects is special relativity. The combination of quantum mechanics and special relativity is called quantum field theory (QFT). In QFT, every particle is described by a quantum field, which is defined by its wave function. The quantum field is the underlying object, and particles are manifestations of these fields. Since the basic building blocks of QFT are fields, there is only little structural difference between the objects that interact, and the force fields. For example, the particle called electron is a phenomenon of the electron field, while the photon is an expression of the electromagnetic force field. Particle realisations of the force field are called force carrier particles or *gauge bosons*.

QFT describes forces by an exchange of force carrier particles between the interacting particles. The force carriers carry momentum from one interacting particle to another. The term "force" can be understood as "a mechanism that leads to a momentum change". An exchange of a force carrier particle does indeed define such a mechanism. The idea of particles mediating the interaction can be compared to two ice-skaters passing a ball to each other. Imagine both persons are initially standing still. Then, if ice-skater A throws the ball, she will slide away from person B, and if ice-skater B catches the ball, he will slide away from person A. The exchange of the ball has made the two ice-skaters move apart, and the ball has acted as carrier of a repulsive force.

The aim of particle physics is to describe all forces by force carrier exchange between indivisible particles. Electrons for example are electrically charged particles, which interact by exchanging photons. Which forces can influence a particle depends on properties of the particle. So far, experiments have revealed four fundamental interactions: Gravitational, electromagnetic, strong and weak forces. Gravity – the force governing most natural phenomena our senses experience – does not yet have a quantum description. The three other fundamental forces are formulated in analogy to electromagnetism. A particular force can only act on a particle if the particle has the correct "charge" property. The Standard Model (SM) of particle physics contains

- ◇ Electromagnetic force carriers (*photons*) coupling to electric charge;
- ◇ Weak force carriers (W- *and* Z-*bosons*) acting on weak isospin charge;
- ◇ Strong force carriers (*gluons*) coupling to colour charge.

Details of the SM will be discussed in the next section.

i.1.2 The road towards the Standard Model

The Standard Model of particle physics describes three fundamental interactions within one framework. It is useful to repeat the most important points of the last section:

1. Symmetries – transformations that do not change the equations of motion – play a fundamental role in physics. Such symmetries cause the conservation of particular quantities.
2. Quantum mechanics governs phenomena at small distances. Every particle is defined by its wave function.
3. Forces can be described by exchange of force carrier particles (called *bosons*) between charged particles. Every force couples to its own type of charge.

In quantum field theory, these points are intimately linked. Take, as an example, electromagnetism. Experiments show that electric charge cannot be destroyed. This means that the quantum field theory describing electromagnetism must have a symmetry that leads to this conservation. When constructing the theory, the electron wave functions are the basic building blocks. Thus, the symmetry transformation has to "act" on the electron wave function, which is possible only if the particle described by the wave function is charged. The symmetry transformations can also directly be used to derive the wave function of the force carrier (the photon), and its precise interaction with the electron.

Before outlining how symmetries can be used to derive the properties of the force carriers, let us have a look at which particles are believed to be fundamental so far. We have already encountered the electron. Two heavier copies of the electron, the muon and tauon, have been found as well. Nuclear reactions furthermore produce copious amounts of electrically neutral *neutrinos*, which seem closely connected to electron-like particles. Three types of neutrinos (electron-neutrino, mu-neutrino, tau-neutrino) have been found. These six fundamental particles are collectively called *leptons*.

The core of the hydrogen atom (the simplest atomic system) consists of a single proton. Protons are not fundamental particles, but bound states of elementary particles called *up-* and *down-quarks*. The proton is composed of two up-quarks and one down-quark, and is part of a family of bound states of three quarks called *baryons*. They form, together with *mesons* (bound states of one quark and one anti-quark[5]), a

[5]Every "charged" particle has a partner with exactly opposite charges, called the anti-particle.

wider group of particles called *hadrons*. To explain the multitude of observed hadrons, two heavier copies of the down-quark, the strange- and bottom-quarks, and another up-like quark, the charm quark, have to be assumed. The Tevatron particle collider finally added another up-type quark, the top-quark, to this picture. The Standard Model of particle physics organises these twelve fundamental particles into three generations, which are subdivided into a neutrino/charged-lepton pair and an up-type/down-type quark pair. All these particles are *fermions*.

Let us again examine the electron more closely. The electron is electrically charged, and experiments show that electric charge is conserved. This conservation law is tied to an underlying symmetry of the electron wave function. To find this symmetry, note that the electron wave function Ψ is a *complex* function, which has both an absolute value ψ and a phase Φ, i.e. $\Psi = \psi e^{i\Phi}$, where $e^{i\Phi}$ is an imaginary function. However, the result of a measurement is always a set of *real* numbers, so that any measurable quantity can only depend on the real parts of Ψ. In particular, shifting the phase of the electron wave function Ψ by the amount ϕ (i.e. $\psi \to e^{i\phi}\psi$) cannot change the equations of motion. This invariance under "phase shift" transformations is the aforementioned symmetry. The transformation does not depend on the space-time point x at which the wave-function is evaluated. If we make the transformation local (i.e. assume $\phi = \phi(x)$), we find that that the mathematical form of the equations of motion does change, unless we introduce a quantity that exactly counteracts this change in form. The quantity we have to introduce has exactly the properties we expect from a photon field. To endow this promising "fix" with a physical meaning, a term describing the propagation of the photon candidate is introduced. Once this is done, a theory of *quantum electrodynamics* (QED) has been constructed, with a massless, non-charged gauge boson – the photon – mediating the force.

This recipe is called *gauge theory*. The gauge theory reasoning can be extended to incorporate all forces described in the SM. The construction of the theory then proceeds along the lines

1. Experimentally determine conserved charges. Then attempt to construct a Lagrange (density) function.
2. Find the corresponding symmetry transformations of the lepton and/or quark wave functions.
3. Require invariance under the corresponding local symmetry transformation, i.e. that the mathematical form of the equations of motion remains the same after an x-dependent transformation. To ensure

this, include the force-carrier terms to counteract the changes due to shifted lepton/quark wave functions.

4. Add a kinetic term for the force-carrier fields.
5. This leads to massless bosons, which mediate the interaction.

One major ingredient is still missing. Experiments show that at distances comparable to the size of the atomic core, the weak interaction is as strong as electromagnetism. At larger distances however, the weak force is almost negligible. The explanation is that the weak force carriers (the W- and Z-bosons) are massive and unstable, and decay rapidly. The existence of W- and Z-masses are reconciled with the local symmetries of the SM, if another quantum field, the Higgs field, is introduced.

After these steps, we arrive at the structure pictured in Figure *i*.1. Leptons and quarks interact weakly by W- and Z-boson exchange, electrically charged particles couple to the photon (γ) and quarks interact through gluon (g) exchange. The weak force is, because of a complex symmetry structure, mediated by three bosons, one neutral boson (Z), and two electrically charged $W^{\pm}$-bosons. These three bosons further interact amongst each other. Self-interactions are also present for gluons.

All massive particles (i.e. leptons, quarks and the W- and Z-bosons) interact with the Higgs boson H, which in turn is self-interacting. Particle masses are "generated" by the Higgs field, which has been introduced specifically for this purpose.

We have deliberately glossed over all difficulties in deriving the standard model. Let us pick up one particular thread here. Until today, all measurements indicate that electric charge is quantised, and that the quantum of electric charge is $e = 1.602 \cdot 10^{-19}$ C, precisely the charge of the proton. The proton is a composite object, formed from two up-quarks and one down-quark. Other bound states of three quarks exist. The neutron, an electrically neutral particle that makes multiply charged atomic cores stable, consists for example of one up- and two down-quarks, while the doubly-charged Delta-particle (Δ^{++}) consists of three up-quarks. The only way to accommodate these charges in three-quark bound states is to assume that quarks are fractionally charged. This means that a mechanism must exist that "hides" this fractional charge. The strong interaction, which is responsible for this mechanism, is discussed in the next section.

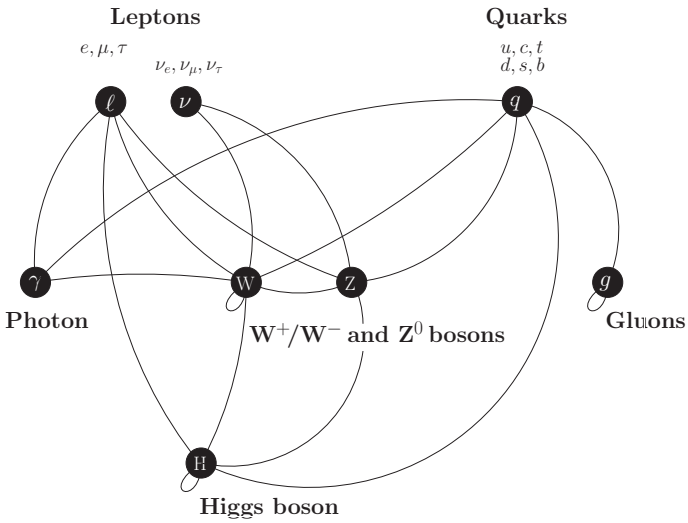

Figure *i*.1: The Standard Model of particle physics, with lines indicating interactions. Electrically charged particles exchange photons. Leptons further interact through W- and Z-boson exchange, as do the quarks, which also communicate through gluon exchange. Every massive particle interacts with the Higgs field. Gluons interact among themselves, as do W- and Z-bosons, and the Higgs boson.

i.1.3 Quantum Chromodynamics (QCD)

The existence of a "strong" force between neutrons and protons was originally postulated to explain the stability of atomic nuclei. In particular, an additional force was necessary to overcome the electromagnetic repulsion of protons. QCD can furnish a mechanism for this strong binding.

QCD describes the interaction amongst quarks through gluon exchange. In order to explain the copious amount of detected hadrons[6], it is necessary to assume that

- ◇ Hadrons are bound states of quarks. Baryons (e.g. the proton, neutron or Δ^{++}) consist of three quarks, while mesons are bound states of one quark and one anti-quark.
- ◇ Five quarks are needed to describe all known hadrons. Together with the extremely heavy top quark, these form three generations of up-type/down-type pairs. Quarks have fractional electric charge.

[6]So far, 41 Baryons and 118 Mesons are considered well-established [2].

◇ The quarks have "QCD-charges" in order to interact via QCD. The "charge" of QCD is called colour. Quarks can have either of the *three different* colour charges "red", "blue" or "green".

In order to motivate these complications, let us have a closer look at the Δ^{++}-baryon. This composite particle is slightly heavier than the proton, but has electric charge $2e$, and spin $\frac{3}{2}$. In the quark model, the electric charge of the Δ^{++} can be explained if it consists of three up-quarks, each carrying an electric charge $\frac{2}{3}e$. That the Δ^{++} has spin of $\frac{3}{2}$ means that the intrinsic angular momenta of all three up-quark building blocks need to to be aligned. Since so far, all up-quarks "look" identical, any interchange of the quarks could not be noticed: The wave function of the Δ^{++} state is completely symmetric. However, quantum mechanics requires that any wave function of a quantum with non-integer spin be completely anti-symmetric. This can only be achieved if the up-quarks exhibit another property, in which all of them differ. An up-quark thus needs to have three different states, for example red, blue and green. This property is called colour charge.

Colour charge conservation, i.e. the requirement that colour charge does not spontaneously disappear, can be used to derive the interactions that bind quarks into hadrons. The resulting theory, QCD, is more complicated than QED, since instead of one electric charge, the theory now contains three colour charges, which are all interacting. As in electrodynamics, it is possible to construct (colour-) neutral objects by combining positive and negative charges. In the quark model, we speak of quarks carrying colour, and anti-quarks carrying anti-colour. However, in contrast to electric charge, it is possible to combine three different colour charges into a colour-neutral object, much like overlaying red, green and blue light results in white, i.e. the absence of colour. QCD interactions are mediated through *gluons*. These massless spin-1 particles are colour-charged, unlike the photon, which does not have an electric charge. Since gluons mediate the force between colour charges, and are colour-charged themselves, gluons self-interact. To transmit QCD interactions between particles that can have one of three colour charges (or one of three anti-colour charges) eight types of gluons are necessary.

These facts make QCD very different from QED, and helps understand why no unbound quarks have been found. This important fact derives from the form of the colour force field. While the electromagnetic force between electrically charged objects decreases with increasing distance, the force between a quark and an anti-quark remains constant when the particles are "pulled apart". This happens because the

gluon self-interactions compress the QCD force field into a narrow tube (string) of field lines connecting the quark colour charge to the anti-quark anti-colour charge. If colour charges are pulled apart, the energy stored in this string increases steadily, until it is energetically favourable that the string breaks, just like a rubber band would snap if stretched too much. The colour string can break if enough energy is stored in the force field to create a quark-antiquark pair in between the ends of the string, which is the case if the distance of the quarks is much larger than 10^{-15} m (i.e. at roughly the size of the proton). After the breaking, two decoupled strings coexist. Instead of isolating a colour charge by separating the quark from the anti-quark, we have produced two new colour-neutral objects. This mechanism, that only further colour-neutral objects are produced whenever the liberation of a colour-charged particle is attempted, illustrates why no free quarks or gluons seem to exist – a phenomenon called colour *confinement*.

In the beginning of this chapter, we have motivated the need for a theory of strong interactions by an attempt to explain the stability of atomic nuclei. We have just argued that the effect of the colour field is confined within mesons and baryons. This would mean that protons do not interact via the strong force. Colour-exchange between hadronic bound states is indeed forbidden – what binds protons and neutrons is instead only a secondary effect of the strong force, which allows the exchange of mesons between the constituents of the atomic core. This is similar to forces between induced charges for water molecules, when slight shifts in the distribution of electric charge distribution allows water molecules to form bonds and crystallise, although the water molecules themselves are electrically neutral.

That this secondary consequence of the strong interaction can outweigh electromagnetism is an indication of the strength of the QCD force. When performing calculations in QCD, we commonly start from simple non-interacting quarks, then calculate the result of exchange of one gluon, then the result of exchanging two gluons and so on. This method is called perturbation theory. If the force is indeed very strong, it would be questionable if we could arrive at sensible results by only relying on calculations involving a finite number of gluon exchanges. However, QCD exhibits the miraculous property of asymptotic freedom: for very large momentum transfers, interactions between colour charges gradually vanish. This means that at large momentum transfers (i.e. high energies), QCD has a well-behaved perturbation theory. Particle colliders, the "microscopes" needed to pursue fundamental particle

physics research, produce such high energies that we can investigate the proton substructure by using perturbation theory. The available energies are however not high enough to simply ignore multi-gluon processes. An improved handling of such "higher order" corrections is the topic of this thesis.

i.1.4 Collider measurements and QCD

Collider experiments are the main means of gathering knowledge in fundamental particle physics, and as such, high hopes for new discoveries are tied to every boost in collision energy. The Large Hadron Collider (LHC) at the CERN research facility in Geneva, Switzerland, currently holds the collision energy record. The high collision energies at LHC are possible because the colliding protons have a non-negligible rest mass, which means that they can be accelerated efficiently. Since protons are composite objects bound by QCD, the imprint of QCD is omnipresent at the LHC.

The ubiquity of QCD effects at the LHC is established through collimated particle sprays called jets. It is important to understand how such sprays are formed, since jets appear so abundantly that signals for unexpected discoveries might be swamped in jet background noise.

Let us attempt to illustrate how LHC measurements can be interpreted. The LHC experiments measure scattering cross sections, i.e. likelihoods of two protons A and B to exchange momentum and scatter into particles within a certain momentum interval. The scattering is often so dramatic that parts of the incoming protons are disintegrated, and completely new outgoing particles $c_1, c_2, \ldots$ are produced from the energy of the collision. The allowed momentum interval for outgoing particles is called their phase space. Scattering cross sections are calculated by integrating transition probabilities over the phase space of all outgoing particles.

Particles undergo a wealth of transitions in one single collision event at the LHC. At the very collision centre, a hard inelastic scattering $a + b \to c_1 + c_2 + \cdots + c_n$ of two components a and b of the incoming protons A and B produces a small number of final particles $c_1 \ldots c_n$, while annihilating the incoming particles a and b. The resulting state contains highly energetic colour-charged particles (called *partons*) that speed apart, dragging the colour-field along. The inter-parton distances at this stage are still very small, so that the colour-fields can produce additional gluons, rather than break apart. Since multiple gluon emissions are allowed, and because gluons can themselves emit further radiation, this

produces a radiation cascade, or *parton shower*. The emissions predominantly move collinear with their parents, or have a very low energy, because the transition probabilities for evolving into such configurations are very high. This leads to sprays of partons moving into roughly the same direction, still at distances smaller than the proton radius. Particles produced in this parton shower cascade are then bound into composite objects (e.g. protons or pions), once the momentum transfer of emissions becomes very low, i.e. when inter-parton distances become comparable to the proton radius. The resulting hadrons will, since the partons before this *hadronisation* have been moving along a similar direction, be collimated into a hadronic jet, which approximately moves along the direction of the underlying partons.

Since the typical energies associated to the three transitions (inelastic scattering, radiation cascade, hadronisation) are vastly different, it is customary to talk about the hard, intermediate and soft regime. This picture is still missing another important piece. Protons are complex, composite objects. It is highly unlikely that if colliding protons interact, only a single scattering (of a parton a in proton A with a parton b in proton B) occurs. Experimental evidence for secondary scatterings (theoretically modelled by *multi-parton interactions*) is indeed abundant.

It is fair to say that QCD effects make conclusive measurements at the LHC challenging. Reliable theoretical models of QCD effects are thus mandatory for data analysis. Here, we should note that none of the "evolution" stages of the collision event before hadronisation can be measured directly, since these evolution steps happen at distances comparable to the proton radius. However, the meter-long jet-like objects that detectors at the LHC observe strongly reflect the underlying production mechanism.

QCD has, as part of the SM, been well established as the theory of the strong interaction for more than two decades. However, we know that the Standard Model of particle physics is, due to its failure to include gravity, ultimately incomplete. This certainly means that particle physics should be concerned with Beyond-the-Standard-Model approaches. However, measurements at the LHC can only reveal signals of new phenomena if a detailed description of QCD jets allows to eliminate these "known" backgrounds.

The aim of General-Purpose Monte Carlo Event Generator (MCEG) computer programs is to give an as complete description of collision events as possible, with main focus on QCD modelling. The structure of these programs is tailored after the energy-dependence of the transi-

tions as follows:

1. Calculate the "hard" transition probability for $a + b \to c_1 + c_2 + \cdots + c_n$ within perturbation theory.
2. Dress the particles $a, b, c_1, c_2, \ldots, c_n$ in a radiative cascade, i.e. a parton shower.
3. Add secondary scatterings to the event, and allow these to initiate further parton showers.
4. At low energies, convert all partons into hadrons.

Processing the output of a MCEG with a detector simulation, which simulates the interaction of hadrons with the material of the detector cells, allows to directly compare this "theory output" with data recorded by the experiment. The research presented in this thesis aims at improving the transition between the first two points of this list, by allowing more complicated perturbative input for event generators. In particular, I have been involved in the PYTHIA8 event generator, which is developed in Lund.

This concludes the general introduction to the topic. In the following, we would like to briefly introduce some mathematical concepts.

i.2 Mathematical concepts

The aim of this section is to recapitulate some concepts in a more mathematical language and to give an introduction to quantum field theory calculations of SM scattering processes. A pedagogical introduction is unfortunately beyond the scope of this introduction, so that some familiarity with the topic has to be assumed.

i.2.1 Symmetries of the Standard Model Lagrangian density.

In field theory, the motions and interactions of particles are governed by equations of motion, which in turn can be derived from a Lagrangian density[7]. In this section, we would like to discuss the structure of the SM Lagrangian.

The SM contains twelve fundamental fermions, which interact via the electromagnetic, weak and strong forces. However, electromagnetism and weak force are consequences of a mixed force, called the electro-weak force. The electro-weak model has to produce the observations that

a) The weak force is parity-violating.

b) Electrically charged force carriers change the flavour of fermions[8].

c) The weak force carriers are massive, the photon massless.

d) Weak isospin and hypercharge are only approximately conserved, while the electric charge is conserved.

These facts can be accommodated if the electro-weak interaction is described by a gauge symmetry of the group $SU(2)_L \otimes U(1)_Y$, which is spontaneously broken to the electromagnetic group $U(1)_{em}$. The index L indicates that left- and right-handed fermions transform differently under the $SU(2)_L$-rotations. Parity is thus explicitly violated. The fundamental fermions are organised is three generations of four particles. Each generation contains a (left- and right-handed) up-type quark, a (left- and right-handed) down-type quark, a (left- and right-handed) electron-type lepton and a (left-handed) neutrino. All naive mass terms, for bosons and fermions alike, are forbidden in the unbroken $SU(2)_L \otimes U(1)_Y$ gauge symmetry. Spontaneous breaking however

[7] In any theory respecting local symmetries, it is more convenient to begin from a Lagrangian density rather than from a Lagrange function.

[8] The flavour of a fermion is given by its name. The up quark for example has "up" flavour.

Quarks	$\binom{u}{d}_{L,i}$	$u_{R,i}$	$d_{R,i}$
	$\left(\mathbf{3},\mathbf{2},\frac{1}{6}\right)$	$\left(\mathbf{3},\mathbf{1},\frac{2}{3}\right)$	$\left(\mathbf{3},\mathbf{1},-\frac{1}{3}\right)$
Leptons	$\binom{\nu}{e}_{L,i}$		$e_{R,i}$
	$\left(\mathbf{1},\mathbf{2},-\frac{1}{2}\right)$		$(\mathbf{1},\mathbf{1},-1)$

Table *i*.1: Classification of the fundamental fermions in the i'th generation through their representation of $SU(3)_C \otimes SU(2)_L \otimes U(1)_Y$. Singlet-representations are indicated by **1**, doublet-representations by **2** and triplets by **3**. The first term in brackets gives the representation of $SU(3)_C$, the second the representation of $SU(2)_L$ and the third term gives the $U(1)_Y$-hypercharge. The z-component of the weak isospin and the hypercharge are related to the electric charge by $Q = I_3 + Y$. Note that the neutrinos only enter in the left-handed lepton doublet. The initial SM did not include a right-handed neutrino, which would be necessary to construct neutrino masses. However, such a particle could be added to the SM.

gives a mechanism to generate boson masses (called the *Higgs mechanism*) and a possibility to accommodate fermion masses (via so-called *Yukawa couplings*). The introduction of fermion mass terms induces a mismatch between flavour- and mass-eigenstates in the Lagrangian density. "Physical" quarks are an admixture of akin (flavour-eigenstate) quarks of different generations.

The QCD part of the Lagrangian density is, because colour-charge is conserved and no spontaneous breaking occurs, structurally simpler. The theory of the strong interaction has to accommodate the facts that

a) Colourless bosonic quark- anti-quark bound states (i.e. mesons) exist.

b) Colourless fermionic bound states of three quarks (i.e. baryons) exist, even if all three quarks have identical flavour.

c) No free, strongly charged particles have been found, and no particle with fractional electric charge has been observed.

The model of the strong force should also, from a technical viewpoint, be at least partially calculable. The requirements $a)$ and $b)$ can be incorporated by assuming that quarks transform under the fundamental (triplet) representation of $SU(3)_C$. The force is transmitted by eight gluon fields.

This model, called QCD, treats left- and right-handed quarks on equal footing, which means that the mass terms introduced in the

electro-weak sector are allowed. The twelve fundamental fermions transform under the combined SM gauge group $SU(3)_C \otimes SU(2)_L \otimes U(1)_Y$ according to Table *i*.1.

QCD is very attractive as theory for the strong interaction, since it is calculable perturbatively at large momentum transfers, and exhibits a phase transition at scales comparable to the proton radius. The reason for this behaviour is founded in renormalisation.

The parts of a Lagrangian density we have introduced so far include arbitrary parameters[9]. Truly physical results measured in experiments are independent of any re-parametrisation (e.g. $g_3 \rightarrow g_3'$) of the Lagrangian density. More precisely, the elements of the scattering matrix (*S*-matrix) should be invariant under such re-parametrisation. The requirement leads to the *renormalisation group equation* for the vertex functions[10]. The solution of this equation implicitly yields masses and coupling constants that vary with the momentum scale Q^2 at which the vertex functions are evaluated. If e.g. the *running, or renormalised* QCD coupling $\alpha_s(Q^2)$ is evaluated within perturbation theory at one-loop level, we find

$$\alpha_s(Q^2) = \frac{\alpha_s(\mu^2)}{1 + \frac{\alpha_s(\mu^2)}{4\pi}\,\beta_0 \ln \frac{Q^2}{\mu^2}} \qquad (i.1)$$

$$\text{with} \quad \alpha_s(Q^2) = \frac{\overline{g_3}^2(Q^2)}{4\pi} \quad \text{and} \quad \overline{g_3}(\mu^2) = g_3 \,,$$

where μ^2 is called renormalisation scale. Explicit calculation for QCD shows

$$\beta_0 \quad = \quad 11 - \frac{2}{3} \cdot N_f \,, \qquad (i.2)$$

where N_f is the number of quark flavours. Thus, $\alpha_s(Q^2)$ is a decreasing function of Q^2 for a theory with six quarks, rendering QCD a non-interacting theory at infinitely large momentum transfers. This property, called asymptotic freedom, allows the application of perturbative methods to calculate QCD transition probabilities at large momentum transfers.

If the running coupling is rewritten as

$$\alpha_s(Q^2) \;=\; \frac{4\pi}{\beta_0 \ln \frac{Q^2}{\Lambda^2}} \,, \quad \text{where} \quad \Lambda^2 = \mu^2 \cdot \exp\left(-\frac{4\pi}{\beta_0 \alpha_s(\mu^2)}\right) \,, \qquad (i.3)$$

[9] For example masses, couplings g_1, g_2, g_3 (appearing the interaction terms of fermions with the $U(1)_Y$, $SU(2)_L$ and $SU(3)_C$ gauge bosons), and the overall normalisation of fields.

[10] Vertex functions are the basic building block of the (connected) *S*-matrix. Vertices define which primitive branchings / annihilations are possible in the theory.

it becomes obvious that $\alpha_s(Q^2)$ can in fact exceed unity, or even diverge. This is taken as evidence that QCD exhibits a phase transition for momentum transfers $Q^2 \approx \Lambda^2$, which gives rise to the formation of hadrons.

i.2.2 Matrix elements and factorisation

Particle physics detectors are highly sophisticated counting experiments. An analysis of available LHC data would for example involve counting the occurrence of a specific event, i.e. of a particular configuration of hadrons, leptons and photons, within a certain detector region, and with three-momenta within some (machine-dependent or deliberately chosen) boundaries. The number of occurrences is directly related to the likelihood of the relevant scattering processes. An experiment measures the (differential) cross section of scattering processes which produce the measured topology.

The calculation of scattering cross sections is thus a major task of theoretical particle physics. The cross section of proton A and proton B to in-elastically scatter, thereby producing non-coloured final state particles[11] $c_1 \dots c_n$ and proton remnants X, is given by

$$\begin{aligned}\sigma\left(A+B \to c_1 + \cdots + c_n + X\right) \qquad (i.4)\\ = \sum_{a,b \in \{\text{allowed partons}\}} \int_0^1 dx_b \int_0^1 dx_a f_{a/A}(x_a, \mu_F) f_{b/B}(x_b, \mu_F)\\ d\widehat{\sigma}\left(a+b \to c_1 + \cdots + c_n\right)\end{aligned}$$

Before explaining eq. (*i*.4) in detail, let us introduce the partonic cross section

$$\begin{aligned}d\widehat{\sigma}\left(a+b \to c_1 + \cdots + c_n\right) \qquad (i.5)\\ = \frac{1}{4\sqrt{\left(p_a p_b\right)^2 - M_a^2 M_b^2}} \left|\mathcal{M}\left(a+b \to c_1 + \cdots + c_n\right)\right|^2\\ d\phi_n\left(p_a, p_b;\ p_1, \dots, p_n\right)\end{aligned}$$

Some clarifications are in order[12]. Equation *i*.4 defines the hadronic cross section of two protons interacting and producing final state particles. This hadronic cross section *factorises* into a hadronic part given by

[11] The situation is more complicated when discussion additional final state partons. These can, in principle, be absorbed into hadrons by using fragmentation functions. Fragmentation can be achieved dynamically by using hadronisation models, which require high-multiplicity partonic input, as provided by a parton shower.

[12] The "kinematic variables" in eqs. *i*.4 and *i*.5 are defined as follows. We use p_A (p_B) as the 4-momentum of the incoming proton A (B), and p_a (p_b) as the 4-momentum of the interacting parton

functions describing the distribution of partons inside the proton, the parton distribution functions (PDFs) $f_{a/A}$, and partonic part $d\widehat{\sigma}$ which involves calculations with unbound quarks and gluons. To a first approximation, the function $f_{a/A}(x_a, \mu_F)$ is the probability of finding a parton a with a momentum fraction in the interval $[x_a, x_a + dx]$ in the proton A, if the proton is probed at the momentum scale μ_F. The dependence of $f_{a/A}$ on the momentum scale μ_F derives from absorbing infrared singularities into the PDF by redefinition. This is in a way reminiscent of the emergence of scale dependent parameters by absorbing ultraviolet divergences in the course of renormalisation. PDFs are descriptions of the hadronic bound states, and can as such not be calculated rigorously in perturbation theory. However, since the $f_{a/A}$ only depend on x_a and μ_F, it is possible to measure these quantities. If we assume the universality of parton distribution functions, i.e. that the PDFs do not depend on the details of the "hard process" $a + b \to c_1 + \cdots + c_n$, it will be possible to calculate the partonic cross section $d\widehat{\sigma}$ independently, and simply convolute the result (for particular incoming momenta p_a and p_b) with PDFs describing the colliding protons. This means that the computational task is to calculate $d\widehat{\sigma}$ to a high precision.

The first factor in the partonic cross section ($1/[\,4\sqrt{(p_a p_b)^2 - M_a^2 M_b^2}\,]$) is called flux factor, and is related to the relative velocities and the energies of the incoming partons. The factor $|\mathcal{M}|^2$ is called squared *invariant matrix element* (ME), and directly related to the scattering matrix S by

$$\begin{aligned}\langle c_1, \ldots, c_n \,|S|\, a, b\rangle &= \langle c_1, \ldots, c_n | a, b\rangle \\ &+\; i\,(2\pi)^4\,\delta^{(4)}\left(p_a + p_b - \sum_{i=1}^{n} p_i\right)\mathcal{M}\left(a + b \to c_1 + \cdots + c_n\right)\,.\end{aligned} \tag{i.6}$$

Flux factor and ME are finally integrated over the phase space

$$d\phi_n\left(p_a, p_b;\; p_1, \ldots, p_n\right) = (2\pi)^4\,\delta^{(4)}\left(p_a + p_b - \sum_{i=1}^{n} p_i\right)\frac{d^3p_1}{(2\pi)^3 2E_{p_1}} \cdots \frac{d^3p_n}{(2\pi)^3 2E_{p_n}}\,. \tag{i.7}$$

The $\delta^{(4)}$-functions guarantee 4-momentum conservation, and the integration measures $d^3p_i/\,(2\pi)^3\,2E_{p_i}$ are chosen to make the phase space integrations Lorentz-invariant.

The basic building blocks of the invariant ME are *vertex functions, propagators and wave functions for external particles*. Vertices describe the

a (b) in proton A (B). The parton and proton momenta are connected by $p_{a,b} = x_{a,b}p_{A,B}$, where $x_{a,b}$ is called the momentum fraction. The mass of parton a (b) is M_a (M_b). The 4-momentum of the outgoing particle i is p_i, while its energy is given by E_{p_i}. All other symbols are discussed in the main text.

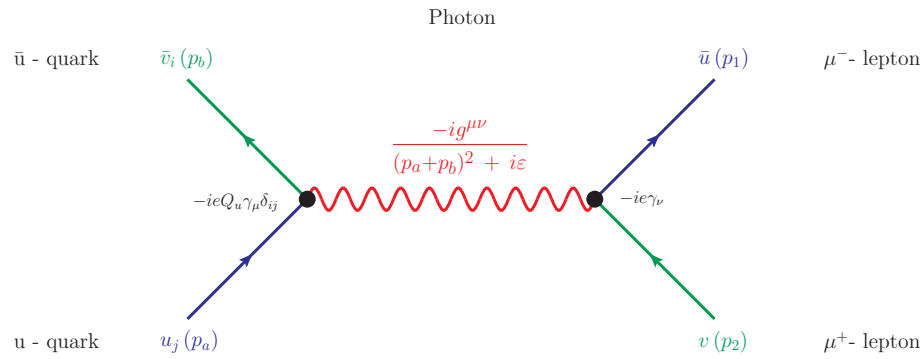

$$= \quad -e^2 Q_u\ \bar{u}\,(p_1)\gamma_\nu v\,(p_2)\ \frac{-g^{\mu\nu}}{(p_a+p_b)^2\ +\ i\varepsilon}\ \bar{v}_i\,(p_b)\gamma_\mu\delta_{ij}\,u_j\,(p_a)$$

Figure *i*.2: Invariant matrix element for a scattering $\bar{\mathrm{u}}(p_b)\mathrm{u}(p_a) \to \mu^+(p_2)\mu^-(p_1)$. The subscripts i and j indicate the colour of the external ū- and u-quarks. Polarisation indices are suppressed. The upper part gives the Feynman diagram, with vertices in black, the photon propagator (in Feynman gauge) in red, and the external wave functions in green and blue. The corresponding factors in the ME are indicated with the same colours. The lower part shows the actual ME expression, which is read off the Feynman diagram by moving from the right to the left side, against the fermion-number flow indicated by arrows, and multiplying all encountered expressions.

interaction of particles with the force fields by exchange of quanta, while propagators describe the propagation of (virtual) interacting fields. The perturbative approximation of these building blocks can be derived from the Lagrange density. Once propagators and vertices have been derived, the calculation of matrix elements can be conveniently organised by using a pictorial representation called Feynman diagrams. The matrix element $\mathcal{M}\left(\bar{\mathrm{u}}(p_b)\mathrm{u}(p_a) \to \mu^+(p_2)\mu^-(p_1)\right)$ is for example illustrated in Figure *i*.2.

Calculations with Feynman diagrams become however unwieldy when many final state particles are involved, since the number of relevant graphs grows very rapidly. It is however possible to derive an approximation of matrix elements with additional final state partons, and use the result to calculate approximate cross sections for an (in principle) arbitrary number of outgoing partons. Parton shower programs, which are investigated in this thesis, rely on such approximations.

To acquaint the reader with this concept, we will describe how the cross section for $\bar{u}u \to \mu^+\mu^- g$ can be approximated[13] when the additional gluon stems from a collinear emission off the incoming u-quark in Figure *i*.2. The ME for this process is

$$\begin{aligned}\mathcal{M}\left(\bar{u}(p_b)\,u(p) \to \mu^+(p_2)\,\mu^-(p_1) g(k)\right) \\ = \overline{u}(p_1) e\gamma_\nu v(p_2) \frac{g^{\mu\nu}}{(p_1+p_2)^2+i\epsilon} \\ \times\ \overline{v}_i(p_b) e Q_u \gamma_\mu \frac{i\left(\not{p}-\not{k}+m\right)}{(p-k)^2-m^2+i\epsilon}\, i g_3 T^a_{ij}\, \not{\varepsilon}^*_a(k) u_j(p)\,,\end{aligned} \tag{i.8}$$

If the mass of the incoming u-quark is neglected, the momenta entering the gluon vertex (i.e. the initial u-quark momentum p, the gluon momentum k and the intermediate u-quark momentum p_a) can be expressed by Sudakov kinematics[14]. If the intermediate u-quark momentum is very close to its mass shell, it is further allowed replace the numerator of the quark propagator (after neglecting the quark mass) by the polarisation sum,

$$\frac{i\left(\not{p}-\not{k}+m\right)}{(p-k)^2-m^2+i\epsilon} \to \frac{u(p_a)\overline{u}(p_a)}{p_a^2}\,. \tag{i.9}$$

This polarisation sum allows to factorise the ME into two parts. Using Sudakov kinematics, inserting the polarisation sum, squaring, and summing over polarisations gives

$$\left|\mathcal{M}\left(\bar{u}u \to \mu^+\mu^- g\right)\right|^2 = \left|\mathcal{M}\left(\bar{u}\,u \to \mu^+\mu^-\right)\right|^2 \ \ 2g_3^2\,\tfrac{1-z}{zp_\perp^2}\,C_F\,\tfrac{1+z^2}{1-z} \tag{i.10}$$

Thus, for collinear gluons (i.e. small $p_\perp$), the squared ME for the scattering $\bar{u}u \to \mu^+\mu^- g$ is proportional to the ME for $\bar{u}u \to \mu^+\mu^-$. If we further rewrite the phase space element of the emitted gluon as

$$\frac{d^3k}{(2\pi)^3\,2E_k} = \frac{dz\,d\phi\,dp_\perp^2}{4\,(2\pi)^3\,(1-z)} + \mathcal{O}(p_\perp^2)\,, \tag{i.11}$$

and relate the flux factors

$$\frac{1}{4\sqrt{(pp_b)^2 - M^2M_b^2}} \approx \frac{1}{4\sqrt{(pp_b)^2}} = z\frac{1}{4\sqrt{(p_ap_b)^2}}\,, \tag{i.12}$$

[13] Apart from considering g-emissions, this discussion closely follows section 2.8.3.1 of [3].

[14] Momenta are parametrised in terms of the energy fraction $z \approx 1$ of the intermediate u-quark ($E_{p_a} \approx zE_p$) and a small transverse momentum $p_\perp$ by
$k^\mu = (1-z)p^\mu + \frac{p_\perp^2}{2(1-z)pn}n^\mu + p_\perp^\mu$ and $p_a^\mu = zp^\mu - \frac{p_\perp^2}{2(1-z)pn}n^\mu - p_\perp^\mu$, where
$p^\mu = (E,0,0,E)$, $n^\mu = (E,0,0,-E)$, $p_\perp^\mu = (0, |\vec{p}_\perp|\cos\phi, |\vec{p}_\perp|\sin\phi, 0)$, $p_a^2 = -\frac{p_\perp^2}{1-z}$.

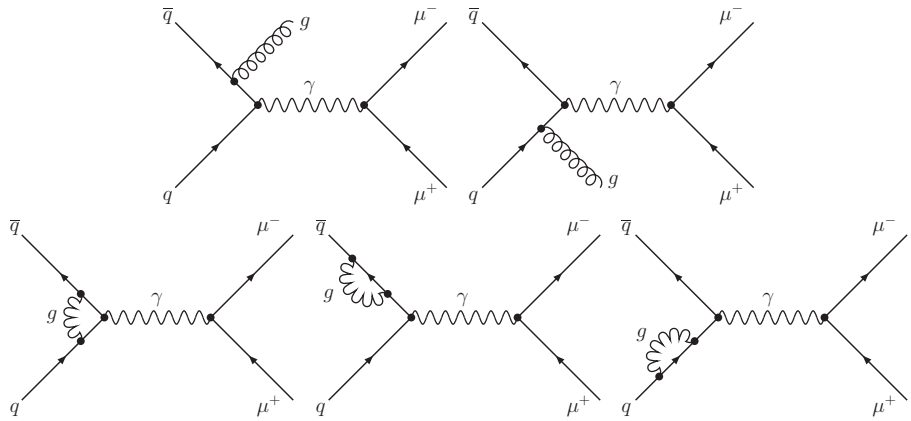

Figure *i*.3: Set of Feynman diagrams that lead to a finite cross section. Real emission corrections are depicted in the upper row, while virtual (or loop) corrections are given in the lower row.

we find that the cross section with an additional collinear gluon can be expressed as

$$d\widehat{\sigma}^{\,\bar{\mathrm{u}}\mathrm{u}\to\mu^+\mu^-\mathrm{g}}\left(p, p_b, p_1, p_2, k\right) \tag{*i*.13}$$
$$= \int_{p^2_{\perp min}}^{p^2_{\perp max}} \frac{dp^2_\perp}{p^2_\perp} \int_0^1 dz\, \frac{\alpha_\mathrm{s}}{2\pi}\, C_F\, \frac{1+z^2}{1-z}\, d\widehat{\sigma}^{\,\bar{\mathrm{u}}\mathrm{u}\to\mu^+\mu^-}\left(p_a, p_b, p_1, p_2\right) ,$$

where we have used $\alpha_\mathrm{s} = g_3^2/4\pi$. Here, $p_{\perp max}$ is of the order of the energy of the process, and thus determined by the phase space limits or experimental constraints. If we had been more careful with quark mass terms, the lower limit $p_{\perp min}$ (introduced by hand here), could be found to be of the order of the quark mass.

When performing the integral in eq. (*i*.13), the result is proportional to $\ln\left(p^2_{\perp max}/p^2_{\perp min}\right)$, i.e. singular for $p_{\perp min} \to 0$. This divergence can, according to the Kinoshita-Lee-Nauenberg theorem [4], be cancelled by including virtual perturbative corrections. A set of Feynman diagrams that, after renormalisation, yield a finite cross section, is given in Figure *i*.3. This set of diagrams gives the next-to-leading order (NLO) QCD prediction for muon pair production in hadronic collisions.

Equation *i*.13 means that the radiative cross section factorises into a non-radiative "hard" cross section, multiplied by a function determin-

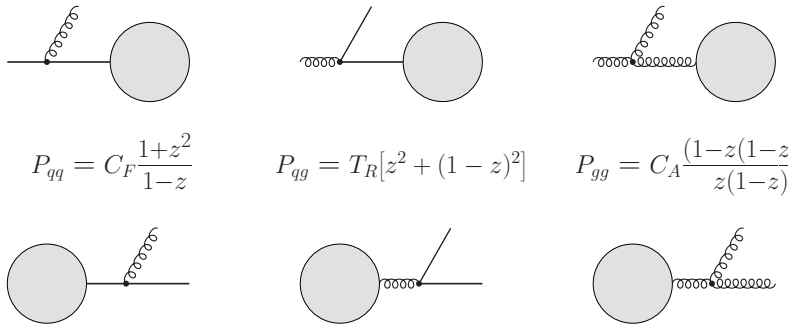

Figure *i*.4: Possible splittings in QCD. The grey circle represents the "hard" process, straight lines indicate quarks or anti-quarks, and spring-like denote lines gluons. The corresponding splitting functions for each column are given between the upper and lower graphs.

ing the splitting. Because the splitting function

$$P_{qq}(z) = C_F \, \frac{1+z^2}{1-z} \tag{i.14}$$

does not depend on the details of the hard process, this exercise can be repeated when adding another gluon emission with $p_{\perp,2} \ll p_{\perp,1}$. This gives the approximate cross section

$$\begin{aligned} & d\widehat{\sigma}^{\,\bar{\mathrm{u}}\mathrm{u}\to\mu^+\mu^-\mathrm{gg}}\,(p, p_b, p_1, p_2, k) \qquad (i.15) \\ & = \int_{p^2_{\perp min}}^{p^2_{\perp max}} \frac{dp^2_{\perp 1}}{p^2_{\perp 1}} \int_0^1 dz_1 \, \frac{\alpha_s}{2\pi} \; P_{qq}(z_1) \int_{p^2_{\perp min}}^{p^2_{\perp 1}} \frac{dp^2_{\perp 2}}{p^2_{\perp 2}} \int_0^1 dz_2 \, \frac{\alpha_s}{2\pi} \; P_{qq}(z_2) \\ & \quad d\widehat{\sigma}^{\,\bar{\mathrm{u}}\mathrm{u}\to\mu^+\mu^-}\,(p_a, p_b, p_1, p_2) \; . \end{aligned}$$

The approximation of three gluon emissions would contain three nested integrals. The procedure can approximate the result of including an arbitrary number of (collinear) gluon emissions.

This iterative splitting procedure can directly be generalised to include other splittings as well. Figure *i*.4 shows possible QCD splittings. Knowledge of these splitting functions (and of a suitable parametrisation of the particle momenta) allows to construct computer programs that provide an approximation of the cross section for any number of collinear partons. Splitting functions have a simple probabilistic inter-

pretation. The term

$$\int_{p_{\perp min}^2}^{p_{\perp max}^2} \frac{dp_\perp^2}{p_\perp^2} \int_0^1 dz \frac{\alpha_s}{2\pi} P_{qq}(z) \tag{i.16}$$

can, for example, be regarded as the probability of emitting a gluon (with energy fraction $(1-z)$ in the interval $[0,1]$) between the momentum scales $p_{\perp max}$ and $p_{\perp min}$. This interpretation has to be slightly amended when taking into account that if the first gluon was emitted at exactly the scale $p_\perp$, then no other "first gluon" can be emitted at $p'_\perp > p_\perp$. The derivation of such a no-emission probability factor will be discussed in the next section.

i.2.3 Parton showers and resummation

In the last section, we have found that cross sections for processes containing "additional" splittings factorise into a hard cross section and process-independent splitting functions. This universal factorisation can be used to construct calculations for cross sections that approximate the effect of an arbitrary number of additional final state particles. It is clear from eq. (*i*.15) that such calculations will always have a "least-collinear" particle given by the "hardest emission" off the hard core process.

The probabilistic interpretation of the splitting kernels makes it tempting to construct numerical programs for this task. Such programs will have to generate a hardest emission. We will in the following mainly be concerned with gluon and quark emissions. Let us, for simplicity, consider gluon emissions. The naive probability for an emission within a small momentum interval $\delta p_\perp^2 = p_{\perp max}^2 - p_{\perp 1}^2$ is

$$\frac{\delta p_\perp^2}{p_\perp^2} \int_0^1 dz \frac{\alpha_s}{2\pi} P_{qq}(z)\,, \tag{i.17}$$

with P_{qq} defined in Figure *i*.4. The probability for no emission is then

$$1 - \frac{\delta p_\perp^2}{p_\perp^2} \int_0^1 dz \frac{\alpha_s}{2\pi} P_{qq}(z) \tag{i.18}$$

If the interval $\delta p_\perp^2$ is subdivided into n parts, and no emission inside $\delta p_\perp^2$ is found, the no-emission probability will be the product of no-emission probabilities for all the sub-intervals,

$$\left[1 - \frac{\delta p_\perp^2/n}{p_\perp^2} \int_0^1 dz \frac{\alpha_s}{2\pi} P_{qq}(z)\right]^n \tag{i.19}$$

For infinitely small steps ($n \to \infty$), this means the probability for no emission between $p_{\perp max}$ and $p_{\perp 1}$ becomes

$$\Delta(p^2_{\perp max}, p^2_{\perp 1}) = \exp\left(- \int_{p^2_{\perp 1}}^{p^2_{\perp max}} \frac{dp^2_\perp}{p^2_\perp} \int_0^1 dz \frac{\alpha_s}{2\pi} P_{qq}(z) \right) \qquad (i.20)$$

Once a hardest emission has been produced, no other emissions can be harder. The probability for the hardest emission with $p_{\perp 1}$ and energy fraction z is thus

$$\Delta(p^2_{\perp max}, p^2_{\perp 1}) \frac{\alpha_s}{2\pi} \frac{P_{qq}(z)}{p^2_{\perp 1}} \qquad (i.21)$$

Calculations inspired by collinear factorisation will always have one hardest emission, followed by a second hardest emission, and so forth. The probability of each sequential emission will contain a no-emission piece and a "naive" factor. An algorithm to generate a final state with an arbitrary number of gluons emitted from an initial quark is:

a) Start at the scale $p_{\perp 0}$. Before the first emission, set $p_{\perp 0} = p_{\perp max}$.

b) Choose a $p_\perp < p_{\perp 0}$ and an energy fraction z.

c) Decide if the emission should be generated. If so, construct the emission momentum.

d) Reset the starting scale $p_{\perp 0} \to p_\perp$ and start from *a*).

This algorithm is the foundation of *parton shower* (PS) programs[15].

The emergence of no-emission probabilities in parton showers is highly fortuitous. These all-order expressions are known as *Sudakov form factors* in the context of resummation. When inferred fully *inclusively*, meaning without exploiting any knowledge of additional emissions, the PS can be seen as resummation tool which resums logarithms enhancements $L = \ln\left(p^2_{\perp max}/p^2_{\perp min}\right)$, which are due to undetectable (virtual) emissions, to all perturbative orders. This resummation is formally of leading-logarithmic accuracy, but can contain – depending on the actual implementation – major improvements. Since parton showers offer a description how to construct the momenta after an emission, they can also be used as an approximation of processes with detectable emissions. Used in this *exclusive* mode, the Sudakov form factors provide the

[15] Actual implementations are considerably more complicated. Also, the algorithm is by no means limited to gluon emissions only, but directly applies to as many different splitting processes as desired. A pure QCD parton shower for example should at least contain all splittings in Figure *i*.4 as competing choices.

necessary approximations to virtual corrections to ensure that logarithmic divergences of real emission contributions are correctly cancelled. These cancellations also ensure that the total inclusive cross section after the application of the PS is still given by the "hard" cross section – a property dubbed *unitarity*.

Parton showers are a core component of wider simulation frameworks called "general-purpose Monte Carlo event generators". Event generators aim at describing particle collision events in detail. This task is accomplished by interfacing the parton-showered hard process with methods that

- ◇ Add multiple interactions between the incoming beam particles,
- ◇ Decay unstable particles (e.g. τ-leptons),
- ◇ Convert colour-charged partons into un-coloured hadrons,
- ◇ Decay unstable hadrons (e.g. B-mesons).

The implementation of these tasks varies widely between the most popular projects HERWIG, PYTHIA and SHERPA – as do their PS approaches. The current incarnations (HERWIG++ [5] and PYTHIA8 [6]) of the older projects were recently rewritten in `C++`, while SHERPA [7] has been developed in `C++` from the event generator's conception. A review of the current event generators for LHC physics can be found in [8].

The hard process calculation in event generators has traditionally been limited to $2 \to 2$ scatterings, at leading order in perturbation theory. More complicated calculations require other, more specialised tools called matrix element generators (MEGs)[16]. The virtue of these tools is an accurate description of multi-parton hard processes at a fixed order in perturbation theory without having to resort to collinear (or soft) approximations. State-of-the-art methods can calculate the cross section for up to $\mathcal{O}(10)$ outgoing particles to leading-order (LO) accuracy (i.e. when only keeping real-emission diagrams), or for fewer final state particles to next-to-leading order (NLO) precision (i.e. including both real-emission and virtual corrections).

MEG and PS methods are complementary. The PS is valid close to the boundaries of phase space, meaning for very collinear or soft emissions, but does not yield a satisfactory description of large-$p_\perp$ emissions. MEG calculations give a more accurate description of large-$p_\perp$ configurations, but break down close to the phase space boundaries.

[16] SHERPA has always put strong focus on improving the PS with higher-multiplicity matrix elements. This is achieved by two built-in MEGs, AMEGIC and COMIX.

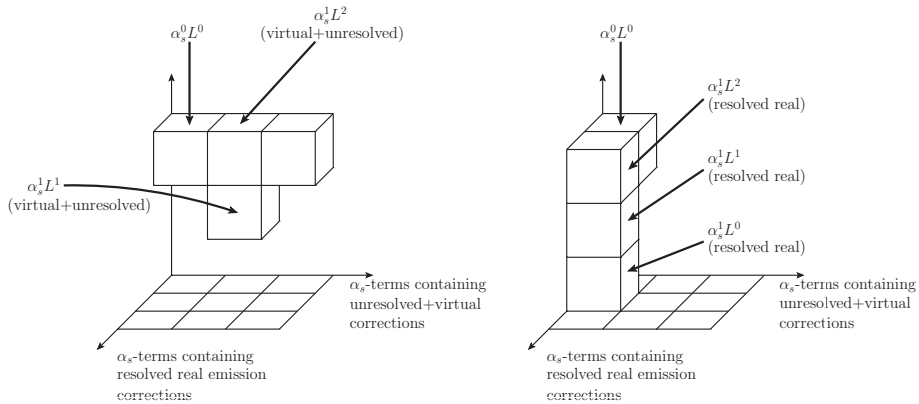

Figure *i*.5: A simplified representation of the accuracy of fixed-order and resummed QCD calculations. We will use the shorthand $L = \ln(\tau)$. Each box represents the correct description of one logarithmic term. The "origin" is in the upper left corner, i.e. attached to the $\alpha_s^0 L^0$-box. The figures represent:
◇ Unresolved emissions + virtual corrections as boxes in rows from left to right,
◇ Resolved emissions as boxes from back to front,
◇ Logarithmic contributions (for a fixed power of α_s) from top to bottom, with the most dominant term on top.

The description of LHC data requires a combination of both approaches.

i.2.4 Combining matrix elements and parton showers

QCD parton showers and matrix elements overlap in addressing the questions how the momenta of states with an intermediate number of final state partons can be simulated, and which (real- and/or virtual) corrections are necessary to describe collider data. When attempting an accurate calculation, we should aspire to combine the virtues of both methods consistently. The following section will consider scattering processes that do not contain final state partons at lowest order in QCD. Also, the lowest-order final state will be kept implicit: when e.g. referring to one-emission states, we will think of a state containing both the lowest-order final state particles and an additional final state parton. Prescriptions to combine matrix elements and parton showers are of course not limited to colour-neutral lowest-order states. Here, this limitation is made for pedagogical reasons only.

Before we discuss possible methods, remember that "accuracy" has different meanings in fixed-order and resummation contexts. To find

a common language for both approaches, let us examine the structure of QCD matrix elements. Fixed-order calculations develop logarithmic divergences when approaching phase space boundaries. There are of course multiple phase space boundaries. The boundary defining soft emissions is for example different (though overlapping) from collinear regions. If we define a boundary by some variable τ approaching zero, we find that a fixed-order calculation at $\mathcal{O}(\alpha_s^n)$ can contains logarithmic divergences proportional to $\alpha_s^n \ln^{2n}(\tau), \alpha_s^n \ln^{2n-1}(\tau), \ldots, \alpha_s^n \ln^1(\tau)$ and regular terms $\alpha_s^n \ln^0(\tau)$. The precision of QCD calculations can then be judged by realising the following:

- ◇ Fixed-order matrix elements contain all logarithmic contributions at one particular order in α_s. Next-to-leading order calculations will for example include $\alpha_s^1 \ln^2(\tau), \alpha_s^1 \ln^1(\tau)$ and $\alpha_s^1 \ln^0(\tau), \alpha_s^0 \ln^0(\tau)$ terms. We will call this precision *fixed-order accuracy*.
- ◇ Resummed calculations include a particular type of logarithmic contributions to all orders in α_s. Leading-logarithmic calculations will for example include $\alpha_s^0 \ln^0(\tau), \alpha_s^1 \ln^2(\tau), \alpha_s^2 \ln^4(\tau), \ldots, \alpha_s^n \ln^{2n}(\tau)$. This precision is called *logarithmic accuracy*.

Fixed order calculations can further be classified into leading-order (or tree-level) calculations (i.e. calculations that do not contain any virtual corrections) and next-to-leading (NLO) calculations (i.e. calculations that contain one-loop virtual corrections). Resummed calculations are called leading-log (LL) accurate if the terms $\alpha_s^n \ln^{2n}(\tau)$ are correctly described, and next-to-leading-log (NLL) if $\alpha_s^n \ln^{2n-1}(\tau)$-terms are also correct.

To discuss fixed-order MEGs and PS resummation on equal footing, we will use the simplified representation defined in Figure *i*.5. Each box represents the correct description of a logarithmic term, and "unfilled" regions represent contributions beyond the formal accuracy of the calculation[17]. Dashed lines are only included to guide the eye when e.g. boxes in the back of the figures are missing.

Figure *i*.6 illustrates a parton shower. If the PS does not generate an additional emission above the lower cut-off $p_{\perp min}$, it supplies a resummation of leading logarithms for the hard process. The PS also includes a LL resummation for states with n emissions. Let the PS for example produce one gluon emission at $p_\perp$ with probability eq. (*i*.21), and then continue the PS from $p_{\perp 1}$ without producing further emissions, i.e. sim-

[17] For a general process, PS resummation is formally only LL accurate. However, it contains many improvements that push the accuracy beyond naive LL calculations.

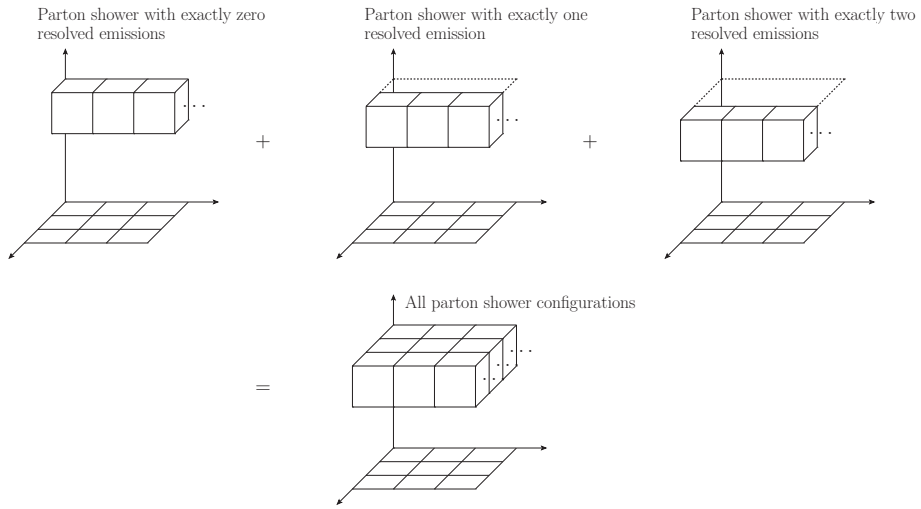

Figure *i*.6: Contributions in a LL parton shower. The "…" indicate that the complete row is correctly included. Resolved here means "above the PS cut-off $p_{\perp min}$". The upper panels shows different PS events. The full PS result consists of the sum of all possible outcomes, i.e. the "layer of boxes" in the lower panel. NLL parton showers would give a second layer of boxes.

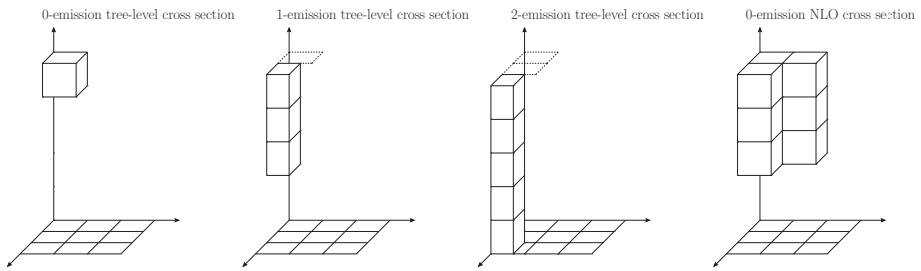

Figure *i*.7: Examples of fixed-order cross sections. Note that the one- and two-jet tree-level samples do not completely fill the box, since such calculations have to be regularised to avoid soft and collinear singularities. This means that a part (the part in the vicinity of the divergence) is missing. In the NLO calculation in the rightmost panel, it is possible to avoid regularisation cuts.

ply multiply the no-emission probability $\Delta(p^2_{\perp 1}, p^2_{\perp min})$. This gives

$$\Delta(p^2_{\perp max}, p^2_{\perp 1}) \frac{\alpha_s}{2\pi} \frac{P_{qq}(z)}{p^2_{\perp 1}} \Delta(p^2_{\perp 1}, p^2_{\perp min}) \,, \tag{i.22}$$

which is a resummed one-emission prediction.

The strength of fixed-order calculations (see e.g. Figure *i*.7) lies in describing the cross section up to a particular order in α_s in detail, including correlations and interference effects. It is highly desirable to absorb these features into event generators. Ideally, we would like to describe the n hardest jets of a multi-parton configuration, where the jets have been defined by some jet algorithm, by the n-parton MEG calculation, dressed in soft and collinear radiation[18]. This cannot be achieved by using the PS in an unconstrained manner, since then, some hard jets after showering could be derived from hard PS emissions. Two ways to avoid this overlap have been proposed:

a) *Multi-jet merging* uses higher-multiplicity matrix elements above above a certain value in some resolution criterion, and parton showers below this value. This procedure can be used for any number of additional partons, since the "resolution-cut" can be defined for arbitrary parton multiplicity. This also means that "inclusive" samples can be constructed, which describe a variable number of hard jets simultaneously.

b) *Matrix element matching* ensures that the lowest-multiplicity states correctly include all fixed-order terms (often including virtual corrections as well), and that all-order terms are included already at the MEG level. The parton shower can then, with appropriate starting conditions, be used to approximate further, softer emissions. This procedure allows to conveniently include NLO corrections into the event generation, but is difficult to generalise to a variable number of emissions.

The most common matrix element matching methods (at NLO accuracy) are MC@NLO [9–12] and POWHEG [13–16]. Both of these are generalisations of the "matrix-element-correction" method [17, 18]. This method uses the full real-emission matrix (instead of the approximate splitting function) as probability to generate the first PS emission, thus leading, apart from a better description of the first emission, to an improved resummation. Though matching methods are very appealing, it is difficult to accommodate a varying number of "hard" jets simultaneously. This is the strength of *multi-jet merging* schemes.

Figure *i*.8 illustrates how multi-jet tree-level merging algorithms change the (pre-calculated) tree-level inputs, which have been regularised by a jet measure cut[19] to remove soft- and collinear divergences

[18] We will ignore the fact that the definition of "hardest" can be a fairly subtle point.

[19] From now on, we will call this regularisation cut *merging scale* or t_{MS}.

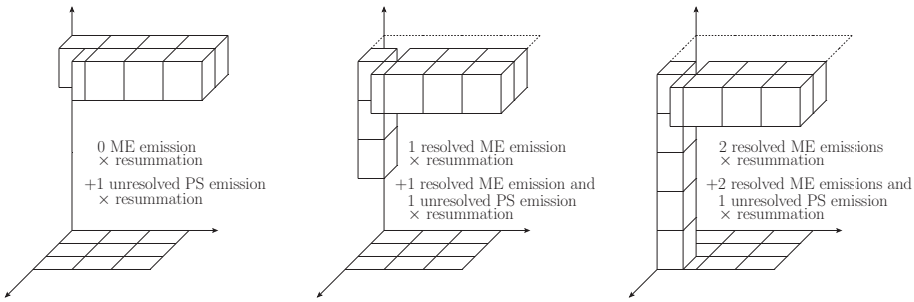

Figure *i*.8: An example of matrix element + parton shower merging. The term "resolved" ("unresolved") refers to a parton with a jet-separation to other partons above (below) the t_{MS} cut. If only the left part of a leftmost box is filled, this indicates that only resolved jets are included. If only the right part of a leftmost box is filled, this indicates that only unresolved jets are included. The leftmost front box in the right panel would be completely filled by the PS if we would only attempt merging with up to two additional jets.

(i.e. the three left panels in Figure *i*.7). This input is processed with the parton shower, by

1. Multiplying the result of parton shower resummation.
2. Disallowing the parton shower to produce "resolved" emissions (i.e. emissions above the merging scale t_{MS}) if tree-level inputs for such configurations are available.
3. Adding the processed inputs to yield the multi-jet merged result.

After applying, for example, the first two steps on the zero-jet input (Figure *i*.8, left panel), we are left with a sample that exactly fills the holes (due to the merging scale cut) in the one-jet input (Figure *i*.8, central panel). Add the left and central panels, we find

$$
\begin{aligned}
&\text{States with 0 emissions} \times \text{resummation} \\
&\quad + \text{States with 1 PS emission below } t_{\text{MS}} \text{ only} \times \text{resummation}' \\
&\quad + \text{States with 1 ME emission above } t_{\text{MS}} \text{ only} \times \text{resummation}'' \\
&\quad + \text{States with 1 ME emission above } t_{\text{MS}} \textit{ and } \text{1 PS emission below } t_{\text{MS}} \times \text{resummation}''' \,,
\end{aligned}
$$

where the first and second (third and fourth) lines correspond to the left (central) panel in Figure *i*.8, and primes indicate that, depending on the input sample, the factors multiplied by resummation may differ. Only if the resummation factors included by adding a PS emission to the zero-jet input are identical to the ones produced by the reweighting of the

one-jet input does this lead to

$$\begin{aligned}
&\text{States with 0 emissions} \times \text{resummation} \\
&+ \left[\text{States with 1 PS emission below } t_{\text{MS}} \text{ only} + \text{States with 1 ME emission above } t_{\text{MS}} \text{ only} \right] \\
&\qquad \times \text{resummation}' \\
&+ \quad \text{States with 1 ME emission above } t_{\text{MS}} \textit{ and } \text{1 PS emission below } t_{\text{MS}} \times \text{resummation}''' \,.
\end{aligned}$$

This is a non-trivial demand on the multi-jet merging scheme. In Figure *i*.8, we also see that the PS only describes the LL terms of the unresolved emission. Thus, the sum [States with 1 PS emission below t_{MS} only + States with 1 ME emission above t_{MS} only] depends on the merging scale t_{MS} through terms beyond LL, i.e. the lowest and second-lowest boxes in the central panel. Modern PS resummation actually contains many improvements beyond LL accuracy, which somewhat ameliorate the merging scale dependence.

The goal of multi-jet merging schemes must be to precisely reproduce the PS resummation that is to multiply the tree-level input, and to ensure that the t_{MS} dependence cancels to a large extent. This requires a thorough understanding of the details of the event generator that we wish to improve. Also, some choices in multi-jet merging schemes are not restricted by formal accuracy arguments. In the next section, we would like to give a short summary of the publications contributing to this doctoral thesis, which are centred around multi-jet merging schemes in the PYTHIA8 event generator.

i.3 The papers

This section is intended to give brief summaries of the publications accounting for the major part of this doctoral thesis. All the articles published during the course of four years of Ph.D. studies are concerned with improving the precision of event generators (in particular the PYTHIA8 program) by including multi-jet fixed-order matrix element information.

i.3.1 Paper I

The goal of Paper I was a flexible implementation of the Catani Kuhn Krauss Webber - Lönnblad (CKKW-L) multi-jet merging method [19–22] in the PYTHIA8 event generator. The CKKW-L merging scheme aims at describing the first n hardest jets (in the $p_\perp$-definition used as evolution variable in PYTHIA8), which are also above a merging scale cut t_{MS} (defined in another jet algorithm), with n-parton tree level matrix elements. The CKKW-L prescription is very close to the one discussed in the last section:

- ◇ Pre-calculate MEG input, with jets above t_{MS}, in the form of event files.
- ◇ For each event, construct all PS histories, choose one, reweight the event with no-emission probabilities, PDF- and α_s-ratios.
- ◇ Veto any event in which the first PS emission would be above the t_{MS}, if MEG input for the resulting configuration were available.

Though the CKKW-L prescription is hardly new, its implementation in PYTHIA8 required a through understanding of numerous details. The construction of all possible histories was e.g. more involved in PYTHIA8, compared to previous work in ARIADNE, because splittings of dipole ends rather than dipoles are book-kept.

Another important step was to understand the impact of PYTHIA8's interleaved multiparton interactions (MPI). In particular, our method ensures that "hard" MPI are not artificially suppressed. This means our method should not (drastically) invalidate previous MPI tuning efforts. Furthermore, we investigated different prescriptions to choose a PS history, and discussed the impact of states that only yield $p_\perp$-unordered splitting sequences. Constraining the phase space of PS emissions by enforcing rapidity ordering can have a visible impact on merging uncertainties, because the a limitation to a smaller phase space volume

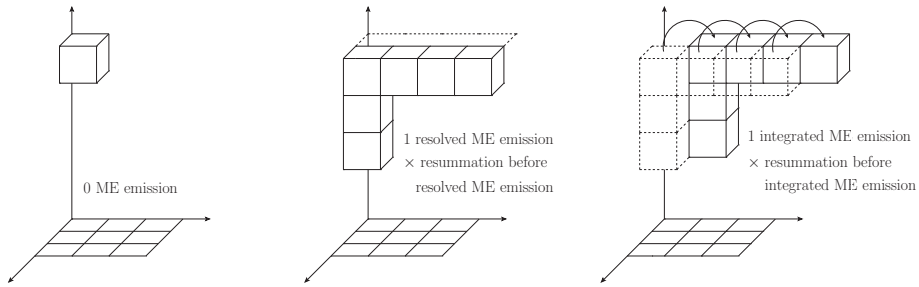

Figure *i*.9: Illustration UMEPS merging, with merging scale at the PS cut-off, for one additional jet. The term "resolved emission" refers to a parton above the PS cut-off. The arrows in the right panel indicate that the emission in the one-emission states is integrated out, and used to construct the resummation in the zero-jet state. The right panel enters with a negative sign into the cross section, while the central and left panels enter with positive sign. In the inclusive cross section, the central and right panels cancel exactly.

degrades the PS approximation. A reduced PS accuracy leads to more pronounced uncertainties.

The implementation was applied to $e^+e^- \to$ jets at LEP, vector boson + jets at the Tevatron and LHC, di-boson production with hadronic Z-decay and QCD di-jet production at the Tevatron. The effect of CKKW-L merging on multi-jet observables is significant and leads to a better description of collider data.

i.3.2 Paper II

Paper II tries to tackle the problem of merging scale dependence of the inclusive cross section in the CKKW-L method, without having to resort to higher-accuracy resummation. The resulting new method is dubbed unitarised matrix element + parton shower (UMEPS) merging.

The main idea of the UMEPS method is to discard the simple, additive, prescription of combining tree-level input in CKKW-L. Instead, an add-and-subtract scheme is put forward. This scheme is derived from PS unitarity, which at its core means that the probability of no emission is defined as unity minus the integral of the emission probability (eq. (*i*.18)). The emission probability in turn contains a no-emission probability, multiplying the "full" fixed-order result. We can, for states with resolved jets in the matrix element, construct the reweighting with no-emission probabilities, PDF- and α_s-ratios. Then, we include the

MEG input state with an additive sign, but also explicitly perform the integration, and subtract the integrated, reweighted state from lower-multiplicity results. This method is illustrated in Figure *i*.9. In this way, we explicitly construct a unitary method, i.e. the lowest-multiplicity cross section is conserved.

An interesting issue in the UMEPS method is the treatment of integrated states that do not have the right number of resolved partons. We choose to perform integrations until a valid state is reached. This then includes merging-scale-unordered contributions into the resummation in lower-multiplicity configurations. We think that this is reasonable, since it might allow to correctly include enhancements that are not governed by $t_{\text{MS}} \to 0$.

We have applied the method to W-boson + jet and QCD di-jet production at the LHC. We find that the t_{MS}-dependence is reduced, and that the inclusive cross section is stable even for very small merging scale values. This leads us to prefer UMEPS over CKKW-L.

i.3.3 Paper III

Paper III is concerned with extending the tree-level merging methods developed in Papers I and II to next-to-leading order accuracy. These generalisations lead to two different algorithms – the Nils Lavesson + Leif Lönnblad (NL^3) method to extend CKKW-L, and the unitarised NLO + parton shower (UNLOPS) merging scheme improving UMEPS.

Moving to NLO accuracy leads to some complications, because the PS already contains approximate virtual corrections, which need to removed and replaced by the corresponding terms of the full NLO calculation. To understand which terms exactly have to be removed from the PS resummation, a good understanding of the NLO inputs is necessary. We choose to work with "exclusive" NLO cross sections, i.e. NLO cross sections that do not contain resolved real-emission contributions. Resolved in this context means that we restrict the real emission to from an underlying n-parton Born configuration to not lead to $n+1$ partons above the merging scale t_{MS}.

The NL^3 scheme presented in this article is based on [23]. The major difficulty in applying NL^3 lies in generating the PS approximation of virtual corrections in the presence of reweighting with PDF-ratios.

The UNLOPS method uses most of the NL^3-code to generate $\mathcal{O}(\alpha_s)$-terms. However, in order to conserve the inclusive cross section, we again apply the add-and-subtract scheme of UMEPS, this time also considering NLO cross sections containing additional jets.

NLO cross sections are taken from the POWHEG-BOX program, and shaped into exclusive cross sections in two ways: Either by explicit phase space subtraction or by modifying the POWHEG-BOX program. The differences between these choices are found to be non-vanishing because of different phase space mappings. To assess the uncertainties of the NLO merging methods, we choose the "explicit subtraction" prescription and apply the methods to W- and Higgs-boson + jets at the LHC. NL^3 and UNLOPS lead to extremely similar results for W-boson + jets, with the uncertainties in both schemes well under control. In Higgs-boson + jets however, we find that a formally allowed rescaling of higher orders produces large renormalisation and factorisation scale uncertainties, and leads to significant changes in the NL^3 inclusive cross section. UNLOPS is reasonably well-behaved for Higgs-boson + jets. This instills confidence that the UNLOPS method is worth pursuing in the future.

i.3.4 List of contributions

- **Paper I:** The ideas in this publication were developed by Leif Lönnblad. My contribution to this paper was the implementation of the method, the production of results and plots. The major part of the article was written by Leif Lönnblad, with me contributing the sections 4.2, 4.3, 5 and appendix A.
- **Paper II:** The ideas in this paper are a collaborative effort of Leif Lönnblad and me. However, the most useful ideas came from Leif Lönnblad. I have further contributed the implementation and the results, and have written most of the publication.
- **Paper III:** The initial idea for NL^3 merging came from Leif Lönnblad. The actual incarnation of the method presented then formed in a collaborative process. The UNLOPS method was a joined project from the start. I have implemented the method and produced results, and have written the major part of the article.

Acknowledgments

I feel privileged to have been given the opportunity to experience Lund. Before I moved to Lund, I visited the Theoretical Physics department for a few days, and decided to study in Lund based on the people I met – I was not disappointed in the slightest.

First and foremost I would like to thank Leif Lönnblad, my supervisor. Leif has always supported me throughout these years, accepted my (irritating) quirks, and taught me a great deal – about physics, computers, and (though it sounds cheesy) life in general. Thank you for being my friend, and for this four-year road trip.

Torbjörn Sjöstrand has been an inspiration and an incessant source of advise, and I would like to express my most heartfelt thanks for all his help. You have taught me that the mind should think subtle thoughts, and that the first rule of science is "know your question". Though so far, I have failed to learn these lessons, I thank you for for pushing me when I needed pushing, and for not giving on me yet.

I would also like to thank Peter Skands, who has supervised my MCnet studentship at CERN, and helped me stay even after its end. I have immensely enjoyed my stay in Geneva, and am very grateful to have had the opportunity to collaborate with Peter.

I like to also express my warmest gratitude to the proof-readers: Leif Lönnblad, Torbjörn Sjöstrand, Johan Bijnens, Christina Isaxon, Christian Bierlich and Jesper Roy Christiansen. Thank you for scrutinising my introduction, and for giving highly useful feedback[20].

Furthermore, I would like to express my sincerest thanks to the whole Theoretical physics group for making the Department my home for four years. Thank you, and be happy that I do not own a comfortable sleeping pad.

Thanks to all my friends, old and new, meaning the people I've continuously neglected, and been rude to, and which still seem to tolerate me. Being an emotionally disabled person, I hope you'll forgive me if I do not list names here, but just say (in my finest Michael Jackson voice) that I lov… sorry, have to go now.

Most importantly, thanks to my family. I love you.

[20] I will use fewer footnotes from now on.

i References

[1] P. Dirac, "The Principles of Quantum Mechanics, Fourth Edition," *International Series of Monographs on Physics* (1958) .

[2] **Particle Data Group** Collaboration, J. Beringer *et al.*, "Review of Particle Physics (RPP)," *Phys.Rev.* **D86** (2012) 010001.

[3] M. Bohm, A. Denner, and H. Joos, "Gauge theories of the strong and electroweak interaction, Third edition," *B. G. Teubner* (2001) .

[4] T. Kinoshita, "Mass singularities of Feynman amplitudes," *J.Math.Phys.* **3** (1962) 650–677 *and* T. Lee and M. Nauenberg, "Degenerate Systems and Mass Singularities," *Phys.Rev.* **133** (1964) B1549–B1562.

[5] M. Bahr, S. Gieseke, M. Gigg, D. Grellscheid, K. Hamilton, *et al.*, "Herwig++ Physics and Manual," *Eur.Phys.J.* **C58** (2008) 639–707, arXiv:0803.0883 [hep-ph].

[6] T. Sjöstrand, S. Mrenna, and P. Skands, "A Brief Introduction to PYTHIA 8.1," *Comput. Phys. Commun.* **178** (2008) 852–867, arXiv:0710.3820 [hep-ph].

[7] T. Gleisberg *et al.*, "Event generation with SHERPA 1.1," *JHEP* **02** (2009) 007, arXiv:0811.4622 [hep-ph].

[8] A. Buckley, J. Butterworth, S. Gieseke, D. Grellscheid, S. Hoche, *et al.*, "General-purpose event generators for LHC physics," *Phys.Rept.* **504** (2011) 145–233, arXiv:1101.2599 [hep-ph].

[9] S. Frixione and B. R. Webber, "Matching NLO QCD computations and parton shower simulations," *JHEP* **06** (2002) 029, arXiv:hep-ph/0204244.

[10] S. Höche, F. Krauss, M. Schönherr, and F. Siegert, "A critical appraisal of NLO+PS matching methods," *JHEP* **1209** (2012) 049, arXiv:1111.1220 [hep-ph].

[11] S. Höche, F. Krauss, M. Schönherr, and F. Siegert, "W+n-jet predictions with MC@NLO in Sherpa," *Physical Review Letters* (2012) , arXiv:1201.5882 [hep-ph].

[12] V. Hirschi, R. Frederix, S. Frixione, M. V. Garzelli, F. Maltoni, *et al.*, "Automation of one-loop QCD corrections," *JHEP* **1105** (2011) 044, arXiv:1103.0621 [hep-ph].

[13] P. Nason, "A new method for combining NLO QCD with shower Monte Carlo algorithms," *JHEP* **11** (2004) 040, arXiv:hep-ph/0409146.

[14] S. Frixione, P. Nason, and C. Oleari, "Matching NLO QCD computations with Parton Shower simulations: the POWHEG method," *JHEP* **11** (2007) 070, arXiv:0709.2092 [hep-ph].

[15] S. Alioli, P. Nason, C. Oleari, and E. Re, "A general framework for implementing NLO calculations in shower Monte Carlo programs: the POWHEG BOX," *JHEP* **1006** (2010) 043, arXiv:1002.2581 [hep-ph].

[16] S. Platzer and S. Gieseke, "Dipole Showers and Automated NLO Matching in Herwig++," *Eur.Phys.J.* **C72** (2012) 2187, arXiv:1109.6256 [hep-ph].

[17] M. Bengtsson and T. Sjostrand, "A Comparative Study of Coherent and Noncoherent Parton Shower Evolution," *Nucl.Phys.* **B289** (1987) 810.

[18] M. Bengtsson and T. Sjostrand, "Coherent Parton Showers Versus Matrix Elements: Implications of PETRA - PEP Data," *Phys.Lett.* **B185** (1987) 435.

[19] S. Catani, F. Krauss, R. Kuhn, and B. R. Webber, "QCD matrix elements + parton showers," *JHEP* **11** (2001) 063, arXiv:hep-ph/0109231.

[20] L. Lönnblad, "Correcting the colour-dipole cascade model with fixed order matrix elements," *JHEP* **05** (2002) 046, arXiv:hep-ph/0112284.

[21] N. Lavesson and L. Lönnblad, "W + jets matrix elements and the dipole cascade," *JHEP* **07** (2005) 054, arXiv:hep-ph/0503293.

[22] S. Höche, F. Krauss, S. Schumann, and F. Siegert, "QCD matrix elements and truncated showers," *JHEP* **05** (2009) 053, arXiv:0903.1219 [hep-ph].

[23] N. Lavesson and L. Lönnblad, "Extending CKKW-merging to One-Loop Matrix Elements," *JHEP* **12** (2008) 070, arXiv:0811.2912 [hep-ph].

I

Matching Tree-Level Matrix Elements with Interleaved Showers

Leif Lönnblad and Stefan Prestel
Dept. of Astronomy and Theoretical Physics, Lund University, Sweden,
and
CERN Theory Division, Geneva, Switzerland
Journal of High Energy Physics **1203** (2012) 019 [hep-ph/1109.4829].

We present an implementation of the so-called CKKW-L merging scheme for combining multi-jet tree-level matrix elements with parton showers. The implementation uses the transverse-momentum-ordered shower with interleaved multiple interactions as implemented in PYTHIA8. We validate our procedure using e^+e^--annihilation into jets and vector boson production in hadronic collisions, with special attention to details in the algorithm which are formally sub-leading in character, but may have visible effects in some observables.

We find substantial merging scale dependencies induced by the enforced rapidity ordering in the default PYTHIA8 shower. If this rapidity ordering is removed the merging scale dependence is almost negligible. We then also find that the shower does a surprisingly good job of describing the hardness of multi-jet events, as long as the hardest couple of jets are given by the matrix elements.

The effects of using interleaved multiple interactions as compared to more simplistic ways of adding underlying-event effects in vector boson production are shown to be negligible except in a few sensitive observables.

To illustrate the generality of our implementation, we also give some example results from di-boson production and pure QCD jet production in hadronic collisions.

I.1 Introduction

Production rates for multi-jet events at the LHC are very large, and the understanding of such events is important, not least as most discovery channels for new physics involve jets. The main irreducible, and often huge, background for such signals comes from QCD processes. To distill a signal one therefore needs to make complicated cuts to decrease the QCD background, sometimes by several orders of magnitude. For this it is very important that we have a good understanding, not only of the average behaviour of multi-jet processes, but also the fluctuations and very rare events coming from standard QCD.

The state-of-the-art for simulating multi-jet final states with Monte Carlo event generators is to use CKKW-based algorithms to combine exact tree-level matrix elements (ME) with parton showers (PS) in a consistent way. Here, the matrix elements describe accurately the production of several hard, well-separated partons, while the parton shower encodes how these are evolved into partonic jets by accurately modelling the soft and collinear partonic emissions, in a way such that standard hadronisation models can be applied to produce realistic exclusive hadronic multi-jet final states.

However, CKKW merging algorithms mainly focus on the jets produced in the primary interaction, and little attention is normally given to jets which may arise from rare, but hard fluctuations in the underlying events. If at all, the underlying-event contribution is typically added to the merged sample assuming that the additional scatterings are completely independent of the primary interaction. This may be a good approximation in most cases, but it is clear that there are correlations between the primary interaction and the underlying event, which we think are important to investigate carefully.

The multiple interaction model in PYTHIA8 is arguably the most advanced model for the underlying event today. It contains several sources of correlations between the primary interaction and the underlying event. In particular, the model for multiple scatterings is tightly tied to the parton shower in that additional scatterings are *interleaved* with the parton evolution.

In this paper we implement the CKKW-L algorithm for merging parton showers with tree-level matrix elements in PYTHIA8, and in doing so we consider possible effects of the fact that the PYTHIA8 shower is interleaved with multiple interactions. Although the effects turn out to be small, we note that there may be more sources of correlations which

are currently not taken into account by PYTHIA8, and our scheme is a way to automatically take into account any such correlations also in the merging with tree-level matrix elements.

It should be noted that this is not the first implementation of matrix-element merging with the PYTHIA shower. Interfaces exists for the FORTRAN version of PYTHIA to the ALPGEN [1] program by employing the MLM matching prescription [2], and to MADGRAPH/ MADEVENT [3] using so-called Pseudo-Shower merging [4].

The outline of this article is as follows. First in sections I.2 and I.3 we briefly recapitulate the main features of the CKKW-L merging scheme and the interleaved showers respectively, before we describe the details of our PYTHIA8 implementation in section I.4. Then we present results in section I.5, starting with some control plots to validate the implementation before we study the effects of multiple interactions and other formally sub-leading features on the production of vector bosons with additional jets at the LHC. We end with showing some comparisons with data, and some preliminary results also from di-boson and pure QCD jet production. Finally we present our conclusions in section I.6.

I.2 The CKKW-L merging scheme

Here we will present the main features of the CKKW-L merging procedure. For a more detailed discussion of CKKW-L and other similar merging algorithms we refer to [5,6] and the original publications [7,8].

The starting point for CKKW-L is that we have a tree-level matrix-element generator capable of generating the Born-level process of interest, as well as the same process with up to N additional partons. The matrix elements used are regularised with a jet cutoff which we refer to as the merging scale, t_{MS}. To the states generated in this way we want to add a parton shower to *dress up* the hard partons with emissions below the merging scale in a way such that the soft and collinear emissions are properly modelled.

As the matrix elements are inclusive, in that they give the cross section for states with *at least n* additional partons resolved above the merging scale, it is obvious that we cannot simply add the event samples generated with different parton multiplicities. Instead we want to make the samples exclusive by reweighting them with Sudakov form factors taken to be the no-emission probabilities the parton shower would have used to produce the same partonic states.

To calculate the form factor we first have to reconstruct a parton-

shower history for the states with n additional partons, S_{+n}, given by the matrix element generator. This means that we have to answer the question, *how would my parton shower have generated this state?* The answer to this question is not necessarily unique. The parton shower may produce a given final parton state in several ways, just as a given state may be represented by many different Feynman diagrams. In CKKW-L, these different path are considered by reconstructing all possible parton shower histories, and picking one of them according to probabilities calculated from the relevant splitting functions.

Doing this, we arrive at a history, in which a sequence of parton shower emissions are specified by the ordering scale of each emission ρ_i and other splitting variables such as the energy fractions, and azimuthal angles, denoted by z_i. We also obtain a sequence of intermediate parton states, S_{+i}. The requirement on the parton shower is therefore that it must have complete on-shell intermediate parton states between each splitting. Until fairly recently this was only true for the ARIADNE program [9], which also was the first to use the CKKW-L merging [8].

Let us denote Sudakov form factors by

$$\Delta_{S_i}(\rho_i, \rho_{i+1}) = \exp\left[-\int_{\rho_{i+1}}^{\rho_i} d\rho \int dz \alpha_s(\rho) P_i(\rho, z)\right] . \tag{I.1}$$

This is the probability that there are no parton shower emissions from the state S_{+i} between the scales ρ_i, and ρ_{i+1}. The reweighting with Sudakov form factors now proceeds by starting the parton shower at a given intermediate state S_{+i}, setting ρ_i as the maximum scale, and generating one emission (ρ, z). The probability that this emission is above ρ_{i+1} is exactly $1 - \Delta_{S_i}(\rho_i, \rho_{i+1})$, so throwing away the event if the emission is above ρ_{i+1} is equivalent to reweighting with the Sudakov form factor.

A special treatment is called for in the Sudakov between the last emission scale, ρ_n, and the merging scale, in the case the cutoff in the matrix elements is not defined in terms of the parton shower ordering variable. In the case of $n < N$, the event is rejected if the trial emission from the state S_{+n} is above the matrix element cut-off, irrespective of how it is defined. In the case of $n = N$, however, no Sudakov-reweighting is done.

The n-parton state is typically generated using matrix elements with a fixed $\alpha_s(\mu)$, so that we also reweight the event with

$$\prod_{i=1}^{n} \frac{\alpha_s(\rho_i)}{\alpha_s(\mu)} \tag{I.2}$$

to obtain the same running of α_s as in the shower.

Finally, note that for initial-state parton-shower splittings, the no-emission probability $\Pi$is not the same as the Sudakov form factor needed to reweight the matrix-element generated state. Instead we have [10, 11],

$$\Delta_{S_i}(\rho_i, \rho_{i+1}) = \frac{f(x, \rho_i)}{f(x, \rho_{i+1})} \times \Pi_{S_{+i}}(\rho_i, \rho_{i+1}), \tag{I.3}$$

and the corresponding ratios of parton density functions are included as an additional weight.

We have thus constructed exclusive final states with an arbitrary number of partons resolved above the parton shower cutoff scale ρ_c. The distribution of these states are resummed to all orders in α_s, according the precision of the parton shower. However, the $n \leq N$ emissions which are considered hardest in the parton-shower sense, and are above the merging scale as well, will have their splitting functions corrected to reproduce the correct tree-level matrix element.

It should be noted that if the merging scale is defined in the same way as the parton shower evolution scale, the CKKW-L is equivalent to standard CKKW, as long as the latter is used with a shower which is properly vetoed and truncated [12]. In Appendix I.A we elaborate on how the logarithmic accuracy of the shower is preserved in CKKW-L and compare with the case of standard CKKW using truncated showers.

I.3 Interleaved showers

As mentioned in the previous section, the requirement on a parton shower to be used in the CKKW-L procedure is that it gives complete on-shell partonic states between each emission. In this respect, the transverse-momentum ordered shower in PYTHIA8 [13] is perfectly suited. However, it is not completely straight forward to implement CKKW-L with PYTHIA8, as the parton shower in the case of hadron collisions is *interleaved* with multiple interactions.

The philosophy behind the interleaved shower is that processes with a high scale in some sense happen *before* processes at lower scales. As the emissions in a parton shower are not completely independent in that every emission will give rise to recoils and will carry away some energy and momentum, it is important that the emissions are performed in the right order. It is, for example, not reasonable that an emission of a gluon with small transverse momentum removes so much energy as to

make an emission with a higher transverse momentum impossible. The argument is based on formation times — a final state parton with large transverse momentum is to some extend formed long before one with small transverse momentum.

If we consider standard QCD jet production in proton collisions, a parton shower is typically initiated by a hard $2 \to 2$ matrix element at some transverse momentum. The parton shower then evolves these hard jets by emitting final-state radiation from the outgoing partons and initial-state radiation from the incoming partons. This is done iteratively, ordering the emissions in transverse momentum.

There is also a chance for a second (semi-)hard interaction between the colliding protons. Also, one of the outgoing partons from the hard interaction can rescatter with one of the spectator partons in one of the colliding protons, and in addition, outgoing partons are allowed to rescatter among themselves. In PYTHIA8 such scatterings are included in the shower procedure such that an additional scattering at a scale ρ_{MI} will happen before e.g. an initial-state splitting at a scale, $\rho_{\mathrm{i}} < \rho_{\mathrm{MI}}$.

This means that the no-emission probabilities are modified in PYTHIA8, and now consist of several pieces,

$$\Pi_{S_{+i}}(\rho_i, \rho) = \Pi^{\mathrm{PS}}_{S_{+i}}(\rho_i, \rho)\Pi^{\mathrm{MI}}_{S_{+i}}(\rho_i, \rho)\Pi^{\mathrm{RS}}_{S_{+i}}(\rho_i, \rho), \tag{I.4}$$

where the superscript refers to the standard parton shower (PS), multiple interactions (MI) and rescattering (RS). If we have resolved a state S_{+i} at a scale ρ_i, the probability for a change of type a at scale ρ is

$$\mathcal{P}^a(\rho) = P^a(\rho) \times \Delta^{\mathrm{PS}}_{S_i}(\rho_i, \rho)\Delta^{\mathrm{MI}}_{S_i}(\rho_i, \rho)\Delta^{\mathrm{RS}}_{S_i}(\rho_i, \rho), \tag{I.5}$$

where P^a is the inclusive probability.

PYTHIA8 uses an interleaved treatment of spacelike (initial-state radiation — ISR) and timelike showers (final-state radiation — FSR), so that the no-emission probability $\Pi^{\mathrm{PS}}_{S_{+i}}$ is further subdivided as

$$\Pi^{\mathrm{PS}}_{S_{+i}}(\rho_i, \rho) = \Pi^{\mathrm{ISR}}_{S_{+i}}(\rho_i, \rho)\Pi^{\mathrm{FSR}}_{S_{+i}}(\rho_i, \rho). \tag{I.6}$$

The ordering scale, ρ, is defined in different ways for different processes, but they all correspond to a relative transverse momentum of emitted partons. For ISR the scale is

$$\rho^{\mathrm{ISR}} = (1 - z)\, Q^2, \tag{I.7}$$

where $-Q^2$ is the virtuality of the incoming original parton and z is its momentum fraction, and for FSR we have

$$\rho^{\mathrm{FSR}} = z(1 - z)\, Q^2\,, \tag{I.8}$$

where Q^2 is the invariant mass of the radiating parton, and z the energy fraction (in the dipole rest frame) of the emitted parton. For MI and RS the scale is simply given by the squared transverse momentum of the emitted partons.

The full interleaving of all shower components makes PYTHIA8 ideal for our prescription of matrix element merging, since the full no-emission probability can, as will be explained below, easily be generated in only one step.

I.4 Implementation in PYTHIA8

Due to the requirement of fully on-shell intermediate states, CKKW-L merging has so far only been implemented in the ARIADNE shower. Here, we present a new implementation within PYTHIA8, which is conceptually equivalent to the former, but differs in details relating to the differences in the parton showers.

I.4.1 Constructing the parton shower history

A key concept of the merging algorithm is the assignment of a shower history — a sequence of shower states and evolution scales — to each n-particle configuration supplied by the matrix element generator. In the CKKW-L approach, this is done by constructing every possible path from a core Born-level process to the current n-particle state.

Here we encounter the first difference between ARIADNE and PYTHIA8. The first gluon emission is particularly simple in e^+e^- in ARIADNE, where the evolution variable and the splitting kernel for the first splitting are symmetrical between both outgoing legs, thus resulting in only one possible path: One dipole splitting into two dipoles. In PYTHIA8, the approach is slightly different. Also here a dipole-like approach is used, but the emission is explicitly divided up into two contributions stemming from each of the dipole ends, where the radiation close to one end of the dipole is considered more likely to come from this dipole end itself. Different splitting probabilities for either dipole end will thus result in two different ways in which PYTHIA8 could have arrived at the $+1$-parton state. In general there are more possible paths in PYTHIA8 than in ARIADNE. We therefore try to investigate in some detail the effects of different ways of choosing a path.

What we basically want to do is to reconstruct which Feynman diagram gives the largest contribution to the state produced by the matrix

element generator. The preferred option would be to ask the matrix element generator itself, but this information is not always easily accessible. Even if such details were available, it is not always enough, as a given Feynman diagram may also correspond to different parton shower histories. As is discussed in Appendix I.B, we approach this issue by constructing all possible path of collinear splittings, and pick a path according to the product of splitting probabilities. For the hardest emission, the splitting probability is supplemented so that the matrix element transition probability is assured. More precisely, we choose a path according to the probability

$$w_p \;=\; \frac{w_{1p}(z_{1p})\prod_{i=2}^{n}\frac{P_{ip}(z_{ip})}{\rho_{ip}}}{\sum_r w_{1r}(z_{1r})\prod_{i=2}^{n}\frac{P_{ir}(z_{ir})}{\rho_{ir}}} \qquad \text{where} \tag{I.9}$$

P_{ip} : Splitting kernel for splitting number i in path number p,

ρ_{ip} : Evolution scale of splitting number i in path number p,

z_{ip} : Energy fraction carried by the parton emitted in splitting number i in path number p,

w_{1p} : Improved splitting probability for hardest splitting, including weights of ME corrections in the shower.

The precise forms of these terms are derived in Appendix I.B, where we also elaborate on how the intermediate states S_{+i} in path p are constructed.

It must be noted that in the limit of strong ordering, which is the relevant limit when looking at the formal logarithmic accuracy of the procedure, picking the most likely path is trivial. Hence, the way a path is selected will only give sub-leading effects on any observable. We will nevertheless investigate how large these effects are by implementing two different schemes. One is similar to the original ARIADNE-implementation, and is based on eq. (I.9). The other is inspired by the CKKW-implementation in HERWIG++ [14], where the path which has the smallest sum of transverse momenta in the splittings is chosen exclusively. Clearly, in the strongly ordered limit, both of these will find the "right" path, but as we will see in section I.5, there are visible differences.

For higher jet multiplicities, minor complications of the path concept arise. First, we know that shower emissions are always ordered in some scale variable ρ (virtuality, angle, transverse momentum). This is not

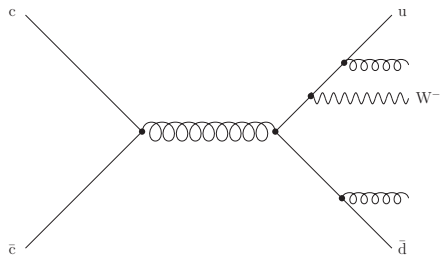

Figure I.1: An example of a matrix element contribution without a complete shower history. In this case, only the two gluon emission can be reclustered, $c\bar{c} \to u\bar{d}W^-$ is regarded a separate hard process.

always true for consecutive clusterings of jets from a matrix element. We choose to interpret a sequence of such unordered splittings as a single step in the algorithm such that all steps will be ordered. We must then decide which scale to use for this combined emission step. Assume that we have a sequence of reconstructed scales given by $\rho_1 > \rho_3 > \rho_2 > \rho_4$. The combined emission then corresponds to ρ_2 and ρ_3 and we can generate the total no-emission probability as

$$\Pi_{S_+}(\rho_0, \rho_4) = \Pi_{S_{+0}}(\rho_0, \rho_1)\Pi_{S_{+1}}(\rho_1, \rho_3)\Pi_{S_{+3}}(\rho_3, \rho_4) \tag{I.10}$$

or

$$\Pi_{S_+}(\rho_0, \rho_4) = \Pi_{S_{+0}}(\rho_0, \rho_1)\Pi_{S_{+1}}(\rho_1, \rho_2)\Pi_{S_{+3}}(\rho_2, \rho_4)\,. \tag{I.11}$$

In the former case, the no-emission probability between the scales ρ_3 and ρ_2 is calculated using the 1-parton state, while in the latter, the 3-parton state is used. We will investigate the difference between using the higher (ρ_3) or lower scale (ρ_2) as minimal scale for rejecting trial emissions off the 1-parton state in section I.5.1.

Some rare matrix element configurations, e.g. massive electroweak corrections to an underlying QCD process, as shown in Figure I.1, could never have been produced in the shower algorithm. For such processes, clustering will be attempted as far as possible. The last, irreducible, state will be treated as a new hard process, and be assigned a shower starting scale in the same way PYTHIA8 normally would have assigned a scale when presented with such processes. When handling externally generated processes, PYTHIA8 would by default start the evolution at the factorisation scale defined in the matrix element evaluation. However, different user choices are allowed. In section I.5.1, we will also investigate the effects of other scale choices.

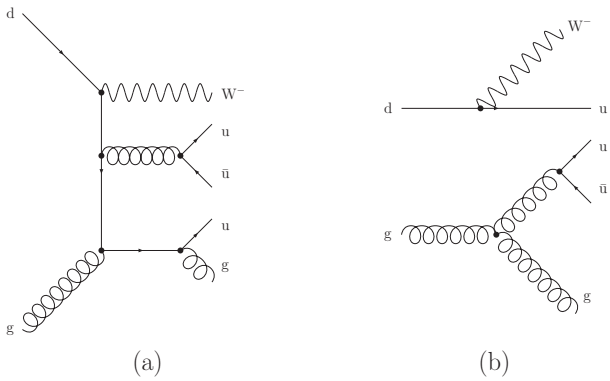

Figure I.2: An example of two different ways the iterative clustering may interpret of a particular colour configuration in a $dg \to W^- u\bar{u}ug$ process. Since (b) has disconnected external particles, no valid shower history can be found.

On a more technical note, we disallow clusterings that will result in a unreasonable Born-level process. An example would involve starting from the configuration shown in Figure I.2 (a). From only recombining colour and flavour, alternative (b) would be identical, and, albeit being disconnected, allowed. The interpretation of the configuration as either (a) or (b) is tied to which $u\bar{u}$ pair is clustered to a gluon. Since we will always be able to find sensible paths like (a), impossible paths (b) leading to disconnected diagrams will be discarded.

In other merging prescriptions, these problems are addressed with other strategies. In HERWIG++ [14], the authors found that results where insensitive to the treatment of unordered or incomplete paths and chose to retain incomplete contributions. SHERPA [15] follows a different approach in that no incomplete histories are constructed, since if necessary, electroweak bosons will be clustered as well. This would interpret the diagram in Figure I.1 as an electro–weak matrix element correction to di-jet production.

I.4.2 Interleaved multiple interactions

At the LHC, events with only one parton–parton scattering per collision are highly improbable, and a lot of effort has gone in to the modelling of multiple scatterings in PYTHIA8. When merging the PYTHIA8 shower with matrix elements, it is therefore desirable to keep the modelling of multiple scatterings as intact as possible.

In PYTHIA8, multiple interactions and radiation compete for the

available phase space. To make sure that some part of phase space is exclusively filled by matrix element configurations, another part by shower radiation and multiple interactions, we minimally modify the CKKW-L algorithm. The generation of no-emission probabilities has to be slightly refined to keep the effect of multiple interactions on the no-emission probability, while assuring the validity of our algorithm.

The formal proof that the merging scale dependence cancels to the accuracy of the shower rests on the assumption that the factorisation scheme defined by the shower evolution equation is uniform over all of phase space. In CKKW-L, this is realised by allowing trial emissions in the matrix element domain, i.e. off reclustered states, without phase space restrictions, and vetoing events if the first emission off a ME configuration produced another ME configuration, i.e. a parton above t_{MS}. In this way, events with non-zero weight have been treated identically in the ME and PS regions. This prescription has to be generalised to include additional sources of emissions, e.g. multiple interactions.

The requirement that the shower evolution is identical in ME and PS domains forces us to treat multiple interactions on equal footing with radiative emissions, once secondary scatterings are included in the evolution of partons by allowing for competition over phase space. When performing trial showers on a reclustered state, we thus treat multiple interactions identical to "ordinary" emissions. The treatment of the first emission off ME configurations defines the border between ME and PS regions. We choose to slightly refine this definition by requiring that the matrix element region contains only radiative emissions above a cut t_{MS}. This means that once a different type of emission has been produced, we are in the parton shower domain, and we should continue the shower without any additional phase space restriction. More concretely, when checking the first shower evolution response from a ME configuration, we keep the state if an emission below t_{MS} or a secondary scattering has been generated. Hence, the lower bound on the matrix-element-corrected region is changed to $t'_{\text{MS}} = \max(t_{\text{MS}}, \rho_{\text{MI}})$. The reason for this treatment is that we want to keep hard multiple interactions generated by the shower, rather than unjustifiably restricting them to be below t_{MS}.

Let us describe our procedure with a specific example for merging up to three additional jets. Consider a $\text{W} + 3$ gluon event, with scales $\rho_1 \geq \rho_2 \geq \rho_3$. When only allowing QCD radiation and multiple scatter-

ings, this state could be produced by

1. Three gluon emissions off W production;
2. One gluon emission off W production, and one secondary $gg \to gg$ or $q\bar{q} \to gg$ scattering;

Clearly, the first possibility can and should be corrected with matrix elements according to the standard CKKW-L procedure. In the second case, the hardest scale can be attributed to either MI ($\rho_1 = \rho_{MI} = \rho_2 > \rho_3$) or an emission. In the former, we think of the state as inside the PS domain. This means that the shower would have produced the secondary interaction first, "freeing" the subsequent emissions from phase space restrictions. Thus, we have to generate this state from the 0-jet matrix element, and, to avoid double counting, veto it in trial showers off reconstructed configurations. If the hardest scale was associated with an emission ($\rho_1 > \rho_2 = \rho_{MI} = \rho_3$), we can distinguish two cases. If the hardest emission is in the PS domain already, there is no reason to restrict the event generation further by disallowing MI above a certain scale. In effect, the configuration is taken from the evolution of the 0-jet ME sample, while removing it from the 1-jet sample by vetoing configurations with $\rho_{MI} > \rho_{1,reclus}$ in the trial showers. Finally, the emission with ρ_1 can be in the matrix element phase space. Adding one secondary interaction will produce a state of two correlated $2 \to 2$ processes. Since no matrix elements can include this state, it is unambiguously inside the PS region, even without applying additional constraints related to a merging scale. This reasoning leads us to define the cross-over of ME and PS domains by a phase space cut for emissions, or the existence of more than one $2 \to 2$ process. Coming back to the example, we will generate this state from the 1-jet matrix element by adding a secondary scattering. In order to avoid double counting, in trial showers off reconstructed states, we veto the event if the trial emission resulted in $\rho_{1,reclus} > \rho_{MI} > \rho_{2,reclus}$.

This example illustrates the algorithm and sheds light on how particular configurations are generated. The bottom line is that every event where the n hardest (according to the parton shower ordering) partons can produced in one of the matrix elements samples, it will be taken from this sample. Hence, we are still true to the philosophy of CKKW-L merging. Note that in this publication, we will only consider merging matrix elements with additional QCD-induced jets. Therefore we will e.g. treat photon radiation in the shower in the same way as to multiple interactions.

To validate our algorithm, we chose to implement an alternative

treatment of multiple interactions, which is similar to the prescription applied in SHERPA [15]. For this, we exclude multiple interactions when performing trial showers on reclustered states, keeping only the shower emissions in the Sudakov form factors. Then, when showering the matrix element configurations, we allow additional interactions below the scale ρ_1 of the reclustered $2 \to 2$ process. For the $+0$ jet contribution, we choose $\rho_0 = t_{\text{MS}}$ as maximal scale. Differences between both treatments are investigated in section I.5.1.

I.4.3 The algorithm step-by-step

After choosing a parton shower history for the matrix element state, the weight the parton shower would have generated while evolving to this state has to be calculated. This includes the running of α_s in the shower, the no-emission probabilities generated by choosing particular splittings and the way parton distribution functions guide the space-like evolution. In the CKKW-L scheme, a seamless inclusion of ME configurations into the parton shower is then achieved by reweighting the state with the parton shower weight

$$
\begin{aligned}
w_{\text{CKKWL}} &= \frac{x_0^+ f_0^+(x_0^+,\rho_0)}{x_n^+ f_n^+(x_n^+,\mu_F^2)} \frac{x_0^- f_0^-(x_0^-,\rho_0)}{x_n^- f_n^-(x_n^-,\mu_F^2)} \times \left(\prod_{i=1}^{n} \frac{x_i^+ f_i^+(x_i^+,\rho_i)}{x_{i-1}^+ f_{i-1}^+(x_{i-1}^+,\rho_i)} \frac{x_i^- f_i^-(x_i^-,\rho_i)}{x_{i-1}^- f_{i-1}^-(x_{i-1}^-,\rho_i)} \right) \\
&\quad \times \left(\prod_{i=1}^{n} \frac{\alpha_s(\rho_i)}{\alpha_{\text{sME}}} \right) \times \left(\prod_{i=1}^{n} \Pi_{S_{+i-1}}(\rho_{i-1},\rho_i) \right) \times \Pi_{S_{+n}}(\rho_n, t_{\text{MS}}) \qquad \text{(I.12)} \\
&= \frac{x_n^+ f_n^+(x_n^+,\rho_n)}{x_n^+ f_n^+(x_n^+,\mu_F^2)} \frac{x_n^- f_n^-(x_n^-,\rho_n)}{x_n^- f_n^-(x_n^-,\mu_F^2)} \\
&\quad \times \prod_{i=1}^{n} \left[\frac{\alpha_s(\rho_i)}{\alpha_{\text{sME}}} \frac{x_{i-1}^+ f_{i-1}^+(x_{i-1}^+,\rho_{i-1})}{x_{i-1}^+ f_{i-1}^+(x_{i-1}^+,\rho_i)} \frac{x_{i-1}^- f_{i-1}^-(x_{i-1}^-,\rho_{i-1})}{x_{i-1}^- f_{i-1}^-(x_{i-1}^-,\rho_i)} \right. \\
&\qquad \left. \Pi_{S_{+i-1}}(\rho_{i-1},\rho_i) \right] \Pi_{S_{+n}}(\rho_n, t_{\text{MS}}) \,, \qquad \text{(I.13)}
\end{aligned}
$$

where ρ_i are the reconstructed scales of the splittings. The first PDF ratio in eq. (I.12) means that the total cross section is given by the lowest order Born-level matrix element, which is what the non-merged PYTHIA8 shower uses. The PDF ratio in brackets comes from of the fact that shower splitting probabilities are products of splitting kernels and PDF factors. The running of α_s is correctly included by the second bracket. Finally, the event is made exclusive by multiplying no-emission probabilities. In our implementation, we chose to reorder the PDF ratios according to eq. (I.13), so that only PDFs of fixed flavour and x-values

are divided, thus making the weight piecewise numerically more stable. The algorithm to calculate and apply this weight can be summarised as follows:

I. Produce *Les Houches* event files (LHEF) [16] with a matrix element generator for $n = 0, 1 \dots N$ extra jets with a regularisation cut-off, t_{MS}, typically using a fixed factorisation scale, μ_F, and a fixed α_{sME}.

II. Pick a jet multiplicity, n, and a state S_n according to the cross sections given by the matrix element generator.

1. Find all shower histories for the state S_n, pick a sequence according to the product of splitting probabilities. Only pick unordered sequences if no ordered sequence was found. Only pick incomplete paths if no complete path was constructed.
2. Perform reweighting according to eq. (I.13): For each $0 \leqslant i-1 < n$,
   i. Start the shower off the state S_{i-1} at ρ_{i-1}, generate a trial state R_i with scale ρ_{R_i}. If $\rho_{R_i} > \rho_i$, veto the event and start again from II.
   ii. Calculate the weight factor

$$w_{i-1} = \frac{\alpha_{\text{s}}(\rho_i)}{\alpha_{\text{sME}}} \frac{x_{i-1}^{+} f_{i-1}^{+}(x_{i-1}^{+}, \rho_{i-1})}{x_{i-1}^{+} f_{i-1}^{+}(x_{i-1}^{+}, \rho_i)} \frac{x_{i-1}^{-} f_{i-1}^{-}(x_{i-1}^{-}, \rho_{i-1})}{x_{i-1}^{-} f_{i-1}^{-}(x_{i-1}^{-}, \rho_i)} \tag{I.14}$$

3. Start the shower from S_n at ρ_n, giving a state R_{n+1} with the scale $\rho_{R_{n+1}}$.
   i. If $n < N$, and R_{n+1} was produced from S_n by QCD radiation, and $k_\perp(R_{n+1}) > t_{\text{MS}}$, reject the event and start again from II. Otherwise, accept the event and the emission and continue the shower. If a multiple interaction was generated, keep it and continue the shower without restrictions.
   ii. If $n = N$, continue the shower without vetoing.

III. If the event was not rejected, multiply the event weight by

$$\frac{x_n^{+} f_n^{+}(x_n^{+}, \rho_n)}{x_n^{+} f_n^{+}(x_n^{+}, \mu_F^2)} \times \frac{x_n^{-} f_n^{-}(x_n^{-}, \rho_n)}{x_n^{-} f_n^{-}(x_n^{-}, \mu_F^2)} \times \prod_{i=1}^{n} w_{i-1} \tag{I.15}$$

IV. Start again from II.

Our merging approach is, with dynamically generated Sudakov factors, tailored to always reproduce what PYTHIA8 would most probably have done to arrive at the current configuration. Starting scales are of course no exception. Thus, we will start (trial) showering of electroweak $2 \to 2$ processes at the kinematical limit $\sqrt{s}$, both for radiation and for multiple interactions, which is the default procedure in PYTHIA8. In this way, the question for a starting scale of multiple interactions when merging additional emissions is irrelevant.

For jet production in the pure QCD case, by default we set the transverse momentum of the outgoing partons in the $2 \to 2$ process as starting scale in the shower and multiple interactions. This should be adequate as long as the merging scale is not too small. For very small merging scales we have the option of including a Sudakov form factor giving the probability that no additional scatterings are produced between the maximum scale, $\sqrt{s}$, and the transverse momentum of the $2 \to 2$ process. This would make the primary process exclusive, in the sense that we make sure that there are no harder scatterings in the event.

Note also that in pure QCD, the Born-level $2 \to 2$ process is in itself divergent and we must introduce a cutoff regularisation. This cutoff need not be the same as the merging scale. In fact we will here choose a much lower scale to avoid having a large fraction of the reclustered multi-jet ME-states ending up below the cut and resulting in un-ordered paths. In addition, the procedure must be changed slightly since also the scale of the reclustered $2 \to 2$ state is included in the classification of un-ordered histories.

In all cases, we implemented the scale settings such that user choices (e.g. forcing "power showers") are always transferred to the trial showers off $2 \to 2$ processes. For higher-order tree-level matrix elements, we use the reconstructed splitting scale of the state as starting point.

When comparing alternative MI treatments, special care is required when setting the starting scale. For the SHERPA-inspired prescription, we will set the scale ρ_1 of the reclustered $2 \to 2$ process as the MI starting scale for states $S_{+n>0}$, and allow multiple scatterings below $\rho_0 = t_{\text{MS}}$ for the $+0$ jet matrix element contributions.

I.5 Results

We have implemented the necessary code for CKKW-L merging in PYTHIA8, where it has been publicly available as of version 8.157.

In the following, we will first show some validation plots on parton

level for jet production in e^+e^- collisions and weak boson production at hadron colliders. We then move to more realistic observables for these processes, and compare to data. Thereafter, di-boson production and pure QCD jet production are examined.

As input matrix element kinematics, we choose Les Houches Event Files generated with MADGRAPH/MADEVENT and the following settings[1]:

- Fixed renormalisation scale $\mu_R = M_Z$.
- CTEQ6L1 parton distributions used for hadron collisions.
- $\alpha_s(M_Z) = 0.118$ for lepton collisions and to $\alpha_s(M_Z) = 0.129783$ for hadron collisions.
- Fixed factorisation scale μ_F set to M_W for W+jets, M_Z for Z+jets, $M_W + M_Z$ for WZ+jets and M_Z for pure QCD di-jets.
- Durham/$k_\perp$-cut

$$k_\perp^2 = \begin{cases} \min\left\{2 \cdot \min(E_i^2, E_j^2)(1-\cos\theta_{ij})\right\} & \text{for } e^+e^- \to \text{jets} \\ \min\left\{\min(p_{T,i}^2, p_{T,j}^2), \min(p_{T,i}^2, p_{T,j}^2)\frac{(\Delta\eta_{ij})^2+(\Delta\phi_{ij})^2}{D^2}\right\} & \text{for } pp(p\bar{p}) \to (V+) \text{ jets.} \end{cases}$$

  with $D = 0.4$, to regularise the QCD divergences and act as merging scale t_{MS}.
- Require $p_{T,\ell} > 20$ GeV in Z+ jets to avoid low momentum in γ propagators.
- Require $p_{T,j} > 10$ GeV in QCD di-jet events.

For brevity, we will refer to results of merging of up to N additional jets as MENPS. Contributions for a fixed number $n \leq N$ of jets from the matrix element will be indicated by a superscript n, as in ME^{n}NPS. Also, we will write `PYTHIA8` when talking about the default PYTHIA8 behaviour. For all distributions, we use routines of the `fastjet` package [17] to define and analyse jets. If not otherwise indicated, we present plots at the parton level, i.e. after shower and multiple interaction evolution, since merging effects are more visible without smearing due to hadronisation.

[1] Note that the values of α_s and the factorisation scales used here are somewhat irrelevant, as they will nevertheless be divided out in eq. (I.13).

I.5.1 Validation

We begin by considering the simplest case, with only one extra parton added to the Born-level state. This is a very useful benchmark for any matching or merging algorithm, as emphasised in [5], because many parton shower programs, such ARIADNE and PYTHIA8, implement directly the tree-level matching by modifying the splitting functions for the first emission. Hence, when comparing a merged parton shower with the matched one, it is very easy to see if the merging algorithm, for example, has any non-trivial dependence on the merging scale.

Merging scale dependence in $e^+e^- \to jjj$

The PYTHIA8 parton cascade by default includes reweighting of the first splitting of the hard process with the correct matrix element expression, thus giving an excellent handle to check our implementation of $e^+e^- \to$ jets. To compare our result with PYTHIA8, we however have to make a minor change to the shower. When supplied with a $e^+e^- \to q\bar{q}$ state, PYTHIA8 will use the three body matrix element as splitting kernel for the first splitting of q *and* the first splitting of $\bar{q}$. This is done since the $e^+e^- \to q\bar{q}g$ matrix element provides a better estimate of the dipole splitting kernel than the DGLAP kernel. However, when starting from $e^+e^- \to q\bar{q}g$ input, PYTHIA8 will use DGLAP kernels in the evolution of the quarks. Thus the showers response to LHEF input of $e^+e^- \to q\bar{q}$ and $e^+e^- \to q\bar{q}g$ will slightly differ when constructing additional jets. Since we want to merge also higher jet multiplicities with the PYTHIA8 cascade, it is natural to exclude the improvement in the $e^+e^- \to q\bar{q}$ case, and switch off the usage of matrix element correction weights for more than three final partons. In the most recent versions of PYTHIA8, such a switch is available for user input.

Doing this, we can compare ME1PS with PYTHIA8. The variable used as a separation cut t_{MS} between matrix element and parton shower domains is most sensitive to the implementation of the merging procedure. In Figure I.3, we show the value of $k_\perp$ for which three jets would be clustered to two jets. As desired, we find excellent agreement, and, when examining different values of the separation cut t_{MS}, vanishing merging scale dependence.

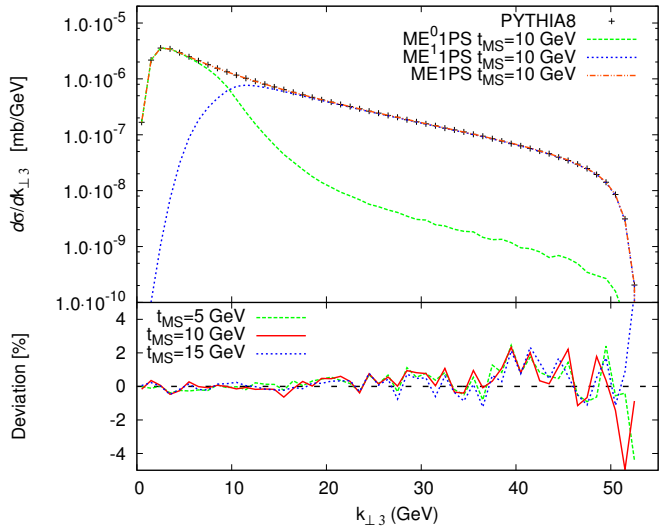

Figure I.3: $k_\perp$ separation of the third jet in e^+e^- collisions at $E_{CM} = 91.25$ GeV. Jets were defined with the Durham algorithm. Hadronisation was switched off. The bottom in-set shows the deviation of the merged samples for three different merging scales t_{MS} with respect to default, matrix-element-corrected PYTHIA8.

Merging scale dependence in $pp \to V + 1$ jet

Similarly, the implementation of V+1 jet merging can be validated against default PYTHIA8. In accordance with the discussion above, we switch off additional matrix element reweighting factors in default PYTHIA8 after the first initial state emission. Further, it is important to note that in PYTHIA8, infrared divergences in space-like splittings are regularised by shifting the denominator of the integration measure in the evolution equation by a small ρ_{reg}. This shift is inspired by the interleaved evolution of space-like splittings and multiple interactions, where colour screening will dampen the number of interactions. Not strictly perturbative effects like these will be present in the default PYTHIA8 distributions, even at $p_\perp \approx \mathcal{O}(10\,\text{GeV})$. That the merging is well under control is shown in Figure I.4, where we set $\rho_{reg} = 0$ for the first splitting in default PYTHIA8 to remove the deliberate mismatch in integration measures. We then find complete agreement in the $k_\perp$ distributions.

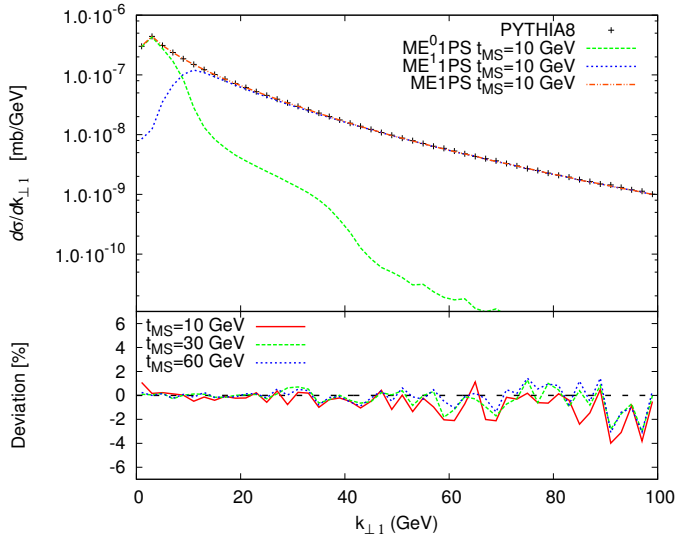

Figure I.4: Transverse momentum of the hardest jet in $W + 1$ jet events at $E_{CM} = 7000$ GeV in pp collisions. Jets were defined with the $k_\perp$-algorithm with $D = 0.4$. Multiple interactions and hadronisation have been switched off. The bottom in-set shows the deviation of the merged sample with respect to default matrix-element corrected PYTHIA8, for three different merging scales.

Influence of the prescription on how to choose a shower history

That different prescriptions to choose amongst reconstructed histories differ only by sub-leading terms is exemplified in Figure I.5. We see a small merging scale dependence when always choosing the history with the smallest sum of transverse momenta. The smallness of the effect stems from the fact the probabilistic choice — on average giving the "correct" shower history — is dominated by a $\frac{1}{\rho}$ factor, so that picking a history by lowest scale ρ or probabilistically almost equally well answer the question "*how would my parton shower have generated this state*".

Variation when changing the starting scales for un-ordered histories

In the following, we refrain from setting the infrared regularisation parameter ρ_{reg} to zero. When facing histories with unordered emission sequences, different ways to assign an emission scale to the combined splitting are conceivable, as discussed in section I.4.1. To investigate this we turn to two-jet merging, the lowest non-trivial jet multiplicity at which non-ordered histories may occur. Figure I.6 highlights that when

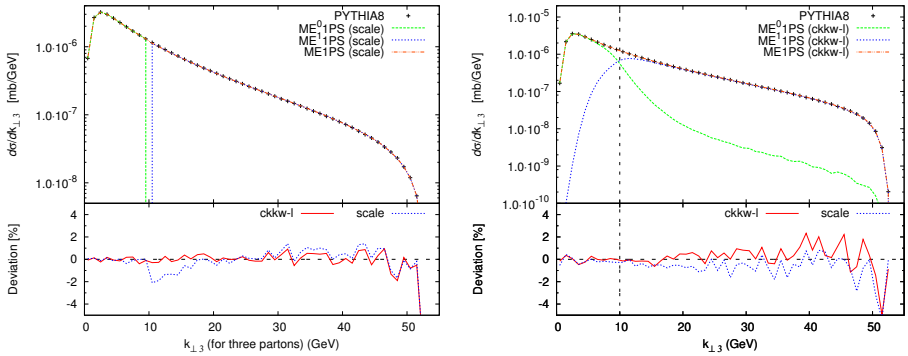

Figure I.5: A comparison of different prescriptions of choosing the history for $e^+e^- \to 3$ jets. Results for choosing in a probabilistic way, with splitting probabilities defined in eqs. I.B10 and I.B11, are labelled "ckkw-l", while adopting a winner-takes-it-all strategy of picking the history with lowest scale carries the label "scale". The plots were produced with a merging scale $t_{\text{MS}} = \min\{k_{\perp i}\} = 10$ GeV. Hadronisation was switched off. The left panel shows the $k_\perp$-separation (in the Durham algorithm) between the third and second hardest parton in the first (reconstructed) emission. The distributions for ME^{0}1PS and ME^{1}1PS for a scale-dependent choice are shown in the upper part, whereas the bottom in-set gives the deviation of both prescriptions from default PYTHIA8. In the right panel we show the $k_\perp$-separation the third and second hardest *jets* defined in the exclusive Durham algorithm for the probabilistic approach, with the bottom in-set again giving the deviation of both prescriptions from default PYTHIA8.

choosing the lower scale as a common scale, the transverse momentum of the second jet has a harder tail compared to setting the higher of both scales as the scale of the combined emission. Also, back-to-back jets are more prominent. This is an effect of the reweighting with a running coupling constant, which produces a more pronounced enhancement of the cross section when choosing smaller scales. For all further results, we will use the larger scale when evaluating $\alpha_s(\rho)$.

Variation due the choice of starting scales for incomplete histories

Figure I.7 shows the consequence of adopting different shower starting scales for incomplete histories. Particularly the consistency of distributions for $\rho_0 = \mu_F^2 = (80.4\,\text{GeV})^2$ and $\rho_0 = s = (1960\,\text{GeV})^2$ allows to conclude that the dependence on the starting scale for incomplete emissions is negligible, which reflects the fact that the corresponding states are very rare.

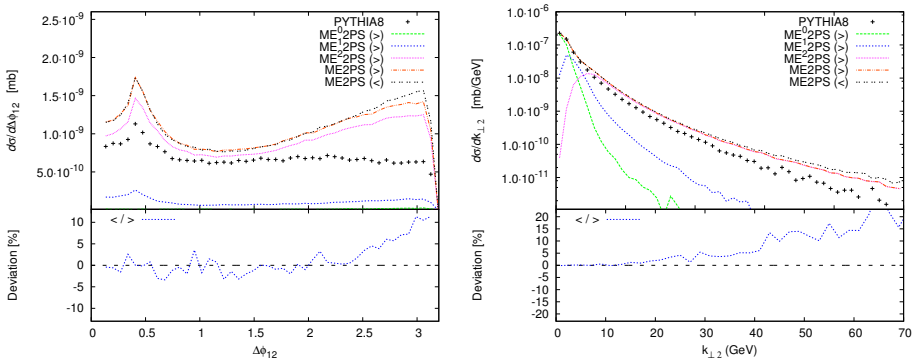

Figure I.6: Two different ways of choosing a combined scale for unordered emissions, in $W + 2$ jet events at $E_{CM} = 1960$ GeV in $p\bar{p}$ collisions. The merging scale is $t_{MS} = 10$ GeV. The curves are labelled with "$>$" when assigning the higher scale $\rho_{combined} = \max(\rho_i, \rho_{i+1})$, and with "$<$" when assigning the lower scale $\rho_{combined} = \min(\rho_i, \rho_{i+1})$, as the combined scale of two unordered emissions. The bottom in-sets show the deviation of the lower scale sample with respect to the higher scale sample. Jets were defined in the $k_\perp$-algorithm with $D = 0.4$, while multiple scatterings and hadronisation were turned off. The left panel shows the azimuthal difference $\Delta\phi_{12}$ between the hardest and second hardest jet. The right panel shows the $k_\perp$ separation $k_{\perp 2}$ of the second hardest jet.

Differences between treatments of multiple interactions

Different treatments of multiple interactions are presented in Figure I.8, which illustrates that at the LHC, variations of up to 10% may occur between the default CKKW-L recipe and the SHERPA-inspired alternative. Due to the phase space restriction $\rho_0 = t_{MS}$ for additional scatterings in $Z + 0$ jet matrix element samples, the alternative treatment produces fewer multiple interactions. Thus, the $k_{\perp 1}$ spectrum for intermediate scales $15\,\text{GeV} < k_{\perp 1} < 30\,\text{GeV}$ is softer than the CKKW-L result. At scales $k_{\perp 1} > 50\,\text{GeV}$, the two prescriptions become indistinguishable. The behaviour at low scales is also anticipated, since the alternative sample does not include suppression due to MI no-emission probabilities. Since these are present in default PYTHIA8, the alternative recipe exhibits a higher maximum, whereas the default prescription reproduces the showers low scale features closely.

Our goal when developing a generalisation of the CKKW-L method including interleaved showers was to be as similar for low scales to the event generator as possible, meaning that the modelling of PYTHIA8 in regions where multiple interactions are important should be left un-

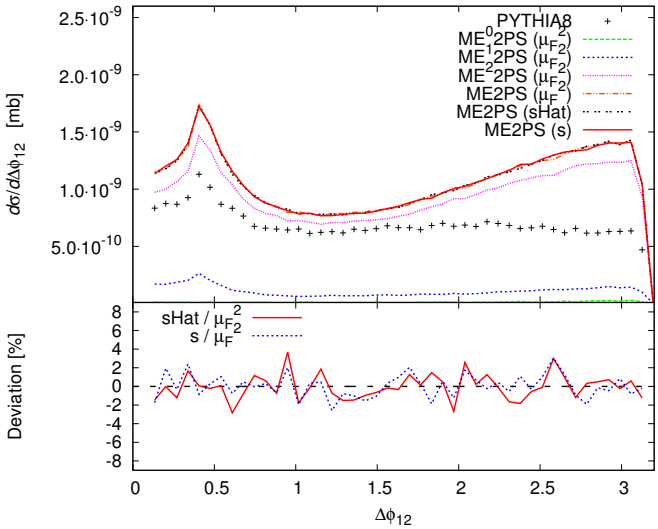

Figure I.7: Azimuthal difference $\Delta\phi_{12}$ between the hardest and second hardest jet, for three different ways of choosing the starting scale ρ_0 for incomplete histories, in W + 2 jet events at $E_{CM} = 1960$ GeV in $p\bar{p}$ collisions. The merging scale is $t_{MS} = \min\{k_{\perp i}\} = 10$ GeV. The curves are labelled "μ_F^2" for $\rho_0 = \mu_F^2$, "sHat" if $\rho_0 = \hat{s}$ and "s" if $\rho_0 = s$. Jets were defined by the $k_\perp$-algorithm with $D = 0.4$. Multiple scatterings and hadronisation were switched off. The bottom in-sets show the deviation of the $\rho_0 = \hat{s}$ and $\rho_0 = s$ samples with respect to the μ_F^2 sample.

changed. As pointed out in I.4.2, this can be formally be achieved in PYTHIA8 by employing the "CKKW-L" prescription. The discussion of the last paragraph also showed that in the implementation of the method, low scale features of PYTHIA8 are retained. Hence, we choose the "CKKW-L" prescription of adding the influence of multiple scatterings as the default. As can be inferred from Figure I.16 below, this method succeeds in not changing the underlying event description of PYTHIA8.

Because in weak boson measurements at low scales, the shape and position of maxima is unchanged in the CKKW-L approach, we also minimise the need for changes of some tuning parameters, e.g. primordial $p_\perp$. This is not obviously true for the alternative method, in which some changes in primordial $p_\perp$ might be necessary. Meanwhile, once hadronisation is added and experimental cuts are applied, Z+ jets observables at the Tevatron show only little dependence on the strategy how multiple interactions are included in merged samples.

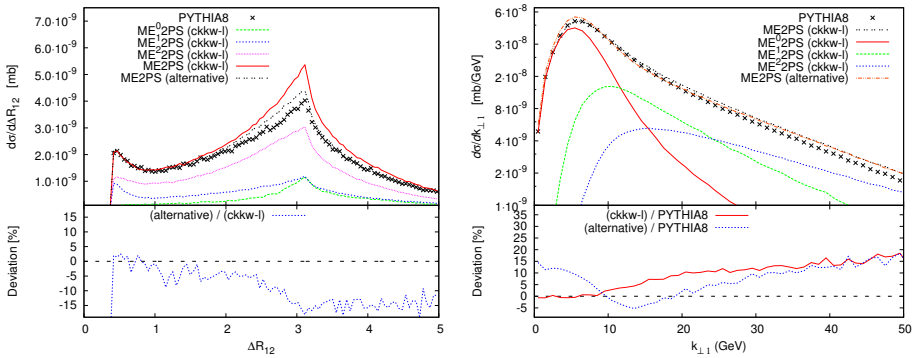

Figure I.8: Two examples for differences in the treatment of secondary interactions, for $Z + 2$ jet events at $E_{CM} = 7000$ GeV in pp collisions. The merging scale is $t_{MS} = \min\{k_{\perp i}\} = 10$ GeV. Jets were defined with the $k_\perp$-algorithm with $D = 0.4$. The left panel shows the R separation ΔR_{12} between the hardest and second hardest jet, with the bottom in-set giving the difference of the SHERPA-inspired sample with respect to the CKKW-L treatment. The right panel shows the jet $k_\perp$ after hadronisation, when clustering to exactly one jet. Ratios of the two MI treatments to default PYTHIA8 are found in the bottom right in-set.

Process	t_{MS}	$2 \to 2$	ME1PS	ME2PS	ME3PS	ME4PS
$e^+e^- \to$ jets	5 GeV		32.92(2) nb	32.50(2) nb	—	—
	10 GeV	32.91(3) nb	32.93(2) nb	32.81(2) nb	32.79(2) nb	32.87(3) nb
	15 GeV		32.90(3) nb	32.88(3) nb	32.87(3) nb	32.87(3) nb
$p\bar{p} \to Z^0$+jets	10 GeV		194.9(5) pb	199.7(5) pb	200.3(5) pb	—
	15 GeV	194.0(1) pb	194.5(6) pb	196.8(6) pb	197.2(6) pb	—
	30 GeV		194.0(6) pb	194.7(6) pb	194.6(6) pb	—
	45 GeV		193.9(6) pb	194.3(6) pb	194.3(6) pb	—
$p\bar{p} \to W^+$+jets	10 GeV		1038(3) pb	1066(3) pb	1074(3) pb	1076(3) pb
	15 GeV	1034(1) pb	1034(3) pb	1048(3) pb	1051(3) pb	1053(3) pb
	30 GeV		1034(3) pb	1039(3) pb	1038(3) pb	1039(3) pb
	45 GeV		1034(3) pb	1036(3) pb	1036(3) pb	1036(3) pb

Table I.1: Impact of changing the merging scale t_{MS} and maximum number of jets on the process cross sections, for three different processes. $e^+e^- \to$ jets is evaluated LEP energy ($E_{CM} = 91.25$), and cross sections for $p\bar{p} \to Z$+jets and $p\bar{p} \to W^+$+jets are calculated at Tevatron Run II energy ($E_{CM} = 1960$). Results were produced with PYTHIA8 Tune 4C. Multiple interactions and hadronisation were switched off.

Unitarity violations

We finish our validation by discussing a theoretical issue. Parton shower resummation alone does not change the cross section of the hard

Process	t_{MS}	$2 \to 2$	ME1PS	ME2PS	ME3PS	ME4PS
$p\bar{p} \to W^+$+jets	10 GeV		1037(3) pb	1048(3) pb	1047(3) pb	1045(3) pb
	15 GeV	1034(1) pb	1034(3) pb	1043(3) pb	1044(3) pb	1043(3) pb
	30 GeV		1034(3) pb	1038(3) pb	1038(3) pb	1038(3) pb
	45 GeV		1034(3) pb	1036(3) pb	1036(3) pb	1036(3) pb

Table I.2: Impact of changing the merging scale t_{MS} and maximum number of jets on the W+ jets cross sections in $p\bar{p}$ collisions at $E_{\mathrm{CM}} = 1960$. Multiple interactions and hadronisation were switched off. Results were produced using Tune 4C, with enforced rapidity ordering switched off.

process, since the probability of having no emission, together with the sum of probabilities to evolve into states with an arbitrary number of emissions adds to unity — a property dubbed unitarity. This however is only true if the transition probabilities used in generating additional emissions are identical to the terms exponentiated in Sudakov form factors. As pointed out in [18, 19], unitarity is violated by tree level merging due to the fact that the transition probabilities above and below t_{MS} are different, while Sudakov factors are always generated with shower splitting kernels, i.e. the transition probabilities below t_{MS}. The magnitude of the resulting unitarity violations for different merging scales is assessed for W+ jets in Table I.1. We have also verified that the main points of the following discussion apply to all example processes used in this report.

First, we note that including one additional jet does not lead to unitarity violations for vector boson production, since PYTHIA8 is already matrix element corrected, so that the full tree-level splitting probability is exponentiated. When including more than one jet, we observe smaller deviations from the hard process cross section as we increase the merging scale. This is expected since for larger t_{MS}, the Sudakov form factors generated by trial showering quickly approach unity. Because of the higher merging scale, phase space regions with low scale emissions (where Sudakov factors differ from unity) are generated by the parton shower. Thus, identical splitting probabilities are used to generate the emissions and Sudakov form factors, and unitarity is preserved to reasonable accuracy. One immediate consequence is that we should not choose t_{MS} too low, since otherwise, sizable violations can occur.

Unitarity violations give a measure of how well the shower splitting probability, integrated over the PS phase space (ordered in the evolution variable), captures the matrix element features and the allowed phase

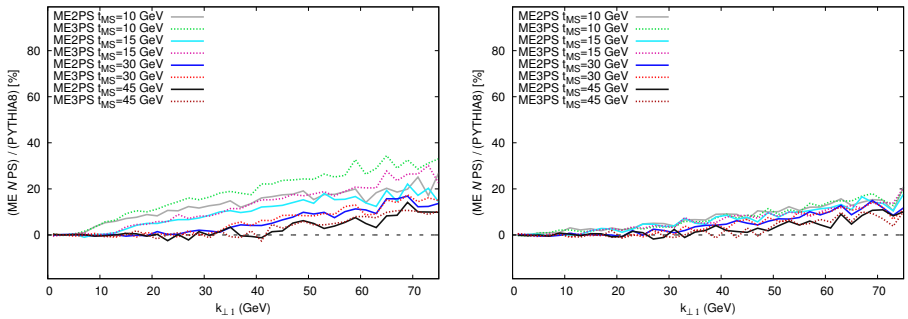

Figure I.9: Comparison of the $k_\perp$ of the first jet in W+ jets events at $E_{\mathrm{CM}} = 1960$ GeV in $p\bar{p}$ collisions, between default, first-order corrected PYTHIA8, and CKKW-L, for different number of merged jets and different merging scales. Jets were defined with the $k_\perp$-algorithm with $D = 0.4$, clustering to exactly one jet. Multiple interactions and hadronisation were switched off. Left panel: Results when using Tune 4C, which by default includes ordering emissions in rapidity as well as ρ. Right panel: Results when using Tune 4C, with enforced rapidity ordering switched off.

space. Different choices of PS evolution variables can lead to different regions of the full phase space — which includes unordered emissions — being neglected in the parton shower approximation. These regions of unordered emission sequences are formally beyond the accuracy of the shower. Figure I.9 shows the differences in transverse momentum distributions between merged distributions and PYTHIA8, for two different ways of ordering emissions. Deviations from unitarity are more significant if the shower evolution is ordered both in ρ and rapidity. This is due to neglecting larger regions of the full phase space in the parton shower. We have verified that when only keeping ME configurations for which a history ordered in ρ and rapidity can be constructed, unitarity violations are greatly reduced. Nonetheless, we have to conclude that ordering the cascade in these two variables makes the parton shower approximation worse than ordering in ρ alone. Only ordering in ρ, we find in Table I.2 that the inclusive $2 \to 2$ cross section is not changed drastically when including additional jets. Also, the $k_{\perp 1}$ spectrum becomes only slightly harder in this case, as is seen in the right panel of Figure I.9.

It should be noted that the rapidity ordering was introduced in PYTHIA8 to suppress the high transverse momentum emissions from dipoles between incoming and outgoing partons. However, this is now achieved through another damping mechanism described in [20], which

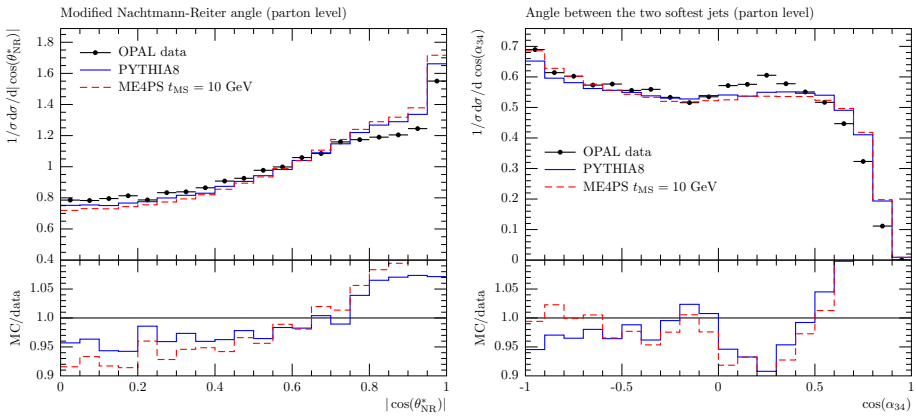

Figure I.10: Four jet angular correlations in e^+e^- collisions at $E_{CM} = 91.25$ GeV, as measured by OPAL [23]. Up to four additional jets were included in the merged samples. Effects of hadronisation are included. Left panel: Modified Nachtmann-Reiter angle $|\cos\theta_{NR}|$. Right panel: Angle between the two lowest energy jets $\cos\alpha_{34}$. The plots were produced with RIVET [24].

means that the rapidity ordering is no longer needed to achieve a reasonable description of data.

We checked that deviations from unitarity can be even further reduced when excluding unordered emissions. However, in CKKW-L, we want to include states which are out of the reach of the shower, and thus, as discussed in section I.4.1, by default keep ME configurations for which only unordered histories can be found. For enthusiasts, switches for rejecting configurations with unordered histories are available in the public code. Provided considerable unitarity violations remain after excluding differences between the full allowed and the PS phase space, this could suggest large higher-order corrections, since by choosing a low merging scale we effectively include major parts of the real emission phase space of an NLO calculation [21]. It should be noted that unitarity is a parton shower concept and need not be fulfilled in other contexts, see e.g. [22].

I.5.2 e^+e^- four-jet observables

Merging procedures aim for a better description of well separated jets in the parton shower. Historically, angular correlations in $e^+e^- \to 4$ jet production have been used to investigate the 3-gluon vertex. The description of these observables should be improved when includ-

ing additional jets. More specifically, we look at the the (modified) Nachtmann-Reiter angle

$$|\cos\theta_{NR}| = \left| \frac{(\vec{p}_1 - \vec{p}_2)\cdot(\vec{p}_3 - \vec{p}_3)}{|\vec{p}_1 - \vec{p}_2|\,|\vec{p}_3 - \vec{p}_4|} \right| , \tag{I.16}$$

and the angle between the two lowest energy jets

$$\cos\alpha_{34} = \frac{\vec{p}_3 \cdot \vec{p}_4}{|\vec{p}_3|\,|\vec{p}_4|}, \tag{I.17}$$

where $\vec{p}_i$ are the energy ordered three-vectors of the jets. As shown in Figure I.10, the default PYTHIA8 description of these observables is fairly good to start with, reflecting the fact that some azimuthal correlations are included in the shower, and it is only slightly changed when merging additional jets. We notice that $|\cos\theta_{NR}|$ becomes slightly worse when including additional jets. The different shape of the generator curves can be explained by the fact that the data was corrected to the parton level, whereas the MC samples where generated with full hadronisation. In $|\cos\theta_{NR}|$, the hadronisation corrections [23] would change the MC shapes towards a better agreement. $\cos\alpha_{34}$ is captured slightly better for $\cos\alpha_{34} \approx -1$, when including additional jets. The trend to overshoot at $\cos\alpha_{34} \geq 0.5$ can again be explained by the fact that we have generated the distributions at the hadron level, whereas the data was corrected to the parton level. We have checked by excluding hadronisation that these statements are true, and that the irregularities are reduced. However, the general trends in both $|\cos\theta_{NR}|$ and $\cos\alpha_{34}$ remain, albeit less pronounced. This might be explained with the fact that the hadronisation corrections applied to the data are estimated with a model different from the one used by PYTHIA8. Since the cross-over from partonic to hadronic states is a highly model-dependent statements, artifacts of the model used to estimate corrections could be present in the data. Even so, we think Figure I.10 illustrates that when including higher-order tree-level matrix elements in the description of $e^+e^- \to$ jets, changes as compared to the default shower are fairly modest, which indicates that PYTHIA8 already nicely describes observables at LEP. When checking further LEP observables, we find that CKKW-L does as good or moderately better than default PYTHIA8. This means that when developing a new tune including additional matrix elements, the hadronisation parameters, which are predominantly constrained at LEP, may not have to be touched.

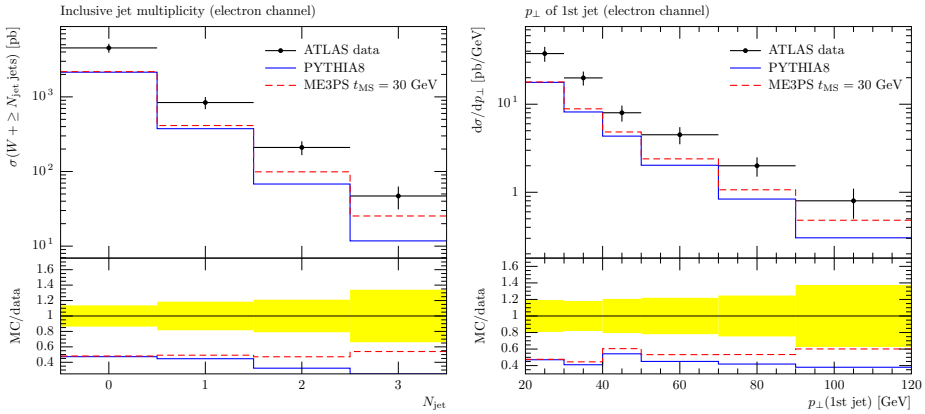

Figure I.11: Jet multiplicity and transverse momentum of the hardest jet in W + jet events as measured in the electron channel by ATLAS [25]. The merging scale is $t_{MS} = \min\{k_{\perp i}\} = 15$ GeV. Effects of multiple scatterings and hadronisation are included. The plots were produced with RIVET [24].

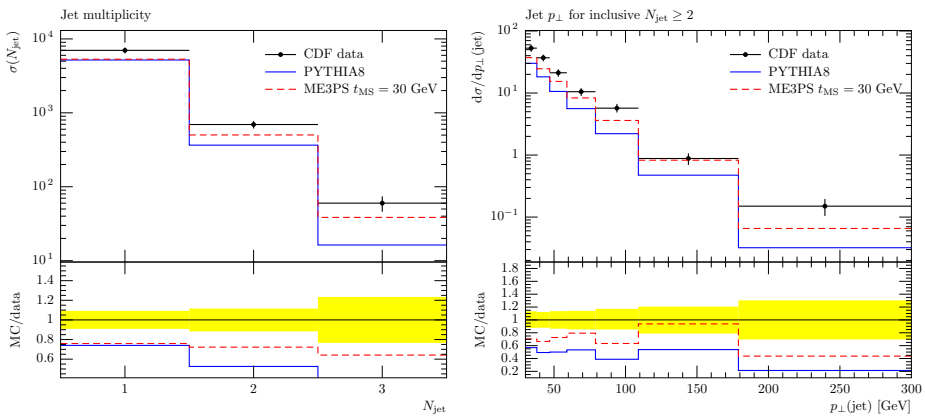

Figure I.12: Jet multiplicity and inclusive jet transverse momentum in Drell-Yan events, as measured by CDF [26]. The merging scale is $t_{MS} = 30$ GeV. Effects of multiple scatterings and hadronisation are included, and Tune 4C was chosen. The plots were produced with RIVET [24].

I.5.3 Vector boson production

In hadron collisions, we can assess the extent of change when including additional jets by looking at vector boson production with two or more additional jets. In Figures I.11 and I.12, we compare jet $k_\perp$ spectra and jet multiplicities for W production and in Drell-Yan events to data, respectively. In general, we find more jets with high $k_\perp$ and better agreement

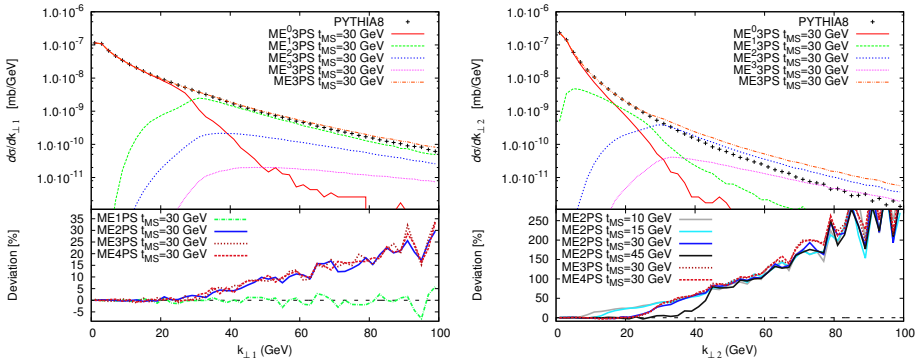

Figure I.13: $k_\perp$ of the hardest and second hardest jet, for different number of merged jets, in W+ jets events at $E_{\mathrm{CM}} = 1960$ GeV in $p\bar{p}$ collisions. The merging scale is defined in $t_{\mathrm{MS}} = \min\{k_{\perp i}\}$. Jets were defined with the $k_\perp$-algorithm with $D = 0.4$. Multiple interactions and hadronisation were switched off. Plots produced with PYTHIA8 Tune 4C. The bottom in-sets show the deviation of the merged samples from default, first-order corrected PYTHIA8.

with jet multiplicity data.

It is particularly instructive to investigate the change of $k_\perp$ distributions when increasing the numbers of jets in the matrix element generation. Figure I.13 again shows that the $k_\perp$ spectra develop harder tails when including higher multiplicity matrix element configurations.

Analysing the $k_{\perp 2}$ separation when two jets are clustered into a single jet in the right panel, it is interesting to see how this increase arises. For small merging scales (e.g. 10, 15 GeV), $k_{\perp 2}$ in two-jet merging quickly grows at the merging scale and remains flat until a more gradual ascend sets in at $k_{\perp 2} \approx 60$ GeV. There, the ME2PS distributions for $t_{\mathrm{MS}} = 10, 15$ GeV also join the curves for larger merging scales (30, 45 GeV). This behaviour of ME2PS for low t_{MS} can more clearly be seen in the left panel of Figure I.14. When inspecting the ME3PS curves for $t_{\mathrm{MS}} = 10, 15$ GeV, we again see a hardening of the spectrum, which is to some extent stable when going to ME4PS. Such a stabilisation inspires the conclusion that the $k_{\perp n \leq N}$ separation between the n'th and $(n-1)$'th hardest jets is stable once the maximal number of merged jets is increased above n, as was found in [21].

One possible argument for this effect is that when looking at the $k_{\perp 2}$ separation at which a jet a_1 and a jet a_2 are clustered into a single jet in ME3PS, the parent jets b_1, b_2, b_3 which produced a_1 and a_2 were harder than in ME2PS, thus again favouring harder jets $a_{1,2}$, i.e. larger separations, $k_{\perp 2}$. The stabilisation could then be explained by assuming that

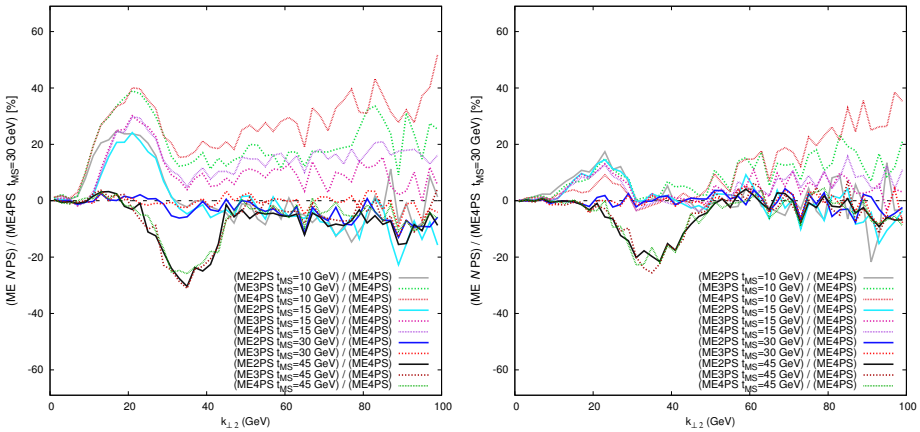

Figure I.14: $k_{\perp 2}$ separation of the second jet in W+ jets events at $E_{\mathrm{CM}} = 1960$ GeV in $\mathrm{p\bar{p}}$ collisions. The curves are normalised to the $k_{\perp 2}$ distribution in ME4PS at $t_{\mathrm{MS}} = 30$ GeV. Jets were defined with the $k_{\perp}$-algorithm with $D = 0.4$. Multiple interactions and hadronisation were switched off. Left panel: Plots produced with PYTHIA8 Tune 4C. Right panel: Plots produced with PYTHIA8 Tune 4C, with enforced rapidity ordering switched off.

the parent jets producing $b_{1,2,3}$ in ME4PS will not greatly increase the hardness of $b_{1,2,3}$ because in ME4PS, most jets will be just above the merging scale due to a steeply falling $k_{\perp 4}$ spectrum.

However, in our implementation, the question arises if a stable $k_{\perp 2}$ distribution will also be stable to changing the value of the merging scale. First, notice that there is no shape change in the $t_{\mathrm{MS}} = 45$ GeV curves when going from ME2PS to ME3PS (or ME4PS), even though by the above reasoning, further distortions should be more pronounced at high merging scales. It is critical to notice (see Figure I.14) that for low merging scales, the spectrum in ME4PS is significantly harder than the ME4PS reference at $t_{\mathrm{MS}} = 30$ GeV, whereas once their initial ascend is over, the curves for $t_{\mathrm{MS}} = 45$ GeV nicely join the $t_{\mathrm{MS}} = 30$ GeV ones. These observations can again be explained by unitarity violation for $t_{\mathrm{MS}} = 10$ GeV and $t_{\mathrm{MS}} = 15$ GeV, which stabilise when merging more jets, but do not decrease. Since the changed cross section is stable while the sample composition changes between ME2PS and ME3PS, the shape of $k_{\perp 2}$ has to change. In support of this rationale, the right panel of Figure I.14 shows that when reducing unitarity violations by not enforcing rapidity ordering in the shower, the effects are significantly reduced as well. These considerations can be applied to jet separations $k_{\perp n \geq 2}$ as well.

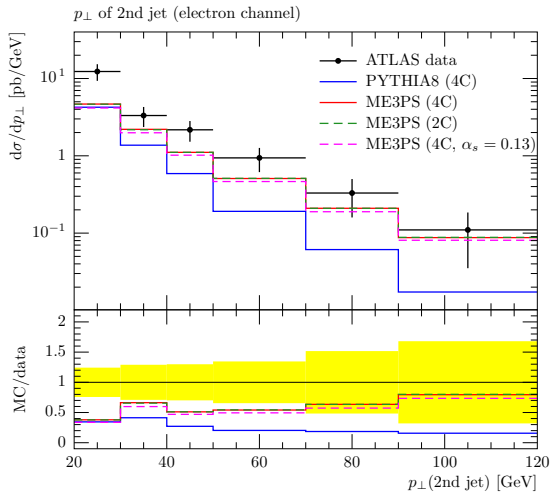

Figure I.15: Transverse momentum of the second hardest jet in W + jet events as measured in the electron channel by ATLAS [25], for different tunes. "2C" indicates that Tune 2C was used, while "4C" uses Tune 4C, the current default tune in PYTHIA8.157. The label "$\alpha_s = 0.13$" stands for fixing $\alpha_s(M_Z) = 0.129783$ in Tune 4C, as discussed in the text. The merging scale is $t_{MS} = \min\{k_{\perp i}\} = 30$ GeV. Effects of multiple interactions and hadronisation are included. The plot was produced with RIVET [24].

Every parton shower relies on phenomenological models to confine partons into hadrons, thus making systematic tuning is a critical step in the development of an event generator. Tuning however should not hide the shortcomings due to approximations made. If residual tuning effects because of correlations between tuning parameters remain in phase space regions with well-separated jets, we expect such changes to be stabilised when correcting with higher multiplicity matrix elements. The impact of changing between different tunes in PYTHIA8 is shown in Figure I.15, where we show the results of using Tune 2C, Tune 4C and forcing $\alpha_s(M_Z) = 0.129783$ (the CTEQ6L1 fit value) in all components of PYTHIA8, in comparison with ATLAS data [25]. We find that the pp $\to$ W+jets predictions are fairly stable with respect to changing tunes. As expected, we observe that the ME3PS sample is harder than default PYTHIA8.

Finally in Figure I.16 we show the effect of our treatment of multiple interactions. The associated hadronic activity in Z production events, especially in the azimuthal direction direction of the Z, is very sensitive to underlying event effects, and hence also to multiple interactions [27].

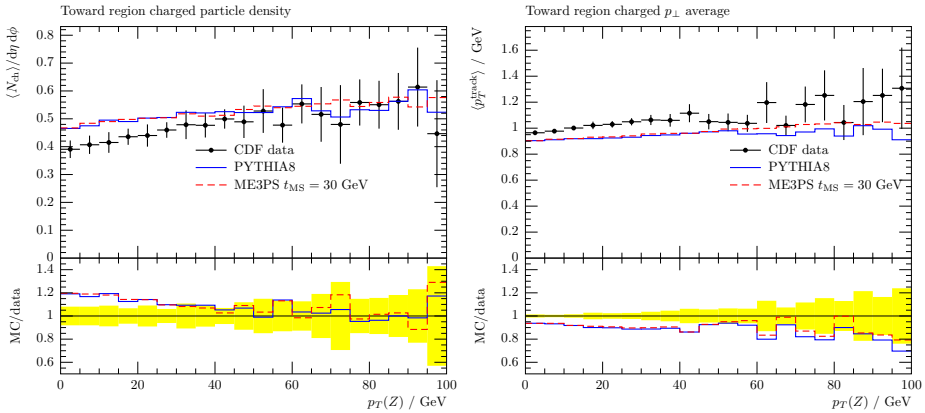

Figure I.16: Toward region charged particle density and average $p_\perp$ in Drell-Yan events, as measured by CDF [27]. The merging scale is $t_{\text{MS}} = \min\{k_{\perp i}\} = 30$ GeV. Effects of multiple scatterings and hadronisation are included, and Tune 4C was chosen. The plots were produced with RIVET [24].

In our merging scheme we have been very careful to make sure that multiple interactions are treated exactly the same way as in standard PYTHIA8 without inclusion of matrix element configurations. And, as seen in Figure I.16, the differences between the merged sample and default PYTHIA8 are indeed very small.

I.5.4 Di-boson and QCD jet production

Our implementation is in principle general enough to be applied to any process that can be handled by PYTHIA8. However, in this publication, we restrict ourselves to two further examples. First, let us examine di-boson production, with one of the bosons decaying hadronically. Allowing hadronic decays of weak bosons in the underlying Born process provides another complication, and for technical reasons we here restrict the matrix element to only produce extra jets in from the incoming partons, while additional jets in the hadronic boson decay are only produced by the shower. As the first emission in the boson decay is anyway ME-corrected in standard PYTHIA8, this is not a severe restriction. Note however that this means that we have to treat emissions from the boson decay on the same footing as multiple interactions (and QED radiation). This means that they are included in the Sudakov form factors generated from reclustered states, but when showering from a $n < N$ state, if the first emission is from the boson decay, the event is never vetoed. The

partons from the boson decay are also not involved in the reclustering of matrix element states.

The performance of our implementation concerning these issues can be tested when merging $pp \to W^+Z \to e^+\nu_e\, jj$+jets matrix elements. The left panel of Figure I.17 shows that also in the case of di-boson production, the $k_{\perp 3}$ spectrum becomes harder on inclusion of additional jets. There are no visible differences in the default PYTHIA8 results when changing between only ordering emissions in evolution ρ and ordering both in ρ and rapidity, since $k_{\perp 3}$ is dominated by the hardest shower emission, which is not affected by the additional rapidity ordering. We observe only small differences between merged samples with and without enforced rapidity ordering in the shower. Relative changes in $k_{\perp 3}$ are, as expected, comparable to the effects on $k_{\perp 1}$ when including additional jets in $pp \to W^+ \to e^+\nu_e$ (see e.g. Figure I.13). We have checked that different jet definitions do not change this trend.

A consequence of harder jets can be seen in the right panel of Figure I.17, where we show the di-jet invariant mass distribution with cuts and jet definition from CDF [28]. The spectrum develops a harder tail compared to default PYTHIA8. Particularly in the region $140 < m_{jj} < 200$ GeV we find an increase around 10%. Also, the distribution is sensitive to the unitarity violations due to enforced rapidity ordering, so that care has to taken when comparing MEPS distributions to experimental data. In [28], the shape of the di-boson backgrounds was modelled by PYTHIA6.216, which should behave similar to default PYTHIA8. Merging additional jets in $pp \to W^+Z \to e^+\nu_e\, jj$ can affect the shape of the di-jet invariant mass spectrum in a way which will reduce the significance of the effect found by CDF. We plan to further investigate these issues in a future publication.

Finally, we examine QCD jet production. For such events, we set the shower starting scale for the $2 \to 2$ process to the transverse momentum of the outgoing partons. The maximal scale for secondary scatterings is set to the same value. In PYTHIA8, users are generally allowed to choose a different prescription of setting a maximal scale of multiple interactions, e.g. the energy of the colliding hadrons. Adopting this example, we risk double-counting configurations, since interactions identical to the hard process can be generated.

To remove this double counting, an additional veto on the transverse momentum of multiple interactions in the trial shower has to be applied. We have checked that when allowing secondary scatterings up to the kinematical limit and applying a veto, distributions are not changed

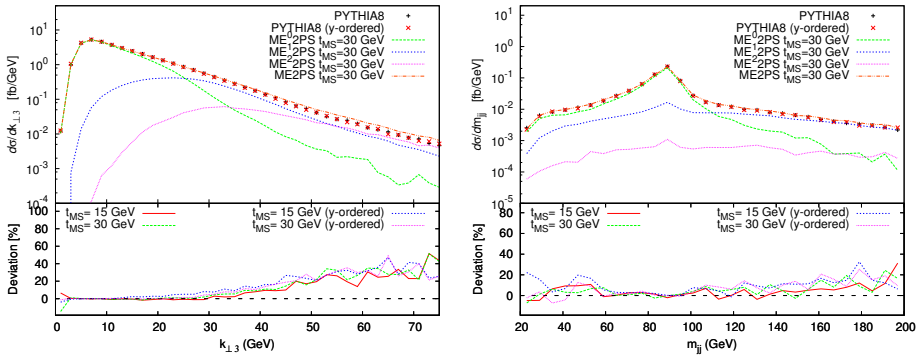

Figure I.17: Sample results of including matrix elements with additional jets in $pp \to W^+Z \to e^+\nu_e\, jj$ events, at $E_{CM} = 1960$ GeV in $p\bar{p}$ collisions. The merging scale is defined in $t_{MS} = \min\{k_{\perp i}\}$. Multiple interactions are included. Curves with enforced rapidity ordering in the shower carry an additional label "y-ordered". The bottom in-set shows the deviation of the merged samples to PYTHIA8. Left panel: $k_{\perp 3}$ of the third and second hardest jet at hadron level. Jets were defined with the $k_\perp$-algorithm with $D = 0.4$. Right panel: Di-jet invariant mass in at hadron level. Cuts are taken from the recent CDF publication [28]. Jets were defined with the CDF JETCLU algorithm [29] as implemented in `fastjet`.

with respect to setting $\rho_{MI,max} = p_{\perp,2\to2}$. The results presented here have been produced with fixing the starting scales for the hard process to the transverse momentum, as is the default in PYTHIA8.

Figure I.18 shows that for QCD jets as well, inclusion of additional jets increases the hardness $k_{\perp 3}$ of the third jet. Compared to the changes in $k_{\perp 1}$ for W+jets, the effect is, however, moderate. This is in accord with the findings in [20], which showed good agreement in the $p_\perp$ of the softest of three partons (there called $p_{\perp 5}$), when comparing $2 \to 3$ matrix elements to the default shower after the first emission from a $2 \to 2$ core process. There, the shower was slightly harder than the matrix element until $p_{\perp 5} \approx 80$ GeV. A similar effect can be seen in the $k_{\perp 3}$ separation of jets, which is related to the $p_{\perp 5}$ of partons.

The inclusion of a sample with two additional jets does not change the situation dramatically, leading us to the conclusion that once the first few hard jets are generated according to the tree-level matrix elements, the parton shower does a fairly good job in describing the hardness of additional jets. This is supported by the upper panel of Figure I.19, showing the $k_{\perp 3}$ separation between the third and second hardest jets in W+jets events. Clearly, there are only little changes in the hardness

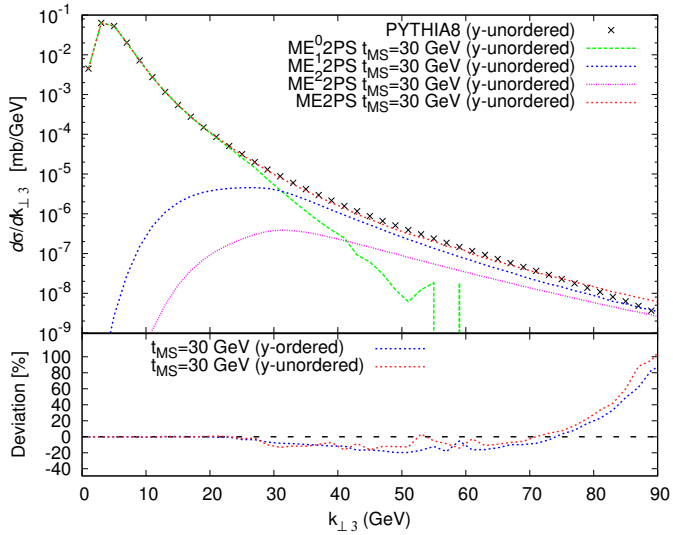

Figure I.18: $k_{\perp 3}$ separation of the third jet in pure QCD jet events at $E_{\mathrm{CM}} = 1960$ GeV in $\mathrm{p\bar{p}}$ collisions. The merging scale is $t_{\mathrm{MS}} = 30\,\mathrm{GeV}$. Jets were defined with the $k_\perp$-algorithm with $D = 0.4$. Multiple interactions are included and hadronisation was switched off. Curves with enforced rapidity ordering in the shower carry the label "y-ordered", while results without explicit rapidity ordering are labelled "y-unordered". The bottom in-set shows the deviation of the merged sample default PYTHIA8.

of the third jet when going from ME2PS to ME4PS, i.e. the merging has less impact once a couple of jets are included from the matrix element states[2].

Coming back to pure QCD, we show in Figure I.20 that also in this case, results for $k_{\perp 3}$ are fairly stable when changing the merging scale. We register only small unitarity violations of $\mathcal{O}(10\%)$, which matches the changes in $k_{\perp 3}$ in W+jets events when going from ME2PS to ME4PS without requiring rapidity ordering, as illustrated in the upper part of Figure I.19. As $\mathrm{W} + n$ jets contains colour configurations similar to di-jet+$(n-2)$ jets, this is another indication for the consistency of the implementation. However, in Figure I.20, we find only minor changes between different treatments of rapidity ordering for di-jet events, whereas for W+jets events, we observe dramatic effects (see lower plot in Figure I.19). This can be explained by the fact that when

[2] As can be seen in the lower panel of Figure I.19, this statement does not hold if there are major unitarity violations – which should be avoided anyway.

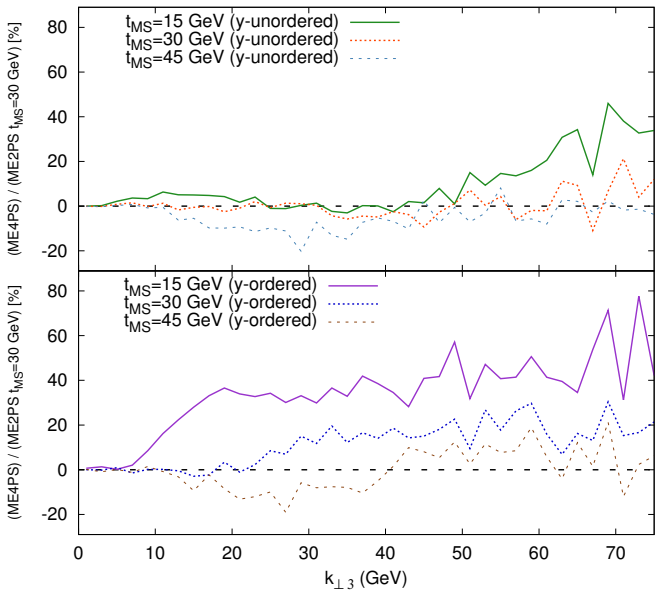

Figure I.19: $k_{\perp 3}$ separation of the second and third jet in W+jets events at $E_{\mathrm{CM}} = 1960$ GeV in $\mathrm{p\bar{p}}$ collisions. The curve shows the deviation in $k_{\perp 3}$ of ME4PS for three different merging scales, with respect to ME2PS for $t_{\mathrm{MS}} = 30$ GeV. Jets were defined with the $k_\perp$-algorithm with $D = 0.4$. Hadronisation and multiple interactions were switched off. Curves with enforced rapidity ordering in the shower carry the label "y-ordered", while results without explicit rapidity ordering are labelled "y-unordered".

requiring rapidity ordering, PYTHIA8 orders all emissions *after the first shower emission* in rapidity, meaning that for di-jet events, $k_{\perp 3}$ is virtually unaffected by the constraint, while in W+jets events, major restrictions on the phase space of the second and third jet lead to large unitarity violations. This argument is substantiated by Figure I.21, which shows that once rapidity ordering becomes relevant, the additional ordering results in larger deviations for low merging scales.

It is worth noting that since jet spectra are not changed dramatically when including additional jets, only small differences are expected when comparing to experimental data. In Figure I.22, we examine the description of CDF jet shapes [30] for two exemplary $p_\perp^{jet}$ bins. For a $p_\perp^{\mathrm{jet}}$ in 55 GeV $< p_\perp^{\mathrm{jet}} <$ 63 GeV, we find only very minor changes. However, for higher $p_\perp^{\mathrm{jet}}$ in the region 128 GeV $< p_\perp^{\mathrm{jet}} <$ 148 GeV the differences between default PYTHIA8 and the merged sample ME2PS with two additional jets are more pronounced, and we see that the latter gives a

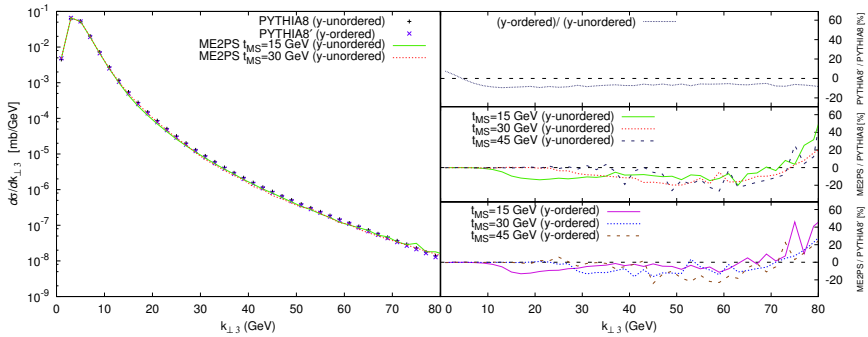

Figure I.20: $k_{\perp 3}$ separation of the third jet in pure QCD jet events at $E_{\mathrm{CM}} = 1960$ GeV in $\mathrm{p\bar{p}}$ collisions, for three different merging scales. Jets were defined with the $k_\perp$-algorithm with $D = 0.4$. Multiple interactions and hadronisation were switched off. Curves with enforced rapidity ordering in the shower carry the label "y-ordered", while results without explicit rapidity ordering are labelled "y-unordered". Left panel: $k_{\perp 3}$ separation of the third jet. Upper right panel: Deviation in $k_{\perp 3}$ between default PYTHIA8 (Tune 4C) and PYTHIA8 (Tune 4C) with no enforced rapidity ordering. Centre right panel: Deviation in $k_{\perp 3}$ between ME2PS sample and PYTHIA8 (Tune 4C) with no enforced rapidity ordering. Lower right panel: Deviation in $k_{\perp 3}$ between ME2PS sample and default PYTHIA8 (Tune 4C).

slightly broader shape. This is expected as at high transverse momentum the effect of the harder third jet in Figure I.18 should come into play, resulting in more jets containing two partons from the matrix element. Such jets are of course broader.

When checking differential jet shapes for other $p_\perp^{\mathrm{jet}}$ bins, we find that ME2PS does as good or slightly better than PYTHIA8 for $p_\perp^{\mathrm{jet}} \lesssim 120$ GeV, while decreasing too slowly for $p_\perp^{\mathrm{jet}} \gtrsim 120$ GeV. This indicates that at least some revisions need to be made when tuning matrix-element-merged PYTHIA8 to pure QCD jet data. Since the influence of multiple interactions on jets with $p_\perp^{\mathrm{jet}} \gtrsim 120$ GeV is likely to be small, a possible new tune would potentially feature changes in $\alpha_{\mathrm{s}}(\mathrm{M_Z})$ and other parameters to prescribe the physics of hard jets.

I.6 Conclusions and Outlook

We have implemented CKKW-L merging inside the PYTHIA8 framework, and have shown that it works well for several sample processes: $\mathrm{e^+e^-} \to$ jets, (di-) boson and pure QCD jet production in hadronic colli-

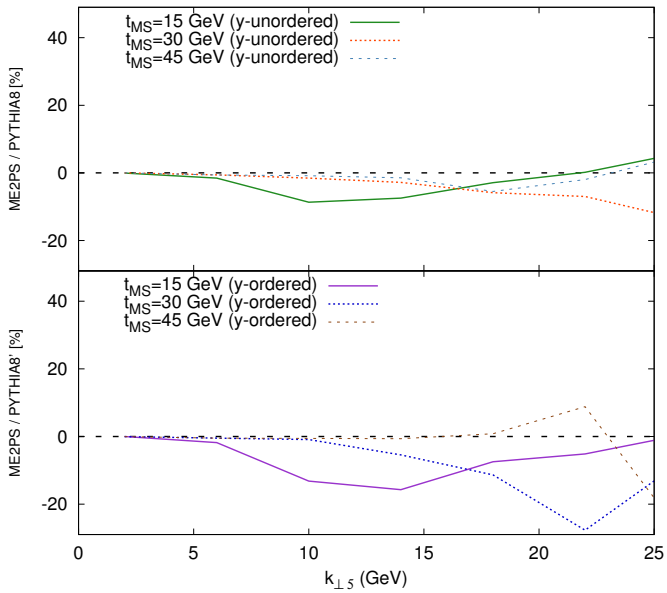

Figure I.21: $k_{\perp 5}$ separation between the fourth and fifth jet in di-jet events at $E_{\mathrm{CM}} = 1960$ GeV in $\mathrm{p\bar{p}}$ collisions. The curves show the deviation of $k_{\perp 5}$–distributions in ME2PS for three different merging scales, with respect to PYTHIA8. Jets were defined with the $k_\perp$-algorithm with $D = 0.4$. Hadronisation and multiple interactions were switched off. Curves with enforced rapidity ordering in the shower carry the label "y-ordered", while results without explicit rapidity ordering are labelled "y-unordered".

sions. The implementation is, however, quite general and could be used for any process which PYTHIA8 is able to handle.

The algorithm is true to the CKKW-L spirit, in that if matrix element samples are provided for up to N extra partons, every event where the $n \leq N$ hardest (in the parton shower sense) partons can be produced by the matrix element, it will be evolved from the corresponding matrix element state.

By construction, the dependence on the merging scale vanishes to the logarithmic precision of the PYTHIA8 parton shower. Nevertheless, we find visible sub-leading effects due to different choices that can be made in the procedure. In particular we have investigated

- different ways of choosing parton shower histories,
- different strategies for handling unordered histories,
- different starting scales for incomplete histories,

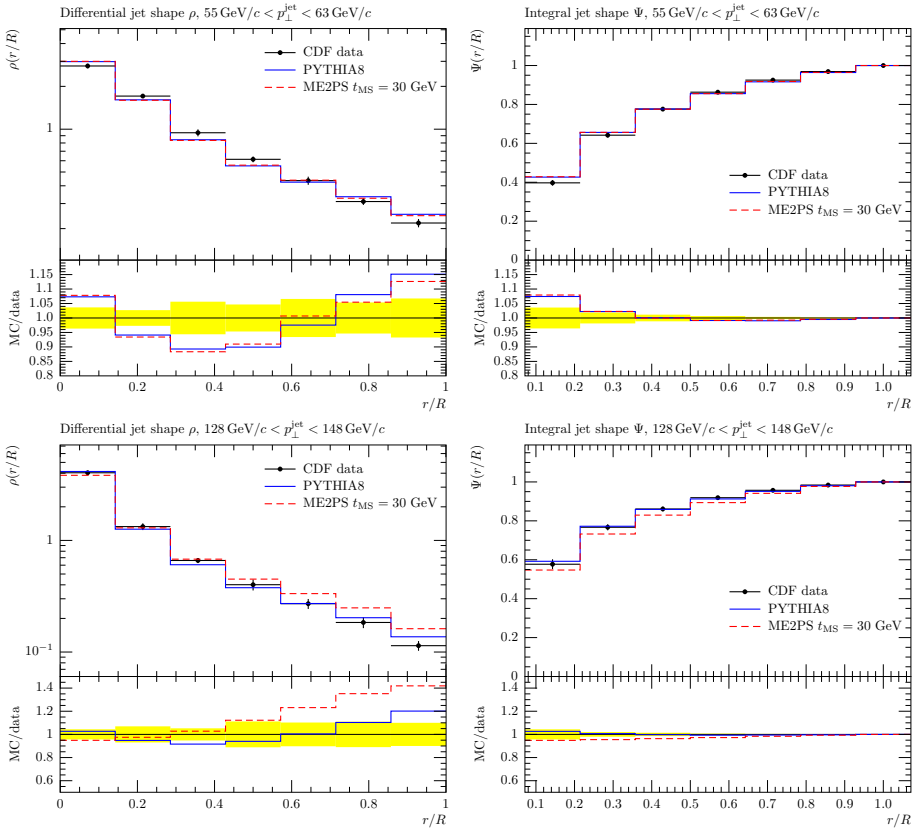

Figure I.22: Jet shapes in QCD events as measured by CDF [30]. The merging scale is $t_{\text{MS}} = \min\{k_{\perp i}\} = 30\,\text{GeV}$. Effects of multiple scatterings and hadronisation are included. The plots were produced with RIVET [24].

- different options for including multiple scatterings.

In all these cases we found the effects to be small.

However, we found that in some cases there are large merging scale dependences from unitarity violations. These problems have been noted before in other CKKW-based algorithms [18, 19], and arise from the fact that what is exponentiated in the Sudakov form factors is only the parton shower approximation to the matrix elements, rather than the matrix elements themselves. In addition, the phase space integrated over in the Sudakov may differ from the full phase space available to the matrix element.

For our implementation, one would expect the unitarity violations to be diminished in the cases where PYTHIA8 already include a matrix-

element reweighting of the first parton shower emission (similar to what is done in POWHEG [12, 31]). However, we found that the effects on the contrary are very large, and traced the reason for this to the fact that the default tune of PYTHIA8 uses a rapidity ordering for the initial-state shower in addition to the ordering in the transverse momentum evolution scale. This results in a severe restriction of the phase space over which Sudakov form factors are integrated, giving increased merging scale dependences. When removing the rapidity ordering, the unitarity violations are reduced to an almost negligible effect.

An important result of our investigations is that the PYTHIA8 shower (without enforced rapidity ordering) actually is quite good at describing the hardness of multi-jet events, as long as the hardest few jets are generated according to the exact matrix elements. Of course, there may be special observables related to details in the correlations between jets, where merging with high-multiplicity matrix elements is still necessary to get a correct description, but for the main features of multi-jet event it seems to be enough to merge with a limited number of extra jets.

Before our CKKW-L implementation can be used for reliable predictions and comparisons with experimental data, the parameters of PYTHIA8 need to be retuned. We have shown that for $e^+e^- \to$ jets, the merging with multi-jet matrix elements barely changes the description of data, and we can assume that the parameters for the hadronisation and final state showers will not need to be substantially changed. Furthermore, for pure QCD processes in hadronic collisions, the effects of multi-jet merging are again very modest, except for very high transverse momentum jets, so also for minimum bias and underlying event observables the tuning needed can be assumed to be minor. On the other hand, for electro-weak processes and for very hard jets in pure QCD processes in hadronic collisions the merging gives quite substantial effects, which means retuning is necessary. To get stable results, this new tune should be done without the rapidity ordering discussed above.

Acknowledgements

We are grateful to Richard Corke and Torbjörn Sjöstrand for useful discussions and explanations of the technical details of the PYTHIA8 machinery.

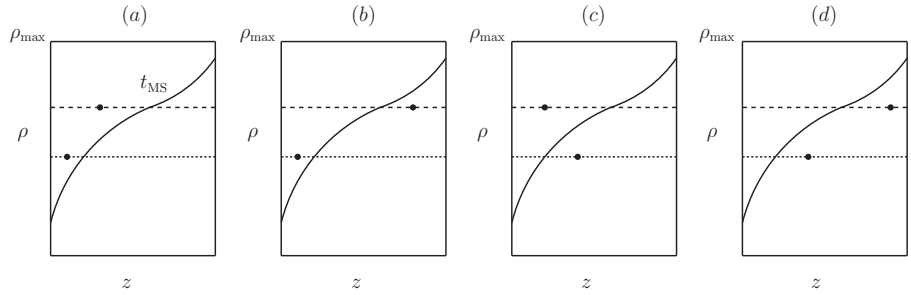

Figure I.A1: A schematic view of how the two-parton phase space is filled in CKKW-L. The figure illustrates how two partons at evolution scales ρ_1 and ρ_2 can be classified in terms of a merging scale t_{MS} defined in the variable t. The vertical axis is the shower ordering scale (which is different from the t-scale) and the horizontal axis is an auxiliary splitting variable. The different states are evolved from different matrix-element samples: (a) starts from the 2-jet ME, (b) the 0-jet ME, (c) the 1-jet ME, and finally (d) is evolved starting from the 0-jet ME.

I.A Comments on the logarithmic accuracy of CKKW-L

Here, we would like to elaborate on how the logarithmic accuracy of the shower is preserved in CKKW-L. This discussion is independent of the functional form of the merging scale variable. For the sake of illustration, let us analyse how the phase space for two additional partons is filled by the merging. As shown in Figure I.A1, there are four different ways in which two shower emissions at scales ρ_1 and ρ_2 can be classified in the variable t. Let the merging scale t_{MS} separate the regions of low and high t, as sketched in the Figure I.A1.

In panel (a), the two partons are inside the matrix element region and as such should be generated by the matrix element generator. Sudakov form factors are added in the way discussed in I.4.3. Notice that this is done by performing trial showers, i.e. that we discard the event if $\rho_1 > \rho_{trial} > \rho_2$, and we never change reclustered states or the matrix element configuration. In this way, for non-zero weighted events, every ME configuration is treated exactly as in the parton shower. It is also clear that panel (d), a configuration with two jets which are soft in t should come from the parton shower. Panel (c) provides the next complicated region. Since region (a) is already correctly accounted for, we veto shower emissions that would evolve the state into one in (a). This means that all states which evolved from a matrix element state

with one jet above t_{MS}, and which have non-zero weight, i.e. with the first emission below t_{MS} or no emission at all, are produced by PS evolution. As outlined in section I.4.3, Sudakov form factors below the reconstructed evolution scale of the ME emission are added by using the full shower when producing trial emissions. We ensure in this way that form factors are added to the ME one-jet configuration in the correct parton shower manner.

To our understanding, the truncated shower approach and CKKW-L only differ in their treatment of panel (b). Let us clarify this statement. In CKKW-L, we define the ME region to contain the $n \leq N$ hardest jets in the evolution variable ρ, which are also above the cut in t. Once we are inside the PS region, we believe the shower is performing well, so that all further emissions will be taken from the parton shower. The first emission in panel (b) is already in the PS region. Thus, every further splitting is taken from the shower. For the example this means that this two jet state is generated from the 0-jet ME sample. Since the shower is the only ingredient in how the state is produced, the accuracy of the shower is preserved.

Truncated showers differ, in that they allow what we call a pure PS state to evolve into something which could have evolved from a ME 1-jet state. Here, the emission is kept, the reclustered state changed, and evolved further until the scale ρ_2 is reached. Then, an emission with the reconstructed ME splitting variables is forced. In this way, the path how the state was reached is correctly described, and the accuracy of the shower is retained. Truncated showering is allowed if the emissions that were inserted before the hard emission are soft and did not change the flavour of the line that will emit the hard jet.

This example reveals the different philosophies behind the CKKW-L and Truncated Shower approaches. In CKKW-L, a compromise is made in that only the $n \leq N$ emissions hardest in the evolution variable, and above the merging scale cut t_{MS}, are corrected with matrix element configurations. Thus, in comparison to using truncated showers, a smaller region of phase space have a matrix element structure. However, we are allowed to use the full shower to generate no-emission probabilities.

When using truncated showers, the flavour of the splitting lines has to be conserved in order to be able to attach the ME emission, i.e. truncated showers only allow gluon emissions. Also, splittings in the truncated showers cannot be allowed to remove too much momentum from the line, since otherwise, the ME emission could not be forced. These restrictions make the Sudakov form factors differ slightly between the full

shower and the truncated shower, though differences are sub-leading and might be tiny in an actual implementation.

Summarising, we believe that both CKKW-L and the Truncated Shower approach have to compromise in regions with t_{MS}-unordered splittings. In CKKW-L, only the hardest partons in the evolution variable will be corrected with tree-level matrix elements, as long as they are above t_{MS} as well. This effectively means that the shower evolution variable should be some measure of hardness, since otherwise, only small regions of the relevant phase space will be endowed with corrections. Choosing e.g. a shower with an ordering variable defined by angles would not be suitable. Truncated Shower prescriptions allow correcting larger parts of the phase space with ME configurations, though at the expense of compromising in the generation of Sudakov form factors. This approach is particularly suited if the evolution variable does not provide a hardness measure, since then, the differences in the Sudakov form factors are vanishing, while large fractions of the phase space can be described by ME emissions. Since the evolution in transverse momentum provides a good hardness measure, CKKW-L provides a natural merging scheme in PYTHIA8.

I.B Reconstructing shower splitting probabilities and intermediate states

In a numerical fixed order calculation, different Feynman graphs can contribute to a particular phase space point. The analogue in a parton shower is that a multitude of different sequences of shower splittings can fill the same phase space point. We describe in this appendix the construction and choice of parton shower histories. The prescriptions below are implemented in PYTHIA8, with the code being publicly available from version 8.157 onwards. Given a matrix element state S_{+n}, all possible intermediate states, splitting probabilities and splitting scales are reconstructed. We first detail how splitting probabilities are calculated and used to choose a particular path of shower splittings. We will after this outline how intermediate states are constructed.

I.B.1 Calculation of splitting probabilities

When assigning a parton shower history to a matrix element state, we have to decide on how to choose amongst all possible splitting sequences. Our choice of a suitable discriminant between these "paths" is

guided by the collinear factorisation of n-particle matrix elements:

$$d\sigma_n = \mathcal{L}_n(x_n, t_n) F_n \left|\mathcal{M}_n\right|^2 d\Phi_n \approx \frac{\alpha_s}{2\pi}\frac{1}{Q^2} P(z) \mathcal{L}_n(x_n, t_n) F_n \left|\mathcal{M}_{n-1}\right|^2 \frac{dk_\perp^2 dz}{z(1-z)} \frac{d\phi}{2\pi} d\Phi_{n-1} \tag{I.B1}$$

where F_m is the flux factor and $\mathcal{L}_m$ the parton luminosity for the m-parton final state using the factorisation scale t_n, while $(k_\perp^2, z, \phi)$ are the splitting variables, Q^2 the virtuality of the splitting parton, and $P(z)$ is the DGLAP splitting kernel for the splitting. The integration measure is given by

$$d\Phi_m = d\phi_m \frac{dx_m^+}{x_m^+} \frac{dx_m^-}{x_m^-}, \tag{I.B2}$$

where $d\phi_m$ is the m-particle phase space volume and $x_m^\pm$ are the momentum fractions of the incoming partons moving in $\pm z$ direction. Using the fact that

$$\mathcal{L}_n(x_n, t_n) = x_n^+ f_n^+(x_n^+, t_n) x_n^- f_n^-(x_n^-, t_n) \text{ , with } \mathcal{L}_n(x_n, t_n) = \mathcal{L}_{n-1}(x_{n-1}, t_{n-1}) \text{ for FSR, and} \tag{I.B3}$$

$$F_n = \begin{cases} F_{n-1} & \text{for FSR} \\ z F_{n-1} & \text{for ISR} \end{cases}$$

as well as the definition of the evolution variable in eqs. (I.7) and (I.8), we can write the factorised transition cross section as

$$d\sigma_n \approx \begin{cases} \left[\frac{\alpha_s}{2\pi}\frac{P(z)}{\rho} dk_\perp^2 dz \frac{d\phi}{2\pi}\right] d\sigma_{n-1}, & \text{for FSR;} \\ \left[\frac{\alpha_s}{2\pi}\frac{x_n^+ f_n^+(x_n^+, t_n)}{x_{n-1}^+ f_{n-1}^+(x_{n-1}^+, t_{n-1})}\frac{P(z)}{\rho} dk_\perp^2 dz \frac{d\phi}{2\pi}\right] d\sigma_{n-1} & \text{for ISR.} \end{cases} \tag{I.B4}$$

To illustrate initial state radiation, we have here chosen the parton moving along $+z$ direction to split. Iterating this procedure down to the desired Born-level state represented by $m = 0$, we can construct one path of collinear splittings by which we may have arrived at the n-particle state. We can use the sum over all different possible paths p,

$$d\sigma_n \approx \left[\sum_p \prod_{i=1}^{n} \frac{\alpha_s}{2\pi} \frac{x_{ip} f_{ip}(x_{ip}, \rho_{ip})}{x_{i-1p} f_{i-1p}(x_{i-1p}, \rho_{ip})} \frac{P_{ip}(z_{ip})}{\rho_{ip}} dk_{\perp ip}^2 dz_{ip} \frac{d\phi_{ip}}{2\pi}\right] d\sigma_0 \,, \tag{I.B5}$$

where $(\rho_{ip}^2, z_{ip}, \phi_{ip})$ and P_{ip} are the reconstructed splitting variables and splitting function for the i'th splitting in the path p, as an approximation of the n-parton cross section. The PDF ratio will equal unity for

final state splitting. We can make this correspondence exact for the very first splitting, by adding matrix element corrections to the splitting kernel and finding a common integration measure for the joined evolution along the possible paths, as will be addressed in the following. The very first emission can be attributed to either a splitting of dipole end "1", or of dipole end "2". If the momentum of dipole end $i \in \{1,2\}$ after the splitting is p_i, and the momentum of the emitted parton is p_3, we define

$$Q^2_{1i} = \begin{cases} (p_i + p_3)^2 & \text{for FSR} \\ (p_i - p_3)^2 & \text{for ISR} \end{cases} \qquad z_{1i} = \begin{cases} \frac{x_i}{x_i+x_3}, \text{with } x_k = \frac{2p_k \sum_{j=1}^3 p_j}{(p_1+p_2+p_3)^2} & \text{for FSR} \\ \frac{(p_1+p_2-p_3)^2}{(p_1+p_2)^2} & \text{for ISR} \end{cases}$$

$$Q^2_{1q\neq p} = \begin{cases} Q^2_{11} & \text{if } p = 2 \\ Q^2_{12} & \text{if } p = 1 \end{cases} \qquad m^2_{Dip} = (p_1 + p_2 + p_3)^2 \text{ for FSR}$$

With this notation, a joined evolution equation is given by

$$d\mathcal{P}_{\text{FSR}} = \left[\sum_{p=1}^{2} \frac{\alpha_s}{2\pi} \frac{P_{1p}(z_{1p}) P_{p\text{MEcorr}}}{Q^2_{1p}} \frac{(1-z_{1p}) m^2_{Dip}}{Q^2_{11} + Q^2_{12}} \right] dp^2_\perp dy \tag{I.B6}$$

$$d\mathcal{P}_{\text{ISR}} = \left[\sum_{p=1}^{2} \frac{\alpha_s}{2\pi} \frac{x_{1p} f_{1p}(x_{1p}, \rho_{1p})}{x_{0p} f_{0p}(x_{0p}, \rho_{1p})} P_{1p}(z_{1p}) P_{p\text{MEcorr}} \frac{(1-z_{1p}) Q^2_{1q\neq p} + \rho_{reg}}{(1-z_{1p})^2 Q^2_{11} Q^2_{12} + (1-z_{1p})^2 \rho_{reg} \hat{s} + \rho^2_{reg}} \right] dQ^2 dz \,. \tag{I.B7}$$

The common integration measures for both paths were defined by introducing the variables

$$p^2_\perp = \frac{Q^2_{11} Q^2_{12}}{m^2_{Dip}}, \quad y = \frac{1}{2} \ln \frac{Q^2_{12}}{Q^2_{11}} \quad \text{for the FSR case, and} \tag{I.B8}$$

$$dQ^2 = d\,|Q_{11,12}| \quad z = z_{11} = z_{12} \quad \text{for the ISR case.} \tag{I.B9}$$

For initial state splittings, the weight takes a more complicated form since in PYTHIA8, infrared singularities are regularised by the introduction of a small scale ρ_{reg}. This is inspired by the regularisation of multiple interactions using arguments relating to colour screening effects [20]. For vanishing ρ_{reg}, the weight for the first splitting of initial particles again takes the form given in eq. (I.B4). Note that we keep α_s fixed, as the running of α_s is corrected for later in the algorithm. Also, the change in incoming parton content, compensated by ratios of parton distributions, will be corrected later on. Hence, the weight for each splitting should not contain α_s or PDF ratio factors. The product of these

weights of individual splittings in a path will then be used as the weight when choosing a path with the normalised probability

$$w_p = \frac{w_{1p}(z_{1p}) \prod_{i=2}^{n} \frac{P_{ip}(z_{ip})}{\rho_{ip}}}{\sum_r w_{1r}(z_{1r}) \prod_{i=2}^{n} \frac{P_{ir}(z_{ir})}{\rho_{ir}}} \quad \text{where} \tag{I.B10}$$

$$w_{1p}(z_{1p}) = \begin{cases} \frac{P_{1p}(z_{1p}) P_{p\text{MEcorr}}}{Q_{1p}^2} \frac{(1-z_{1p}) m_{Dip}^2}{Q_{11}^2 + Q_{12}^2} & \text{for FSR} \\ P_{1p}(z_{1p}) P_{p\text{MEcorr}} \frac{(1-z_{1p}) Q_{1q\neq p}^2 + \rho_{reg}}{(1-z_{1p})^2 Q_{11}^2 Q_{12}^2 + (1-z_{1p})^2 \rho_{reg} \hat{s} + \rho_{reg}^2} & \text{for ISR} \end{cases} \tag{I.B11}$$

In section I.5, we compare this probabilistic prescription with a winner-takes-it-all strategy based on the smallest sum of transverse momenta, and observe minor, though visible, differences.

I.B.2 Reconstruction of intermediate states

Given an n-parton phase space point S_{+n} from a matrix element generator, we explicitly construct all possible intermediate states $S_{+0} \ldots, S_{+n-1}$ in all paths p by reclustering allowed shower emissions. For the construction of the state S_{+i}, given that we have the state S_{+i+1}, this rather complicated step is achieved by inverting all the changes the shower would have applied in the construction of the emission. This means that we need construct

1. The underlying momenta $\tilde{p} = \{\tilde{p}_0, \ldots, \tilde{p}_{k+i}\}$ from the momenta $p = \{p_0, \ldots, p_{k+i+1}\}$;
2. The underlying flavour configuration $\widetilde{\mathcal{F}}_{+i}$ from the configuration $\mathcal{F}_{+i+1}$;
3. The underlying colour configuration $\widetilde{\mathcal{C}}_{+i}$ from $\mathcal{C}_{+i+1}$.

In the following, write "before" for values before the clustering, and "after" for values after the clustering.

Reclustering of momenta

The construction of the reclustered momenta $\tilde{p}$ from the momenta p is achieved by exactly reverting all changes PYTHIA8 would have done if the showers would have constructed an emission resulting in the momenta p. Formally speaking, this means that we invert the radiative phase space mapping of the shower. The construction of the momentum of an emission in PYTHIA8 differs between initial state and final state splittings, leading to different prescriptions how underlying kinematics $\tilde{p}$ are constructed.

For a final state emission with a final state recoiler, this means that the momenta of the reconstructed radiator and recoiler in the rest frame of the dipole are set to

$$p^{\mu}_{\text{radiator, after}} = \left(0,\, 0,\, \frac{m_{Dip}}{2},\, \frac{m_{Dip}}{2}\right), \qquad p^{\mu}_{\text{recoiler, after}} = \left(0,\, 0,\, -\frac{m_{Dip}}{2},\, \frac{m_{Dip}}{2}\right)$$

and then rotated and boosted from the rest frame of the decaying dipole[3] to the event centre-of-mass frame[4].

For final state splittings with an initial state recoiler, the shower would have taken the energy (four-momentum) for the emitted particle from the beam. This steps is undone after the boost to the event centre-of-mass frame by setting the recoiler momentum according to

$$p^{\mu}_{\text{recoiler, after}} = 2 \cdot p^{\mu}_{\text{recoiler, before}} - p^{\mu,\,\text{after Lorentz transformation}}_{\text{recoiler, after}}.$$

For initial state splittings, PYTHIA8 distributes the recoil among all final state particles, making the inversion of this momentum mapping more complicated. We will denote all unchanged momenta of the original $2 \to n$ process by p_i. The momenta of the partons involved in the splitting are denoted by p_{mother}, p_{sister} and p_{partner}. When referring to p_{mother}, p_{sister} or p_{partner} in the following we always think about the momenta of these particles at the current step in the construction of reclustered kinematics. Inverting the construction of kinematics of PYTHIA8 proceeds as follows:

1. Undo the rotation with

$$\phi = \arctan\left(\frac{[p_{\text{sister}}]_y}{[p_{\text{sister}}]_x}\right)$$

   that PYTHIA8 would have done, by rotating all momenta with $-\phi$.

2. Transform all momenta from the event centre-of-mass frame[5] to the centre-of-mass frame[6] of the momenta $p^{\mu}_b = p^{\mu}_{\text{daughter}} = p^{\mu}_{\text{mother}} - p^{\mu}_{\text{sister}}$ and $p^{\mu}_{\text{recoiler}} = p^{\mu}_{\text{partner}}$. Notice that we transform to the centre-of-mass frame of the off-shell momentum p_{daughter}.

[3] Defined by $\vec{p}_{\text{radiator, before}} + \vec{p}_{\text{emitted, before}}$ aligned along $+z$-direction, $\vec{p}_{\text{recoiler, before}}$ aligned along $-z$-direction.

[4] Defined by the orientation of the momenta $\vec{p}_{\text{radiator, before}} + \vec{p}_{\text{emitted, before}}$ and $\vec{p}_{\text{recoiler, before}}$ taken from the unchanged $2 \to n$ state, where these are not anti-parallel.

[5] Defined by the orientation of the momenta p_{daughter} and p_{recoiler} in the rotated, but otherwise unchanged $2 \to n$ process.

[6] Defined by $\vec{p}_{\text{daughter}}$ being aligned to the $+z$-direction and p_{recoiler} aligned to -z-direction.

3. Undo the
$$-\theta = -\arctan\left(\frac{\sqrt{[p_{\text{mother}}]_x^2 + [p_{\text{mother}}]_y^2}}{[p_{\text{mother}}]_z}\right)$$
rotation that PYTHIA8 would have done by rotating all momenta with θ.
4. Construct the on-shell momenta p_{daughter} and p_{recoiler} by resetting
$$p^\mu_{\text{daughter}} = \left(0,\, 0,\, \tfrac{1}{2}\hat{s},\, \tfrac{1}{2}\hat{s}\right) \qquad p^\mu_{\text{recoiler}} = \left(0,\, 0, -\frac{1}{2}\hat{s},\, \frac{1}{2}\hat{s}\right),$$
where
$$\hat{s} = z x_1 x_2 \cdot E^2_{\text{CM}} \qquad \text{and} \qquad x_1 = \frac{2E_1}{E_{\text{CM}}},\; x_2 = \frac{2E_2}{E_{\text{CM}}},\; z = \frac{\left(p_1^\mu + p_2^\mu - p_3^\mu\right)^2}{\left(p_1^\mu + p_2^\mu\right)^2}.$$
5. Boost along the z-axis to the frame where the energy fraction of the newly constructed p^μ_{recoiler} is the original value x_2, i.e. along the vector
$$\vec{p}_{\text{boost}} = \left(0,\, 0, \frac{z \cdot x_1 - x_2}{z \cdot x_1 + x_2}\right).$$
After this boost, the newly constructed p^μ_{recoiler} should be identical to p_2^μ
6. Undo the initial $-\phi$ rotation by a rotation with ϕ.

These changes allow us to reconstruct the state from which PYTHIA8 would have constructed the matrix element momenta if the shower would have produced a splitting at the reconstructed splitting scale. We tested that this method of inverting the shower splitting kinematics exactly reproduces lower multiplicity states from states with additional shower emissions. We found complete agreement, since this construction explicitly inverts the momentum mapping of the shower.

Reconstruction of the underlying flavour structure

To reconstruct the intermediate state S_{+i}, we further have to assign the correct flavour structure $\widetilde{\mathcal{F}}_{+i}$. With the notation $f(k)$ and $\bar{f}(k)$ for the flavour of particle k and the antiparticle to k, the flavour mapping can be accomplished by following the rules:

1. If the emitted parton is a gluon, then
$$f(\text{radiator, after}) = f(\text{radiator, before})$$
2. If the emitted parton is a quark, and the radiating parton is a gluon, then
$$f(\text{radiator, after}) = \begin{cases} f(\text{emitted, before}) & \text{in FSR,} \\ \bar{f}(\text{emitted, before}) & \text{in ISR,} \end{cases}$$
3. If the emitted parton is a quark, and the radiating parton is the corresponding antiquark, then
$$f(\text{radiator, after}) = \begin{cases} \text{g} & \text{in FSR,} \\ \text{not possible} & \text{in ISR,} \end{cases}$$
4. If the emitted parton is a quark, and the radiating parton is a quark of the same flavour, then
$$f(\text{radiator, after}) = \begin{cases} \text{not possible} & \text{in FSR,} \\ \text{g} & \text{in ISR,} \end{cases}$$

This exhausts the list of QCD flavour mappings in PYTHIA8, so that following these rules, the flavour configuration $\widetilde{\mathcal{F}}_{+i}$ of the state S_{+i} can be reconstructed.

Reconstruction of the underlying colour structure

Finally, we need to construct the colour configuration $\widetilde{\mathcal{C}}_{+i}$. Let us write c ($\bar{c}$) for the colour (anticolour) of partons, and indicate the parton to be reconstructed by a subscript r. After flavours have been assigned, the colour of the parton p_r can be found by following the rules

1. For final state splittings with a gluon involved as either emitted or radiating parton, i.e.
$$\text{q}_r \to \text{q}\text{g}_{emt}\,, \quad \text{q}_r \to \text{g}\text{q}_{emt}\,, \quad \bar{\text{q}}_r \to \bar{\text{q}}\text{g}_{emt}\,, \quad \bar{\text{q}}_r \to \text{g}\bar{\text{q}}_{emt}\,, \quad \text{g}_r \to \text{g}\text{g}_{emt} \quad \text{(FSR)}$$
remove the index appearing both as colour and anticolour in the (emitted, radiating)–parton pair. Set the leftover colour and anticolour as the colour and anticolour of p_r, i.e.
$$\begin{aligned} &c_{\text{q}_r} = c_{g_{emt}}\,,\ \bar{c}_{\text{q}_r} = 0 \\ &c_{\bar{\text{q}}_r} = 0\,,\ \bar{c}_{\bar{\text{q}}_r} = \bar{c}_{g_{emt}} \\ &c_{\text{g}_r} = c_{g_{emt}}\,,\ \bar{c}_{\text{g}_r} = \bar{c}_{\text{g}_{rad}} \qquad \text{or} \qquad c_{\text{g}_r} = c_{g_{rad}}\,,\ \bar{c}_{\text{g}_r} = \bar{c}_{g_{emt}} \end{aligned}$$

The second possibility for $g_r \to g g_{emt}$ can occur if the matrix element generator produced a non-planar colour flow.

2. For final state splittings with quark and antiquarks as emitted and radiating partons, i.e.

$$g_r \to q\bar{q}_{emt}\,, \quad g_r \to \bar{q}q_{emt} \qquad \text{(FSR)}$$

set the colour of g_r to the quark colour, the anticolour to the antiquark anticolour. This means

$$c_{g_r} = c_q\,,\ \bar{c}_{g_r} = \bar{c}_{\bar{q}}$$

irrespectively of whether the quark or the antiquark is considered the emitted parton.

3. For initial state splittings with an emitted gluon, i.e.

$$g \to g_r g_{emt}\,, \quad q \to q_r g_{emt} \qquad \text{(ISR)}$$

remove the index appearing as colour (or anticolour) both in the emitted and radiating parton. If a colour (anticolour) index remains in the initial state, set the colour (anticolour) of p_r to the remaining initial state colour (anticolour), and set the p_r anticolour (colour) to the remaining final state colour (anticolour) index.

4. For initial state splittings with an emitted quark (antiquark) and a gluon radiator, i.e.

$$g \to q_r\bar{q}_{emt}\,, \quad g \to \bar{q}_r q_{emt} \qquad \text{(ISR)}$$

set the p_r colour (anticolour) to the colour (anticolour) of the radiating gluon.

5. For initial state splittings with an emitted quark (antiquark) and a quark (antiquark) radiator, i.e.

$$q \to g_r q_{emt}\,, \quad \bar{q} \to g_r\bar{q}_{emt} \qquad \text{(ISR)}$$

set the g_r colour (anticolour) to the anticolour (colour) of the emitted parton. Set the reconstructed gluon anticolour (colour) to the anticolour (colour) of the radiating parton.

Once a pair of radiating and emitted partons is chosen, these rules can be applied to deduce the colour configuration $\widetilde{\mathcal{C}}_{+i}$ of the state S_{+i}.

Combining the inversion of the parton shower kinematics, the construction of the underlying flavour configuration and reclustering of

colours, the complete state S_{+i} can be generated. We have extensively tested that, given a state S_{+n}, our implementation exactly reproduces all states $S_{+(m<n)}$, if the states $S_{+m+1}, \ldots S_{+n}$ were generated by shower splittings, verifying that we have used the exact inversion of the radiative mappings of PYTHIA8.

I References

[1] M. L. Mangano, M. Moretti, F. Piccinini, R. Pittau, and A. D. Polosa, "ALPGEN, a generator for hard multiparton processes in hadronic collisions," *JHEP* **07** (2003) 001, arXiv:hep-ph/0206293.

[2] M. Mangano, "The so-called MLM prescription for ME/PS matching." http://www-cpd.fnal.gov/personal/mrenna/tuning/nov2002/mlm.pdf. Talk presented at the Fermilab ME/MC Tuning Workshop, October 4, 2002.

[3] F. Maltoni and T. Stelzer, "MadEvent: Automatic event generation with MadGraph," *JHEP* **02** (2003) 027, hep-ph/0208156.

[4] S. Mrenna and P. Richardson, "Matching matrix elements and parton showers with HERWIG and PYTHIA," *JHEP* **05** (2004) 040, arXiv:hep-ph/0312274.

[5] N. Lavesson and L. Lönnblad, "Merging parton showers and matrix elements – back to basics," *JHEP* **04** (2008) 085, arXiv:0712.2966 [hep-ph].

[6] J. Alwall *et al.*, "Comparative study of various algorithms for the merging of parton showers and matrix elements in hadronic collisions," *Eur. Phys. J.* **C53** (2008) 473–500, arXiv:0706.2569 [hep-ph].

[7] S. Catani, F. Krauss, R. Kuhn, and B. R. Webber, "QCD matrix elements + parton showers," *JHEP* **11** (2001) 063, arXiv:hep-ph/0109231.

[8] L. Lönnblad, "Correcting the colour-dipole cascade model with fixed order matrix elements," *JHEP* **05** (2002) 046, arXiv:hep-ph/0112284.

[9] L. Lönnblad, "ARIADNE version 4: A Program for simulation of QCD cascades implementing the color dipole model," *Comput. Phys. Commun.* **71** (1992) 15–31.

[10] F. Krauss, "Matrix elements and parton showers in hadronic interactions," *JHEP* **08** (2002) 015, arXiv:hep-ph/0205283.

[11] N. Lavesson and L. Lönnblad, "W + jets matrix elements and the dipole cascade," *JHEP* **07** (2005) 054, arXiv:hep-ph/0503293.

[12] P. Nason, "A new method for combining NLO QCD with shower Monte Carlo algorithms," *JHEP* **11** (2004) 040, arXiv:hep-ph/0409146.

[13] T. Sjöstrand, S. Mrenna, and P. Skands, "A Brief Introduction to PYTHIA 8.1," *Comput. Phys. Commun.* **178** (2008) 852–867, arXiv:0710.3820 [hep-ph].

[14] J. Tully, "Monte Carlo simulations of hard QCD radiation," *Monte Carlo simulations of hard QCD radiation. Doctoral Thesis, Durham University* (2009) .

[15] T. Gleisberg *et al.*, "Event generation with SHERPA 1.1," *JHEP* **02** (2009) 007, arXiv:0811.4622 [hep-ph].

[16] J. Alwall *et al.*, "A standard format for Les Houches Event Files," *Comput. Phys. Commun.* **176** (2007) 300–304, hep-ph/0609017.

[17] M. Cacciari and G. P. Salam, "Dispelling the N**3 myth for the k(t) jet-finder," *Phys. Lett.* **B641** (2006) 57–61, arXiv:hep-ph/0512210.

[18] K. Hamilton and P. Nason, "Improving NLO-parton shower matched simulations with higher order matrix elements," *JHEP* **1006** (2010) 039, arXiv:1004.1764 [hep-ph].

[19] S. Höche, F. Krauss, M. Schönherr, and F. Siegert, "NLO matrix elements and truncated showers," arXiv:1009.1127 [hep-ph].

[20] R. Corke and T. Sjöstrand, "Interleaved Parton Showers and Tuning Prospects," *JHEP* **03** (2011) 032, arXiv:1011.1759 [hep-ph].

[21] S. Höche, F. Krauss, S. Schumann, and F. Siegert, "QCD matrix elements and truncated showers," *JHEP* **05** (2009) 053, arXiv:0903.1219 [hep-ph].

[22] J. R. Andersen and J. M. Smillie, "Multiple Jets at the LHC with High Energy Jets," *JHEP* **06** (2011) 010, arXiv:1101.5394 [hep-ph].

[23] **OPAL** Collaboration, G. Abbiendi *et al.*, "A Simultaneous measurement of the QCD color factors and the strong coupling," *Eur.Phys.J.* **C20** (2001) 601–615, arXiv:hep-ex/0101044 [hep-ex].

[24] A. Buckley *et al.*, "Rivet user manual," arXiv:1003.0694 [hep-ph].

[25] **ATLAS** Collaboration, G. Aad *et al.*, "Measurement of the production cross section for W-bosons in association with jets in pp collisions at sqrt(s) = 7 TeV with the ATLAS detector," *Phys.Lett.* **B698** (2011) 325–345, arXiv:1012.5382 [hep-ex].

[26] **CDF** Collaboration, T. Aaltonen *et al.*, "Measurement of inclusive jet cross-sections in Z/gamma*($\rightarrow e^+e^-$) + jets production in $p\bar{p}$ collisions at $\sqrt{s}$ = 1.96-TeV," *Phys.Rev.Lett.* **100** (2008) 102001, arXiv:0711.3717 [hep-ex].

[27] **CDF** Collaboration, T. Aaltonen *et al.*, "Studying the Underlying Event in Drell-Yan and High Transverse Momentum Jet Production at the Tevatron," *Phys. Rev.* **D82** (2010) 034001, arXiv:1003.3146 [hep-ex].

[28] **CDF** Collaboration, T. Aaltonen *et al.*, "Invariant Mass Distribution of Jet Pairs Produced in Association with a W boson in $p\bar{p}$ Collisions at $\sqrt{s} = 1.96$ TeV," *Phys.Rev.Lett.* **106** (2011) 171801, arXiv:1104.0699 [hep-ex].

[29] G. C. Blazey *et al.*, "Run II jet physics," arXiv:hep-ex/0005012.

[30] **CDF** Collaboration, D. Acosta *et al.*, "Study of jet shapes in inclusive jet production in $p\bar{p}$ collisions at $\sqrt{s} = 1.96$ TeV," *Phys.Rev.* **D71** (2005) 112002, arXiv:hep-ex/0505013 [hep-ex].

[31] S. Frixione, P. Nason, and C. Oleari, "Matching NLO QCD computations with Parton Shower simulations: the POWHEG method," *JHEP* **11** (2007) 070, arXiv:0709.2092 [hep-ph].

II

Unitarising Matrix Element + Parton Shower merging

Leif Lönnblad and Stefan Prestel

Dept. of Astronomy and Theoretical Physics, Lund University, Sweden

Accepted for publication in the Journal of High Energy Physics.
LU-TP 12-42
MCnet-12-14
e-Print: arXiv:1211.4827 [hep-ph].

We revisit the CKKW-L method for merging tree-level matrix elements with parton showers, and amend it with an add/subtract scheme to minimise dependencies on the merging scale. The scheme is constructed to, as far as possible, recover the unitary nature of the underlying parton shower, so that the inclusive cross section is retained for each jet multiplicity separately.

II.1 Introduction

Particularly after the discovery of a Higgs-candidate resonance at ATLAS and CMS, the precise description of multi-jet Standard Model (SM) processes at the LHC remains crucial. Major progress has recently been made in combining calculations of next-to-leading order (NLO) perturbative QCD corrections with Parton Shower (PS) based Monte Carlo event generators [1–8].

In light of the rapid succession of publications on merging multiple NLO calculations with event generators [1, 6–8], it seems hardly arguable that this long-standing issue is resolved. From the point of next-to-leading order accuracy, scepticism about state-of-the-art methods is baseless. It has however also been pointed out that sub-leading logarithmic enhancements could be left after the merging procedure [9–11]. It has to be stressed that initially, this problem is not caused by the extension of tree-level methods to NLO, but already appears for CKKW-inspired tree-level merging schemes [12–16]. The introduction of a merging scale (t_{MS}) introduces logarithmic dependencies, $L = \ln \mu_F / t_{\text{MS}}$, with a dominant leading logarithm $\alpha_{\text{s}}^n L^{2n}$, in the multi-jet tree-level configurations. This leading logarithmic contribution is completely cancelled by the parton shower higher-order corrections to low-multiplicity states, but terms beyond the leading approximation are only partly cancelled. Let us look at one-jet merging in W-boson production, with a strictly leading-logarithmic parton shower. Integrating the W+jet matrix element (ME) over the one-jet phase space introduces the dependencies $\alpha_{\text{s}} L^2$ and $\alpha_{\text{s}} L^1$, while unresolved PS emissions in the zero-jet state produce $\alpha_{\text{s}} L^2$ terms, but with negative sign. In the total cross section, the $\alpha_{\text{s}} L^2$ terms cancel, and only a t_{MS}-dependence beyond the accuracy of the parton shower (i.e. $\alpha_{\text{s}} L^1$-terms) remains. This example is rather academic, since modern parton showers include a matrix-element correction for W+jet production, thus ensuring that in one-jet merging, all dependencies on t_{MS} are cancelled[1]. After the inclusion of matrix element corrections [17–20], the merging scale dependence enters for two-jet merging. However, since control of beyond-leading logarithmic contributions cannot be universally exerted in a parton shower, it is clear that dependencies enter at some level, commonly hoped to be at next-to-next-to-leading logarithmic accuracy. The logarithmic structure of a two-jet tree-level cross section for example has only an approximate

[1] Note that the introduction of ME corrections already endows the PS with the tree-level description of the hardest jet, so that one-jet merging would not be necessary.

equivalent in parton showers, meaning that certainly at $\mathcal{O}(\alpha_s^2)$, subleading contributions are not fully cancelled. This is often, for lack of a better term, referred to as violation of PS unitarity.

We believe it important to investigate this issue more closely. In this publication, we take a step back from the remarkable progress in NLO merging and outline a tree-level merging method that amends the behaviour of parton showers to ensure that no spurious logarithmic enhancements are introduced by including multi-jet matrix elements. The foundation of this method is PS unitarity, i.e. the requirement that the lowest order cross section remains unchanged by methods introduced to ameliorate the description of shapes of observables. It should be noted that in particular the GKS matrix-element-correction method in VINCIA [21, 22] has emphasised a unitarity-based approach before. The aim of this article is more modest, in that we offer a novel prescription of combining the input used in multi-jet merging procedures, moving from the additive scheme of CKKW-inspired methods to an add-and-subtract method that preserves the total inclusive cross section.

This article is structured as follows. Section II.2 is intended as introduction to our perspective on PS unitarity. This will be succeeded by a brief discussion of tree-level merging in the CKKW-L scheme [13, 14, 16] and its problems in section II.3, before we move on to construct a LO merging method that preserves PS unitarity in section II.4. Section II.5 presents results for including additional jets in W-production and QCD dijet processes in the novel procedure, which we call UMEPS (Unitary Matrix Element + Parton Shower merging). Finally, we give a discussion in section II.6 and conclude in section II.7.

II.2 Parton shower unitarity

Without any outside intervention, parton showers act on a lowest order seed cross section as a unitary operator. In other words, showering dresses the constituents of a perturbatively calculated $2 \to 2$ process with radiation, in order to set the stage for hadronisation. By generating soft and collinear emissions, parton showering sums (at least) leading double-logarithmic enhancements to all orders.

Before detailing how this is achieved, let us introduce some notation in order to make the formulae less cluttered. We will also classify partons to be either resolved or unresolved at a particular scale ρ_{MS}. By this, we mean that in a jet algorithm that exactly inverts the parton shower, a parton would be resolved as a jet if the evolution scale at which it was

emitted (ρ), as well as jet separations that have been changed by the emission due to recoil effects, are above ρ_{MS}. For the parton shower to be invertible in a well-defined way, we assume the existence of on-shell intermediate states between splittings. The index MS foreshadows the use of this jet definition as merging scale[2].

The parton shower approximates the effect of virtual corrections on observables sensitive to the scales ρ_i and ρ_{i+1} by integrating DGLAP splitting kernels $P(z)$ over the unresolved phase space. This gives a term

$$\begin{aligned} &- \int_{\rho_{i+1}}^{\rho_i} d\rho\, dz\, \frac{\alpha_s(\rho)}{2\pi} \left\{ \sum_{a\in\{\text{outgoing}\}} \sum_j P_j^a(z) + \sum_{a\in\{\text{incoming}\}} \sum_j \frac{f_j^a(\frac{x_i^a}{z},\rho)}{f_i^a(x_i^a,\rho)} P_j^a(z) \right\} \\ &\qquad \equiv - \int_{\rho_{i+1}}^{\rho_i} d\rho dz \alpha_s(\rho)\, \mathcal{P}_{i+1}(z,\rho)\ , \end{aligned} \tag{II.1}$$

where the first terms on the left-hand side sums all possible unresolved final state emissions, and the second term includes all unresolved initial state splittings. The ratios of parton distribution functions f is only absent if no initial parton is taking part in the (unresolved) emissions. The $\mathcal{P}_{i+1}$ (and P) notation is rather symbolic to permit a certain degree of simplicity. We include symmetry factors and the typical ρ- and z-fractions from approximating the matrix element or multiplying Jacobian factors in P and $\mathcal{P}_{i+1}$, e.g. for an initial state splitting $\bar{q} \to \bar{q}g$, we would have $P = \frac{1}{\rho}\frac{1}{z}\frac{1+z^2}{1-z}$. It can be shown, by performing the z-integration for a specific splitting kernel P, that the PS "virtual corrections" in eq. (II.1) indeed capture the leading logarithmic contributions of virtual corrections. Let us introduce the short-hand

$$f_i(x_i,\rho_i) = f_i^+(x_i^+,\rho_i) f_i^-(x_i^-,\rho_i) \tag{II.2}$$

The Sudakov form factor, resumming unresolved emissions between scales ρ_i and ρ_{i+1}, is given by

$$\Delta_{S_i}(x_i,\rho_i,\rho_{i+1}) \quad = \quad \frac{f_i(x_i,\rho_i)}{f_{i+1}(x_i,\rho_{i+1})} \Pi_{S_{+i}}(x_i,\rho_i,\rho_{i+1}) \tag{II.3}$$

where $\Pi_{S_{+i}}(x_i,\rho_i,\rho_{i+1})$ is the probability of no emission from state S_{+i} between the ρ_i and ρ_{i+1}. The no-emission probability in turn can be

[2] We here restrict ourselves to a particular jet (merging scale) definition, for the sake of clarity. We further assumed that the PS evolution variable is a measure of "hardness", i.e. that soft and collinear divergences are located at $\rho \to 0$. All the following arguments apply for a general merging scale t_{MS}.

expressed as

$$\Pi_{S_{+i}}\left(x_i,\rho_i,\rho_{i+1}\right)=\exp\left\{-\int_{\rho_{i+1}}^{\rho_i}d\rho dz\alpha_{\mathrm{s}}\left(\rho\right)\mathcal{P}_{i+1}\left(z,\rho\right)\right\} \tag{II.4}$$

We have kept x_i as an argument to remember that $\Pi_{S_{+i}}\left(x_i,\rho_i,\rho_{i+1}\right)$ contains x_i-dependent PDF factors through $\mathcal{P}_{i+1}$.

Let us consider the case when no PS emission above a scale ρ_{MS} is generated. The parton shower approximation of the resummed exclusive zero-jet cross section is then

$$\begin{aligned}\frac{d\sigma_0^{ex}}{d\phi_0} &= f_0(x_0,\rho_0)\left|\mathcal{M}_0\left(\rho_0,\mu_R\right)\right|^2\Pi_{S_{+0}}\left(x_0,\rho_0,\rho_{\mathrm{MS}}\right)\\ &= f_0(x_0,\rho_0)\left|\mathcal{M}_0\left(\rho_0,\mu_R\right)\right|^2\\ &- f_0(x_0,\rho_0)\left|\mathcal{M}_0\left(\rho_0,\mu_R\right)\right|^2\int_{\rho_{\mathrm{MS}}}^{\rho_0}d\rho dz\alpha_{\mathrm{s}}\left(\rho\right)\mathcal{P}_1\left(z,\rho\right)\\ &+ f_0(x_0,\rho_0)\left|\mathcal{M}_0\left(\rho_0,\mu_R\right)\right|^2\int_{\rho_{\mathrm{MS}}}^{\rho_0}d\rho_1dz_1\alpha_{\mathrm{s}}\left(\rho_1\right)\mathcal{P}_1\left(z_1,\rho_1\right)\\ &\qquad\times\int_{\rho_{\mathrm{MS}}}^{\rho_1}d\rho_2dz_2\alpha_{\mathrm{s}}\left(\rho_2\right)\mathcal{P}_1\left(z_2,\rho_2\right)+\mathcal{O}(\alpha_{\mathrm{s}}^3)\,,\end{aligned} \tag{II.5}$$

where we have used the fact that

$$\begin{aligned}&\frac{1}{2}\left(\int_{\rho_{\mathrm{MS}}}^{\rho_0}d\rho dz\alpha_{\mathrm{s}}\left(\rho\right)\mathcal{P}_1\left(z,\rho\right)\right)^2\\ &=\int_{\rho_{\mathrm{MS}}}^{\rho_0}d\rho_1dz_1\alpha_{\mathrm{s}}\left(\rho_1\right)\mathcal{P}_1\left(z_1,\rho_1\right)\int_{\rho_{\mathrm{MS}}}^{\rho_1}d\rho_2dz_2\alpha_{\mathrm{s}}\left(\rho_2\right)\mathcal{P}_1\left(z_2,\rho_2\right)\,.\end{aligned} \tag{II.6}$$

The zero-jet PS cross section is exclusive in the sense that no resolved emissions (i.e. emissions above ρ_{MS}) are produced. Beside resumming unresolved contributions to the zero-jet cross section, the parton shower also produces resolved emissions. The parton shower approximation to the cross section for emitting the hardest jet at scale ρ_1 is

$$\frac{d\sigma_1^{in}}{d\phi_0} = d\rho_1dz_1f_0(x_0,\rho_0)\left|\mathcal{M}_0\left(\rho_0,\mu_R\right)\right|^2\alpha_{\mathrm{s}}\left(\rho_1\right)\mathcal{P}_1\left(z_1,\rho_1\right)\Pi_{S_{+0}}\left(x_0,\rho_0,\rho_1\right)\,.$$

$\mathcal{P}_1$ contains PDF ratios and kinematical factors (see definition II.1). The cross section is labelled with *in* for "inclusive", because the emission of further jets below ρ_1, but above ρ_{MS}, is still allowed. Note that $\frac{d\sigma_1^{in}}{d\phi_0}$ is also exclusive in the sense that no resolved emissions above ρ_1 – the scale of the *first* emission – are possible. In the following, we will always call a cross section inclusive if the parton shower can (at least in principle) produce further resolved emissions, and exclusive otherwise.

If only zero- and one-jet states are generated, the total cross section is given by the sum of exclusive zero-jet and inclusive one-jet cross sections. Let us analyse the total cross section in the approximation of having maximally one parton shower emission. It useful to rewrite eq. (II.5) with help of definition eq. (II.4):

$$\begin{aligned}\frac{d\sigma_0^{ex}}{d\phi_0} &= f_0(x_0,\rho_0)\left|\mathcal{M}_0\left(\rho_0,\mu_R\right)\right|^2 \qquad \text{(II.7)}\\ &- f_0(x_0,\rho_0)\left|\mathcal{M}_0\left(\rho_0,\mu_R\right)\right|^2 \int_{\rho_{\text{MS}}}^{\rho_0} d\rho dz \alpha_{\text{s}}\left(\rho\right)\mathcal{P}_1\left(z,\rho\right)\Pi_{S_{+0}}\left(x,\rho_0,\rho\right)\end{aligned}$$

so that the total cross section is[3]

$$\begin{aligned}\sigma^{in} &= \int d\phi_0\left(\frac{d\sigma_0^{ex}}{d\phi_0}+\int d\phi^{(1)}\frac{d\sigma_1^{in}}{d\phi_1}\right)\\ &= \int d\phi_0\Bigg(f_0(x_0,\rho_0)\left|\mathcal{M}_0\left(\rho_0,\mu_R\right)\right|^2\\ &\qquad - f_0(x_0,\rho_0)\left|\mathcal{M}_0\left(\rho_0,\mu_R\right)\right|^2\int_{\rho_{\text{MS}}}^{\rho_0} d\rho dz\alpha_{\text{s}}\left(\rho\right)\mathcal{P}_1\left(z,\rho\right)\Pi_{S_{+0}}\left(x,\rho_0,\rho\right)\Bigg)\\ &+ \int d\phi_0 f_0(x_0,\rho_0)\left|\mathcal{M}_0\left(\rho_0,\mu_R\right)\right|^2\int_{\rho_{\text{MS}}}^{\rho_0} d\rho dz\alpha_{\text{s}}\left(\rho\right)\mathcal{P}_1\left(z,\rho\right)\Pi_{S_{+0}}\left(x_0,\rho_0,\rho\right)\\ &= \int d\phi_0 f_0(x_0,\rho_0)\left|\mathcal{M}_0\left(\rho_0,\mu_R\right)\right|^2 . \qquad \text{(II.8)}\end{aligned}$$

Thus, if the parton shower would stop after the first emission, the total cross section is not changed by the application of the parton shower.

This small sketch does not really ensure that the total cross section is preserved after PS resummation. Parton showering usually generates more than one emission, so that only being concerned with a single emission might not be enough. The above argument can however be extended to any number of emissions. As an example, assume the PS had generated two emissions. Then, the one-jet cross section becomes exclusive by demanding that only one resolved emission has been produced,

$$\begin{aligned}\frac{d\sigma_1^{ex}}{d\phi_0} &= d\rho_1 dz_1 f_0(x_0,\rho_0)\left|\mathcal{M}_0\left(\rho_0,\mu_R\right)\right|^2\\ &\qquad \alpha_{\text{s}}\left(\rho_1\right)\mathcal{P}_1\left(z_1,\rho_1\right)\Pi_{S_{+0}}\left(x_0,\rho_0,\rho_1\right)\Pi_{S_{+1}}\left(x_1,\rho_1,\rho_{\text{MS}}\right) \qquad \text{(II.9)}\end{aligned}$$

[3] We use the notation $\int d\phi_0 \int d\phi^{(1)} \ldots \int d\phi^{(n)} \frac{d\sigma_n^{in}}{d\phi_n}$ to indicate that $d\sigma_n^{in}$ is integrated over the full phase space, i.e. the phase space of the of core process and all n additional emissions.

and we need to add the PS approximation to the two-jet cross section

$$\begin{aligned}\frac{d\sigma_2^{in}}{d\phi_0} &= d\rho_1 dz_1 d\rho_2 dz_2 f_0(x_0,\rho_0)\left|\mathcal{M}_0\left(\rho_0,\mu_R\right)\right|^2 \\ &\quad\times \alpha_s\left(\rho_1\right)\mathcal{P}_1\left(z_1,\rho_1\right)\Pi_{S_{+0}}\left(x_0,\rho_0,\rho_1\right) \\ &\quad\times \alpha_s\left(\rho_2\right)\mathcal{P}_2\left(z_2,\rho_2\right)\Pi_{S_{+1}}\left(x_1,\rho_1,\rho_2\right)\Theta\left(\rho_1-\rho_2\right) \qquad \text{(II.10)}\end{aligned}$$

Now we rewrite II.9 by expanding the second no-emission probability

$$\begin{aligned}\frac{d\sigma_1^{ex}}{d\phi_0} &= d\rho_1 dz_1 f_0(x_0,\rho_0)\left|\mathcal{M}_0\left(\rho_0,\mu_R\right)\right|^2\alpha_s\left(\rho_1\right)\mathcal{P}_1\left(z_1,\rho_1\right)\Pi_{S_{+0}}\left(x_0,\rho_0,\rho_1\right) \\ &\quad\times\left(1-\int_{\rho_{MS}}^{\rho_1}d\rho_2 dz_2\alpha_s\left(\rho_2\right)\mathcal{P}_2\left(z_2,\rho_2\right)\right. \\ &\quad\left.+\int_{\rho_{MS}}^{\rho_1}d\rho_2 dz_2\alpha_s\left(\rho_2\right)\mathcal{P}_2\left(z_2,\rho_2\right)\int_{\rho_{MS}}^{\rho_2}d\rho_3 dz_3\alpha_s\left(\rho_3\right)\mathcal{P}_2\left(z_3,\rho_3\right)+\mathcal{O}(\alpha_s^3)\right) \\ &= d\rho_1 dz_1 f_0(x_0,\rho_0)\left|\mathcal{M}_0\left(\rho_0,\mu_R\right)\right|^2\alpha_s\left(\rho_1\right)\mathcal{P}_1\left(z_1,\rho_1\right)\Pi_{S_{+0}}\left(x_0,\rho_0,\rho_1\right) \\ &\quad\times\left(1-\int_{\rho_{MS}}^{\rho_1}d\rho dz\alpha_s\left(\rho\right)\mathcal{P}_2\left(z,\rho\right)\Pi_{S_{+1}}\left(x_1,\rho_1,\rho\right)\right) \qquad \text{(II.11)}\end{aligned}$$

where we have again used definition II.4 to derive the last equality. If parton showering stops after generating maximally two emissions, the total cross section is given by

$$\sigma^{in} = \int d\phi_0\left(\frac{d\sigma_0^{ex}}{d\phi_0}+\int d\phi^{(1)}\frac{d\sigma_1^{ex}}{d\phi_1}+\int d\phi^{(1)}\int d\phi^{(2)}\frac{d\sigma_2^{in}}{d\phi_2}\right) \qquad \text{(II.12)}$$

By comparing the second term in eq. (II.11) with eq. (II.10), we see that any PS contribution of two resolved partons cancels with terms containing one resolved and one unresolved parton. Already earlier, we saw that contributions with one resolved parton cancel against terms with zero resolved partons. Thus, we again find

$$\sigma^{in} = \int d\phi_0 f_0(x_0,\rho_0)\left|\mathcal{M}_0\left(\rho_0,\mu_R\right)\right|^2$$

It is easy to extend this argument to as many emissions as wanted: Whenever the parton shower generates one emission, the change in the total cross section is counteracted exactly by unresolved contributions to states with one emission less. There is no need to correct the PS approximation of the zero-jet exclusive cross section in the presence of two-jet states – the zero-jet resummation is oblivious of two-jet states. That parton showers are unitary is understandable directly from their construction, since the branching of an underlying n-jet state produces a $n+1$-jet state, which overwrites (i.e. removes) the n-jet state in the wake of the branching.

II.3 The problem with CKKW-L

Let us now review tree-level matrix element merging, more specifically the CKKW-L scheme[4]. We here focus mainly on issues related to parton shower unitarity, and refer to [16] for a detailed description of CKKW-L in PYTHIA8 [23] and to [12–15] for a more general introduction.

Matrix element merging procedures are designed to improve the PS description of multi-jet observables. For this purpose, tree-level matrix element (ME) calculations are combined with the parton shower, i.e. tree-level-weighted phase space points with m "hard process particles" and n additional partons are included in the shower. In the following, we will often use the terms state, event, configuration or the symbol S_{+n} to refer to these $n+m-$body phase space points. As can be inferred from the form of S_{+n}, we will most often understand that the state contains m hard process particles, but not mention these particles explicitly.

A consistent merging removes all overlap between ME states and the PS approximation. This is ensured by introducing a phase space cut ρ_{MS} to separate the ME region from the PS region, and applying no-emission probabilities. The cut dependence is minimised by weighting configurations above and below ρ_{MS} in identical fashion. The CKKW-L scheme constructs and chooses a sequence of lower-multiplicity states (a so-called parton shower history) for each ME event, since factors need to be generated that would, in the parton shower evolution, have contributed though intermediate stages. With the help of the history, ME events will be reweighted with

$$\begin{aligned} w_n &= \frac{x_0 f_0(x_0,\rho_0)}{x_n f_n(x_n,\mu_F)} \times \left(\prod_{i=1}^{n} \frac{x_i f_i(x_i,\rho_i)}{x_{i-1} f_{i-1}(x_{i-1},\rho_i)}\right) \\ &\quad \times \left(\prod_{i=1}^{n} \frac{\alpha_s(\rho_i)}{\alpha_s(\mu_R)}\right) \times \left(\prod_{i=1}^{n} \Pi_{S_{+i-1}}(\rho_{i-1},\rho_i)\right) \times \Pi_{S_{+n}}(\rho_n,\rho_{\text{MS}}) \qquad \text{(II.13)} \\ &= \frac{x_n f_n(x_n,\rho_n)}{x_n f_n(x_n,\mu_F)} \times \prod_{i=1}^{n}\left[\frac{\alpha_s(\rho_i)}{\alpha_{\text{sME}}} \frac{x_{i-1} f_{i-1}(x_{i-1},\rho_{i-1})}{x_{i-1} f_{i-1}(x_{i-1},\rho_i)} \Pi_{S_{+i-1}}(x_{i-1},\rho_{i-1},\rho_i)\right] \\ &\quad \times \Pi_{S_{+n}}(x_n,\rho_n,\rho_{\text{MS}})\,, \qquad \text{(II.14)} \end{aligned}$$

where ρ_i are the reconstructed splitting scales, and S_{+i} the reconstructed intermediate states. The first PDF ratio in eq. (II.13) ensures that all ME configurations are normalised to the same total cross section, given by the lowest order Born-level matrix element. The PDF ratios in brackets

[4] Although most of what we discuss also applies to other CKKW-inspired merging schemes.

account for PDF factors in the shower splitting probabilities $\mathcal{P}_i$ for initial state backward evolution. The running of α_s is correctly included by the second bracket. Finally, double-counting is prevented by multiplying no-emission probabilities.

Let us investigate how the CKKW-L merging prescription changes the lowest-order inclusive cross section. For simplicity, we will highlight merging matrix elements with up to two additional jets with parton showers. In the simplest conceivable case of one-jet merging, applying CKKW-L defines the cross sections

$$\begin{aligned}\frac{d\sigma_0^{ex}}{d\phi_0} &= f_0(x_0,\rho_0)\left|\mathcal{M}_0\left(\rho_0,\mu_R\right)\right|^2\Pi_{S_{+0}}\left(x_0,\rho_0,\rho_{\mathrm{MS}}\right) &\text{(II.15)}\\ &= f_0(x_0,\rho_0)\left|\mathcal{M}_0\left(\rho_0,\mu_R\right)\right|^2\times\left(1-\int_{\rho_{\mathrm{MS}}}^{\rho_0}d\rho dz\alpha_s\left(\rho\right)\mathcal{P}_1\left(z,\rho\right)+\mathcal{O}(\alpha_s^2)\right)\\ \frac{d\sigma_1^{in}}{d\phi_0} &= d\rho_1 dz_1 f_0(x_0,\rho_0)\frac{\alpha_s(\rho_1)}{\alpha_s(\mu_R)}\frac{f_1(x_1,\rho_1)}{f_0(x_0,\rho_1)}\left|\mathcal{M}_1\left(\rho_0,\mu_R\right)\right|^2\Pi_{S_{+0}}\left(x_0,\rho_0,\rho_1\right) &\text{(II.16)}\end{aligned}$$

It is crucial to note that the tree-level one-jet matrix element is in general different from the approximate PS splitting kernels. The inclusive lowest-order cross section is only preserved if

$$\begin{aligned}&f_0(x_0,\rho_0)\left|\mathcal{M}_0\left(\rho_0,\mu_R\right)\right|^2\int_{\rho_{\mathrm{MS}}}^{\rho_0}d\rho dz\alpha_s\left(\rho\right)\mathcal{P}_1\left(z,\rho\right) &\text{(II.17)}\\ &\quad=\int_{\rho_{\mathrm{MS}}}^{\rho_0}d\rho_1 dz_1 d\varphi_1 f_0(x_0,\rho_0)\frac{\alpha_s(\rho_1)}{\alpha_s(\mu_R)}\frac{f_1(x_1,\rho_1)}{f_0(x_0,\rho_1)}\left|\mathcal{M}_1\left(\rho_0,\mu_R\right)\right|^2\ ,\end{aligned}$$

i.e. in the case where the first parton shower emission is distributed exactly according to the one-jet matrix element. In this case, we would not have needed a merging prescription, since the PS would have already produced the correct result.

Though correcting the first PS splitting to the full tree-level result is reasonably simple, correcting higher multiplicities requires significantly more work. The VINCIA program aims at solving this issue [21, 22]. In general however, we are currently forced to rely on tree-level merging to improve the descriptions of multi-jet observables.

If a first-splitting-corrected PS is available, unitarity violations will enter when including matrix elements for the next higher jet multiplicity. Since the case of two-jet merging is also instructive for later consid-

erations, we will list the contributions to the cross section below.

$$\frac{d\sigma_0^{ex}}{d\phi_0} = f_0(x_0,\rho_0)\,|\mathcal{M}_0(\rho_0,\mu_R)|^2\,\Pi_{S_{+0}}(x_0,\rho_0,\rho_{\mathrm{MS}}) \tag{II.18}$$

$$= f_0(x_0,\rho_0)\,|\mathcal{M}_0(\rho_0,\mu_R)|^2 \times\left(1-\int_{\rho_{\mathrm{MS}}}^{\rho_0} d\rho dz \alpha_s(\rho)\,\mathcal{P}_1(z,\rho)\,\Pi_{S_{+0}}(x_0,\rho_0,\rho)\right) \tag{II.19}$$

$$\frac{d\sigma_1^{ex}}{d\phi_0} = d\rho_1 dz_1 d\varphi_1 f_0(x_0,\rho_0)\frac{\alpha_s(\rho_1)}{\alpha_s(\mu_R)}\frac{f_1(x_1,\rho_1)}{f_0(x_0,\rho_1)}\,|\mathcal{M}_1(\rho_0,\mu_R)|^2 \Pi_{S_{+0}}(x_0,\rho_0,\rho_1)\,\Pi_{S_{+1}}(x_1,\rho_1,\rho_{\mathrm{MS}}) \tag{II.20}$$

$$= d\rho_1 dz_1 d\varphi_1 f_0(x_0,\rho_0)\frac{\alpha_s(\rho_1)}{\alpha_s(\mu_R)}\frac{f_1(x_1,\rho_1)}{f_0(x_0,\rho_1)}\,|\mathcal{M}_1(\rho_0,\mu_R)|^2\,\Pi_{S_{+0}}(x_0,\rho_0,\rho_1) \times\left(1-\int_{\rho_{\mathrm{MS}}}^{\rho_1} d\rho dz \alpha_s(\rho)\,\mathcal{P}_2(z,\rho)\,\Pi_{S_{+1}}(x_1,\rho_1,\rho)\right) \tag{II.21}$$

$$\frac{d\sigma_2^{in}}{d\phi_0} = d\rho_1 dz_1 d\varphi_1 d\rho_2 dz_2 d\varphi_2 f_0(x_0,\rho_0)\frac{\alpha_s(\rho_1)}{\alpha_s(\mu_R)}\frac{f_1(x_1,\rho_1)}{f_0(x_0,\rho_1)}\frac{\alpha_s(\rho_2)}{\alpha_s(\mu_R)}\frac{f_2(x_2,\rho_2)}{f_1(x_1,\rho_2)} \times|\mathcal{M}_2(\rho_0,\mu_R)|^2\,\Pi_{S_{+0}}(x_0,\rho_0,\rho_1)\,\Pi_{S_{+1}}(x_1,\rho_1,\rho_2) \tag{II.22}$$

For a first-splitting-corrected PS all contributions not containing $\Pi_{S_{+1}}$ cancel between II.19 and II.21, except for the lowest order inclusive cross section. Unitarity is then guaranteed if

$$\begin{aligned}&\int_{\rho_{\mathrm{MS}}}^{\rho_0} d\rho_1 dz_1 d\varphi_1 \int_{\rho_{\mathrm{MS}}}^{\rho_1} d\rho_2 dz_2 d\varphi_2 f_0(x_0,\rho_0)\frac{\alpha_s(\rho_1)}{\alpha_s(\mu_R)}\frac{f_1(x_1,\rho_1)}{f_0(x_0,\rho_1)} \\ &\qquad\times|\mathcal{M}_1(\rho_0,\mu_R)|^2\,\alpha_s(\rho_2)\,\mathcal{P}_2(z_2,\rho_2)\,\Pi_{S_{+0}}(x_0,\rho_0,\rho)\,\Pi_{S_{+1}}(x_1,\rho,\rho_2) \\ =&\int_{\rho_1}^{\rho_0} d\rho_1 dz_1 d\varphi_1 \int_{\rho_{\mathrm{MS}}}^{\rho_1} d\rho_2 dz_2 d\varphi_2 f_0(x_0,\rho_0)\frac{\alpha_s(\rho)}{\alpha_s(\mu_R)}\frac{f_1(x_1,\rho)}{f_0(x_0,\rho)}\frac{\alpha_s(\rho_2)}{\alpha_s(\mu_R)}\frac{f_2(x_2,\rho_2)}{f_1(x_1,\rho_2)} \\ &\qquad\times|\mathcal{M}_2(\rho_0,\mu_R)|^2\,\Pi_{S_{+0}}(x_0,\rho_0,\rho)\,\Pi_{S_{+1}}(x_1,\rho,\rho_2)\end{aligned} \tag{II.23}$$

For this, the splitting kernels need to exactly reproduce the matrix element, phase space must be fully covered by the parton shower, and the no-emission probabilities need to be produced identically in both cases. Particularly the requirement that the phase space is completely covered is problematic, since parton showers commonly fill only phase space regions in which consecutive emissions are ordered in a decreasing evolution variable.

Clearly, eq. (II.23) is not fulfilled in standard PS programs, which at best are correct to next-to-leading logarithmic (NLL) accuracy. This means that the dependence on the merging scale would vanish to order $\alpha_s^2 L^4$ and $\alpha_s^2 L^3$, but that there will be a residual logarithmic dependence of order $\alpha_s^2 L^2$.

In the next section, we would like to outline a method that sidesteps these problems by using multi-jet matrix elements from the very beginning to build the resummation for low-multiplicity states.

II.4 Concepts of UMEPS

The main concept we would like to emphasise is that appropriately weighted matrix elements with additional jets can be used to induce resummation in lower-multiplicity states.

For example, one-jet inclusive cross sections (eq. (II.7)) can, by integrating over the phase space of the resolved parton, be manipulated to induce resummation in zero-jet cross section. No parton shower resummation above ρ_{MS} would then be necessary in zero-jet contributions. This means that we can reorder the parton shower formula for the inclusive cross section:

$$\begin{aligned}\sigma^{in} &= \int d\phi_0 \left(\frac{d\sigma_0^{ex}}{d\phi_0} + \int d\phi^{(1)} \frac{d\sigma_1^{in}}{d\phi_1} \right) \\ &= \int d\phi_0 \Bigg(f_0(x_0,\rho_0) \left|\mathcal{M}_0\left(\rho_0,\mu_R\right)\right|^2 \\ &\quad \underbrace{- f_0(x_0,\rho_0) \left|\mathcal{M}_0\left(\rho_0,\mu_R\right)\right|^2 \int_{\rho_{\mathrm{MS}}}^{\rho_0} d\rho dz \alpha_{\mathrm{s}}\left(\rho\right) \mathcal{P}_1\left(z,\rho\right) \Pi_{S_{+0}}\left(x_0,\rho_0,\rho\right)}_{\frac{d\sigma_{1\to 0}^{in}}{d\phi_0}} + \int d\phi^{(1)} \frac{d\sigma_1^{in}}{d\phi_1} \Bigg)\end{aligned} \tag{II.24}$$

and generate $\frac{d\sigma_{1\to 0}^{in}}{d\phi_0}$ *explicitly from* $\frac{d\sigma_1^{in}}{d\phi_1}$ by integrating over the emission phase space. When including one additional jet into the parton shower, we can explicitly preserve the inclusive cross section by adding the samples[5]

$$\frac{d\sigma_0^{in}}{d\phi_0} = f_0(x_0,\rho_0) \left|\mathcal{M}_0\left(\rho_0,\mu_R\right)\right|^2 \tag{II.25}$$

$$\frac{d\sigma_1^{in}}{d\phi_0} = d\rho_1 dz_1 d\varphi_1 f_0(x_0,\rho_0) \frac{\alpha_{\mathrm{s}}(\rho_1)}{\alpha_{\mathrm{s}}(\mu_R)} \frac{f_1(x_1,\rho_1)}{f_0(x_0,\rho_1)} \left|\mathcal{M}_1\left(\rho_0,\mu_R\right)\right|^2 \Pi_{S_{+0}}\left(x_0,\rho_0,\rho_1\right) \tag{II.26}$$

$$\frac{d\sigma_{1\to 0}^{in}}{d\phi_0} = -\int_{\rho_{\mathrm{MS}}}^{\rho_0} d\rho dz d\varphi f_0(x_0,\rho_0) \frac{\alpha_{\mathrm{s}}(\rho)}{\alpha_{\mathrm{s}}(\mu_R)} \frac{f_1(x_1,\rho)}{f_0(x_0,\rho)} \left|\mathcal{M}_1\left(\rho_0,\mu_R\right)\right|^2 \Pi_{S_{+0}}\left(x_0,\rho_0,\rho\right) \tag{II.27}$$

Before we continue, let us pause and investigate how we attach parton showers to these samples. In zero-jet contributions, the effect of parton

[5] The integration over the azimuthal angle φ is included because the matrix element exhibits a φ-dependence. In the PS approach, this integration was already implicitly contained in the φ-integrated splitting functions P_i (and $\mathcal{P}_i$).

showers above ρ_{MS} is already included, so that we only need to start the parton shower at ρ_{MS}. If the one-jet matrix element is the highest multiplicity sample, we allow the shower to generate emissions below ρ_1, as in traditional merging [13, 15]. Since changes to the cross section from allowing e.g. two resolved partons cancel exactly with unresolved partons in the one-parton state (see eq. (II.10) and eq. (II.11) and the discussion following II.12), allowing the shower to produce resolved emissions does not invalidate unitarity.

We call this method UMEPS, for unitary matrix element + parton shower merging. In principle, this method is as easily generalisable as traditional merging techniques, and shows, on a more detailed level, difficulties reminiscent of CKKW-L. To particularise, let us have a look at how two additional jets can be included by UMEPS. Naively, we would simply add

$$\begin{aligned}\frac{d\sigma_2^{in}}{d\phi_0} &= d\rho_1 dz_1 d\varphi_1 d\rho_2 dz_2 d\varphi_2 f_0(x_0,\rho_0)\frac{\alpha_s(\rho_1)}{\alpha_s(\mu_R)}\frac{f_1(x_1,\rho_1)}{f_0(x_0,\rho_1)}\frac{\alpha_s(\rho_2)}{\alpha_s(\mu_R)}\frac{f_2(x_2,\rho_2)}{f_1(x_1,\rho_2)}\\ &\quad\times|\mathcal{M}_2(\rho_0,\mu_R)|^2\,\Pi_{S_{+0}}(x_0,\rho_0,\rho_1)\,\Pi_{S_{+1}}(x_1,\rho_1,\rho_2) \qquad \text{(II.28)}\\ \frac{d\sigma_{2\to1}^{in}}{d\phi_0} &= -d\rho_1 dz_1 d\varphi\int_{\rho_{\text{MS}}}^{\rho_1} d\rho dz d\varphi f_0(x_0,\rho_0)\frac{\alpha_s(\rho_1)}{\alpha_s(\mu_R)}\frac{f_1(x_1,\rho_1)}{f_0(x_0,\rho_1)}\frac{\alpha_s(\rho_2)}{\alpha_s(\mu_R)}\frac{f_2(x_2,\rho)}{f_1(x_1,\rho)}\\ &\quad\times|\mathcal{M}_2(\rho_0,\mu_R)|^2\,\Pi_{S_{+0}}(x_0,\rho_0,\rho_1)\,\Pi_{S_{+1}}(x_1,\rho_1,\rho) \qquad \text{(II.29)}\end{aligned}$$

and treat II.28 as highest multiplicity sample. It is however possible that due to undoing recoil effects, states with jets below ρ_{MS} are produced by performing the integration in II.29. In this case, we take these contributions to be corrections to the zero-jet cross section, and integrate twice. After this amendment, two-jet UMEPS merging contains the contributions

$$\begin{aligned}\frac{d\sigma_0^{in}}{d\phi_0} &= f_0(x_0,\rho_0)\,|\mathcal{M}_0(\rho_0,\mu_R)|^2 \qquad \text{(II.30)}\\ \frac{d\sigma_1^{in}}{d\phi_0} &= d\rho_1 dz_1 d\varphi_1 f_0(x_0,\rho_0)\frac{\alpha_s(\rho_1)}{\alpha_s(\mu_R)}\frac{f_1(x_1,\rho_1)}{f_0(x_0,\rho_1)}\,|\mathcal{M}_1(\rho_0,\mu_R)|^2\,\Pi_{S_{+0}}(x_0,\rho_0,\rho_1) \qquad \text{(II.31)}\\ \frac{d\sigma_{1\to0}^{in}}{d\phi_0} &= -\int_{\rho_{\text{MS}}}^{\rho_0} d\rho dz d\varphi f_0(x_0,\rho_0)\frac{\alpha_s(\rho)}{\alpha_s(\mu_R)}\frac{f_1(x_1,\rho)}{f_0(x_0,\rho)}\,|\mathcal{M}_1(\rho_0,\mu_R)|^2\,\Pi_{S_{+0}}(x_0,\rho_0,\rho) \qquad \text{(II.32)}\\ \frac{d\sigma_2^{in}}{d\phi_0} &= d\rho_1 dz_1 d\varphi_1 d\rho_2 dz_2 d\varphi_2 f_0(x_0,\rho_0)\frac{\alpha_s(\rho_1)}{\alpha_s(\mu_R)}\frac{f_1(x_1,\rho_1)}{f_0(x_0,\rho_1)}\frac{\alpha_s(\rho_2)}{\alpha_s(\mu_R)}\frac{f_2(x_2,\rho_2)}{f_1(x_1,\rho_2)}\\ &\quad\times|\mathcal{M}_2(\rho_0,\mu_R)|^2\,\Pi_{S_{+0}}(x_0,\rho_0,\rho_1)\,\Pi_{S_{+1}}(x_1,\rho_1,\rho_2) \qquad \text{(II.33)}\\ \frac{d\sigma_{2\to1}^{in}}{d\phi_0} &= -d\rho_1 dz_1 d\varphi_1\int_{\rho_{\text{MS}}}^{\rho_1} d\rho dz d\varphi f_0(x_0,\rho_0)\frac{\alpha_s(\rho_1)}{\alpha_s(\mu_R)}\frac{f_1(x_1,\rho_1)}{f_0(x_0,\rho_1)}\frac{\alpha_s(\rho)}{\alpha_s(\mu_R)}\frac{f_2(x_2,\rho)}{f_1(x_1,\rho)}\\ &\quad\times\Theta(\rho_1-\rho_{\text{MS}})\,|\mathcal{M}_2(\rho_0,\mu_R)|^2\,\Pi_{S_{+0}}(x_0,\rho_0,\rho_1)\,\Pi_{S_{+1}}(x_1,\rho_1,\rho) \qquad \text{(II.34)}\end{aligned}$$

$$\frac{d\sigma^{in}_{2\to 0}}{d\phi_0} = -\int_{\rho_1}^{\rho_0} d\rho_a dz_a d\varphi_a \int_{\rho_{\rm MS}}^{\rho_1} d\rho_b dz_b d\varphi_b f_0(x_0,\rho_0) \frac{\alpha_s(\rho_a)}{\alpha_s(\mu_R)} \frac{f_1(x_1,\rho_a)}{f_0(x_0,\rho_a)} \frac{\alpha_s(\rho_b)}{\alpha_s(\mu_R)} \frac{f_2(x_2,\rho_b)}{f_1(x_1,\rho_b)} \times |\mathcal{M}_2(\rho_0,\mu_R)|^2 \Theta(\rho_{\rm MS}-\rho_a)\Pi_{S_{+0}}(x_0,\rho_0,\rho_a)\,\Pi_{S_{+1}}(x_1,\rho_a,\rho_b) \quad \text{(II.35)}$$

UMEPS can then be extended to arbitrary jet multiplicity. The main idea is that in order to maintain unitarity, we have to subtract all contributions that we add as higher multiplicity matrix elements. The subtractions are constructed with PS unitarity as a guideline. For brevity, we introduce the short-hands

$$\frac{d\sigma^{in}_{n}}{d\phi_0} \equiv \mathrm{B}_n w'_n \equiv \widehat{\mathrm{B}}_n \qquad \text{and} \quad \text{(II.36)}$$

$$\frac{d\sigma^{in}_{n\to m}}{d\phi_0} \equiv -\left[\prod_{a=m+1}^{n-1}\int d\rho_a dz_a d\varphi_a \Theta(\rho_{\rm MS}-\rho_a)\right]\int d\rho_n dz_n d\varphi_n \mathrm{B}_n w'_n \equiv -\int_s \widehat{\mathrm{B}}_{n\to m}$$

where w'_n will be defined below. The symbol $\int_s \widehat{\mathrm{B}}_{n\to m}$ indicates that more than one integrations had to be performed since all of the states $S_{+n-1},\ldots,S_{+m+1}$ contained partons below the merging scale. The integration(s) will be achieved by substituting the input event with a reconstructed lower-multiplicity event of the parton shower history, as will be discussed in section II.4.1. This substitution method is indicated by the subscript s on the integral sign. The weight w'_n that needs to be applied to tree-level events to produce the $\frac{d\sigma^{in}_n}{d\phi}$ sample is given by

$$w'_n = \frac{x_n f_n(x_n,\rho_n)}{x_n f_n(x_n,\mu_F)} \times \prod_{i=1}^{n}\left[\frac{\alpha_s(\rho_i)}{\alpha_s(\mu_R)} \frac{x_{i-1}f_{i-1}(x_{i-1},\rho_{i-1})}{x_{i-1}f_{i-1}(x_{i-1},\rho_i)} \Pi_{S_{+i-1}}(x_{i-1},\rho_{i-1},\rho_i)\right] \quad \text{(II.37)}$$

$$= \frac{x^+_n f^+_n(x^+_n,\rho_n)}{x^+_n f^+_n(x^+_n,\mu_F)} \frac{x^-_n f^-_n(x^-_n,\rho_n)}{x^-_n f^-_n(x^-_n,\mu_F)} \times \prod_{i=1}^{n}\left[\frac{\alpha_s(\rho_i)}{\alpha_s(\mu_R)} \frac{x^+_{i-1}f^+_{i-1}(x^+_{i-1},\rho_{i-1})}{x^+_{i-1}f^+_{i-1}(x^+_{i-1},\rho_i)} \frac{x^-_{i-1}f^-_{i-1}(x^-_{i-1},\rho_{i-1})}{x^-_{i-1}f^-_{i-1}(x^-_{i-1},\rho_i)} \Pi_{S_{+i-1}}(x_{i-1},\rho_{i-1},\rho_i)\right].$$

This weight differs from the CKKW-L weight in eq. (II.14), since it does not contain the last no-emission probability $\Pi_{S_{+n}}(x_n,\rho_n,\rho_{\rm MS})$, i.e. the last line in eq. (II.14). In the UMEPS procedure, this factor is instead included by subtracting the integrated, reweighted, next-higher multiplicity sample, thus conserving unitarity in a way reminiscent of standard parton showers. The probability of having no resolved emissions off the zero-jet states in eq. (II.30) for example, is included through the contributions in eqs. (II.32) and eq. (II.35).

Armed with this notation, the prediction of an observable $\mathcal{O}$ in 2−jet

merged UMEPS becomes

$$\begin{aligned}\langle\mathcal{O}\rangle \;=\; & \int d\phi_0 \Bigg\{ \mathcal{O}(S_{+0j})\widehat{\mathrm{B}}_0 \;-\; \mathcal{O}(S_{+0j}) \int_s \widehat{\mathrm{B}}_{1\to 0} \;-\; \mathcal{O}(S_{+0j}) \int_s \widehat{\mathrm{B}}_{2\to 0} \\ & + \int d\phi^{(1)} \mathcal{O}(S_{+1j})\widehat{\mathrm{B}}_1 \;-\; \int d\phi_1 \mathcal{O}(S_{+1j}) \int_s \widehat{\mathrm{B}}_{2\to 1} \\ & + \int d\phi^{(1)} \int d\phi^{(2)} \mathcal{O}(S_{+2j})\widehat{\mathrm{B}}_2 \Bigg\}, \end{aligned} \tag{II.38}$$

where we have used the notation S_{+nj} to indicate states with n resolved partons, resolved meaning above the cut ρ_{MS} as defined by the merging scale definition. More generally, the outcome of merging n additional partons with the UMEPS method is

$$\begin{aligned}\langle\mathcal{O}\rangle \;=\; & \int d\phi_0 \Bigg\{ \mathcal{O}(S_{+0j}) \left[\widehat{\mathrm{B}}_0 \;-\; \int_s \widehat{\mathrm{B}}_{1\to 0} \;-\; \int_s \widehat{\mathrm{B}}_{2\to 0} \;-\; \cdots \;-\; \int_s \widehat{\mathrm{B}}_{N\to 0} \right] \\ & + \int d\phi^{(1)} \mathcal{O}(S_{+1j}) \left[\widehat{\mathrm{B}}_1 \;-\; \int_s \widehat{\mathrm{B}}_{2\to 1} \;-\; \cdots \;-\; \int_s \widehat{\mathrm{B}}_{N\to 1} \right] \\ & + \;\; \cdots \\ & + \int d\phi^{(1)} \cdots \int d\phi^{(N-1)} \mathcal{O}(S_{+N-1j}) \left[\widehat{\mathrm{B}}_{N-1} \;-\; \int_s \widehat{\mathrm{B}}_{N\to N-1} \right] \\ & + \int d\phi^{(1)} \cdots \int d\phi^{(N)} \mathcal{O}(S_{+Nj}) \, \widehat{\mathrm{B}}_N \Bigg\} \\ =\; & \sum_{n=0}^{N} \int d\phi_0 \int d\phi^{(1)} \cdots \int d\phi^{(n)} \mathcal{O}(S_{+nj}) \left\{ \widehat{\mathrm{B}}_n \;-\; \sum_{i=n+1}^{N} \int_s \widehat{\mathrm{B}}_{i\to n} \right\}. \end{aligned} \tag{II.39}$$

The generation of $\widehat{\mathrm{B}}_n-$ and $\int_s \widehat{\mathrm{B}}_{n\to m}-$events will be summarised in section II.4.1. It should be noted that the treatment $\rho_{\mathrm{MS}}-$unordered integration results is heavily influenced by how CKKW-L includes states with $\rho_{\mathrm{MS}}-$unordered emissions, which was discussed in detail in [16]. Precisely for states which evolve from a state below ρ_{MS} to a state above ρ_{MS} do CKKW-L and the truncated-shower [24] approach differ. It can thus be imagined that other ways of treating such notorious configurations show improved behaviour. For now, we will not discuss such possibilities, and instead, if necessary, integrate multiple times, until a state above ρ_{MS} is produced.

A well-known challenge of merging prescriptions is the treatment of configurations that could never have been produced by a sequence of shower splittings. This can happen if the PS does not include all possible splittings of the model. Figure II.1 for example cannot be produced

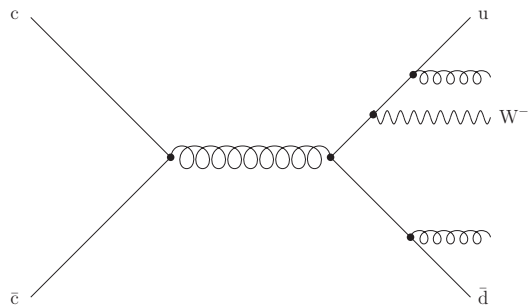

Figure II.1: An example of a matrix element contribution without a complete shower history. If the parton shower does not include W−boson radiation, only the two gluon emissions can be reclustered, and $c\bar{c} \to u\bar{d}W^-$ has to be considered a separate hard process.

by a shower that does not allow W−boson radiation. Such states cannot be projected onto a lower-multiplicity underlying process, and will thus introduce unitarity violations in UMEPS. It is clear, however, that such states will not contain any divergences and the unitarity violations will not blow up at small merging scales. Indeed we have found that these contributions are numerically irrelevant for the processes we have studied.

II.4.1 Procedure step-by-step

To implement UMEPS, we need to be able to perform the necessary integrations. Although the formulae could convey a feeling of complexity, these integrations are factually already needed in traditional merging approaches. All modern CKKW-inspired schemes need to construct a history of parton shower states for input matrix element events, because otherwise, no trial showers can be used to generate Sudakov form factors dynamically. Thus, a sequence of states $S_{+n} \to S_{+n-1} \to \cdots \to S_{+1} \to S_{+0}$ is always available. The sequence is constructed by inverting the shower mapping of radiative phase space on each state, i.e. a parton in S_{+n} is removed, and its momentum distributed amongst the remaining particles, leading to a state S_{+n-1}[6]. This is exactly the integration we need: To produce the integrated version of S_{+n}, we simply replace it by S_{+n-1}, but keep the full weight. $k-$fold integrations can be achieved by replacing S_{+n} with S_{+n-k}.

[6]The mapping used for the current paper is given in Appendix B.2 of [16]

With this, we have all ingredients to construct the UMEPS scheme. If not mentioned explicitly, all weights in UMEPS are generated precisely as in CKKW-L. To avoid unnecessary complications, we will here gloss over many technicalities that have already been addressed in CKKW-L, and are directly borrowed by UMEPS. A discussion of Sudakov reweighting for states without parton-shower ordered histories, for example, can be found in [16].

The UMEPS algorithm has two parts – a part in which we keep the matrix element configurations ($\widehat{\mathrm{B}}_n-$events) and another in which we integrate over emissions ($\int_s \widehat{\mathrm{B}}_{n\to m}-$events):

I. Produce *Les Houches* event files (LHEF) [25] with a matrix element generator for $n = 0, 1 \dots N$ extra jets with a regularisation cut-off, ρ_{MS}, typically using a fixed factorisation scale, μ_F, and a fixed $\alpha_{\mathrm{s}}(\mu_R)$.

II. Pick a jet multiplicity, n, and a state S_{+n} according to the cross sections given by the matrix element generator.

   1. Find all shower histories for the state S_{+n}, pick a sequence according to the product of splitting probabilities. Only pick un-ordered sequences if no ordered sequence was found. Only pick incomplete paths (cf. the discussion of figure II.1 above) if no complete path was constructed.
   2. Perform reweighting: For each $0 \leqslant i < n$,
      i. Start the shower off the state S_{+i} at ρ_i, generate a trial state R with scale ρ_R. If $\rho_R > \rho_{i+1}$, veto the event and start again from II.
      ii. Calculate the weight factor

$$w_i = \frac{\alpha_{\mathrm{s}}(\rho_{i+1})}{\alpha_{\mathrm{s}}(\mu_R)} \frac{x_i^+ f_i^+(x_i^+, \rho_i)}{x_i^+ f_i^+(x_i^+, \rho_{i+1})} \frac{x_i^- f_i^-(x_i^-, \rho_i)}{x_i^- f_i^-(x_i^-, \rho_{i+1})} \qquad \text{(II.40)}$$

   3. Start the shower from S_{+n}.
      i. If $n < N$, start the shower at ρ_n, veto any shower emission producing an additional resolved parton.
      ii. If $n = N$, start the shower at ρ_n.

III. If the event was not rejected, multiply the event weight by

$$w'_n = \frac{x_n^+ f_n^+(x_n^+, \rho_n)}{x_n^+ f_n^+(x_n^+, \mu_F)} \times \frac{x_n^- f_n^-(x_n^-, \rho_n)}{x_n^- f_n^-(x_n^-, \mu_F)} \times \prod_{i=0}^{n-1} w_i \qquad \text{(II.41)}$$

V. Start again from II.

The second part, i.e. producing $\int_s \widehat{\mathrm{B}}_{n\to m}-$events to effect lower-multiplicity PS resummation, requires only two changes:

II.3 Replace the matrix-element state by S_{+n-1}, or the first state S_{+l} with all $l \leq n-1$ partons above the merging scale. If no integrated state can be constructed, i.e. if only incomplete paths were found, reject the event. For valid events, start the shower at ρ_n, veto any shower emission producing an additional resolved parton.

III. If the event was not rejected, multiply the event weight by

$$-w'_n = -\frac{x_n^+ f_n^+(x_n^+,\rho_n)}{x_n^+ f_n^+(x_n^+,\mu_F)} \times \frac{x_n^- f_n^-(x_n^-,\rho_n)}{x_n^- f_n^-(x_n^-,\mu_F)} \times \prod_{i=0}^{n-1} w_i \qquad \text{(II.42)}$$

Finally, all samples generated in the first and second parts are added to give the UMEPS prediction. Note that in order produce correctly normalised cross sections $\frac{d\sigma_i^{ex}}{d\phi_0}$, we need to include ratios of parton distributions and α_s ratios into the weight. This is analogous to the CKKW-L method (see the α_s- and PDF-factors in eq. (II.14)). It is worthwhile to notice that the UMEPS scheme can in principle be implemented by using structures already existing in traditional merging codes. Basically, compared to traditional merging, the $\widehat{\mathrm{B}}_n-$contributions do not carry a no-emission probability for emissions off the ME event. The $\int_s \widehat{\mathrm{B}}_{n\to m}-$samples can easily be extracted from merging codes.

How multiple partonic interactions (MPI) are added to the merged samples requires a short discussion. In principle, we stay true to the philosophy of the algorithm outlined in [16], i.e. we want to make sure that the merging method does not artificially suppress hard secondary scatterings, which in PYTHIA8 are interleaved with the parton shower. The interleaving means that the PS is competing with the MPI's, and the probability of emitting a parton in the PS is not only governed by the standard no-emission probability, $\Pi_{S_{+n}}$ but is also multiplied by a no-MPI probability, $\Pi^{\mathrm{MPI}}_{S_{+n}}$. Hence all m-jet (both $\widehat{\mathrm{B}}_m$ and $\int_s \widehat{\mathrm{B}}_{n\to m}$) samples generated by our algorithm above need to be multiplied by the no-MPI probabilities

$$\prod_{i=0}^{m-1} \Pi^{\mathrm{MPI}}_{S_{+i}}(\rho_i,\rho_{i+1}), \qquad \text{(II.43)}$$

which are easily incorporated in the trial showers described above. We also need to include the actual MPI's. Here the philosophy is that as soon as we have a MPI at some scale, we ignore corrections from the full

tree-level matrix element on softer jets from the primary interaction, and allow them to be described by the PS alone. Hence, when we start the shower from a given m-parton state (with $m < N$) in step II.3, we choose the reconstructed ρ_m as starting scale. As described before, we veto any parton emission above ρ_{MS}. However, if a MPI is generated above ρ_{MS}, it is accepted and the shower is allowed to continue without any further veto. (For the $m = N$ case, the shower including MPI is allowed without restrictions, starting from ρ_N.) In this way we achieve the same goal as in [16]: If the $n \leq N$ hardest jets in an event all belong to the primary interaction, they are described by the tree-level ME, while all other jets are given by the (interleaved) PS. Just as in [16], the treatment of pure QCD jet production means that the Born-level cross section is properly eikonalized by the no-MPI factor, by allowing MPI's all the way from $\sqrt{s}$ in the trial shower for $\Pi^{\mathrm{MPI}}_{S_{+0}}$.

II.5 Results

We have implemented UMEPS merging in PYTHIA8, and will make the necessary code public in the next major release version. In this section, we will concentrate on predictions for W-boson and QCD jet production at the LHC. However, the code aims to achieve the same generality as the implementation of CKKW-L in PYTHIA8.

All input matrix element configurations are taken from Les Houches Event Files generated with MadGraph/MadEvent, with the following settings:

- Fixed renormalisation scale $\mu_R = \mathrm{M}_\mathrm{Z}^2$, fixed factorisation scale $\mu_F = \mathrm{M}_\mathrm{W}^2$ for W-production. For $2 \to 2$ processes in pure QCD, we use $\mu_{r,2\to2} = m_{\perp,1} m_{\perp,1}$ and $\mu_{f,2\to2} = \min\{m^2_{\perp,1}, m^2_{\perp,1}\}$.
- CTEQ6L1 parton distributions and $\alpha_\mathrm{s}(\mathrm{M}_\mathrm{Z}^2) = 0.130$.
- The merging scale ρ_{MS} is defined by the minimal PYTHIA8 evolution $p_{\perp,ijk}$ of all possible combinations of three partons in the event. $p_{\perp,ijk}$ for a single combination of three particles i, j and k is defined as

$$p^2_{\perp,ijk} = \begin{cases} z_{ijk}(1-z_{ijk})Q^2_{ij} & \text{with } Q^2_{ij} = (p_i + p_j)^2 \text{ , } z_{ijk} = \frac{x_{i,jk}}{x_{i,jk}+x_{j,ik}} \text{ , } \\ & x_{i,jk} = \frac{2p_i(p_i+p_j+p_k)}{(p_i+p_j+p_k)^2} \quad \text{for FSR} \\ (1-z_{ijk})Q^2_{ij} & \text{with } Q^2_{ij} = -(p_i - p_j)^2 \text{ , } z_{ijk} = \frac{(p_i-p_j+p_k)^2}{(p_i+p_k)^2} \\ & \text{for ISR} \end{cases} \tag{II.44}$$

- In QCD $2 \to 2$ scatterings, the kinematical transverse momentum of jets is required to be larger than $p_{T,j} = 5$ GeV.

The value of $\alpha_s(M_Z^2)$ was set to match the α_s-value obtained in fitting the PDFs used in the ME calculation. To generate results, we have chosen the merging scale definition to closely match the parton shower evolution variable. The algorithm does however not depend on this particular choice. All jets needed for analysis purposes were defined with help of `fastjet`-routines [26]. The momentum of the intermediate W-boson will, if required, be extracted directly from the Monte Carlo event. We will compare UMEPS to the CKKW-L implementation in PYTHIA8. The problems we choose to highlight should be regarded as criticism of the implementation in PYTHIA8, rather than an assessment of CKKW-inspired methods in general.

II.5.1 W-boson production

We begin by comparing the result of the removal of a jet by integration with the corresponding parton shower contribution. This is useful to assess if performing the integration by the replacement $S_{+n+1} \to S_{+n}$ produces the desired results.

In the left panel of Figure II.2, we compare the integrated one-jet matrix element (i.e. the $\mathcal{O}\left(\alpha_s^1(\mu_R)\right)$-term of eq. (II.32)) with the shower approximation of the $\mathcal{O}\left(\alpha_s^1(\mu_R)\right)$-term in zero-jet events. The second term is of course just the $\mathcal{O}\left(\alpha_s^1(\mu_R)\right)$-contribution in eq. (II.18). The rapidity of the W-boson is identical in these two samples because PYTHIA8 is already matrix-element corrected for $W + j$-states. This demonstrates that in W-boson production, generating the no-emission probability in zero-jet states with PYTHIA8, or by a reweighted, integrated one-jet matrix element are both legitimate ways to produce the same factor.

The right panel of Figure II.2 investigates the difference between the parton shower approximation of no resolved emissions in one-jet states between the scales ρ_1 and ρ_{MS} and the result of constructing an unresolved emission by integrating over one parton in a two-jet matrix element. This means that we compare the one-jet matrix element, multiplied by the $\mathcal{O}\left(\alpha_s^1(\mu_R)\right)$-term of the no-emission probability $\Pi_{S_{+1}}(x_1, \rho_1, \rho_{MS})$ in eq. (II.20), with the $\mathcal{O}\left(\alpha_s^2(\mu_R)\right)$-contribution in eq. (II.34). The comparison shows that, as expected, the parton shower underestimates the hardness of the unresolved (second) emission, which is reminiscent of the fact that the inclusion of two-jet matrix

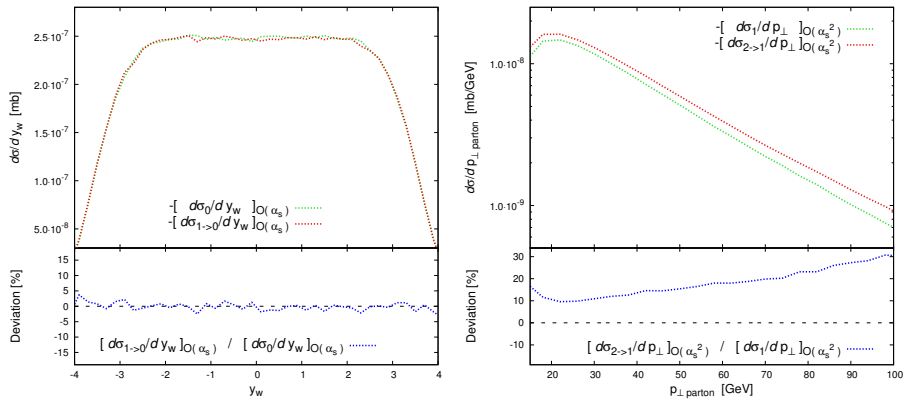

Figure II.2: Comparison between $\mathcal{O}(\alpha_s)$-terms of the parton shower with integrated matrix elements, for W-boson production in pp collisions at $E_{CM} = 7000$ GeV. The numerical value of the merging scale is $\rho_{MS} = 15$ GeV. Left panel: Rapidity of the W-boson, intended for comparison between the integrated one-jet matrix element (labelled $[d\sigma_{1\to 0}/dy_w]_{\mathcal{O}(\alpha_s^1)}$) and the $\mathcal{O}(\alpha_s^1)$-term of the no-emission probability for having no emission above ρ_{MS} radiated off zero-jet states above ρ_{MS} (labelled $[d\sigma_0/dy_w]_{\mathcal{O}(\alpha_s^1)}$). Right panel: Transverse momentum of the parton, for $W + j$ production in pp collisions at $E_{CM} = 7000$ GeV, intended for comparison between the integrated two-jet matrix element (labelled $[d\sigma_{2\to 1}/dp_\perp]_{\mathcal{O}(\alpha_s^2)}$) and the $\mathcal{O}(\alpha_s^1)$-term of the no-emission probability for having no emission above ρ_{MS} radiated off one-jet states, multiplying the $W + j$ matrix element (labelled $[d\sigma_1/dp_\perp]_{\mathcal{O}(\alpha_s^2)}$).

elements into the PS prediction does in general increase the tail of the $p_\perp$ of the hardest jet.

In Figure II.3 we show how matrix element samples contribute to this increase. All jet multiplicities enter, because the merging scale is not defined as the jet-separation of the $k_\perp$-algorithm, and since the merging cut acts on the matrix element state, while the jets are constructed from outgoing particles after the parton shower. In CKKW-L, the high-$p_\perp$ tail is dominated by the two-jet matrix element, with a major contribution from the one-jet states. The latter is, as can clearly be seen in the Figure II.4, significantly lower in UMEPS, a fact that we think crucial. UMEPS correctly cancels the inclusion of phase space points with two resolved partons by using the two-jet matrix element to construct a better approximation of radiating an *unresolved* parton from one-jet states. We see both in CKKW-L (left panel of Figure II.3), and in Figure II.2, that the

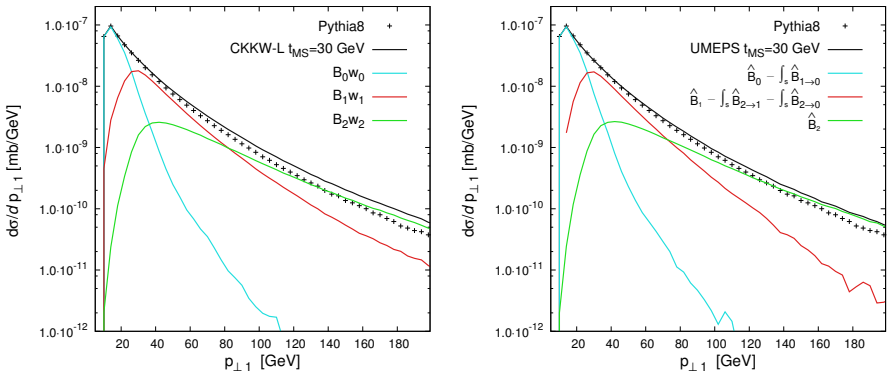

Figure II.3: Transverse momentum of the hardest jet, for W-boson production in pp collisions at $E_{\mathrm{CM}} = 7000$ GeV, when merging up to two additional partons. Jets were defined with the $k_\perp$-algorithm, with $k_{\perp,min} = 10$ GeV. Multi-parton interactions and hadronisation were excluded. Left panel: Results of the CKKW-L scheme. The contributions are labelled $\mathrm{B}_0 w_0$, $\mathrm{B}_1 w_1$ and $\mathrm{B}_2 w_2$ for CKKW-L-reweighted zero-, one- and two-jet matrix elements, respectively. Right panel: Results of the UMEPS scheme. The contributions are labelled $\widehat{\mathrm{B}}_0$, $\widehat{\mathrm{B}}_1$ and $\widehat{\mathrm{B}}_2$ for UMEPS-reweighted zero-, one- and two-jet matrix elements, and $\int_s \widehat{\mathrm{B}}_{1\to 0}$ and $\int_s \widehat{\mathrm{B}}_{2\to 1}$ for UMEPS-reweighted, integrated one- and two-jet samples. $\int_s \widehat{\mathrm{B}}_{2\to 0}$ indicates the two-jet contribution that was integrated twice because the state S_{+1} after the first integration contained an unresolved parton.

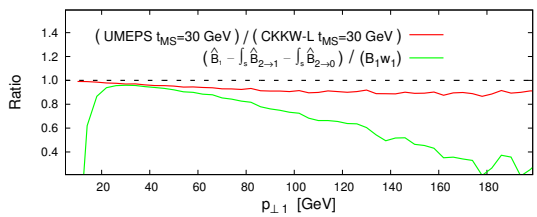

Figure II.4: Ratio of UMEPS and CKKW-L results, for the transverse momentum of the hardest jet in W-boson production for pp collisions at $E_{\mathrm{CM}} = 7000$ GeV, when merging up to two additional partons. Jets were defined with the $k_\perp$-algorithm, with $k_{\perp,min} = 10$ GeV. Multi-parton interactions and hadronisation were excluded. The symbols in the legend are defined in Figure II.3. The green curve shows the "one-jet" contribution in UMEPS divided by the one-jet contribution in CKKW-L. Below the merging scale, the UMEPS result also contains zero-jet contributions due to the double integration in $\int_s \widehat{\mathrm{B}}_{2\to 0}$, which again decrease the UMEPS "one-jet"-curve as compared to CKKW-L.

parton shower underestimates the hardness of two-parton states. The

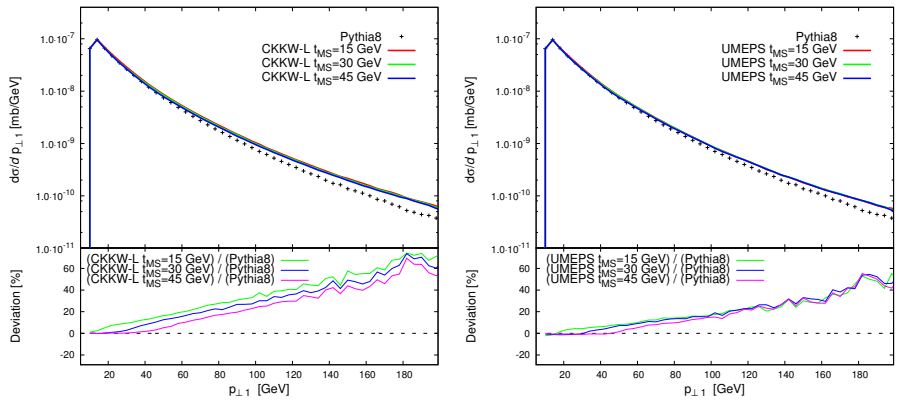

Figure II.5: Transverse momentum of the hardest jet, for W-boson production in pp collisions at $E_{\mathrm{CM}} = 7000$ GeV, when merging up to two additional partons. Jets were defined with the $k_\perp$-algorithm, with $k_{\perp,min} = 10$ GeV. Multi-parton interactions and hadronisation were excluded. The lower insets show the deviation of merged results from default PYTHIA8, for three different ρ_{MS}-values. Left panel: Results of the CKKW-L scheme. Right panel: Results of the UMEPS scheme.

description of unresolved emissions enters into the no-emission probabilities, with a negative $\mathcal{O}(\alpha_s^1)$-term. Thus, the contribution of showered one-jet states to the tail of $p_{\perp 1}$ will be larger if the shower description of two-jet states underestimates hardness. UMEPS improves the description of the no-emission probability by ensuring that in inclusive observables, resolved two-parton states are cancelled, a feature that is at work in the tail of $p_{\perp 1}$.

Variations in the description of $p_{\perp 1}$ are also visible in Figure II.5, where we show the transverse momentum of the hardest jet in CKKW-L and UMEPS[7]. The trend sketched in the previous paragraph is particularly clear in the insets comparing to default PYTHIA8: UMEPS produces a softer tail in $p_{\perp 1}$ than CKKW-L. The harder tail in CKKW-L is due to a worse description of unresolved emissions. It is fair to say that the difference between CKKW-L and UMEPS hints at the size of relic effects from not cancelling the dependence on higher-multiplicity matrix elements in a well-defined way. Merging scale variations in tree-level merging schemes arise from a mismatch of unresolved emissions ex-

[7] Note that the co-variation of merged results in the ratio inset is due to fluctuations in the PYTHIA8 reference curve.

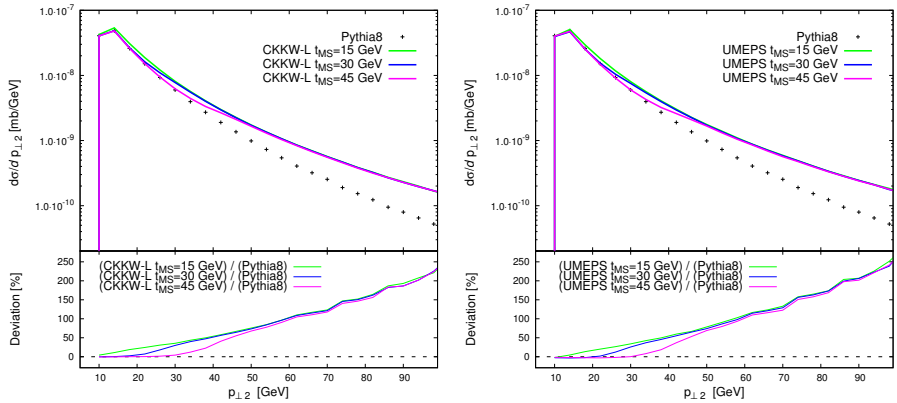

Figure II.6: Transverse momentum of the second-hardest jet, for W-boson production in pp collisions at $E_{\mathrm{CM}} = 7000$ GeV. Jets were defined with the $k_\perp$-algorithm, with $k_{\perp,min} = 10$ GeV, when merging up to two additional partons. Multi-parton interactions and hadronisation were excluded. The lower insets show the deviation of merged results from default PYTHIA8, for three different ρ_{MS}-values. Left panel: Results of the CKKW-L scheme. Right panel: Results of the UMEPS scheme.

ponentiated in no-emission probabilities and tree-level matrix elements for hard, resolved jets. UMEPS has a significantly lower merging scale variation since the method enforces a cancellation of resolved and unresolved contributions.

Figure II.6 shows that for very exclusive observables, CKKW-L and UMEPS are virtually indistinguishable. In this example, this is of course expected since the treatment of the highest multiplicity (here, the two-jet) matrix element is identical for both cases.

We would now like to perform a stress-test of the merging scale dependence. Since UMEPS properly cancels the effects of adding multi-jet matrix elements by subtracting their integrated counter-parts, it is in principle possible to push the merging scale to very small values. The variation of the inclusive cross section is shown in Figure II.7. It is clear that UMEPS does indeed preserve the inclusive cross section, while for CKKW-L, very small merging scales lead to large changes, rendering the method unreliable. However, the error convergence in UMEPS is, due to the negative weights, significantly slower. We will comment on this below.

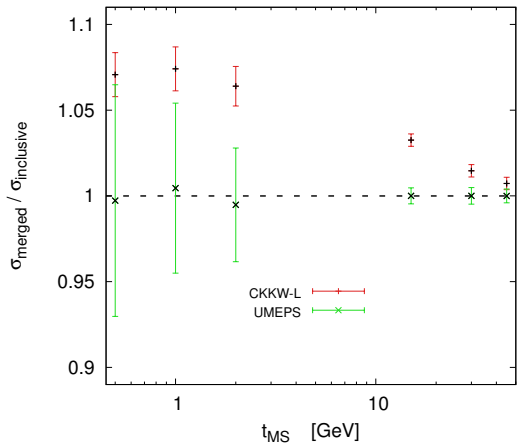

Figure II.7: Inclusive cross section for UMEPS- and CKKW-L merging of up to two additional jets in W-boson production in pp collisions at $E_{\mathrm{CM}} = 7000$ GeV (labelled σ_{merged}), in comparison to the the lowest-multiplicity inclusive cross section $\sigma_{\mathrm{inclusive}}$. The error bars represent only the statistical error on the merged cross section. For the UMEPS sample this becomes large for small merging scales, but as it is the same samples which are added and the subtracted, the central value stays very close to unity.

These unitarity violations might not induce drastic effects in the description of hard-scale observables like the transverse-momentum distribution of the W-boson. However, magnifying the low-scale description of this observable (Figure II.8) reveals problems. Figure II.8 serves two purposes. It clearly shows that by pushing the merging scale to small values in CKKW-L, sub-leading contributions in the multi-jet matrix elements start to contribute more. Since those sub-leading contributions cannot be cancelled by the default parton shower, major increases over PYTHIA8 are found. UMEPS explicitly cancels these sub-leading terms, and thus leads to a reliable prediction. The second observation in Figure II.8 is the dependence on the primordial transverse momentum parameter $k_{\perp,p}$. This parameter was introduced in event generators to account for the transverse momentum of partons in the incoming protons, which cannot be generated in initial state DGLAP evolution. If this were the only effect to be modelled by $k_{\perp,p}$, a value of $k_{\perp,p} \approx 0.3$ GeV per incoming parton would seem appropriate. However, in current event generator tunes, significantly higher values ($k_{\perp,p} \approx 2$ GeV) are required [20,27], potentially to compensate for an incomplete phase space coverage in initial state showers due to the shower cut-off. The

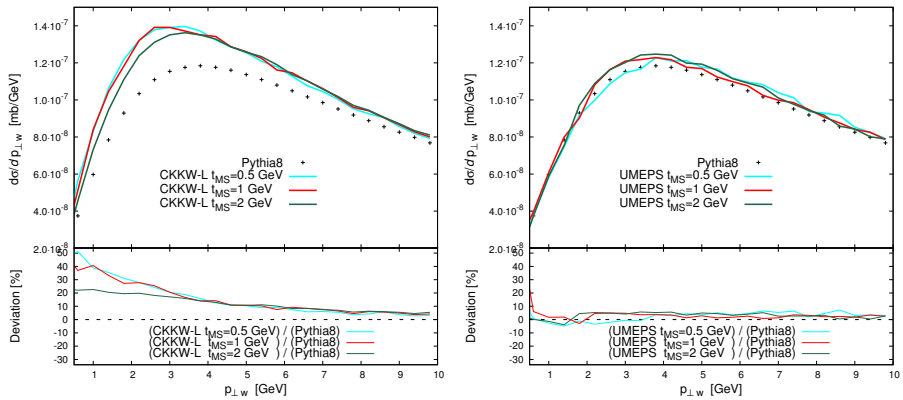

Figure II.8: Transverse momentum of the W-boson, for W-boson production in pp collisions at $E_{\mathrm{CM}} = 7000$ GeV, when merging up to two additional partons. Multi-parton interactions and hadronisation were excluded. The PYTHIA8 results are generated with the default settings, in particular with a primordial transverse momentum of $k_{\perp,p} = 2$ GeV. All merged curves have been generated with $k_{\perp,p} = 0.5$ GeV. The lower insets show the deviation of merged results from default PYTHIA8, for three different ρ_{MS}-values. Left panel: Results of the CKKW-L scheme. Right panel: Results of the UMEPS scheme.

value of $k_{\perp,p}$ is mainly fixed by tuning to the position of the peak of the transverse momentum spectrum of the Z- or W boson. Increasing the value of $k_{\perp,p}$ roughly corresponds to pushing the peak to higher $p_\perp$ values. Figure II.8 compares the UMEPS and CKKW-L predictions for the transverse momentum of the W boson, with $k_{\perp,p} = 0.5$ GeV, to default, tuned PYTHIA8 with $k_{\perp,p} = 2.0$ GeV. Unitarity violations in CKKW-L pull the peak back to lower $p_\perp$. This fact is virtually unchanged if we had used $k_{\perp,p} = 2.0$ for CKKW-L predictions instead, suggesting that if we positively wanted to use a very low merging scale, an increase in $k_{\perp,p}$ would be necessary. UMEPS on the other hand can be used with very low merging scales, and in particular shows the interesting feature of matching the default PYTHIA8 curve *without* having a high $k_{\perp,p}$ value. We believe this is due to a better modelling of logarithms of the form $\ln(1/x)$, which are present in the matrix element, and which are included in a unitary way in UMEPS – allowing for a much more natural value of $k_{\perp,p}$. This result is of course very preliminary, since there are e.g. correlations of the shower cut-off $p_{\perp\mathrm{min}}$ and $k_{\perp,p}$. One would hope that matrix-element merging would allow to lower $p_{\perp\mathrm{min}}$, which might

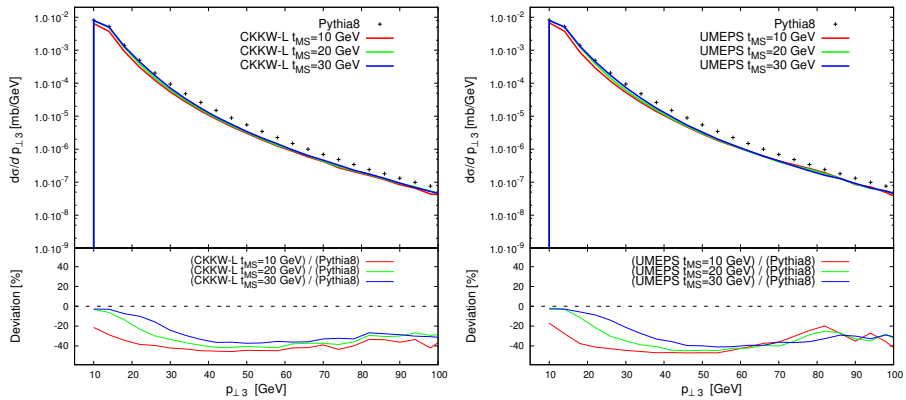

Figure II.9: Transverse momentum of the third hardest jet, for pure QCD dijet production in pp collisions at $E_{\mathrm{CM}} = 7000$ GeV, when merging up to two additional partons. Jets were defined with the $k_\perp$-algorithm, with $k_{\perp,min} = 10$ GeV. Multi-parton interactions and hadronisation were excluded. The lower insets show the deviation of merged results from default PYTHIA8, for three different ρ_{MS}-values. Left panel: Results of the CKKW-L scheme. Right panel: Results of the UMEPS scheme.

mean having to make a compromise for the value of $k_{\perp,p}$. We will come back to these aspects when presenting tunes for matrix-element-merged PYTHIA8 in a future publication.

II.5.2 Dijet production

We would further like to mention QCD dijet production at the LHC, since potential merging scale dependencies enter already when merging dijet- and three-jet matrix elements, and to demonstrate the flexibility of our implementation. The main objective of including QCD dijet production in this publication was to assess the treatment of MPI discussed at the end of section II.4.1. This is most effectively done by comparing to data, and before these we would like to only stress one issue.

Figure II.9 shows the transverse momentum of the third-hardest jet. We see that UMEPS and CKKW-L show very similar changes when compared to PYTHIA8. However, neither curves show the high-$p_\perp$ increase seen in [16]. This is simply because we have revised the choice of the renormalisation scale in the core $2 \to 2$ QCD scattering. In [16], the two powers of $\alpha_{\mathrm{s}}(\mu_R)$ in the core $2 \to 2$ process were never touched,

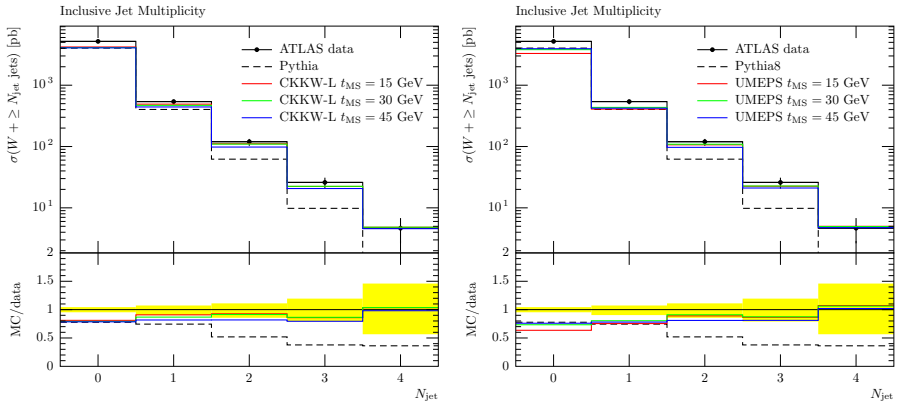

Figure II.10: Jet multiplicity in W-boson production, for three different merging scales, as measured by ATLAS [31]. Effects of multiple scatterings and hadronisation are included.

and thus were evaluated with the rather unfortunate choice $\mu_R = M_Z^2$ in the input Les Houches events. This has been rectified in the current release of (CKKW-L in) PYTHIA8, i.e. the scale choice ($\mu_{r,2\to2} = m_{\perp,1}m_{\perp,1}$) is now dynamical. Potential reweighting (due to the usage of fixed μ_R in the LHEF generation is handled internally in PYTHIA8. The trend that pure QCD multi-jet matrix elements have a softer spectrum of well-separated jets has already been observed in [16, 28]. The merging scale variation in UMEPS is within the statistical error of the samples. The statical uncertainty is larger in UMEPS than in CKKW-L, due to cancellations between positive and negative weights (see the last part on section II.6).

II.5.3 Comparison with data

In this section, we would like to confront UMEPS with experimental data. Event generator predictions were obtained with the settings of Tune A2 [29]. The results should of course not be regarded as final statement, since changes in the perturbative physics in event generators in principle request a full re-tuning. The intention of this section is to investigate if after including matrix-element information, hard-scale features are closer to measurements, and to assess the changes in underlying event description. All plots were produced with RIVET [30]. We apologise if the selection of experimental measurements seems biased.

In Figure II.10, we show jet rates in W-boson production at ATLAS

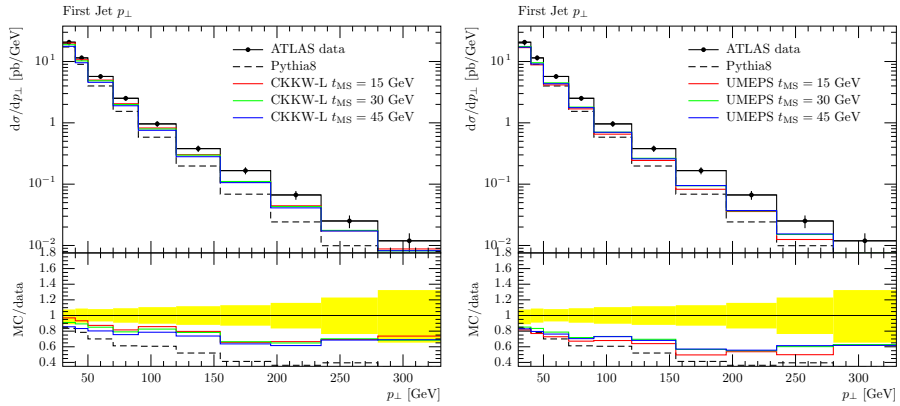

Figure II.11: Transverse momentum of the hardest jet in W-boson production, for three different merging scales, as measured by ATLAS [31]. Effects of multiple scatterings and hadronisation are included.

[31]. We find an improved description after including up to two additional jets, and little differences between UMEPS and CKKW-L.

The transverse momentum of the hardest jet is shown in Figure II.11. Again, we find that the shape description is improved by the CKKW-L and UMEPS methods. CKKW-L shows merging scale variations at lower $p_\perp$-values, since a slightly different inclusive cross section for a low merging scale leads to a slightly different normalisations. UMEPS on the other hand suffers from statistical fluctuations for a low merging scale value ($\rho_{\text{MS}} = 15$ GeV), while the curves for $\rho_{\text{MS}} = 30$ GeV and $\rho_{\text{MS}} = 45$ completely overlap. Note that the $p_\perp$ spectrum of UMEPS is a little softer than CKKW-L, in accordance with Figure II.5.

It is interesting to investigate when tree-level matrix element merging schemes produce large uncertainties. Figure II.12 shows the azimuthal distance $\Delta\phi_{12}$ between the two hardest jets. The parton shower alone cannot describe the peak at π. If the merging scale is low, the two-jet matrix element will give the dominant contribution in the peak region. High merging scales will increase the influence of the shower, thus degrading the description of the peak. The distribution will be determined by the shower if the merging scale is chosen higher than the jet-$p_\perp$ cut. This is precisely the reason why the merging scale is traditionally chosen (and varied) below any experimental $p_\perp$ cut. There is no formal reason to require only small merging scales, other than the goal to ME-correct large regions of phase space. Choosing a merging scale above experimental cuts makes the interplay between ME and PS

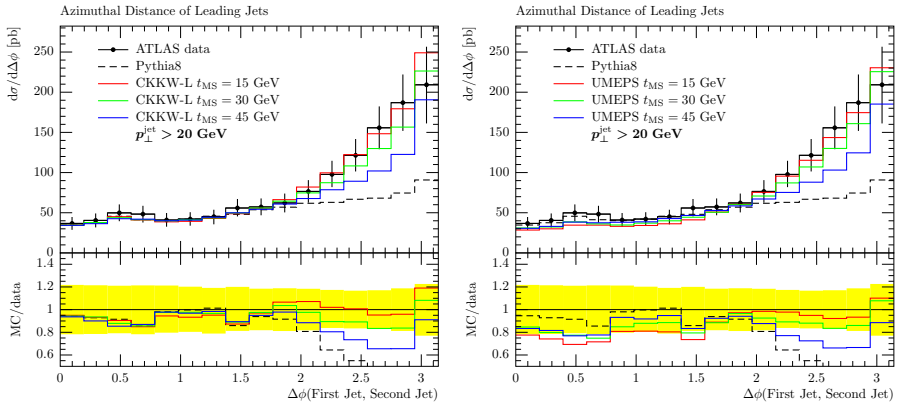

Figure II.12: Azimuthal distance between the two hardest jets in W-boson production, for three different merging scales, as measured by ATLAS [31]. Effects of multiple scatterings and hadronisation are included.

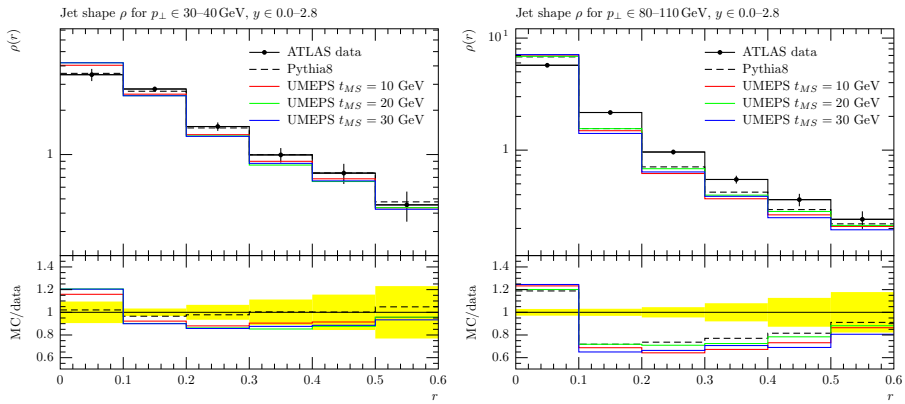

Figure II.13: Jet shapes in QCD events, for three different merging scales, in two $p_{\perp}$ bins, as measured by ATLAS [32]. Effects of multiple scatterings and hadronisation are included.

easy to see, and can provide guidance for future improvements beyond UMEPS, particularly for improvements that apply below the merging scale.

Before moving to the discussion section, we would like to investigate how jet shapes at the LHC are changed by the inclusion of additional matrix elements in the pure QCD case. The ATLAS analysis [32] found that the differential jet shape for relatively low-$p_{\perp}$ jets with $p_{\perp} \leq 160$ GeV depends crucially on the modelling of the underlying event. In Figure II.13, we show the default PYTHIA8 and UMEPS results for two

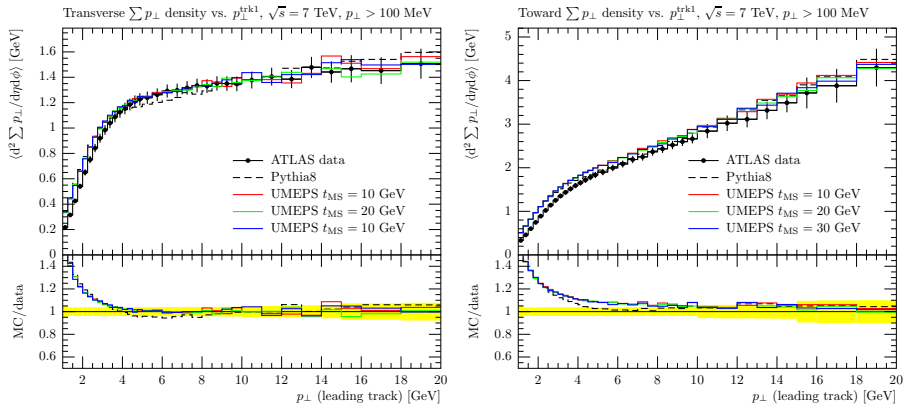

Figure II.14: Sum of transverse momenta of charged particles in QCD events, for three different merging scales, in the transverse and toward region, as measured by ATLAS [33]. Effects of multiple scatterings and hadronisation are included.

$p_\perp$ bins. Although far from perfect, the difference between the pure shower and merged results are similar to what a minor change in α_s would give[8]. We are confident that the prescription for adding MPI (see section II.4.1) does indeed mean that the underlying-event modelling of PYTHIA8 is only marginally perturbed by the inclusion of additional jets. This is supported by Figure II.14, which shows the sum of charged-particle transverse momenta in region close to the leading track (i.e. the toward region) and perpendicular to the leading track (transverse region) [33]. These are typical minimum-bias observables especially designed to investigate the underlying event, and PYTHIA8 tune A2 includes this data in the tuning procedure. It is reassuring that the inclusion of two additional jets through the UMEPS scheme did not invalidate this tuning.

II.6 Discussion

Before concluding this letter, we would like to make some comments to put this method into perspective.

[8]This of course does *not* mean that we will to use this data for tuning, but that α_s-choices for different tunes can have a comparable effect on $\rho(r)$.

Relation to LoopSim

Even though not completely obvious at first sight, UMEPS was heavily influenced by the LoopSim method [34]. This method as introduced to tame order-by-order large logarithmic enhancements by combining matrix elements with different jet multiplicities in a unitary way. The combination is done by joining all combinations to integrate over $1, \ldots, n$ partons in the ME event S_{+n}, and also allowing an integration over hard process particles. In figure II.1, the final state gluons are candidates for integration (or, in the terminology of LoopSim, looping), and the W−boson can be looped as well. With such a procedure, enhancements due to collinear W−boson radiation off a dijet state can be compensated[9].

Apart from major technical differences, one interesting difference is that in the LoopSim method, higher fixed-order corrections are approximated by multiple loopings, whereas in UMEPS, an all-order expression is included in the S_{+n+1} state before one parton is looped. Integrating multiple emissions is only necessary for ρ_{MS}−unordered sequences of splittings, which are not considered in LoopSim. Furthermore, in UMEPS, only integrations of QCD splittings are performed, while LoopSim includes loopings of W−boson radiation. We postpone the inclusion W−boson clusterings in UMEPS until a full electroweak shower is available in PYTHIA8. It would clearly be interesting to combine the Sudakov resummation in UMEPS with the multiple loopings done in LoopSim. To arrive at a better description of S_{+0} configurations, one could e.g. take α_s^1 contributions from the looped S_{+1} state, α_s^2 contributions from the twice-looped S_{+2}, and all higher orders from Sudakov-reweighted thrice-integrated S_{+3} events. The way the inclusive cross section is maintained in such a procedure will be less obvious than in the case of LoopSim or UMEPS.

Merging scale dependence

In the original CKKW-L algorithm it is evident that the dependence on the merging scale is absent to the accuracy of the PS. This means that for any observable, leading logarithmic terms on the form $\alpha_s^n L^{2n}$, where $L = \ln \mu_F / \rho_{\text{MS}}$, are correctly cancelled to all orders. For a shower[10] which in

[9] At very large transverse momenta, the effect of multiple soft/collinear electroweak bosons becomes important. An appraisal of high-$p_\perp$ observables in WZ-production has recently been reported [35].

[10] Note that the shower in PYTHIA8 which is used in simulations in this paper has not been formally proven to be NLL-correct.

addition is correct to next-to-leading logarithmic accuracy, also terms on the form $\alpha_s^n L^{2n-1}$ are correctly cancelled.

What we have accomplished with the UMEPS method is that the total inclusive Born-level cross section is almost completely independent of the merging scale. In addition, if we look at the master formula in eq. (II.39), it is clear that for any phase space point ϕ_n with n resolved partons, the inclusive cross section, integrating all contributions from higher parton multiplicities, is simply given by $\widehat{\mathrm{B}}_n$. Although $\widehat{\mathrm{B}}_n$ includes no-emission probabilities calculated by the shower, it has no dependence on the merging scale, and hence, all inclusive n-jet cross sections are independent of the merging scale. Since exclusive n-jet cross sections are the difference between the n-jet and $n+1$-jet inclusive cross sections, also these are independent of the merging scale.

The independence is, of course, not exact for any real observable. A jet algorithm will not cluster an $n+1$-jet state back to the precise n-parton phase space point as would the mapping of the parton shower, or symbolically for a general observable $\mathcal{O}$, $\int \mathcal{O}(S_{+n+1j})\widehat{\mathrm{B}}_{n+1} \neq \mathcal{O}(S_{+nj}) \int_s \widehat{\mathrm{B}}_{n+1\to n}$. However, as long as the observable is collinear- and infrared-safe this difference will not have any logarithmic enhancements, and as long as the n-jet state is well above the merging scale we can take this scale to be arbitrarily small, without changing the n-jet cross section.

Also, as we have noted before, there are some n-parton states, such as the one in figure II.1, which do not have an underlying $n-1$-parton state reachable with a reconstructed PS emission. Unless the PS is amended with W-strahlung splittings, such contributions will always give a small dependence. However, we have found these to be numerically very small in the cases we have investigated.

Events with negative weight

Contrary to the standard CKKW(-L) algorithms our new UMEPS procedure will produce negatively weighted events. There has in the past been a great reluctance in the experimental community towards using generators with negative event weights. Mostly this has been a question about problems in handling the statistics and that it seems wasteful to spend a huge number of CPU cycles to do a full detector simulation on an event, which in the end will be cancelled by another event with a negative weight. However, the acceptance for negative weights have increased, and today most experiments are using programs such

as MC@NLO [36–39], which do produce a fair amount of events with negative weight.

Clearly UMEPS is more wasteful than CKKW-L in this respect, and the number of events that need to be analysed to get the same statistics is more than doubled. In fact it can be shown that the variance in the event weights, when calculating the no-emission probability for the zero-jet case in CKKW-L with the Sudakov-veto algorithm, is proportional to $\Pi_{S_{+0}} - \Pi_{S_{+0}}^2$. The variance for UMEPS, where the corresponding factor is calculated by reclustering one-jet states multiplied by a no-emission probability, is of the form

$$\frac{1-\Pi_{S_{+0}}}{-\ln\Pi_{S_{+0}}} - \left(\frac{1-\Pi_{S_{+0}}}{-\ln\Pi_{S_{+0}}}\right)^2. \tag{II.45}$$

Thus, for small merging scales (giving small no-emission probabilities), UMEPS becomes very inefficient as compared to CKKW-L.

We believe that the benefits of UMEPS outweigh this drawback. Also we note that the algorithm works in a way such that all events will either have zero weight or a weight of order ($\pm$) unity. This is because the no-emission probabilities are generated by the Sudakov-veto algorithm and are therefore either zero or unity, while the PDF- and α_s-reweighting typically is of $\mathcal{O}(1)$. Had the no-emission probabilities been calculated analytically, they would be very small for small merging scales, and e.g. each single 0-jet ME event would have to be cancelled by large number of small-weight reclustered 1-jet events. This would be very inefficient if a CPU-heavy detector simulation would have to be run on each event.

On the other hand, the Sudakov-veto algorithm causes some problem in the case full detector simulation is not used. In this case the computational bottle neck is typically in the ME generation of high jet multiplicities, and the problem is that most of these events are given zero weight and will be thrown away by the Sudakov-veto algorithm, especially for small merging scales. This can in principle be handled by a modification of the veto algorithm [40] where all events are kept but are given a small weight.

II.7 Conclusions and Outlook

In this article, we have presented a new method for tree-level matrix element merging called UMEPS. This method is heavily indebted to the CKKW-L prescription, but explicitly keeps the total inclusive cross

section fixed. Since it builds on the implementation of CKKW-L in PYTHIA8, all developments of CKKW-L are immediately available to UMEPS. This for example includes improvements for BSM processes [41] and multiple pre-defined merging scales.

The UMEPS scheme uses an add-subtract prescription inspired by parton shower unitarity to combine the improved description of observable shapes of CKKW-L with a fixed total inclusive cross section. This means that significantly lower the merging scale values are possible, which allows for controlled improvement of low-scale features of the parton shower. Tuning efforts will be subject of a future article. When confronted with data, UMEPS and CKKW-L perform equally well.

UMEPS is an ideal candidate for further improvements, since the lowest-multiplicity cross section is not reweighted, making replacements with the full NLO or NNLO results possible. We have successfully implemented an NLO extension, and will present it in a separate publication [42].

Finally, while finishing this article, it came to our attention that a very similar approach has been developed in parallel by Plätzer [43], which further describes the extension of an inclusive-cross-section preserving merging method to NLO accuracy.

Acknowledgements

Work supported in part by the Swedish research council (contracts 621-2009-4076 and 621-2010-3326). We would like to thank Simon Plätzer, Stefan Höche and Frank Tackmann for helpful discussions.

II References

[1] N. Lavesson and L. Lönnblad, "Extending CKKW-merging to One-Loop Matrix Elements," *JHEP* **12** (2008) 070, arXiv:0811.2912 [hep-ph].

[2] K. Hamilton and P. Nason, "Improving NLO-parton shower matched simulations with higher order matrix elements," *JHEP* **1006** (2010) 039, arXiv:1004.1764 [hep-ph].

[3] S. Höche, F. Krauss, M. Schönherr, and F. Siegert, "NLO matrix elements and truncated showers," arXiv:1009.1127 [hep-ph].

[4] S. Alioli, K. Hamilton, and E. Re, "Practical improvements and merging of POWHEG simulations for vector boson production," *JHEP* **1109** (2011) 104, arXiv:1108.0909 [hep-ph].

[5] K. Hamilton, P. Nason, and G. Zanderighi, "MINLO: Multi-Scale Improved NLO," *JHEP* **1210** (2012) 155, arXiv:1206.3572 [hep-ph].

[6] T. Gehrmann, S. Höche, F. Krauss, M. Schönherr, and F. Siegert, "NLO QCD matrix elements + parton showers in e+e- $\to$ hadrons," arXiv:1207.5031 [hep-ph].

[7] S. Höche, F. Krauss, M. Schönherr, and F. Siegert, "QCD matrix elements + parton showers: The NLO case," arXiv:1207.5030 [hep-ph].

[8] R. Frederix and S. Frixione, "Merging meets matching in MC@NLO," arXiv:1209.6215 [hep-ph].

[9] C. W. Bauer, F. J. Tackmann, and J. Thaler, "GenEvA. I. A New framework for event generation," *JHEP* **0812** (2008) 010, arXiv:0801.4026 [hep-ph].

[10] C. W. Bauer, F. J. Tackmann, and J. Thaler, "GenEvA. II. A Phase space generator from a reweighted parton shower," *JHEP* **0812** (2008) 011, arXiv:0801.4028 [hep-ph].

[11] S. Alioli, C. W. Bauer, C. J. Berggren, A. Hornig, F. J. Tackmann, *et al.*, "Combining Higher-Order Resummation with Multiple NLO Calculations and Parton Showers in GENEVA," arXiv:1211.7049 [hep-ph].

[12] S. Catani, F. Krauss, R. Kuhn, and B. R. Webber, "QCD matrix elements + parton showers," *JHEP* **11** (2001) 063, arXiv:hep-ph/0109231.

[13] L. Lönnblad, "Correcting the colour-dipole cascade model with fixed order matrix elements," *JHEP* **05** (2002) 046, arXiv:hep-ph/0112284.

[14] N. Lavesson and L. Lönnblad, "W + jets matrix elements and the dipole cascade," *JHEP* **07** (2005) 054, arXiv:hep-ph/0503293.

[15] S. Höche, F. Krauss, S. Schumann, and F. Siegert, "QCD matrix elements and truncated showers," *JHEP* **05** (2009) 053, arXiv:0903.1219 [hep-ph].

[16] L. Lönnblad, and S. Prestel, "Matching Tree-Level Matrix Elements with Interleaved Showers," *JHEP* **1203** (2012) 019, arXiv:1109.4829 [hep-ph].

[17] M. Bengtsson and T. Sjostrand, "A Comparative Study of Coherent and Noncoherent Parton Shower Evolution," *Nucl.Phys.* **B289** (1987) 810.

[18] M. Bengtsson and T. Sjostrand, "Coherent Parton Showers Versus Matrix Elements: Implications of PETRA - PEP Data," *Phys.Lett.* **B185** (1987) 435.

[19] G. Miu, "A Matrix element based modification of the parton shower," arXiv:hep-ph/9804317 [hep-ph].

[20] G. Miu and T. Sjostrand, "W production in an improved parton shower approach," *Phys.Lett.* **B449** (1999) 313–320, arXiv:hep-ph/9812455 [hep-ph].

[21] W. T. Giele, D. A. Kosower, and P. Z. Skands, "A Simple shower and matching algorithm," *Phys.Rev.* **D78** (2008) 014026, arXiv:0707.3652 [hep-ph].

[22] W. Giele, D. Kosower, and P. Skands, "Higher-Order Corrections to Timelike Jets," *Phys.Rev.* **D84** (2011) 054003, arXiv:1102.2126 [hep-ph].

[23] T. Sjöstrand, S. Mrenna, and P. Skands, "A Brief Introduction to PYTHIA 8.1," *Comput. Phys. Commun.* **178** (2008) 852–867, arXiv:0710.3820 [hep-ph].

[24] P. Nason, "A new method for combining NLO QCD with shower Monte Carlo algorithms," *JHEP* **11** (2004) 040, arXiv:hep-ph/0409146.

[25] J. Alwall *et al.*, "A standard format for Les Houches Event Files," *Comput. Phys. Commun.* **176** (2007) 300–304, hep-ph/0609017.

[26] M. Cacciari, G. P. Salam, and G. Soyez, "FastJet User Manual," *Eur.Phys.J.* **C72** (2012) 1896, arXiv:1111.6097 [hep-ph].

[27] C. Balazs, J. Huston, and I. Puljak, "Higgs production: A Comparison of parton showers and resummation," *Phys.Rev.* **D63** (2001) 014021, arXiv:hep-ph/0002032 [hep-ph].

[28] R. Corke and T. Sjöstrand, "Interleaved Parton Showers and Tuning Prospects," *JHEP* **03** (2011) 032, arXiv:1011.1759 [hep-ph].

[29] T. A. collaboration, "Summary of ATLAS Pythia 8 tunes,".

[30] A. Buckley *et al.*, "Rivet user manual," arXiv:1003.0694 [hep-ph].

[31] **ATLAS Collaboration** Collaboration, G. Aad *et al.*, "Study of jets produced in association with a W boson in pp collisions at $\sqrt{s} = 7$ TeV with the ATLAS detector," *Phys.Rev.* **D85** (2012) 092002, arXiv:1201.1276 [hep-ex].

[32] **Atlas Collaboration** Collaboration, G. Aad *et al.*, "Study of Jet Shapes in Inclusive Jet Production in pp Collisions at $\sqrt{s} = 7$ TeV using the ATLAS Detector," *Phys.Rev.* **D83** (2011) 052003, arXiv:1101.0070 [hep-ex].

[33] **Atlas Collaboration** Collaboration, G. Aad *et al.*, "Measurement of underlying event characteristics using charged particles in pp collisions at $\sqrt{s} = 900GeV$ and 7 TeV with the ATLAS detector," *Phys.Rev.* **D83** (2011) 112001, arXiv:1012.0791 [hep-ex].

[34] M. Rubin, G. P. Salam, and S. Sapeta, "Giant QCD K-factors beyond NLO," *JHEP* **1009** (2010) 084, arXiv:1006.2144 [hep-ph].

[35] F. Campanario and S. Sapeta, "WZ production beyond NLO for high-pT observables," *Phys.Lett.* **B718** (2012) 100–104, arXiv:1209.4595 [hep-ph].

[36] S. Frixione and B. R. Webber, "Matching NLO QCD computations and parton shower simulations," *JHEP* **06** (2002) 029, arXiv:hep-ph/0204244.

[37] S. Höche, F. Krauss, M. Schönherr, and F. Siegert, "A critical appraisal of NLO+PS matching methods," *JHEP* **1209** (2012) 049, arXiv:1111.1220 [hep-ph].

[38] S. Höche, F. Krauss, M. Schönherr, and F. Siegert, "W+n-jet predictions with MC@NLO in Sherpa," *Physical Review Letters* (2012) , arXiv:1201.5882 [hep-ph].

[39] V. Hirschi, R. Frederix, S. Frixione, M. V. Garzelli, F. Maltoni, *et al.*, "Automation of one-loop QCD corrections," *JHEP* **1105** (2011) 044, arXiv:1103.0621 [hep-ph].

[40] L. Lönnblad, "Fooling Around with the Sudakov Veto Algorithm," arXiv:1211.7204 [hep-ph].

[41] H. K. Dreiner, M. Kramer, and J. Tattersall, "How low can SUSY go? Matching, monojets and compressed spectra," *Europhys.Lett.* **99** (2012) 61001, arXiv:1207.1613 [hep-ph].

[42] L. Lönnblad and S. Prestel, "Merging Multi-leg NLO Matrix Elements with Parton Showers," arXiv:1211.7278 [hep-ph].

[43] S. Plätzer, "Controlling inclusive cross sections in parton shower + matrix element merging," `arXiv:1211.5467 [hep-ph]`.

III

Merging Multi-leg NLO Matrix Elements with Parton Showers

Leif Lönnblad and Stefan Prestel
Dept. of Astronomy and Theoretical Physics, Lund University, Sweden
Submitted to the Journal of High Energy Physics.
LU-TP 12-43
MCnet-12-17
e-Print: arXiv:1211.7278 [hep-ph].

We discuss extensions of multi-jet matrix element and parton shower merging approaches, to also include next-to-leading order accuracy. Specifically, we generalise the so-called CKKW-L prescription and the recently developed unitarised matrix element + parton shower (UMEPS) scheme. Endowing tree-level merging methods with NLO corrections greatly enhances the perturbative accuracy of parton shower Monte Carlo programs.

To generalise the CKKW-L approach, we augment the Nils-Lavesson-Leif-Lönnblad (NL^3) scheme, which was previously developed for e^+e^--annihilation, with a careful treatment of parton densities. This makes the application of the NL^3 method to hadronic collisions possible. NL^3 is further updated to use for more readily accessible next-to-leading order input calculations.

We also extend the UMEPS scheme to NLO accuracy. The resulting approach, dubbed unitarised next-to-leading order + parton shower (UNLOPS) merging, does not inherit problematic unitarity-breaking features of CKKW-L, and thus allows for a theoretically more appealing definition of NLO order merging.

Both schemes have been implemented in PYTHIA8. We present results for the merging of W- and Higgs-production events, where the zero- and one-jet contribution are corrected to next-to-leading order simultaneously, and higher jet multiplicities are described by tree-level matrix elements. We find that NL^3 and UNLOPS yield a very similar description for W production. For Higgs production however, UNLOPS produces more stable results.

The implementation of the NLO merging procedures is completely general and can be used for higher jet multiplicities and other processes, subject to the availability of programs able to correctly generate the corresponding partonic states to leading and next-to-leading order accuracy.

III.1 Introduction

Particle physics phenomenology has been awed by the accuracy of LHC analyses. The precision at which, for example, the Higgs candidate mass has been measured could only be achieved through a very detailed understanding of the structure of collision events in an environment that can safely be called messy. Remnants of single collisions alone give rise to large numbers of hadronic jets, leptons and photons – even before pile-up events are taken into account. In order to separate and determine the characteristics of rare signal events, highly accurate methods have evolved to describe background processes.

Precise theoretical calculations for scatterings with multiple jets in particular are necessary for reliable background estimates. For generic processes this, until recently, meant that multi-jet tree-level matrix element and parton shower merging (MEPS) techniques were the method of choice, with CKKW-inspired prescriptions [1–5] being widely used. These methods impose a weight containing the parton shower resummation on tree-level-weighted n-parton phase space points. Phase space points with soft and/or collinear partons in the matrix element (ME) event generation are removed by a jet-resolution cut, leaving only n-parton phase space points that contain exactly n resolved jets. The same cut is also used to restrict the parton shower (PS) to only produce unresolved partons as long as tree-level calculations for the resulting state are available. The combination of reweighting and phase space slicing (by the jet separation cut) allows to add tree-level samples with different jet multiplicity without introducing any phase space overlap.

This method has an evident drawback, even if we would be content with a tree-level prescription of multiple jets: Simply adding n-resolved-jet states cannot guarantee a stable inclusive (lowest-multiplicity) cross section. In particular, the inclusive cross will depend on the jet separation parameter, t_{MS}, so that choosing t_{MS} unwisely may result in significant cross section uncertainties. This problem is remedied by the UMEPS method [6], which infers the notion of parton shower unitarity to derive an add-subtract scheme to safeguard a fixed inclusive cross section.

However, MEPS methods only improve the description of the shape of multi-jet observables, and cannot describe overall normalisations or decrease theoretical uncertainties due to scale variations. This requires predictions of next-to-leading order (NLO) QCD. Through formidable efforts of the fixed-order community, we have recently witnessed an

NLO revolution[1], meaning that today, the automation of NLO calculations is practically a solved problem. Such calculations become directly comparable to LHC data by incorporating the NLO results into General-Purpose event generators. NLO matrix element and parton shower matching methods like POWHEG [17–20] and MC@NLO [21–24] have – in parallel with the NLO revolution – become robust tools that allow a coalescence of resummation, low-scale effects and hadronisation with NLO calculations.

The latest step in these developments are multi-jet NLO merging prescriptions [25–28]. These address the problem of simultaneously describing observables for any number of (additional) jets with NLO accuracy, and are thus direct successors of the tree-level schemes. The problem in NLO multi-jet merging is twofold. It is firstly mandatory – as in tree-level merging – to ensure that configurations with n hadronic jets are described by the n-jet ME. If we have a better calculation at hand, we do not want to predict rates for n hadronic jets by adding a parton shower emission to the $(n-1)$-jet NLO calculation. This problem has already been solved in tree-level merging methods. Secondly, each n-jet observable has to be described with NLO accuracy (if an NLO calculation of the $n-$jet cross section was used as input), while all higher orders in α_s should be given by the parton shower resummation (possibly with improvements). This problem can be overcome by

(1) Using tree-level matrix elements only as seeds for higher-order corrections, i.e. including the full resummation in tree-level events, and safeguarding that the weighting of n-jet tree-level configurations does not introduce $\mathcal{O}(\alpha_s^{n+1})$-terms.

(2) Defining an NLO cross section for n-parton states that does not include $n+1$ resolved jets, and making sure that no (uncontrolled) $\mathcal{O}(\alpha_s^{n+2})$-corrections are introduced by the NLO calculation.

(3) Adding the corrected tree-level and the NLO events.

This means that we have to decide how to define NLO cross section for n-parton states that do not include $n+1$ resolved jets. We call an NLO calculation "exclusive" if it contains weights for n-jet phase space points that include Born, virtual and unresolved real corrections, where the resolution criterion is defined by exactly the same function as the merging scale. If *all* real emission corrections are projected onto n-jet kinematics, the calculation will be called "inclusive" instead. It is fea-

[1] We cannot do justice to all results of these intricate calculations, so that we limit ourselves to the more conceptual papers [7–16], which made this progress possible.

sible to make an inclusive calculation exclusive by introducing explicit counter-events that are distributed according to the resolved-emission contribution, and subtracting these events from events generated according to the inclusive NLO cross section.
The points (1) - (3) will schematically lead to an algorithm of the form

- Reweight n-resolved-jet tree-level events with weight used in the tree-level merging scheme.
- Subtract the $\mathcal{O}(\alpha_s^n)$ and $\mathcal{O}(\alpha_s^{n+1})$ terms introduced by this prescription from the tree-level events.
- Add NLO-weighted n-resolved-jet events.

Many variations of this basic form are possible. The first conceptual paper on NLO merging [29] for example advocated subtracting $\mathcal{O}(\alpha_s^{n+1})$-terms from the NLO cross section. This is also the case in the MINLO NLO matching scheme [30], and the NLO merging scheme introduced for aMC@NLO [28]. MEPS@NLO [26, 27] exerts full control over the NLO calculation to avoid point (1). We hope that the near future will bring detailed comparisons of all these schemes.

Moving beyond tree-level merging prescriptions has long been regarded the next crucial step in background simulations for the LHC. The aim of this article is to present a comprehensive guide to NLO merging schemes in PYTHIA8 [31]. We will present two different NLO merging schemes, choosing to generalise both the CKKW-L and UMEPS methods. We will refer to the NLO version of CKKW-L as NL^3, since this is an extension of the NLO merging scheme for e^+e^--collision presented in [25] to hadronic collisions, now also allowing for POWHEG input. The virtue of this method is its relative simplicity in combining NLO accuracy with PS resummation. However, it inherits violations of the inclusive cross section from CKKW-L. Cross section changes are the result of adding higher-multiplicity matrix elements – containing logarithmic terms that are beyond the accuracy of the parton shower, and which can thus not be properly cancelled. At tree-level, this issue was resolved by the UMEPS method. Thus, we believe that a NLO generalisation of UMEPS, which also cancels new logarithmic contributions appearing at NLO, is highly desirable. This method will be coined UNLOPS for unitary next-to-leading-order matrix element and parton shower merging[2].

This publication is split into a main text and a large appendix section. The main text should be regarded as an introduction of the methods,

[2]While finishing this article, a conceptual publication [32] was presented, discussing similar methods.

while all technical details and derivations are collected in appendices. Sections in the main body are intended to give an overview of NL^3 and UNLOPS, and explain some benefits with simple examples. The appendices are aimed at completeness, and in principle allow an expert reader to implement our methods in detail. As such, the appendices can also be considered a technical manual of the PYTHIA8 implementation.

We begin by reviewing the CKWW-L method (section III.2.1) and the UMEPS improvement (section III.2.2). Then, we move to NLO merging methods (section III.3), discuss NL^3 in section III.3.1, and describe UNLOPS in section III.3.2. Comments on the methods, and on the interplay between sub-dominant logarithms and the $\mathcal{O}(\alpha_s^{n+1})$-corrections of the NLO calculations, are given in section III.3.3. After these, we show the feasibility of the NLO merging schemes by presenting results for W-boson production (sections III.4.1 and III.4.3) and for H-boson production in gluon fusion (section III.4.2). The main text concludes with section III.5.

In appendix III.A we discuss some of the prerequisites that we need in order to derive our merging schemes, such as our choice of merging scale (III.A.1), the form of NLO input events that is required for NLO merging in PYTHIA8 (III.A.2), a detailed description of the notation we use (III.A.3) and an outline of how the POWHEG-BOX program can be used to produce the desired NLO input (III.A.4).

All technical details on how weights and subtraction terms are generated is deferred to appendix III.B, ending in a summary (appendix III.B.4). From there, we move to a motivated derivation of the general NL^3 method in appendix III.C, which can also be understood as a validity proof. The corresponding derivation of UNLOPS is given in appendix III.D, to which a comment on pushing this method to NNLO is attached (section III.D.1). We finally discuss the addition of multiparton interactions to NLO-merged results in appendix III.E.

Before moving to the main text, we would like to apologise for the inherent complexity of NLO merging methods. Also, we would like to affirm that in PYTHIA8, intricacies are handled internally, so that with reasonable input, producing NLO-merged predictions should not be difficult. The schemes described in this paper will be part of the next major PYTHIA8 release.

III.2 Tree-level multi-jet merging

Since the methods presented in this article are heavily indebted to tree-level merging methods, we would like to start with a brief discussion of CKKW-inspired schemes. Let us first introduce some technical jargon.

We think of the results of fixed-order calculations as matrix element (ME) weights, integrated over the allowed phase space of outgoing particles. In the following, we will refer to a phase space point (i.e. a set of momentum-, flavour- and colour values for a configuration with *n additional* partons) as a $n-$parton event, $n-$parton state or simply S_{+n}. Let us use the term "n-resolved-jet phase space point" (often shortened to n-jet point, n-jet configuration or n-jet state) for a point in the integration region for which all n partons have a jet separation larger than a cut t_{MS}. We further classify any configuration of hadronic jets by the number of resolved jets from which it emerged. The goal of merging schemes is to describe configurations with n hadronic jets with n-jet fixed-order matrix elements, meaning that the distribution of hadronic jets is governed by the "seed" partons in the $n-$jet phase space point, while parton showers only dress the seed partons in soft/collinear radiation. We will often use the notation $\mathcal{O}\left(S_{+nj}\right)$ to indicate that the observable $\mathcal{O}$ has been evaluated on configurations containing n resolved jets.

Tree-level merging schemes have to ensure that an n-resolved-jet configuration never evolves into a state with $n+1$ well-separated hadronic jets. This can be achieved by applying Sudakov factors to the ME input events and by vetoing emissions above t_{MS}. To capture the full parton shower resummation, it is common to also reweight the input events with a running coupling. Because no n-resolved-jet event evolves to an $(n+1)$-resolved-jet state, it is possible to add all contributions, and combine the tree-level description of well-separated jets with the resummation of parton showers, which can then be processed by hadronisation models.

To summarise, tree-level merging is realised by calculating tree-level-weighted n-jet phase space points for up to N additional jets, reweighting these events, guaranteeing that ME events do not fill overlapping regions of phase space, and combining the different event samples for predictions of observables. It is not reasonable to limit observable predictions to only include configurations with up to N additional resolved jets. Instead, the parton shower is used to generate resolved jets for all multiplicities $n > N$, for which no tree-level calculation is available. This is accomplished by *not* restricting the emissions off the

highest multiplicity (N-jet) ME state to unresolved partons only.

There are in principle different ways how to combine the reweighted samples in tree-level merging. CKKW-inspired methods use an additive scheme, while unitarised MEPS opts for an add-subtract prescription. In the following, we will briefly discuss CKKW-L and UMEPS.

III.2.1 CKKW-L

The CKKW-L method [2,3,5] imposes tree-level accuracy on the parton shower description of phase space regions with $n \leq N$ well-separated partons. To this purpose, tree-level-weighted phase space point are generated in the form of Les Houches Event files [33]. The cross section of producing a state S_{+n} with n partons has to be regularised by a cut t_{MS} on the momenta of the partons. In CKKW-L, any (collection of) cuts that regularise the calculation are allowed. t_{MS} is commonly called merging scale.

The events with $n = 1, \ldots, N$ additional partons will then be reweighted to incorporate parton shower resummation. The parton shower off states $S_{+n<N}$ is further forbidden to generate radiation that passes the cut t_{MS}. Reweighting with no-emission probabilities, and ensuring that parton shower emissions do not fill phase space regions for which events are available from other ME multiplicities, will guarantee that there is no double-counting between events with different number of partons in the ME calculation. In this publication, we will use the minimal parton shower evolution variable ρ as regularisation cut, and hence denote the merging scale by ρ_{MS}. This choice is discussed in appendix III.A.1.

The full CKKW-L weight to make n-parton events exclusive, and minimise the dependence on ρ_{MS}, is given by

$$
\begin{aligned}
w_n =& \frac{x_0^+ f_0^+(x_0^+,\rho_0)}{x_n^+ f_n^+(x_n^+,\mu_F)} \frac{x_0^- f_0^-(x_0^-,\rho_0)}{x_n^- f_n^-(x_n^-,\mu_F)} \times \left(\prod_{i=1}^{n} \frac{x_i^+ f_i^+(x_i^+,\rho_i)}{x_{i-1}^+ f_{i-1}^+(x_{i-1}^+,\rho_{i-1})} \frac{x_i^- f_i^-(x_i^-,\rho_i)}{x_{i-1}^- f_{i-1}^-(x_{i-1}^-,\rho_{i-1})} \right) \\
& \times \left(\prod_{i=1}^{n} \frac{\alpha_s(\rho_i)}{\alpha_s(\mu_R)} \right) \times \left(\prod_{i=1}^{n} \Pi_{S_{+i-1}}(x_{i-1},\rho_{i-1},\rho_i) \right) \times \Pi_{S_{+n}}(x_n,\rho_n,\rho_{\text{MS}}) \qquad \text{(III.1)} \\
=& \frac{x_n^+ f_n^+(x_n^+,\rho_n)}{x_n^+ f_n^+(x_n^+,\mu_F)} \frac{x_n^- f_n^-(x_n^-,\rho_n)}{x_n^- f_n^-(x_n^-,\mu_F)} \\
& \times \prod_{i=1}^{n} \left[\frac{\alpha_s(\rho_i)}{\alpha_s(\mu_R)} \frac{x_{i-1}^+ f_{i-1}^+(x_{i-1}^+,\rho_{i-1})}{x_{i-1}^+ f_{i-1}^+(x_{i-1}^+,\rho_i)} \frac{x_{i-1}^- f_{i-1}^-(x_{i-1}^-,\rho_{i-1})}{x_{i-1}^- f_{i-1}^-(x_{i-1}^-,\rho_i)} \Pi_{S_{+i-1}}(x_{i-1},\rho_{i-1},\rho_i) \right] \\
& \times \Pi_{S_{+n}}(x_n,\rho_n,\rho_{\text{MS}}) \,, \qquad \text{(III.2)}
\end{aligned}
$$

where ρ_i are reconstructed emission scales. The first PDF ratio in eq. (III.1) means that the total cross section is given by the lowest order Born-level matrix element, which is what non-merged PYTHIA8 uses. The PDF ratio in brackets comes from of the fact that shower splitting probabilities are products of splitting kernels and PDF factors. The running of α_s is correctly included by the second bracket. Finally, the event is made exclusive by multiplying no-emission probabilities. The PYTHIA8 implementation reorders the PDF ratios according to eq. (III.2), so that only PDFs of fixed flavour and x-values are divided, thus making the weight piecewise numerically more stable. This will also later be useful when expanding the CKKW-L weight. For the highest multiplicity, the last no-emission probability $\Pi_{S_{+N}}(x_N, \rho_N, \rho_{\text{MS}})$ is absent to not suppress well-separated emissions for which no ME calculation is available.

The calculation of the CKKW-L weight is made possible by using a parton shower history. Parton shower histories are crucial for all merging methods, so it is necessary to elaborate. The matrix element state, S_{+n}, (read from a LHE file) is interpreted as the result of a sequence of PS splittings, evolving from a zero-jet state, S_{+0}, to a one-jet state, S_{+1}, etc. until the the state S_{+n-1} splits to produce the input S_{+n}. All splittings occur at associated scales $\rho_1, \ldots, \rho_n$. A parton shower history (short PS history) for an input state S_{+n}, i.e. a sequence of states, $S_{+0}, \ldots, S_{+n}$, and scales $\rho_1, \ldots, \rho_n$, is constructed from the input event by inverting the parton shower phase space on S_{+n}. This means that in a first step, we identify partons in S_{+n} that could have resulted from a splitting, recombine their momenta, flavours and colours, and iterate this procedure on $S_{+n-1}, \ldots, S_{+0}$. Clearly, there can be many ways of constructing such a history "path". Indeed, we construct all possible parton shower histories for each input state S_{+n}, and then choose one history path probabilistically, using the product of PS branching probabilities as discriminant. More on this matter can be found in [5].

A CKKW-L merged prediction for and observable $\mathcal{O}$ is obtained by adding all contributions for fixed numbers of resolved jets $\mathcal{O}(S_{+nj})$, given by the reweighted (i.e. exclusive) the S_{+n} events, for all multiplicities $n = 1, \ldots, N$. Using the symbol B_n for the fully differential n-parton tree-level hadronic cross section, the prediction for $\mathcal{O}$ is given by

$$\langle \mathcal{O} \rangle = \int d\phi_0 \Bigg\{ \mathcal{O}(S_{+0j}) \text{B}_0 w_0 + \int \mathcal{O}(S_{+1j}) \text{B}_1 w_1 + \iint \mathcal{O}(S_{+2j}) \text{B}_2 w_2 + \qquad \text{(III.3)}$$

$$\left. \ldots + \int\ldots\int \mathcal{O}(S_{+Nj})\mathrm{B}_N w_N \right\}$$
$$= \sum_{n=0}^{N} \int d\phi_0 \int\ldots\int \mathcal{O}(S_{+nj})\ \mathrm{B}_n w_n \ , \tag{III.4}$$

where we have used the symbol S_{+nj} to indicate states with n resolved jets, resolved meaning above the cut ρ_{MS} as defined by the merging scale definition. The contribution of states with more than N resolved jets is included by allowing the parton shower to produce emissions above the merging scale when showering the N-jet ME events.

III.2.2 UMEPS

The idea of unitarised matrix element + parton shower (UMEPS) merging [6] is to supplement CKKW-L merging with approximate higher orders for low-multiplicity states, in order to exactly preserve the n-jet inclusive cross sections. In UMEPS, events with additional jets, which are simply added in CKKW-L, are also subtracted, albeit from lower-multiplicity states. This subtraction is motivated by the mechanism for how non-corrected parton showers would preserve the inclusive cross section. The contribution for a jet being emitted off S_{+0} at scale ρ, for example, is cancelled with contributions for no jet being emitted between ρ_{max} and ρ. UMEPS makes this cancellation explicit by constructing subtraction terms through integration over the phase space of the last emitted jet. The guiding principle is "subtract what you add": If $n-$parton events are added, those events should, in an integrated form, be subtracted from $(n-1)-$parton states. Improvements in multi-jet observables are retained, since integrated n-parton events and "standard" events contribute to different jet multiplicities.
In UMEPS, Les Houches events with (initially) $n-$partons are reweighted with

$$w'_n = \frac{x_n^+ f_n^+(x_n^+,\rho_n)}{x_n^+ f_n^+(x_n^+,\mu_F)} \frac{x_n^- f_n^-(x_n^-,\rho_n)}{x_n^- f_n^-(x_n^-,\mu_F)} \tag{III.5}$$
$$\times \prod_{i=1}^{n} \left[\frac{\alpha_{\mathrm{s}}(\rho_i)}{\alpha_{\mathrm{s}}(\mu_{\mathrm{R}})} \frac{x_{i-1}^+ f_{i-1}^+(x_{i-1}^+,\rho_{i-1})}{x_{i-1}^+ f_{i-1}^+(x_{i-1}^+,\rho_i)} \frac{x_{i-1}^- f_{i-1}^-(x_{i-1}^-,\rho_{i-1})}{x_{i-1}^- f_{i-1}^-(x_{i-1}^-,\rho_i)} \Pi_{S_{+i-1}}(x_{i-1},\rho_{i-1},\rho_i) \right] .$$

This is the CKKW-L weight w_n without the last no-emission probability $\Pi_{S_{+n}}(x_n,\rho_n,\rho_{\mathrm{MS}})$ (i.e. for the highest multiplicity N: $w'_N = w_N$). As before, we make use of a PS history to calculate this weight. Denoting the tree-level differential n-parton cross section by B_n, and introducing the

notation

$$\mathrm{B}_n w'_n \;=\; \widehat{\mathrm{B}}_n \qquad \text{and} \qquad \int d^{n-m}\phi\, \mathrm{B}_n w'_n \;=\; \int_s \widehat{\mathrm{B}}_{n\to m}\,, \tag{III.6}$$

we can write the UMEPS n-jet merged prediction for an observable $\mathcal{O}$ as

$$\begin{aligned}
\langle \mathcal{O} \rangle =& \int d\phi_0 \Bigg\{ \mathcal{O}(S_{+0j}) \left[\widehat{\mathrm{B}}_0 \;-\; \int_s \widehat{\mathrm{B}}_{1\to 0} \;-\; \int_s \widehat{\mathrm{B}}_{2\to 0} \;-\; \ldots \;-\; \int_s \widehat{\mathrm{B}}_{N\to 0} \right] \\
&+ \int \mathcal{O}(S_{+1j}) \left[\widehat{\mathrm{B}}_1 \;-\; \int_s \widehat{\mathrm{B}}_{2\to 1} \;-\; \ldots \;-\; \int_s \widehat{\mathrm{B}}_{N\to 1} \right] \\
&+ \;\; \ldots \\
&+ \int \ldots \int \mathcal{O}(S_{+N-1j}) \left[\widehat{\mathrm{B}}_{N-1} \;-\; \int_s \widehat{\mathrm{B}}_{N\to N-1} \right] \\
&+ \int \cdots \int \mathcal{O}(S_{+Nj})\, \widehat{\mathrm{B}}_N \Bigg\} \\
=& \sum_{n=0}^{N} \int d\phi_0 \int \ldots \int \mathcal{O}(S_{+nj}) \left\{ \widehat{\mathrm{B}}_n \;-\; \sum_{i=n+1}^{N} \int_s \widehat{\mathrm{B}}_{i\to n} \right\}.
\end{aligned} \tag{III.7}$$

Many parts of standard CKKW-L implementations can be recycled to construct UMEPS predictions. The letter s on the integrals in the samples $\int_s \widehat{\mathrm{B}}_{n+i\to n}$ indicates that the integrated states can directly be read off from intermediate states in the parton shower history. If a one-particle integration includes revoking the effect of recoils, it is possible that the state after performing one integration contains unresolved partons. In this case, we decide to perform further integrations (as indicated by the integration measure in III.6), until the reconstructed lower-multiplicity state involves only resolved jets. Multiple integrations will include the effect of ρ_{MS}-unordered emissions into the description of lower-multiplicity states. We think of these (ρ_{MS}-unordered, sub-leading) contributions as improvements to a strictly ordered parton shower.

It might however not always be possible to find any parton shower histories that will permit at least one integration. If the flavour and colour configurations of a $+n$-parton phase space point cannot be projected onto an "underlying Born" configuration with $n-1$ partons, we call the parton shower history of the phase space point incomplete [5]. The existence of configurations with incomplete histories is reminiscent of which particles are consider radiative partons, meaning that if W-radiation were allowed, a history

$$\mathrm{c\bar{c}} \to \mathrm{u\bar{d}W^-} \qquad \Longrightarrow \qquad \mathrm{c\bar{c}} \to \mathrm{u\bar{u}}$$

is possible, while otherwise, the history of $c\bar{c} \to u\bar{d}W^-$ is incomplete. Note that the effect of incomplete configurations on the cross section is minor, since such contributions are related to flavour changes of fermion lines through radiation. Configurations with incomplete histories are not regarded as corrections to the lowest-multiplicity process, and will be treated as completely new process. Therefore, we will not (and cannot) subtract configurations with incomplete histories from lower-multiplicity states, which leads to marginal changes in the inclusive cross section.

III.2.3 Getting ready for NLO merging

Following appendix III.A.1, we define the merging scale in terms of the shower evolution variable, thus putting $t_{\text{MS}} = \rho_{\text{MS}}$. We further rescale the weights w_n and w'_n by a K-factor, $K = \int \bar{B} / \int B$, to arrive at a better normalisation of the total cross section. This means the introduction of additional $\mathcal{O}(\alpha_s(\mu_R))-$terms, which have to be removed later on. Appendix III.B discusses the generation of these K-factors, which were introduced in [25] to avoid discontinuities across the merging scales. Note that we include K-factors only because we do not see a formal reason against rescaling. In this publication, we attempt to provide a general definition of our new NLO merging schemes, and thus include these factors.

Parton showers make α_s a tunable parameter, so that e.g. $\alpha_s(M_Z)$ is chosen to fit data as closely as possible. This means $\alpha_{\text{sPS}}(M_Z)$ used in the parton shower might not be the value $\alpha_{\text{sME}}(M_Z)$ used in the matrix element calculation. We can recover a uniform α_s-definition by shifting

$$\alpha_{\text{sPS}}(\rho) = \alpha_{\text{sME}}(b_i \rho), \tag{III.8}$$

where b_i might be take different values, b_I or b_F, if $\alpha_{\text{sPS}}(M_Z)$ is different for initial and final state splittings. If $\alpha_{\text{sME}}(b_{I/F}\rho)$ would then be used instead of α_s everywhere, a uniform α_s definition would be recovered. For this paper, we choose $\alpha_{\text{sPS}}(M_Z) = \alpha_{\text{sME}}(M_Z) = \alpha_{s,\text{PDF}}(M_Z)$, i.e. fix the value of $\alpha_s(M_Z)$ to the one used in the parton distributions. In the future, when developing a NLO tune, we will interpret $\alpha_{\text{sPS}}(M_Z)$ as a tuning parameter, so that we can check the influence of NLO merging on the (rather high) parton shower α_s value. For the results in this publication, we will drop the index "ME" on α_s, and understand $b_i = 1$. Our starting

point for NLO merging are $n-$parton samples reweighted by

$$w'_n = K \cdot \frac{x_n^+ f_n^+(x_n^+,\rho_n)}{x_n^+ f_n^+(x_n^+,\mu_F)} \frac{x_n^- f_n^-(x_n^-,\rho_n)}{x_n^- f_n^-(x_n^-,\mu_F)} \times \prod_{i=1}^{n} \left[\frac{\alpha_s(\rho_i)}{\alpha_s(\mu_R)} \frac{x_{i-1}^+ f_{i-1}^+(x_{i-1}^+,\rho_{i-1})}{x_{i-1}^+ f_{i-1}^+(x_{i-1}^+,\rho_i)} \frac{x_{i-1}^- f_{i-1}^-(x_{i-1}^-,\rho_{i-1})}{x_{i-1}^- f_{i-1}^-(x_{i-1}^-,\rho_i)} \Pi_{S_{+i-1}}(x_{i-1},\rho_{i-1},\rho_i) \right] \quad \text{(III.9)}$$

$$w_n = w'_n \Pi_{S_{+n}}(x_n,\rho_n,\rho_{\text{MS}}) \,, \quad \text{(III.10)}$$

in the case of UMEPS and CKKW-L, respectively. When referring to the weight in UMEPS and CKKW-L we will from now on always allude to the weights including a K-factor.

Since we aim at interfacing two different program codes – NLO matrix element generators and parton shower event generators – we need to make sure that the output of one stage (i.e. the NLO ME generator) is completely understood, before using it as input for the event generation step. Thus, we require that all fixed-order calculations are performed with fixed factorisation and renormalisation scale, since dynamic scale choices in the fixed-order calculation result in subtle changes in higher orders[3]. All higher-order terms due to α_s-running and PDF evolution will be carefully taken into account in the merging algorithm by reweighting with eq. (III.9) (or eq. (III.10)).

III.3 Next-to-leading order multi-jet merging

Before sketching the NLO merging schemes we want to present here, we apologise that the discussion is (even after shifting most technical details into appendices) unfortunately very notation-heavy.

Multi-jet merging schemes act on exclusive fixed-order input. This, for example, means that all phase space points that are allowed in the evaluation of tree-level matrix elements with n outgoing partons correspond to configurations with exactly n resolved jets, and no unresolved jets. The resolution criterion is given by the minimal separation of jets, with the relative transverse momentum used as shower evolution variable defining the separation[4].

The idea of using exclusive inputs is adopted for NLO merging, however, the notion of exclusive cross section needs to be refined for next-to-leading order calculations: We consider an $n-$jet NLO calculation exclusive if the output consists of $n-$parton phase space points

[3] The preparation of output of the POWHEG-BOX program [19] is outlined in appendix III.A.4

[4] See appendix III.A.1 for details.

with weights that correspond to the sum of Born, virtual and unresolved real radiation terms, where by unresolved real emission, we mean that the additional emission does not produce an additional resolved jet. It is possible to amend the NLO merging scheme if the requirement that all real emission terms are unresolved is not met (see discussion about exclusive vs. inclusive NLO calculations in appendix III.A.2 for details).

For an NLO merging scheme it is however crucial that virtual and unresolved real contributions contribute to the same phase space points, since otherwise, it is not possible to guarantee an implementation that is independent of the infrared regularisation in the NLO calculation. This problem is solved in POWHEG and MC@NLO, where real-emission contributions are projected onto $n-$jet phase space points by integrating over the radiative phase space. In this article, we use the POWHEG-BOX program [19] as NLO matrix element generator[5].

Note that we do not require any change in the NLO matrix element generator. It is acceptable to produce LHE output with only minimal cuts. The merging scale jet separation will then be enforced internally in PYTHIA8, meaning that after reading the input momentum configuration from LHE file, any event not passing the cut will be dismissed. PYTHIA8 itself can decide if the required number of resolved jets are found, thus rendering the input exclusive.

The aim of this section is to briefly describe two NLO merging algorithms. Each description will be split into a more formal part, and an algorithmic section, with the goal of presenting an overview of the NLO merging prescriptions coined NL^3 and UNLOPS. So that the flow of the narrative is not overly cluttered with technicalities, we have shifted all details into appendices. We however wish to introduce the reader to the symbols[6]

B_n:	Tree-level matrix element for n outgoing partons.
$\int_s \mathrm{B}_{n\to m}$:	Sum of tree-level cross sections with n outgoing partons in the input ME events, after integration over the phase space of $n-m$ partons.
$\mathrm{B}_{n+1\|n}$:	Sum of tree-level configurations with $n+1$ partons with a definite correspondence to a n-parton tree-level matrix element.
V_n:	Virtual correction matrix element for n outgoing partons.

[5] See appendix III.A.4 for details.
[6] See appendix III.A.3 for details.

$\mathrm{D}_{n+1\|n}$:	Sum of infrared regularisation terms for n resolved and one unresolved parton.
$\mathrm{I}_{n+1\|n}$:	Sum of integrated infrared regularisation terms for n resolved and one unresolved parton.
$\overline{\mathrm{B}}_n$:	Inclusive NLO matrix element for n outgoing partons, i.e. sum of Born, virtual and all real contributions as weight of $n-$parton phase space points.
$\widetilde{\mathrm{B}}_n$:	Exclusive NLO matrix element for n outgoing partons, i.e. sum of Born, virtual and unresolved real contributions as weight of $n-$parton phase space points.
$\int_s \overline{\mathrm{B}}_{n\to m}$:	Inclusive NLO cross sections with n outgoing partons in the input ME events, after integration over the phase space of $n-m$ partons.
$\int_s \widetilde{\mathrm{B}}_{n\to m}$:	Exclusive NLO cross sections with n outgoing partons in the input ME events, after integration over the phase space of $n-m$ partons.
$\widehat{\mathrm{B}}_n$:	UMEPS-processed n-resolved-jet tree-level events.
$\int_s \widehat{\mathrm{B}}_{n\to m}$:	UMEPS-processed tree-level cross sections with initially n resolved jets in the input ME events, after integration over the phase space of $n-m$ partons.
$[A]_{-a,b}$:	Contribution A, with terms of powers α_s^a and α_s^b removed.
$[A]_{c,d}$:	Contribution A, with only terms of power α_s^c and α_s^d retained.

Appendix III.A.3 is intended to give more thorough explanations of the notation. Particularly the last two short-hands are helpful when isolating orders in α_s. For example, we have

$$
\begin{aligned}
\left[\mathrm{B}_2\right]_{-2} &= 0 \\
\left[\widetilde{\mathrm{B}}_0\right]_1 &= \mathrm{V}_n + \mathrm{I}_{n+1|n} + \int d\Phi_\mathrm{rad}\Big[\,\mathrm{B}_{n+1|n}\Theta\left(\rho_\mathrm{MS} - t(S_{+n+1},\rho)\right) - \mathrm{D}_{n+1|n}\,\Big] \\
\left[\mathrm{B}_0 w_0\right]_{-0,1} &= \mathrm{B}_0\Big\{w_0 - \left[w_0\right]_0 - \left[w_0\right]_1\Big\} \\
&= \mathrm{B}_0\left\{\Pi_{S_{+0}}(x_0,\rho_0,\rho_\mathrm{MS}) - 1\right. \\
&\quad \left. + \int_{\rho_\mathrm{MS}}^{\rho_0} d\rho\, dz\, \frac{\alpha_\mathrm{s}(\mu_R)}{2\pi}\left[\sum_{a\in\{\text{outgoing}\}}\sum_j P_j^a(z) + \sum_{a\in\{\text{incoming}\}}\sum_j \frac{f_j^a(\frac{x_i^a}{z},\mu_F)}{f_i^a(x_i^a,\mu_F)} P_j^a(z)\right]\right\}
\end{aligned}
$$

All details on the expansion of the tree-level weights can be found in ap-

pendix III.B. We are now equipped for extending CKKW-L and UMEPS tree-level merging to next-to-leading order accuracy.

III.3.1 NL^3: CKKW-L at next-to-leading order

The NL^3 prescription [25] in principle starts from the CKKW-L-weighted tree-level cross sections $\mathrm{B}_n w_n$, adds events weighted according to the exclusive NLO cross sections $\widetilde{\mathrm{B}}_n$, and removes approximate $\mathcal{O}(\alpha_s^0(\mu_R))$ and $\mathcal{O}(\alpha_s^1(\mu_R))$ terms in the CKKW-L weight w_n. Since exclusive NLO samples are rarely accessible, we instead use the inclusive NLO cross section $\overline{\mathrm{B}}_n$, and generate explicit subtraction events by using higher-multiplicity tree-level matrix elements. For details of this choice, we refer to appendix III.A.4.

All details about the derivation of the NL^3 method can be found in appendix III.C. Here, let us assume the construction of NLO accuracy + parton shower higher orders is possible for configurations with exactly m resolved jets, and that the desired accuracy is achieved for any number of resolved jets $m \in \{0, \dots, M\}$. On top of these NLO-correct multiplicities, NL^3 allows the inclusion of tree-level matrix elements with $n \in \{M+1, \dots, N\}$ additional partons. The highest-multiplicity tree-level sample further allows the generation of more than N resolved jets, by allowing parton shower emissions to produce resolved partons. The complete result is then obtained by simply adding the partial results for each jet multiplicity. This means that the NL^3 result for an observable $\mathcal{O}$, when merging N tree-level, and $M < N$ next-to-leading order calculations, is

$$\begin{aligned}\langle \mathcal{O} \rangle &= \sum_{m=0}^{M} \int d\phi_0 \int \cdots \int \mathcal{O}(S_{+mj}) \left\{ \left[\mathrm{B}_m w_m \right]_{-m,m+1} + \overline{\mathrm{B}}_m - \int_s \mathrm{B}_{m+1\to m} \right\} \\ &+ \sum_{n=M+1}^{N} \int d\phi_0 \int \cdots \int \mathcal{O}(S_{+nj}) \mathrm{B}_n w_n \end{aligned} \tag{III.11}$$

where the crucial change from CKKW-L (c.f. eq. (III.4)) is in the first line, where we add the exclusive NLO events and remove the corresponding α_s-terms from the CKKW-L weight. From a technical point of view, it is often convenient to think of this in terms of processing the samples

$$\mathbb{T}'_m = \left[\mathrm{B}_m w_m \right]_{-m,m+1} = \mathrm{B}_m \left\{ w_m - \left[w_m \right]_0 - \left[w_m \right]_1 \right\} \quad \text{for } m \le M \tag{III.12}$$

$$\mathbb{V}_m = \overline{\mathrm{B}}_m \quad \text{for } m \le M \tag{III.13}$$

$$\mathbb{S}_m = -\int_s \mathrm{B}_{m+1\to m} \quad \text{for } m \le M \tag{III.14}$$

$$\mathbb{T}_n = \mathrm{B}_n w_n \quad \text{for } M < n \le N \tag{III.15}$$

and writing simply

$$\begin{aligned}\langle\mathcal{O}\rangle &= \sum_{m=0}^{M}\int d\phi_0\int\cdots\int \mathcal{O}(S_{+mj})\left\{\mathbb{T}'_m+\mathbb{V}_m+\mathbb{S}_m\right\}\\ &+ \sum_{n=M+1}^{N}\int d\phi_0\int\cdots\int \mathcal{O}(S_{+nj})\mathbb{T}_n \qquad \text{(III.16)}\end{aligned}$$

The prediction for a generic observable can be obtained by calculating the result $\mathcal{O}_b(S_{+k})$, measured for $k-$jet phase space points, filling the histogram bin $\mathcal{O}_b$ with weight $\mathbb{T}_k$ (or $\mathbb{T}'_k/\mathbb{V}_k/\mathbb{S}_k$, depending on the sample), and summing over all multiplicities k.

The construction of the necessary weights is done with the help of a parton shower history and is detailed in appendix III.B. Once the weights are calculated, further parton showering is attached. The shower off inclusive NLO events and phase space subtractions is started at the last reconstructed scale, and all emissions above ρ_{MS} vetoed. This means that all higher-order terms above the merging scale are taken solely from the reweighted tree-level matrix elements, thus ensuring that the prescription preserves the parton shower description corrections beyond the reach of the NLO calculation. All samples have to be added to produce NLO-accurate $m = 0,\ldots,M$ jet observables, with higher-order corrections given by CKKW-L. Details on how the weights of different samples are motivated, as well as a proof of NLO + PS correctness, are given appendix III.C.

Here, let us illustrate how NLO accuracy is achieved for one particular jet multiplicity. For this, we examine the samples contributing to $M-$jet observables (where M is the highest multiplicity for which an NLO calculation is available). We start by analysing the $\mathcal{O}(\alpha_{\text{s}}^{M})$ and $\mathcal{O}(\alpha_{\text{s}}^{M+1})$ contributions. We find

$$\begin{aligned}&\left[\langle\mathcal{O}\rangle_M\right]_M+\left[\langle\mathcal{O}\rangle_M\right]_{M+1}=\Big[\mathcal{O}(S_{+Mj})\mathbb{V}_M\Big]_M+\Big[\mathcal{O}(S_{+Mj})\Big\{\mathbb{V}_M+\mathbb{S}_M\Big\}\Big]_{M+1}\\ &= \mathcal{O}(S_{+Mj})\Big\{\text{B}_M+\text{V}_M+\text{I}_{M+1|M}+\int d\Phi_{\text{rad}}\left(\text{B}_{M+1|M}-\text{D}_{M+1|M}\right)-\int_s \text{B}_{M+1\to M}\Big\}\\ &= \mathcal{O}(S_{+Mj})\,\widetilde{\text{B}}_M \qquad \text{(III.17)}\end{aligned}$$

Thus, the description of $M-$jet states is NLO-correct. For $M+1-$jet events, we have

$$\left[\langle\mathcal{O}\rangle_{M+1}\right]_{M+1}=\mathcal{O}(S_{+Mj})\,\text{B}_{M+1}\,, \qquad \text{(III.18)}$$

providing tree-level accuracy. Both these facts mirror the NLO description of observables. Keeping only the next-higher powers $\mathcal{O}(\alpha_{\text{s}}^{M+2})$

above ρ_{MS}, we see that

$$\begin{aligned}&\left[\langle\mathcal{O}\rangle_M\right]_{M+2} + \left[\langle\mathcal{O}\rangle_{M+1}\right]_{M+2} + \left[\langle\mathcal{O}\rangle_{M+2}\right]_{M+2} \\ &\quad= \mathcal{O}(S_{+Mj})\,\mathrm{B}_M\left[w_M\right]_2 + \mathcal{O}(S_{+M+1j})\,\mathrm{B}_{M+1}\left[w_{M+1}\right]_1 + \mathcal{O}(S_{+M+2j})\,\mathrm{B}_{M+2}\end{aligned} \tag{III.19}$$

For $M-$jet observables, only the reweighted $M-$parton LO matrix element contributes, while $M+1-$jet observables are described by reweighted $M+1-$parton tree-level states. $M+2-$jet observables are determined by the $M+2-$parton tree-level prediction. These are the results of default CKKW-L. Thus, the method is NLO accurate for $M-$jet observables, and also retains exactly the resummation of CKKW-L in higher orders for $M-$ and $M+1-$jet observables.

NL^3 step-by-step

In the NL^3 algorithm, we have to handle three classes of event samples:

- A: Inclusive next-to-leading order samples $\mathbb{V}_m$ for $m \leq M$ resolved jets.
- B: Tree-level samples $\mathbb{T}'_m$ for $m \leq M$ resolved jets, and tree-level samples $\mathbb{T}_n$ for $M < n \leq N$ jets.
- C: Tree-level samples $\mathbb{S}_m$ with initially $m+1$ partons, after integration over the radiative phase space of the $(m+1)$'th parton (for $m \leq M$).

Samples of class A are produced with the POWHEG-BOX program, by setting the minimal scale for producing radiation to E_{CM}. For calculations that need to be regularised, we use minimal cuts in POWHEG-BOX, and reject events without exactly the number of required jets internally in PYTHIA8. The samples of class A are processed in the most simple manner:

- A.I Pick a jet multiplicity, m, and a state S_{+m}, according to the cross sections given by the (NLO) matrix element generator. Reject any state with unresolved jets.
- A.II Find all parton shower histories for $S_{+0}, \ldots, S_{+m}$, and pick a parton shower history probabilistically.
- A.III Do not perform any reweighting on S_{+m}.
- A.IV Start the shower off S_{+m} at the latest reconstructed scale ρ_m. Veto shower emissions resulting in an additional resolved jet. ρ_{MS}.
- A.V Start again from A.I.

To amend that we have used inclusive NLO cross sections where we should have used exclusive calculations, we have to introduce samples of class C. The first step in the construction of these samples is to generate tree-level weighted events with $1 \leq m \leq M+1$ partons above ρ_{MS}. Then,

- C.I Pick a jet multiplicity, $m+1$, and a state S_{+m+1}, according to the cross sections given by the (LO) matrix element generator. Reject any state with unresolved jets.
- C.II Find all parton shower histories for $S_{+0}, \ldots, S_{+m}, S_{+m+1}$, and pick a parton shower history probabilistically. Replace S_{+m+1} with the S_{+m} of by the chosen history[7].
- C.III Weight S_{+m} with -1.
- C.IV Start the shower off S_{+m} at the latest reconstructed scale ρ_m. Veto shower emissions resulting in an additional resolved jet.
- C.V Start again from C.I.

Higher orders in α_s (in the CKKW-L scheme) are introduced by including events of class B. Again, tree-level weighted events for $0 \leq n \leq N$ partons are needed as input. Then,

- B.I Pick a jet multiplicity, n, and a state S_{+n}, according to the cross sections given by the matrix element generator. Reject any state with unresolved jets.
- B.II Find all parton shower histories for $S_{+0}, \ldots, S_{+n}$, and pick a parton shower history probabilistically.
- B.III Perform reweighting:
  - B.III.1 If $n > M$, weight with w_n, as would be the case in CKKW-L.
  - B.III.2 If $n \leq M$, weight with $\{w_n - [w_n]_0 - [w_n]_1\}$.
- B.IV Start the shower off S_{+n} at the latest reconstructed scale ρ_n.
  - B.IV.1 If $n = N$, allow any shower emission.
  - B.IV.2 If $n < N$, veto shower emissions resulting in an additional resolved jet.
- B.V Start again from B.I.

All samples of all classes are finally added to produce the M-NLO-jet- and N-LO-jet-merged prediction. Both the samples B and C require

[7] We do not apply any further action if S_{+m} contains unresolved jets in NL^3, in contrast UMEPS (or UNLOPS).

tree-level input, i.e. the input events for C-samples can be also be used as input for B-samples. In total, the PYTHIA8 implementation requires M NLO-weighted Les Houches event files, and N tree-level-weighted files as input, but some of the tree-level input files need to be processed twice.

Due to the ubiquity of multiparton interactions (MPI) in hadronic collisions, we are still far from a full event description at the LHC, even after combining multi-jet calculations and parton showers. How MPI can be attached to NL^3 is discussed in appendix III.E.

III.3.2 UNLOPS: UMEPS at next-to-leading order

Although NL^3 accomplishes a merging of multiple NLO calculations to the specified accuracy, it inherits the merging scale dependence of the inclusive lowest multiplicity cross section from CKKW-L. For lack of a better term, we will refer to changes in the inclusive cross section as "unitarity violations". When including additional jets in W-boson production, unitarity violations enter at the same order in α_s as e.g. the NLO corrections to $W + j-$production. Even if changes of the inclusive cross section are generally small as long as the merging scale is not set too small, it is not clear how much of the shape changes we observe are really due to not cancelling logarithms. Thus, we want to promote UMEPS, where these unitarity violations are absent [6], to NLO accuracy as well.

Extending UMEPS to include multiple NLO calculations is slightly more involved than the CKKW-L case. The complete method is derived in appendix III.D. In a sense, NL^3 and UNLOPS are complementary: NL^3 is, in the accuracy claimed by the method, easily applicable to any number of jets, while UNLOPS aims at higher accuracy for the dominant low multiplicities[8]. The strategy to extend UMEPS to NLO accuracy is similar to NL^3. We remove any approximate $\mathcal{O}\left(\alpha_s^0\left(\mu_R\right)\right)$ and $\mathcal{O}\left(\alpha_s^1\left(\mu_R\right)\right)$ terms in the UMEPS weighting procedure, and simply add the correct NLO result. To disturb the description of higher order contributions as little as possible, we only cancel those terms of the UMEPS weight that would have a better description in the NLO matrix element.

The UNLOPS method aims to move beyond UMEPS not only in terms of fixed-order accuracy for multiple exclusive $n-$jet observables, but also in the description of higher orders in low-multiplicity states.

[8] In fact, the UNLOPS zero- and one-jet NLO merging presented here can easily be promoted to a NNLO matching scheme, as outlined in appendix III.D.

This is a direct consequence of requiring unitarity, i.e. that the inclusive cross section be fixed to the zero-jet NLO result. In the spirit of UMEPS, this means that once we want to add a one-jet NLO calculation, we have to subtract its integrated version from zero-jet events. Similarly we need to remove the $\mathcal{O}\left(\alpha_s^0\left(\mu_R\right)\right)$ and $\mathcal{O}\left(\alpha_s^1\left(\mu_R\right)\right)$ in the UMEPS tree-level weights, not only for the one-jet events but also for the corresponding subtracted zero-jet events. In this way we ensure that the inclusive zero-jet cross section is still given by the NLO calculation and we will also improve the $\mathcal{O}(\alpha_s^2)-$term of exclusive zero-jet observables.

The UNLOPS prediction for an observable $\mathcal{O}$, when simultaneously merging inclusive NLO calculations for m=0, ..., M jets, and including up to N tree-level calculations, is given by

$$\begin{aligned}
\langle\mathcal{O}\rangle \;=\; & \sum_{m=0}^{M-1}\int d\phi_0\int\cdots\int\mathcal{O}(S_{+mj})\left\{\overline{\mathrm{B}}_m+\left[\widehat{\mathrm{B}}_m\right]_{-m,m+1}\right. \\
& \qquad\left.-\sum_{i=m+1}^{M}\int_s\overline{\mathrm{B}}_{i\to m}-\sum_{i=m+1}^{M}\left[\int_s\widehat{\mathrm{B}}_{i\to m}\right]_{-i,i+1}-\sum_{i=M+1}^{N}\int_s\widehat{\mathrm{B}}_{i\to m}\right\} \\
+\; & \int d\phi_0\int\cdots\int\mathcal{O}(S_{+Mj})\left\{\overline{\mathrm{B}}_M+\left[\widehat{\mathrm{B}}_M\right]_{-M,M+1}-\sum_{i=M+1}^{N}\int_s\widehat{\mathrm{B}}_{i\to M}\right\} \\
+\; & \sum_{n=M+1}^{N}\int d\phi_0\int\cdots\int\mathcal{O}(S_{+nj})\left\{\widehat{\mathrm{B}}_n-\sum_{i=n+1}^{N}\int_s\widehat{\mathrm{B}}_{i\to n}\right\} \qquad \text{(III.20)}
\end{aligned}$$

Here we see, in the first line, the addition of the $\overline{\mathrm{B}}_m$ and the removal of the $\mathcal{O}\left(\alpha_s^m\left(\mu_R\right)\right)$ and $\mathcal{O}\left(\alpha_s^{m+1}\left(\mu_R\right)\right)$ terms of the original UMEPS $\widehat{\mathrm{B}}_m$ contribution. On the second line we see the subtracted integrated $\overline{\mathrm{B}}_{m+1}$ term to make the m-parton NLO-calculation exclusive and the corresponding $\mathcal{O}\left(\alpha_s^m\left(\mu_R\right)\right)$- and $\mathcal{O}\left(\alpha_s^{m+1}\left(\mu_R\right)\right)$-subtracted UMEPS term together with subtracted terms from higher multiplicities where intermediate states in the clustering were below the merging scale. The third line is the special case of the highest multiplicity corrected to NLO, and the last line is the standard UMEPS treatment of higher multiplicities.

The full derivation of this master formula is given in appendix III.D, where we also discuss the case of exclusive NLO samples and explain the necessity for subtraction terms from higher multiplicities. We will limit ourselves to including only zero- and one-jet NLO calculations in the results section. For the sake of clarity we will thus only discuss this special case here. For this case, the UNLOPS prediction (when including

only up to two tree-level jets) is

$$\begin{aligned}\langle\mathcal{O}\rangle \;=\; & \int d\phi_0 \Bigg\{ \mathcal{O}(S_{+0j}) \left(\overline{\mathrm{B}}_0 \;-\; \int_s \overline{\mathrm{B}}_{1\to 0} \;-\; \left[\int_s \widehat{\mathrm{B}}_{1\to 0} \right]_{-1,2} \;-\; \int_s \widehat{\mathrm{B}}_{2\to 0} \right) \\ & + \int \mathcal{O}(S_{+1j}) \left(\overline{\mathrm{B}}_1 + \left[\widehat{\mathrm{B}}_1 \right]_{-1,2} \;-\; \int_s \widehat{\mathrm{B}}_{2\to 1} \right) \\ & + \iint \mathcal{O}(S_{+2j}) \widehat{\mathrm{B}}_2 \end{aligned} \tag{III.21}$$

In an implementation, this is conveniently arranged in terms of the samples

$$\mathbb{B}_2 \;=\; \mathrm{B}_2 w_2' \tag{III.22}$$

$$\mathbb{B}_1 \;=\; \left[\widehat{\mathrm{B}}_1 \right]_{-1,2} \;=\; \mathrm{B}_1 \left\{ w_1' - \left[w_1' \right]_0 - \left[w_1' \right]_1 \right\} \tag{III.23}$$

$$\mathbb{V}_0 \;=\; \overline{\mathrm{B}}_0 \;=\; \mathrm{B}_0 + \mathrm{V}_0 + \mathrm{I}_{1|0} + \int d\Phi_{\mathrm{rad}} \left(\mathrm{B}_{1|0} - \mathrm{D}_{1|0} \right) \tag{III.24}$$

$$\mathbb{V}_1 \;=\; \overline{\mathrm{B}}_1 \;=\; \mathrm{B}_1 + \mathrm{V}_1 + \mathrm{I}_{2|1} + \int d\Phi_{\mathrm{rad}} \left(\mathrm{B}_{2|1} - \mathrm{D}_{2|1} \right) \tag{III.25}$$

$$\mathbb{I}_1 \;=\; -\int_s \mathrm{B}_{2\to 1} w_2' \;-\; \int_s \mathrm{B}_{2\to 0} w_2' \tag{III.26}$$

$$\mathbb{I}_0 \;=\; -\left[\int_s \widehat{\mathrm{B}}_{1\to 0} \right]_{-1,2} \;=\; -\int_s \mathrm{B}_{1\to 0} \left\{ w_1' - \left[w_1' \right]_0 - \left[w_1' \right]_1 \right\} \tag{III.27}$$

$$\mathbb{L}_0 \;=\; -\int_s \overline{\mathrm{B}}_{1\to 0} \tag{III.28}$$

meaning that we have two tree-level samples ($\mathbb{B}_1$, $\mathbb{B}_2$), two NLO samples ($\mathbb{V}_0$, $\mathbb{V}_1$), two subtractive samples ($\mathbb{I}_0$, $\mathbb{I}_1$) and one integrated NLO sample ($\mathbb{L}_0$). The prediction is formed by reading tree-level input events (for $\mathbb{B}_1$, $\mathbb{B}_2$, $\mathbb{I}_0$ and $\mathbb{I}_1$), or inclusive NLO input (for $\mathbb{V}_0$, $\mathbb{V}_1$ and $\mathbb{L}_0$), generating the necessary merging weights, and filling histogram bins with the product of matrix element and merging weight. For technicalities on the generation of the weights, we refer to appendix III.B.

In the inclusive cross section, it can immediately be checked that all contributions except zero-jet NLO terms cancel exactly, meaning that the inclusive cross section is given by the zero-jet NLO cross section. As in UMEPS however, we have to accept marginal changes of the inclusive cross section in the presence of incomplete histories, i.e. when it is not possible to regard n-jet states as corrections to $n-1$-jet states, because no underlying Born configuration exists. (see discussion at the end of section III.2.2). The contribution from such configurations is, for the results presented in this publication, numerically insignificant.

Let us turn to the UNLOPS description of exclusive observables.

Only looking at zero-jet observables in eq. (III.21), we see

$$\begin{aligned}\langle\mathcal{O}\rangle_0 \;=\; & \int d\phi_0 \mathcal{O}(S_{+0j}) \Bigg\{ \mathrm{B}_0 + \mathrm{V}_0 + \mathrm{I}_{1|0} + \int d\Phi_{\mathrm{rad}} \Big[\mathrm{B}_{1|0} \Theta\left(\rho_{\mathrm{MS}} - t(S_{+1},\rho)\right) - \mathrm{D}_{1|0} \Big] \\ & - \int_s \Big[\mathrm{V}_1 + \mathrm{I}_{2|1} + \int d\Phi_{\mathrm{rad}} \left(\mathrm{B}_{2|1} - \mathrm{D}_{2|1} \right) \Big] \\ & - \int_s \mathrm{B}_{1\to 0} \left\{ w_1' - \left[w_1'\right]_0 - \left[w_1'\right]_1 \right\} - \int_s \mathrm{B}_{2\to 0} w_2' \quad \Bigg\}, \end{aligned} \tag{III.29}$$

where we have, between the first and second lines, cancelled the tree-level contribution of $\int_s \overline{\mathrm{B}}_{1\to 0}$ with the resolved real-emission term $\int_{\rho_{\mathrm{MS}}} d\Phi_{\mathrm{rad}} \mathrm{B}_{1|0}$ appearing in $\overline{\mathrm{B}}_0$. When extracting only the $\mathcal{O}\left(\alpha_{\mathrm{s}}^0\left(\mu_R\right)\right)$ and $\mathcal{O}\left(\alpha_{\mathrm{s}}^1\left(\mu_R\right)\right)$ terms, this gives the contribution of the exclusive NLO matrix element, i.e. of tree-level, virtual correction and unresolved real contributions. At $\mathcal{O}\left(\alpha_{\mathrm{s}}^2\left(\mu_R\right)\right)$, we have

$$\left[\langle\mathcal{O}\rangle_0\right]_2 = \int d\phi_0 \mathcal{O}(S_{+0j}) \Bigg\{ - \int_s \Big[\mathrm{V}_1 + \mathrm{I}_{2|1} + \int d\Phi_{\mathrm{rad}} \left(\mathrm{B}_{2|1} - \mathrm{D}_{2|1} \right) \Big] - \int_s \mathrm{B}_{2\to 0} \Bigg\} \tag{III.30}$$

The first group of terms in the curly brackets gives an approximation of NNLO corrections, since in a NNLO calculation, all logarithmic terms in the NLO $+1-$jet calculation are removed by two-loop and double-real terms. Conversely, we should be able to include the correct logarithmic terms of two-loop and double unresolved terms by integrating over the jet in the $+1-$jet NLO calculation. The last term in curly brackets is sub-dominant and corresponds to emissions that are unordered in ρ_{MS}[9].

Examining the $\mathcal{O}\left(\alpha_{\mathrm{s}}^3\left(\mu_R\right)\right)$ contributions, we are left with

$$\left[\langle\mathcal{O}\rangle_0\right]_3 = \int d\phi_0 \mathcal{O}(S_{+0j}) \left\{ - \int_s \mathrm{B}_{1\to 0} \left[w_1'\right]_2 - \int_s \mathrm{B}_{2\to 0} \left[w_2'\right]_1 \quad \right\} \tag{III.31}$$

This is simply the parton shower approximation, amended with a term corresponding emissions that are unordered in ρ_{MS}.

Let us move on to the discussion of one-jet observables. If we use the fact that we can cancel the contribution of two resolved real-emission jets in $\overline{\mathrm{B}}_1$ by the $\mathcal{O}\left(\alpha_{\mathrm{s}}^2\left(\mu_R\right)\right)$ term in $\int_s \widehat{\mathrm{B}}_{2\to 1}$, we find

$$\begin{aligned} & \left[\langle\mathcal{O}\rangle_1\right]_1 + \left[\langle\mathcal{O}\rangle_1\right]_2 \\ & = \int d\phi_0 \int \mathcal{O}(S_{+1j}) \left\{ \mathrm{B}_1 + \mathrm{V}_1 + \mathrm{I}_{2|1} + \int^{\rho_{\mathrm{MS}}} d\Phi_{\mathrm{rad}} \left(\mathrm{B}_{2|1} - \mathrm{D}_{2|1} \right) \right\}. \end{aligned} \tag{III.32}$$

[9] This term already appears in UMEPS.

Thus, the method describes one-jet observables with NLO accuracy. The $\mathcal{O}\left(\alpha_s^3\left(\mu_R\right)\right)$ −term is given by

$$\left[\langle\mathcal{O}\rangle_1\right]_3 \quad = \quad \int d\phi_0 \int \mathcal{O}(S_{+1j}) \left\{ \mathrm{B}_1\left[w_1'\right]_2 - \int_s \mathrm{B}_{2\to1}\left[w_2'\right]_1 \right\}, \qquad \text{(III.33)}$$

which is simply the UMEPS-improved parton shower approximation. In conclusion, we find the method is NLO-correct, improves the logarithmic behaviour of zero-jet observables, and otherwise includes the parton shower resummation of the UMEPS procedure.

UNLOPS step-by-step

As a complication on top of NL^3, UNLOPS requires four classes of events. We will step-by-step formulate the method for including M inclusive next-to-leading order calculations, combined with N tree-level matrix elements. This means that we need to handle the samples

- A: Inclusive next-to-leading order samples $\mathbb{V}_m$ for m resolved jets.
- B: Tree-level samples $\mathbb{B}_n$ for $n < N$ resolved jets. (There is no zero-jet tree-level sample.)
- C: Tree-level samples $\mathbb{I}_n$ with initially m partons, after integration over the radiative phase space of the one or more emissions, as required by the UMEPS method.
- D: Next-to-leading order samples $\mathbb{L}_m$ with initially m resolved jets, after integration over the radiative phase space of the emission.

Samples of class A are produced with the POWHEG-BOX program, exactly as in NL^3. The POWHEG-BOX output files are then processed:

- A.I Pick a jet multiplicity m, and a state S_{+m}, according to the cross sections given by the (NLO) matrix element generator. Reject any state with unresolved jets.
- A.II Find all parton shower histories for $S_{+0}, \ldots, S_{+m}$, and pick a parton shower history probabilistically.
- A.III Do not perform any reweighting on S_{+m}.
- A.IV Start the shower off S_{+m} at the latest reconstructed scale ρ_m. Veto shower emissions resulting in an additional resolved jet.
- A.V Start again from A.I.

This is exactly the treatment we already know from NL^3. To ensure that the inclusive (lowest-multiplicity) cross section is not changed, we need

to subtract the integrated variants $\mathbb{L}_{m+1}$ of the $(m+1)$-jet NLO calculation, i.e. introduce the samples of class D. This will also remedy the fact that we have used the inclusive m-jet NLO cross sections, while we should have used exclusive $\widetilde{\mathrm{B}}_m$ input for $\mathbb{V}_m$. As starting point, we use the $\overline{\mathrm{B}}_{m+1}-$distributed event sample (i.e. the same input as for $\mathbb{V}_{m+1}$). Then

- D.I Reject any state with unresolved jets.
- D.II Find all parton shower histories for $S_{+0}, \ldots, S_{+m+1}$, and pick a parton shower history probabilistically. Replace S_{+m+1} with the S_{+m}, or the first state S_{+l} with all $l \leq m$ partons above the merging scale. (lower multiplicity states are taken from the intermediate states of the chosen PS history)
- D.III Weight S_{+m} with -1.
- D.IV Start the shower off S_{+m} at the latest reconstructed scale ρ_m. Veto shower emissions resulting in an additional resolved jet.
- D.V Start again from D.I.

To add the UMEPS resummation to these samples (and correct that we have used $\overline{\mathrm{B}}_M$ events rather than exclusive $\widetilde{\mathrm{B}}_M$ input for $\mathbb{V}_M$), we include samples of class C. These are generated from the $(n+1)$-jet tree-level samples, by following the steps

- C.I Pick a jet multiplicity, $n+1$, and a state S_{+n+1}, according to the cross sections given by the matrix element generator. Reject any state with unresolved jets.
- C.II Find all parton shower histories for $S_{+0}, \ldots, S_{+n}$, and pick a parton shower history probabilistically.
- C.III Perform reweighting:
  - C.III.1 If $n+1 > M$, weight with w'_{n+1}, as would be the case in UMEPS.
  - C.III.2 If $n+1 \leq M$, weight with $\left\{ w'_{n+1} - \left[w'_{n+1}\right]_0 - \left[w'_{n+1}\right]_1 \right\}$.
- C.IV Replace S_{+n+1} with the S_{+n}, or the first state S_{+l} with all $l \leq n$ partons above the merging scale (lower multiplicity states are taken from the intermediate states of the chosen history). Start the shower off S_{+n} at the latest reconstructed scale ρ_n. Veto shower emissions resulting in an additional resolved jet.
- C.V Start again from C.I.

The last contributions we have to include are reweighted tree-level samples, i.e. events of class B. There is no zero-jet tree-level contribution in UNLOPS, since the $\mathcal{O}\left(\alpha_s^0\left(\mu_R\right)\right)$ −term is already included by $\mathbb{V}_0$. Samples for class B are generated very similar to events of class C, with no "integration step" required for class B:

- B.I Pick a jet multiplicity, $n > 0$, and a state S_{+n}, according to the cross sections given by the matrix element generator. Reject any state with unresolved jets.
- B.II Find all parton shower histories for $S_{+0}, \ldots, S_{+n}$, and pick a parton shower history probabilistically.
- B.III Perform reweighting:
  - B.III.1 If $n > M$, weight with w'_n, as would be the case in UMEPS.
  - B.III.2 If $n \leq N$, weight with $\left\{w'_1 - [w'_1]_0 - [w'_1]_1\right\}$.
- B.IV Start the shower off S_{+n} at the latest reconstructed scale ρ_n.
  - B.IV.1 If $n = N$, allow any shower emission.
  - B.IV.2 If $n < N$, veto shower emissions resulting in an additional resolved jet.
- B.V Start again from B.I.

Note that although the UNLOPS procedure is more complicated than NL^3, no additional user input is required: PYTHIA8 only needs M inclusive NLO event samples and $N - 1$ tree-level event files, since A and B use the same NLO input, and the same tree-level input can be employed in both C and D. This concludes our discussion of NLO merging prescriptions. Information on how underlying event is added to our prescription is given in appendix III.E.

III.3.3 Short comparison

Before presenting results, let us pause and recapitulate the last section. We have presented two different NLO merging schemes, which differ in several ways

NL^3	UNLOPS
• Generalisation of CKKW-L	◇ Generalisation of UMEPS
• Needs exclusive or inclusive NLO calculations as input.	◇ Needs exclusive or inclusive NLO calculations as input.

• Straight-forward when moving to high jet multiplicities.	◇ Less transparent when moving to high jet multiplicities.
• Changes the inclusive NLO cross sections.	◇ Preserves the NLO inclusive cross sections.
• Reproduces the logarithmic behaviour of the PS in zero-jet observables. Does not fully cancel sub-leading logarithmic enhancements of higher multiplicity NLO calculations.	◇ Explicitly cancels logarithmic enhancements, has improved logarithmic behaviour in low-multiplicity jet observables.
• Produces negative weights.	◇ Produces even more negative weights.

At this point, we will not make comparisons with other NLO merging methods, but hope to be able to contribute to a thorough comparison in a future publication. Here we will only make some brief remarks on the formal accuracy of our methods, compared to the ones presented in [26, 27] (MEPS@NLO) and [28] (aMC@NLO). All of these methods rely on the introduction of a merging scale and it is relevant to investigate how the description of observables are affected by changes in this scale. In particular it is interesting to make sure that the NLO-correctness of the of the methods are not spoiled by large logarithms involving the merging scale, $L = \ln\left(\frac{\mu_{r/f}}{\rho_{\text{MS}}}\right)$. Even if the dependence on the merging scale vanishes to the logarithmic approximation of the shower (normally at best NLL), the sub-leading logarithmic dependence may become as large as the NLO correction which we want include.

To exemplify (following the arguments of Bauer et al. [34–36]) we look at the inclusive n-jet cross section, which in all methods have been corrected to reproduce the NLO cross section, so it is exact to $\mathcal{O}(\alpha_s^n)$ and $\mathcal{O}(\alpha_s^{n+1})$. But if we look at the $\mathcal{O}(\alpha_s^{n+2})$-term there will be dependencies on the merging scale, which we can symbolically expand out in logarithms as $\alpha_s^{n+2}(L^4 + L^3 + L^2 + \ldots)$. Even for a NLL-correct parton shower where the both the $\alpha_s^{n+2}L^4$ and $\alpha_s^{n+2}L^3$ terms will cancel exactly, we will have dependencies of the order $\alpha_s^{n+2}L^2$. This means we that have to choose the merging scale such that $\alpha_s L^2 \ll 1$, to be sure we do not spoil the effect of the $\mathcal{O}(\alpha_s^{n+1})$-correction of the NLO calculation.

For the MEPS@NLO method it was shown that it at most has a dependence of order $\alpha_s^{n+2}L^3$ which is colour-suppressed, but certainly has a dependence of order $\alpha_s^{n+2}L^2$. For the aMC@NLO method we do not know of any formal analysis of the logarithmic correctness, but it is dif-

ficult to see how it could have avoid dependencies of order $\alpha_s^{n+2}L^3$. Also in our NL^3 method, where the dependence is given by the precision of the shower, it cannot be claimed that the dependence of order $\alpha_s^{n+2}L^3$ is absent, as it has not been proven that the PYTHIA8 shower is formally NLL-correct. However, for our UNLOPS method, we explicitly conserve the inclusive NLO cross section, and the merging scale dependence is cancelled almost completely through our "subtract everything that is added" strategy. We say *almost* cancelled, as this is clearly an observable-dependent statement. From eq. (III.20) we see that in order for the addition of a higher order matrix element B_k to completely cancel for an inclusive n-jet observable, we require (symbolically)

$$\int d\phi_0 \int \cdots \int \mathcal{O}_n(S_{+kj})B_k = \sum_{i=n}^{k-1} \int d\phi_0 \int \cdots \int \mathcal{O}_n(S_{+ij})B_{k\to i}\,, \quad \text{(III.34)}$$

which is clearly never an exact cancellation. There is also an implicit merging scale dependence here as, whether or not e.g. B_3 is projected into $B_{3\to 2}$ and measured with $\mathcal{O}(S_{+2j})$ or into $B_{3\to 1}$ and measured with $\mathcal{O}(S_{+1j})$, depends on the merging scale. However, for small enough merging scales, this should not matter for collinear- and infrared-safe observables, and we do not expect any large logarithms of the merging scale to appear. Also we note that there are some n-parton states that cannot be projected down to a lower multiplicity state using parton shower splittings (*incomplete* states in section III.2.2) as described in [6], where we also found that such diagrams give numerically very small contributions.

UNLOPS also shares features with the LoopSim method [37, 38], in particular the use of an integrated version of one-jet NLO calculations. However, we cannot cancel logarithms of the form $\ln\left(\frac{p_{\perp\text{jet}}}{M_W}\right)$, which arise by soft/collinear W-radiation, because we do not allow an integration over the (radiated) W-boson. The study of such "giant K-factor effects" is postponed until a full electroweak shower becomes available in PYTHIA8.

Finally it should be noted that NLO merging methods can be useful even if only the NLO calculation for the lowest multiplicity is available. Since an NLO merging scheme consistently splits the real emission into unresolved and resolved parts by defining a merging scale ρ_{MS}, and uses the same definition to separate states with two resolved jets from states with one resolved and several unresolved jets, any NLO calculation can be improved by merging further tree-level calculations for additional jets. Such schemes go under the name of MENLOPS [39–41]. Promoting

a NLO calculation to a MENLOPS prediction is straight-forward with our methods.

III.4 Results

The UNLOPS and NL^3 methods have been implemented in PYTHIA8, and will be included in the next major release version. In this section, we will present sample results for NLO merging with inclusive NLO calculations. The aim of this section is to affirm that the implementation in PYTHIA8 is working smoothly. We do so by presenting results for W-boson production and Higgs (H) production in gluon fusion, when simultaneously merging zero and one additional jet at next-to-leading order with two additional jets on tree-level.

All input matrix element configurations are taken from Les Houches Event Files. We use the following input:

- $W + 0$, $W + 1$ and $W + 2$ at tree-level generated by MadGraph/MadEvent.
- $W + 0$, $W + 1$ at NLO [42, 43] generated by POWHEG-BOX (see appendix III.A.4).
- $H + 0$, $H + 1$ and $H + 2$ at tree-level generated by MadGraph/MadEvent.
- $H + 0$, $H + 1$ at NLO [44, 45] generated by POWHEG-BOX (see appendix III.A.4).
- Fixed-order input was calculated with three values for fixed renormalisation scales and factorisation scales,
- Central scales: $\mu_R = M_Z^2$ and $\mu_F = M_W^2$ for W-production, $\mu_R = M_Z^2$ and $\mu_F = M_H^2 = (125\text{ GeV})^2$ for H-production.
- Low scales: $\mu_R = (M_Z/2)^2$ and $\mu_F = (M_W/2)^2$ for W-production, $\mu_R = (M_Z/2)^2$ and $\mu_F = (M_H/2)^2$ for H-production.
- High scales: $\mu_R = (2M_Z)^2$ and $\mu_F = (2M_W)^2$ for W-production, $\mu_R = (2M_Z)^2$ and $\mu_F = (2M_H)^2$ for H-production.

In all Figures we will label curves generated from central scale input with *cc*, from low scale input with *ll*, and from high scale input with *hh*.

- CTEQ6M parton distributions and $\alpha_s(M_Z^2) = 0.118$.
- The merging scale ρ_{MS} is defined by the minimal PYTHIA8 evolution variable (see appendix III.A.1).

The value of $\alpha_s(M_Z^2)$ was set to match the α_s-value obtained in the parton distributions used in the ME calculation. We use the same PDFs and $\alpha_s(M_Z^2)$-value in the parton shower evolution. For all internal analyses, we use `fastjet`-routines [46] to define jets. The momentum of the intermediate W-boson will, if required, be extracted directly from the Monte Carlo event.

We will compare our results to the result of the POWHEG-BOX program for W+jet production. For these comparisons, we have generated default POWHEG-BOX output, fixing the renormalisation and factorisation scales, and regularising the Born configuration with a cut $p_{\perp,\text{parton}} = 5$ GeV. To determine a shower starting scale for these POWHEG-BOX output events, we reconstruct all possible (including unordered) parton shower histories, choose one, and start the shower from the last reconstructed scale. No visible effects of using different options to choose history have been found. This is not the default interface to the POWHEG-BOX, which requires truncated showers if the scale definition on the POWHEG-BOX and the parton shower do not match. Appropriately vetoed showers are normally used instead in PYTHIA8, because no truncated showers are available. Since the scale definition in the POWHEG-BOX could change depending on the details of the implementation (being different for Catani-Seymour- and Frixione-Kunzt-Signer-based approaches), we do not use vetoed showers, and rather choose starting scale by constructing a parton shower history. For W+jet production, we found only insignificant differences between both methods.

When taking ratios to default PYTHIA8 (often given by the lower insets of figures), we rescale the PYTHIA8 reference by $K(\mu_R, \mu_F) = \frac{\int \overline{B}_0(\mu_R,\mu_F)}{\int B_0(\mu_R,\mu_F)}$. This guarantees that we remove the variation of the normalisation of the inclusive cross section due to scale choices:

$$\frac{\frac{1}{\int \overline{B}_0(\mu_R,\mu_F)}\langle\mathcal{O}\rangle_{\text{NLO merged}}}{\frac{1}{\int B_0(\mu_R,\mu_F)}\langle\mathcal{O}\rangle_{\text{Pythia8}}} = \frac{\langle\mathcal{O}\rangle_{\text{NLO merged}}}{K(\mu_R,\mu_F)\cdot\langle\mathcal{O}\rangle_{\text{Pythia8}}} \tag{III.35}$$

The variation of the overall normalisation will otherwise obscure interesting features. For Higgs production in gluon fusion for example we will compare merged curves generated with $\mu_R = 2M_Z$ and $\mu_F = 2M_H$ (labelled *hh*) to PYTHIA8, multiplied by with $K(2M_Z, 2M_H)$. For central scales, we would use $K(M_Z, M_H)$.

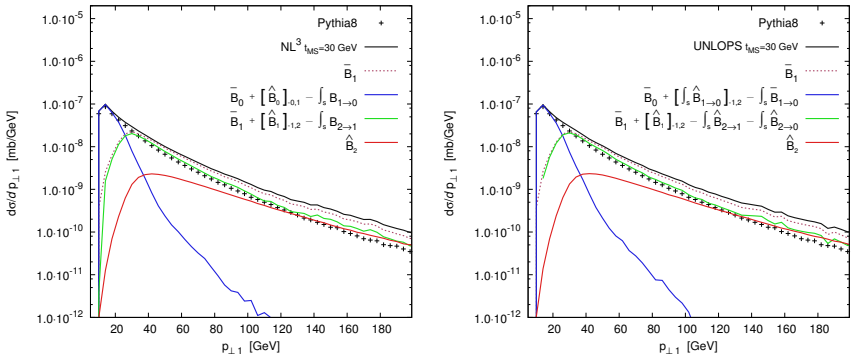

Figure III.1: Transverse momentum of the hardest jet, for W-boson production in pp collisions at $E_{\mathrm{CM}} = 7000$ GeV, when merging up to two additional partons at LO, and zero and one additional parton at NLO. Jets were defined with the $k_\perp$-algorithm, with $k_{\perp,min} = 10$ GeV. Multi-parton interactions and hadronisation were excluded. Left panel: Results of the NL^3 scheme. Right panel: Results of the UNLOPS scheme.

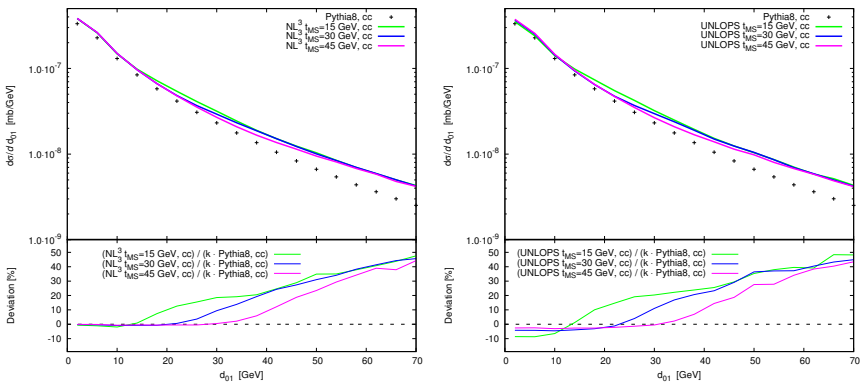

Figure III.2: $k_\perp$- separation d_{01} of the first jet and the beam, for W-boson production in pp collisions at $E_{\mathrm{CM}} = 7000$ GeV, when merging up to two additional partons at LO, and zero and one additional parton at NLO, for three different merging scales. Jets were defined with the $k_\perp$-algorithm, by clustering to exactly one jet. Multi-parton interactions and hadronisation were excluded. Left panel: Results of the NL^3 scheme. Right panel: Results of the UNLOPS scheme.

III.4.1 W-boson production

Let us start by discussing results for W-boson production, when combining inclusive NLO calculations for W + 0- and W + 1 parton with the PYTHIA8 event generator. This section is intended mainly for validation,

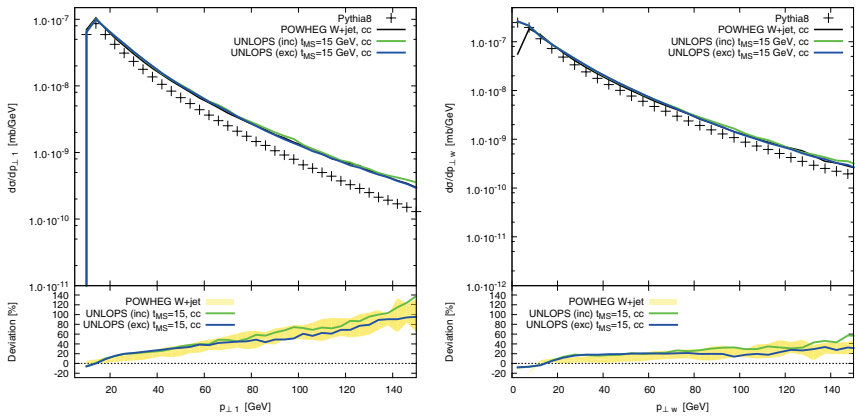

Figure III.3: Comparison of using exclusive and inclusive NLO input for W-boson production in pp collisions at $E_{CM} = 7000$ GeV, when merging up to two additional partons at LO, and zero and one additional parton at NLO. Curves labelled "inc" are produced with the $\overline{B}$-prescription, while "exc" indicate a generation with $\widetilde{B}$-input. The lower inset shows the deviation from PYTHIA8. The band labelled "POWHEG W+jet" is given by the envelope of varying the renormalisation scale in the POWHEG-BOX program between $\frac{1}{2}M_Z, \ldots, 2M_Z$, and the factorisation scale between $\frac{1}{2}M_W, \ldots, 2M_W$.

and we will thus switch off multi-parton interactions and hadronisation. We present results for both NL^3 and UNLOPS. Our preferred method is UNLOPS, since the inclusive cross sections are there handled more consistently. By showing the results for both NL^3 and UNLOPS, we hope to convey a rudimentary idea of the effect of potentially problematic logarithmic enhancements in standard observables.

Figure III.1 shows the transverse momentum of the hardest jet in W-production at the LHC, for both NL^3 and UNLOPS. The sum of the solid, coloured curves gives the full NLO merged result, i.e. the black line. The dashed curve is included only to illustrate that the hard tail of the $p_{\perp 1}$-spectrum is dominated by the the W+jet NLO sample (labelled $\bar{B}_1$), both in NL^3 and UNLOPS, which is of course desired. This fact makes the $p_{\perp 1}$-spectra of NL^3 and UNLOPS very similar.

Differences between NL^3 and UNLOPS are expected in the intermediate- / low-scale regions. This is illustrated by Figure III.2, which shows the d_{01}-distribution of the first jet[10]. Since UNLOPS explicitly preserves the W-production NLO cross section, the increase in

[10]The observable d_{01} is very closely related to $p_{\perp 1}$, but avoids a $k_{\perp,min}$-cut in defining the jet, by clustering to exactly one jet. This allows to show the lowest scale features.

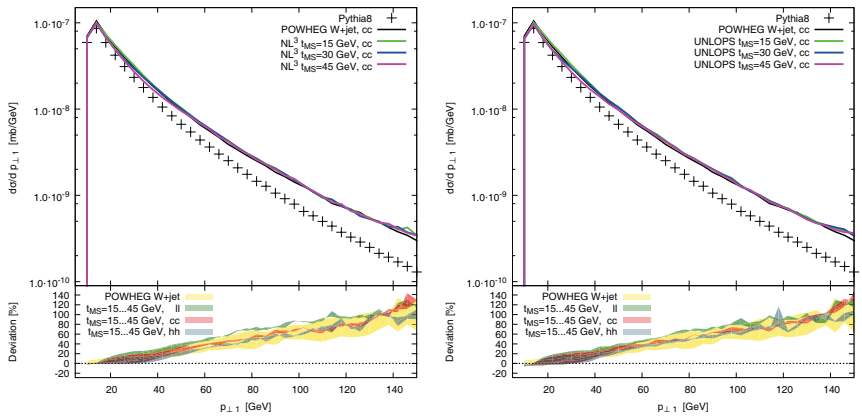

Figure III.4: Transverse momentum of the hardest jet, for W-boson production in pp collisions at $E_{\mathrm{CM}} = 7000$ GeV, when merging up to two additional partons at LO, and zero and one additional parton at NLO. Jets were defined with the $k_\perp$-algorithm, with $k_{\perp,min} = 10$ GeV. Multi-parton interactions and hadronisation were excluded. The lower inset shows the deviation from PYTHIA8. The band labelled "POWHEG W+jet" is given by the envelope of varying the renormalisation scale in the POWHEG-BOX program between $\frac{1}{2}\mathrm{M_Z}, \ldots, 2\mathrm{M_Z}$, and the factorisation scale between $\frac{1}{2}\mathrm{M_W}, \ldots, 2\mathrm{M_W}$. Left panel: Results of NL^3. Right panel: Results of UNLOPS.

the tail has to be compensated by decreasing contributions below the merging scale. The description at low d_{01} in NL^3 is, by construction, completely governed by the PYTHIA8 result.

Before continuing, we would again like to stress that we are using inclusive NLO cross section as input in this publication, as discussed in appendix III.A.2. There, it was found that making inclusive cross sections exclusive by constructing explicit phase space subtractions (through the phase space mapping of PYTHIA8) will produce slightly harder partons in the core process (see Figure III.A1). This tendency persists after showering, as shown in Figure III.3 for the UNLOPS case. Clearly, this is a non-negligible effect, although the differences are contained in the NLO scale variation band. We believe that using exclusive input is conceptually superior. However, this section is intended to give uncertainty estimates for NLO merged parton showers, and in particular to sketch merging scale uncertainty, and there is no reason to assume that the $\overline{\mathrm{B}}$- and the $\widetilde{\mathrm{B}}$-prescription differ in this respect. Using inclusive input, however, makes merging scale variations much simpler and quicker and avoids having to tamper with the internals of the

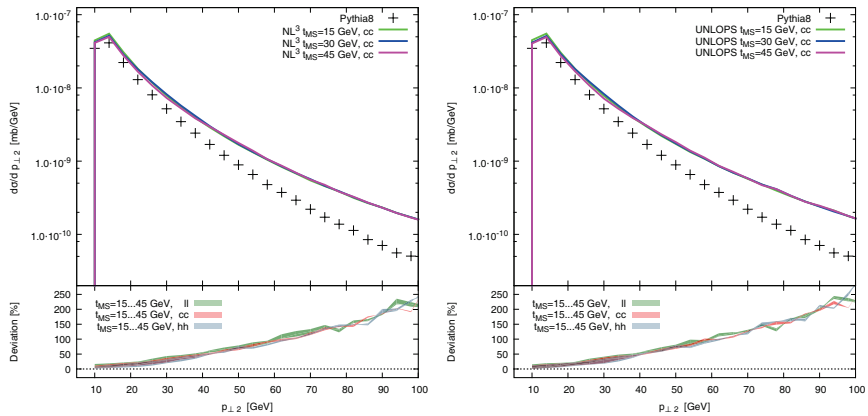

Figure III.5: Transverse momentum of the second hardest jet, for W-boson production in pp collisions at $E_{\mathrm{CM}} = 7000$ GeV, when merging up to two additional partons at LO, and zero and one additional parton at NLO. Jets were defined with the $k_\perp$-algorithm, with $k_{\perp,min} = 10$ GeV. Multi-parton interactions and hadronisation were excluded. The lower inset shows the deviation from PYTHIA8. Left panel: Results of NL^3. Right panel: Results of UNLOPS.

POWHEG-BOX. Because of this speed factor, we chose to use inclusive input for the results of this publication.

In the following, we will often include merging scale variations in the ratio plots. So that the plots become less cluttered, we will give the envelope of curves for merging scales between $\rho_{\mathrm{MS}} = 15$ GeV and $\rho_{\mathrm{MS}} = 45$ GeV as uncertainty band, rather than show the actual curves.

Figure III.4 shows that the transverse momentum of the hardest jet is heavily affected by NLO merging. This is due to the W+jet NLO calculation, as already seen in Figure III.1. The merging scale variations, as well as the μ_R/μ_F-variation for NLO merged results lie within the scale variation band of the NLO calculation, but the combined variation is not significantly smaller. The NLO merged predictions touch the upper limit of the NLO scale variation band, because of the use of inclusive NLO input, as discussed earlier. Merging scale variations alone are minor.

Merging scale uncertainties are also small in Figure III.5, which shows the transverse momentum of the second hardest jet. It is particularly reassuring that even combined with μ_R/μ_F-variation, the bands are smaller than in CKKW-L and UMEPS [6].

We would like to conclude this section by noting that differences between UNLOPS and NL^3 are hardly noticeable for the displayed observ-

ables. This is true for all observables we have investigated in W-boson production, which can be interpreted to mean that the logarithmic improvements in UNLOPS do not result in major changes in W-boson production for the merging scale we have chosen. We anticipate larger effects once scale hierarchies become larger, i.e. if the merging scale is significantly decreased. For now, we will instead investigate if the introduction of a slightly larger mass scale and incoming gluons in the lowest order process leads to visible effects.

III.4.2 H-boson production in gluon fusion

This section is intended to demonstrate that the PYTHIA8 implementation is not specific to W+jets, and that different processes can be used to guide algorithmic choices. We have chosen to investigate Higgs-boson production in gluon fusion, mainly because of the presence of incoming gluons in the lowest order process and the very large NLO corrections.

In Figure III.6, we compare the variation of NLO merged results with the scale variation in the H+jet NLO calculation of the default POWHEG-BOX program. The transverse momentum spectrum of the hardest jet is softer in NLO results than in PYTHIA8. We found the same behaviour in tree-level merging as well. Interestingly, a similar effect was observed in pure QCD dijet production, which might indicate that PYTHIA8 overestimates the hardness of radiation from initial state gluons.

We consider Figure III.6 a cautionary tale. Let us examine the the upper row first. The merging scale variation in $p_{\perp 1}$ is very small. However, when including renormalisation- and factorisation-scale dependence, the uncertainty of the NLO merged results is larger than the variation in the H+jet NLO calculation. This is explained by our choice of K-factor. As discussed in appendix III.B, this rescaling affects only the "higher orders", since the effect on n-jet observables is removed to $\mathcal{O}\left(\alpha_s^{n+1}\left(\mu_R\right)\right)$. Different choices lead to no visible effects in W-boson production, since e.g. a change of $K_0 = \frac{\int \overline{B}_0}{\int B_0} = 1.16 \approx 1$ will only result in changing tree-level samples slightly, and $p_{\perp 1}$ is dominated by the one-jet NLO contribution. However, this does not apply to H production in gluon fusion, where $K_0 \gtrsim 2$ leads to a significantly larger two-jet tree-level contribution. Enhancing the two-jet tree-level contribution will make the leading-order scale variation of this sample more visible, thus leading to an overall larger variation[11].

[11] The same might naively be true for the POWHEG result, since two-jet contributions in H+jet in

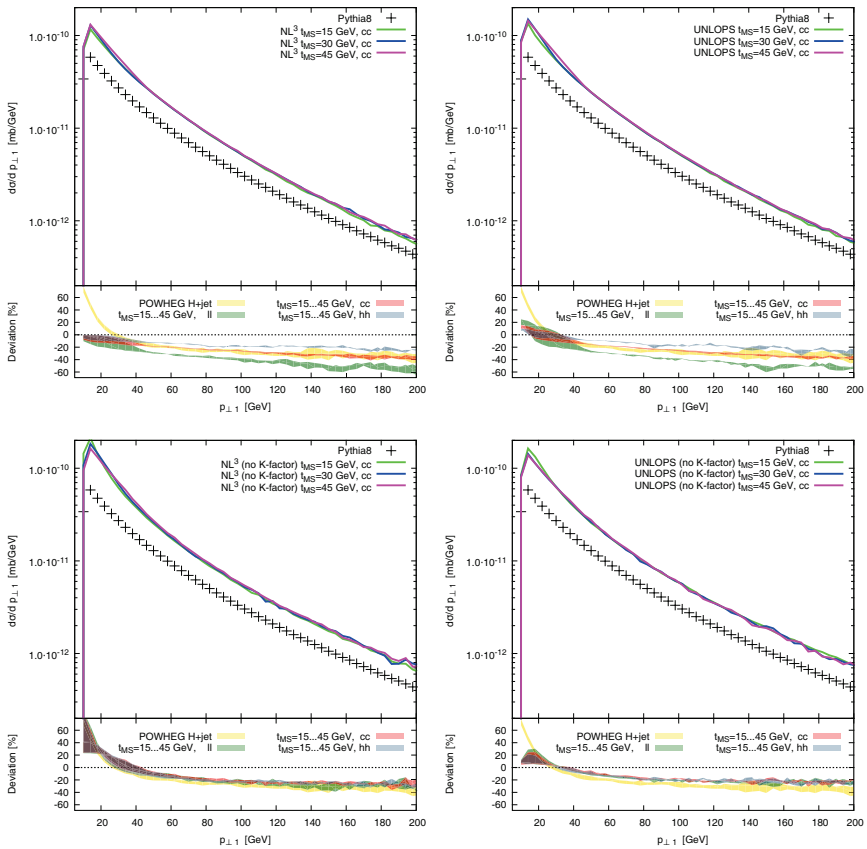

Figure III.6: Transverse momentum of the hardest jet, for H-boson production in pp collisions at $E_{\mathrm{CM}} = 7000$ GeV, when merging up to two additional partons at LO, and zero and one additional parton at NLO. Jets were defined with the $k_\perp$-algorithm, with $k_{\perp,min} = 10$ GeV. Multi-parton interactions and hadronisation were excluded. The lower inset shows the deviation from PYTHIA8. The band labelled "POWHEG W+jet" is given by the envelope of varying the renormalisation scale in the POWHEG-BOX program between $\frac{1}{2}M_Z, \ldots, 2M_Z$, and the factorisation scale between $\frac{1}{2}M_H, \ldots, 2M_H$. The upper panels show the results for using the zero-jet K-factor (i.e. $K = \frac{\int \overline{B}_0}{\int B_0}$) throughout the NLO merging procedures. The lower panel show the result when *not* using any K-factor (i.e. $K = 1$). Left columns: Results of NL^3. Right columns: Results of UNLOPS.

POWHEG also carry a (much more complex, phase-space dependent) K-factor $K = \frac{\overline{B}_1}{B_1}$. This "one-jet K-factor" increases with increasing $\mu_{F,R}$ and counteracts the decrease in H+ 2 jet cross section with increasing scales. This leads – among other improvements – to a small scale variation in the POWHEG-BOX calculation for H+jet.

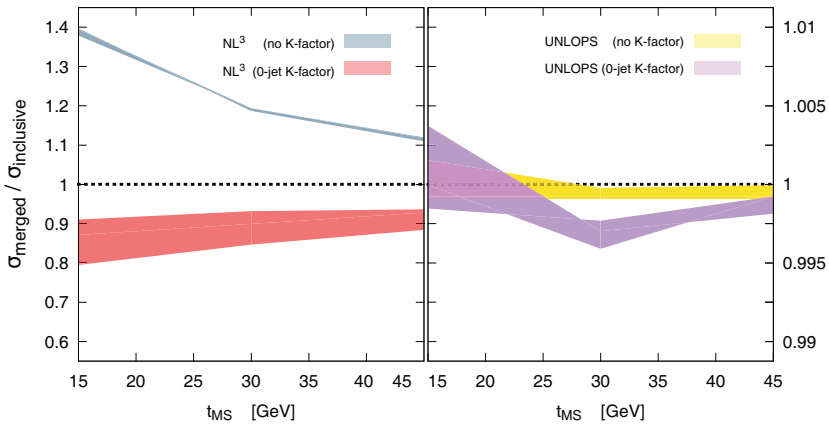

Figure III.7: Comparison of inclusive cross sections for H-production in gluon fusion pp collisions at $E_{\mathrm{CM}} = 7000$ GeV, for NL^3 (left panel) and UNLOPS (right panel), when merging up to two additional partons at LO, and zero and one additional parton at NLO. The results of the merging procedure (labelled σ_{merged}) are normalised to the zero-jet inclusive NLO cross section $\sigma_{\mathrm{inclusive}}$. The coloured bands indicate the variation from choosing μ_F in $\left[(\frac{1}{2}\mathrm{M_H})^2, \dots (2\mathrm{M_H})^2 \right]$ and μ_R in $\left[(\frac{1}{2}\mathrm{M_Z})^2, \dots (2\mathrm{M_Z})^2 \right]$. The results of the NLO merging procedure are presented for two different K-factor treatments. The result of using *no* K-factor is labelled "no K-factor". Usage of the zero-jet K-factor is indicated by the label "0-jet K-factor". The same variations of NL^3 and UNLOPS are plotted, albeit with a smaller ordinate scale for UNLOPS.

Imposing a leading-order scale uncertainty on NLO observables is very conservative, and it seems prudent avoid artificial increases due to K-factors that rescale higher orders. The lower row of III.6 shows the result of not using any K-factors at all. The agreement with POWHEG-BOX is reassuring, and the scale variation is small. The NL^3 result however exhibits major merging scale variations, which are mainly induced by an increased cross section in the results for $t_{\mathrm{MS}} = 15$ GeV. This unitarity violation was previously "masked" by a large K-factor.

To further illustrate the effect of including K-factors, we show the merged prediction of the total inclusive Higgs cross section as a function of the merging scale in Figure III.7. In this figure, we divide the NLO merged results for scales μ_R/μ_F by the input NLO cross section with the same μ_R/μ_F choices. The ideal result should be unity, without scale uncertainties. This is true to a high degree for UNLOPS, which shows that the unitary nature of that method really works as expected.

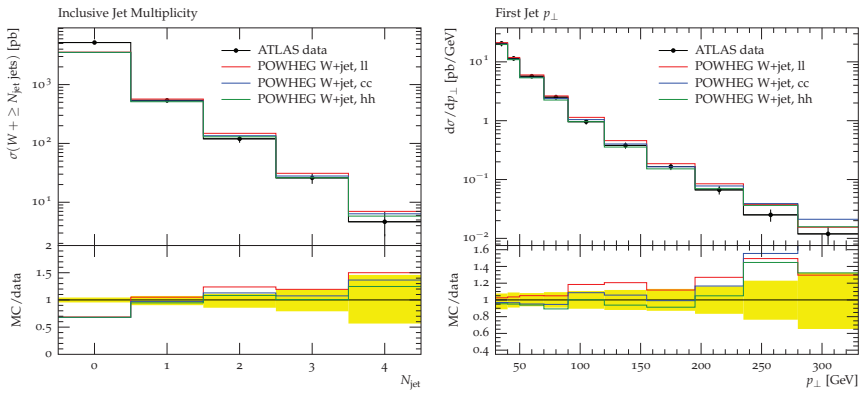

Figure III.8: Jet multiplicity and transverse momentum of the hardest jet in W-boson production, as measured by ATLAS [47]. MC results taken from the POWHEG-BOX program, with three different renormalisation/factorisation scales. Effects of partons showers, multiple scatterings and hadronisation are included.

For NL^3, however, we see that when using K-factors we get a large scale variation with a non-negligible merging scale dependence. Removing the K-factors decreases the scale variations, but on the other hand increases significantly the merging scale dependence.

The K-factor dependence is a major uncertainty in the NLO merged results for Higgs production in gluon fusion. We would like to stress that the current publication is intended as a technical summary, and not aimed at making binding predictions. Rather, we will use this as guidance when improving the implementation further.

III.4.3 W-boson production compared to data

In this section, we would like to show NLO merged predictions in comparison to data. We would like to point out that we have fixed $\alpha_s(M_Z)$ in the PS to $\alpha_s(M_Z) = 0.118$, and use CTEQ6M parton distributions throughout. Please consult appendix III.E for a discussion of multiparton interactions. This means that the results do not correspond to a tuned version of the PYTHIA8 shower. Conclusive results can of course only be presented after the uncertainty of PS tuning has been assessed.

In figure III.9, we show that the jet multiplicity is well under control in NLO merged predictions. The left panel of Figure III.8 shows that, as expected, it is not possible to describe the number of zero-jet events with a W+jet NLO calculation. This is of course exactly the strength of

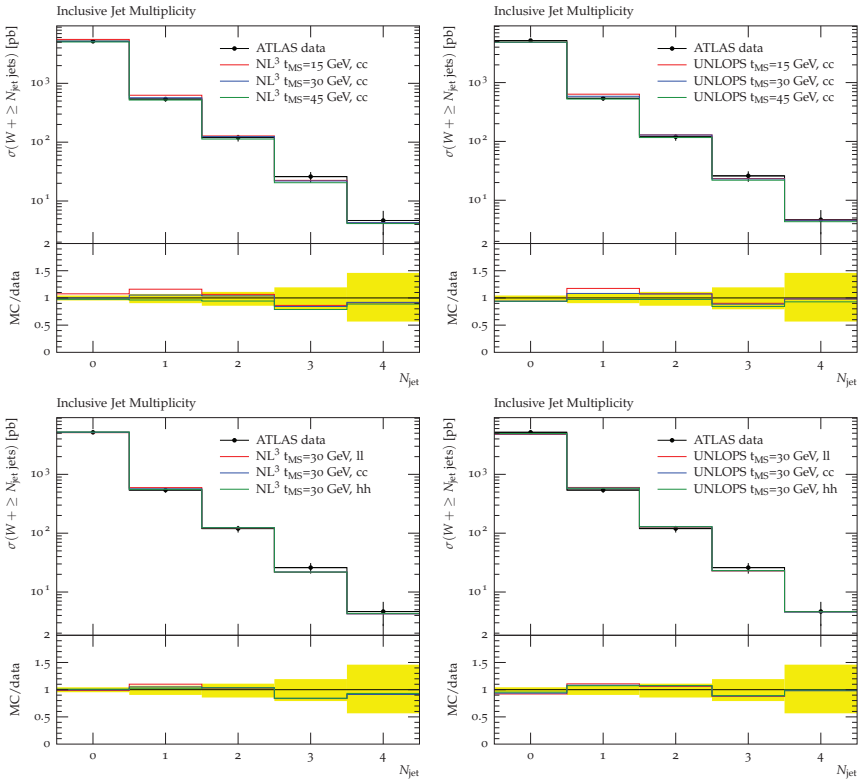

Figure III.9: Jet multiplicity in W-boson production, as measured by ATLAS [47]. The MC results were obtained by merging up to two additional partons at LO, and zero and one additional parton at NLO. MC results are shown for three different merging scales (top panels) and for three different renormalisation/factorisation scales (bottom panels). Effects of multiple scatterings and hadronisation are included. Left panels: Results of NL^3. Right panels: Results of UNLOPS.

merged calculations: Observables with different jet multiplicities can be described in a single inclusive sample.

The transverse momentum of the hardest jet in association with a W-boson is shown in figure III.10 and the right panel of Figure III.8. It is clear that the NLO merged results do not agree with data. We have chosen this particular observable because it exhibits the most unsatisfactory description of data that we have encountered while testing our NLO merging methods. The reason for this disagreement is multifold. First, we have already mentioned that correcting for inclusive NLO input produces harder $p_{\perp 1}$ tails. The two-jet sample will eventually dom-

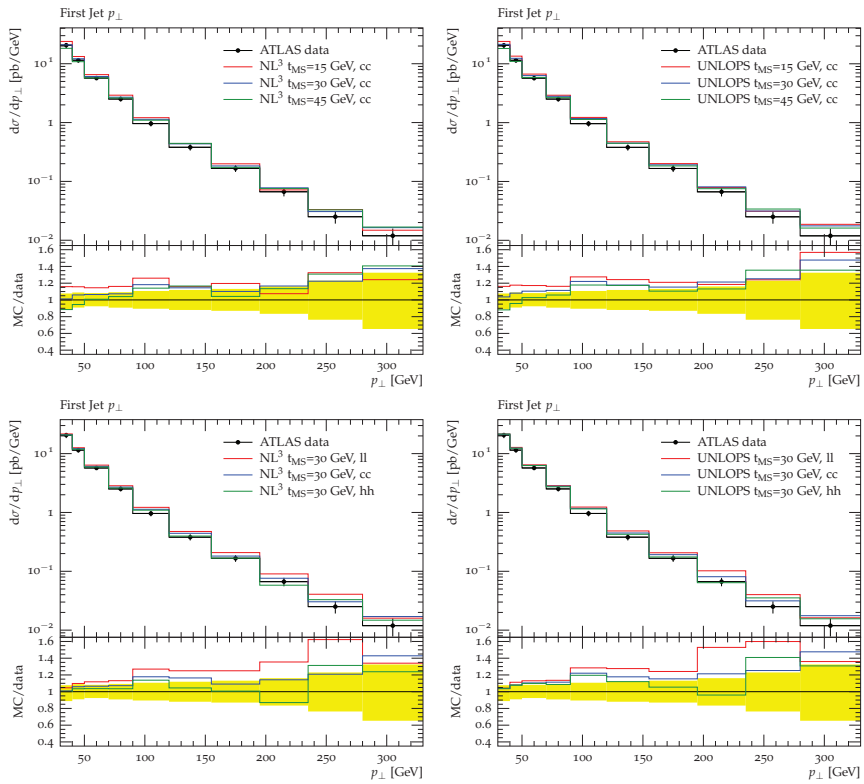

Figure III.10: Transverse momentum of the hardest jet in W-boson production, as measured by ATLAS [47]. The MC results were obtained by merging up to two additional partons at LO, and zero and one additional parton at NLO. MC results are shown for three different merging scales (top panels) and for three different renormalisation/factorisation scales (bottom panels). Effects of multiple scatterings and hadronisation are included. Left panels: Results of NL^3. Right panels: Results of UNLOPS.

inate the tail. We have chosen to rescale the two-jet contribution with a K-factor above unity. It could also be argued that the POWHEG-BOX result in Figure III.8 has slight tendency to overshoot. This might indicate that some part of the "giant K-factor effect" due to enhancements of $\mathcal{O}\left(\alpha_s \ln \frac{p_{\perp 1}^2}{M_W^2}\right)$ is developing in the W+jet NLO calculation of $p_{\perp 1}$ because of soft/collinear W-bosons. The last two points are correlated, since two-jet configurations have a major impact on the $p_{\perp 1}$-dependence of the NLO result, and increasing the two-jet contribution can enhance the visibility of giant K-factors.

The NL^3 and UNLOPS descriptions of data exhibit high similarity.

We have already noted the semblance of both methods in section III.4.1. This observation is specific to W-boson production, and does not hold for other processes, as for instance illustrated in section III.4.2.

III.5 Discussion and conclusions

In this article, we have presented two new methods for combining multiple next-to-leading order calculations consistently with the PYTHIA8 parton shower. The NL^3 method is a generalisation of the CKKW-L scheme, while the UNLOPS prescription accomplishes the same for UMEPS. Both methods achieve a description of zero-, one-, ..., n-jet observables simultaneously at NLO accuracy in one inclusive sample, provided input event files at NLO accuracy for up to n additional jets are supplied. We would like to point the interested reader to appendix III.D.1, in which we argue out that it is feasible to extend the UNLOPS method to a NNLO matching scheme.

Two distinct NLO merging schemes were presented to estimate the magnitude of issues related to sub-leading logarithmic enhancements. Although the UNLOPS method can be considered theoretically preferable, no large differences between NL^3 and UNLOPS have been observed when merging multiple NLO calculations for W-boson production in association with jets. This leads us to conclude that for the observables that were investigated, and the merging scale values that were used, sub-leading logarithmic enhancements are sub-dominant. For H$-$boson production, differences are visible, with UNLOPS delivering a more reliable solution.

This article is intended to give a comprehensive description of the choices that can be made in deriving and implementing an NLO merging method. We hope that this publication provides enough information about the actual implementation to allow the reader to form clear judgements of the rather intricate details. We have tried to remain as general as possible in our choice of inputs. It has been shown that different inputs can, due to mismatches in phase space mappings, have visible, systematic effects. When confronted with such effects, it is clearly preferable to reach an agreement over inputs, and we hope that the current publication can contribute to a discussion.

We have shown that the merging scale dependence in W$+$jets is small, and contained in the scale variation band of the W$+$jet NLO calculation. This also means that the description of data is governed by the input NLO calculation.

The merging scale dependence in Higgs-boson production in gluon fusion is very small. In this case, we highlighted that the dominant uncertainty of the algorithms is given by the choice of the K-factor rescaling higher orders – which is beyond the control of the NLO calculation. This is a manifestation of the magnitude of K-factors in gluon fusion and the scale variation of the cross sections. We would like to stress that this uncertainty is present because we try to be as general as possible, and that the introduction of K-factors does in principle not jeopardise NLO accuracy, or degrade the PS approximation. However, if K-factors are not necessary and instead produce large variations, the removal of K-factors should be considered.

Although we have presented some comparisons to data in this article, we do not attempt to make any definite predictions. To do this, a further investigation of the uncertainties has to be performed – a task we will return to in future publications. We end this article by listing the main issues that need to be addressed.

Our methods require events generated according to the exclusive NLO cross section. There are currently no standard programs that will produce such events, and instead we have used inclusive NLO cross sections and subtracted explicit counter events by integrating tree-level matrix element events over the radiative phase space, using the mapping of the PYTHIA8 parton shower. We have also "hacked" POWHEG-BOX to directly produce the exclusive cross section event, and have found some differences, due to the different phase space mapping used there. Modifying the internals of other programs is, of course, not a viable long-term solution, and we hope that the introduction of our algorithm may inspire authors of NLO matrix element generators to include the generation of exclusive cross sections as an option in their programs.

We have allowed the use of K-factors in the underlying tree-level merging in the hope that the inclusion of NLO corrections will then lead to less merging scale variations. Although this can be done without modifying the formal accuracy of our methods, we see clear differences compared to the case where K-actors are omitted, in the case of Higgs-production, where these K-factors are large. We find indications of reduced factorisation and renormalisation scale uncertainties in the absence of K-factor, but also note larger merging scale variations in the NL^3 case. This needs to be investigated further. Other options, e.g. including multiplicity-dependent K-factors, should also be considered to understand uncertainties.

At very high transverse momenta we expect logarithms of the form

$\ln\left(\frac{p_{\perp\text{jet}}}{M_W}\right)$ to arise, resulting in so-called "giant K-factors" [37,38]. These logarithms can in principle be resummed to all orders, and an inclusion of such resummation is planned for the parton shower in PYTHIA8. We are confident that our methods can be extended also to deal with this full electro-weak shower, but meanwhile we need to understand better the uncertainties arising from these logarithms.

Finally, before we can be confident enough to make precise predictions with our new methods, a re-tuning of the shower (including MPI) of PYTHIA8 must be carried out. The currently available tunes have all been obtained without higher order matrix elements merging, and it is clear that some of the resulting parameters have been obtained from trying to fit distributions where we do not expect an uncorrected parton shower to do a reasonable job. In particular, this applies to the tuning of the scale factor in α_s (see eq. (III.8)) in the shower, and we expect this to change significantly when tuning the ME corrected shower. This will then also directly influence the MPI, which also need to be re-tuned. Needless to say, such a tuning as a major undertaking.

Note added

While finishing this article, it came to our attention that an approach that is similar to UNLOPS has been developed in parallel by Plätzer [32]. Also, on the day of submission, we noted that Alioli et al. [36] presented their work on NLO-matching.

Acknowledgements

Work supported in part by the Swedish research council (contracts 621-2009-4076 and 621-2010-3326). We are grateful to Nils Lavesson and Oluseyi Latunde-Dada for collaboration at the early stages of developing the NL^3 method. We would also like to thank Simon Plätzer and Keith Hamilton for helpful discussions.

Appendices

III.A NLO prerequisites

This appendix is intended to introduce the merging scale definition used throughout this article (see section III.A.1), discuss the prerequisites on NLO input (section III.A.2), introduce the notation we employ (section III.A.3) and finally illustrate how the POWHEG-BOX program can be used to generate the input necessary for NLO merging (section III.A.4).

III.A.1 The Pythia jet algorithm

Throughout this paper, we use cuts on the minimal PYTHIA8 evolution $p_{\perp,evol}$, to disentangle regions of phase space. Since $p_{\perp,evol}$ defines a relative $p_\perp$ distance [48], we think of $p_{\perp,evol}$ as an inter-parton separation criterion. To avoid confusion with other $p_\perp-$definitions, we will use the symbol ρ for $p_{\perp,evol}$.

The phase space regions in which we believe fixed-order calculations to dominate is separated from the resummation region by a cut value ρ_{MS}, defined in a parton separation $t \sim \min\{\rho\}$. This minimal separation is constructed by finding the minimal ρ for any triplet of partons e, r, s, where e is a final state "emitted" parton, r is a radiating parton and s is a spectator. All triplets, irrespectively of flavour (or colour) constraints are included. In a dipole picture, the radiator r can be thought of as the dipole end whose momentum changes most when splitting the dipole (r', s') into two dipoles (r, e), (e, s) while s is the dipole end that absorbs the (small) recoil. The functional definition of this parton separation criterion is

$$t = \min\left[\rho_{\{i,j,k\}}\right] \quad \begin{array}{l}\text{where } i \in \{\text{final state partons}\},\\ \text{and } j \in \{\text{final and initial state partons}\},\\ \text{and } k \in \{\text{final and initial state partons}\}\end{array} \tag{III.A1}$$

where the separation of i for a fixed triplet (i, j, k) of partons with mo-

menta p_i, p_j, p_k is

$$\rho_{ijk} = p_{\perp,evol,ijk}^2 = \begin{cases} z_{ijk}(1-z_{ijk})Q_{ij}^2 & \text{if the radiator } j \text{ is a final state parton, and} \\ & Q_{ij}^2 = (p_i+p_j)^2\,, \quad z_{ijk} = \frac{x_{i,jk}}{x_{i,jk}+x_{j,ik}} \\ & x_{i,jk} = \frac{2p_i(p_i+p_j+p_k)}{(p_i+p_j+p_k)^2} \\ (1-z_{ijk})Q_{ij}^2 & \text{if the radiator } j \text{ is an initial state parton, and} \\ & Q_{ij}^2 = -(p_i-p_j)^2\,, \quad z_{ijk} = \frac{(p_i-p_j+p_k)^2}{(p_i+p_k)^2} \end{cases} \tag{III.A2}$$

The cut value ρ_{MS} is called merging scale. If all ρ_{ijk} for a particular final state parton i are larger than ρ_{MS}, we call this parton a resolved jet. Conversely, if any ρ_{ijk} is below ρ_{MS}, we call i an unresolved jet. We say that a phase space point is in the matrix element region if $t > \rho_{\text{MS}}$, i.e. all minimal parton separations are larger than the cut. In other words, a phase space point is in the matrix element region if it only contains resolved jets. The parton shower region is disjoint: If any jet separation falls below ρ_{MS}, be believe that parton shower resummation is appropriate.

Using eq. (III.A1) and eq. (III.A2) as merging scale definition does not exactly correspond to separating the matrix element- and parton shower regions in $p_{\perp,evol}$. In parton shower algorithms, the resolution scale attributed to a state is given by the scale of the last splitting. This is just one number, since a splitting is generated by a winner-takes-it all strategy: If a splitting is chosen, all scales attributed to splittings of other partons are considered higher. Such a merging scale definition can only be constructed if we know (all) parton shower histories of an input event.

For now, we use eq. (III.A1) and eq. (III.A2) as merging scale definitions, and are content with the fact that ρ_{MS} does still correspond to a single $p_{\perp,evol}-$value. This means that vetoing shower emissions that would result in an additional resolved jet will not introduce no-emission probabilities above ρ_{MS}.

We have to point out that fixing the merging scale definition is necessary in the NLO merging methods illustrated in this article. Otherwise, it would be mandatory to reweight NLO corrections with no-emission probabilities for merging-scale-unordered emissions, which would fundamentally degrade the higher-order description we aim to achieve[12]. One benefit of CKKW-L tree-level merging is that the method allows for a wide class of merging scale definitions. Because of the treatment of

[12] See appendix III.C for details

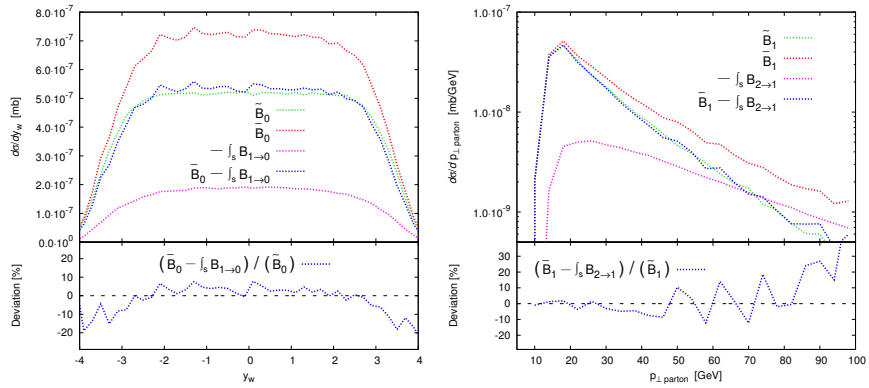

Figure III.A1: Comparisons of two way of generating exclusive NLO cross sections. $\overline{\mathrm{B}}_i$ events are calculated without changing the POWHEG-BOX program, while for $\widetilde{\mathrm{B}}_i$, we have explicitly introduced the necessary cuts in POWHEG-BOX. Left panel: Comparison for zero-jet exclusive NLO cross section, as function of the W-boson rapidity. Right panel: Comparison for one-jet exclusive NLO cross section, as function the kinematical transverse momentum of the parton.

emissions that are unordered in the merging scale, however, the merging scale effectively has to define a hardness-measure, since otherwise, only small portions of phase space will be endowed with ME corrections [5]. Different choices of hardness definitions for different processes in CKKW-L can be helpful for efficiently correcting phase space. The current implementation of CKKW-L in PYTHIA8 allows for both $\min\{\rho\}$ and $\min\{k_\perp\}$ as merging scales. No major efficacy differences between these merging scale definitions has been found so far, leading us to conclude that in practise, defining the merging scale in $\min\{\rho\}$ is reasonable.

III.A.2 Exclusive cross sections

In this section, we would like to introduce the concepts of exclusive and inclusive NLO cross sections, and comment on how inclusive NLO cross sections can be made exclusive by the inclusion of a phase space subtraction sample.

We think of matrix element merging as a two-step measurement. We first measure the number of resolved jets in the input event, by applying a cut. Then, we calculate an interesting observable on events that have

been classified as $n-$jet events. To make the second step independent of the choices in the first measurement, we need to sum over all possible jet multiplicities.

Throughout this publication, we will define jets by the PYTHIA8 evolution $p_\perp$ jet separation criterion, as discussed in appendix III.A.1. Resolved jets are defined as partons whose separation to any other partons in the state is above the value ρ_{MS}. We call ρ_{MS} the merging scale.

The output of a tree-level calculations for k final partons can contain $l = 0, \ldots, k$ partons with soft or collinear momenta. The result of the calculation will diverge as soon as any parton in the calculation becomes soft or collinear. We can remove these regions of phase space, if we enforce that the output only contains exactly k partons with jet separation above ρ_{MS}, i.e. k resolved jets. If the jet definition is infrared and collinear safe, this jet cut will render tree-level calculations finite.

The result of using a next-to-leading order calculation for k partons to describe an observable $\mathcal{O}$ can schematically be written as

$$\langle \mathcal{O} \rangle = \int d^k\phi \, \mathcal{O}(\phi_k) \, d\sigma_{Born} + \int d^k\phi \, \mathcal{O}(\phi_k) \, d\sigma_{Virtual} + \int d^{k+1}\phi \, \mathcal{O}(\phi_{k+1}) \, d\sigma_{Real} \, , \tag{III.A3}$$

where $\int d^k\phi$ indicates an integration over the $k-$parton phase space, $d\sigma_{Born}$ is the tree-level cross section, $d\sigma_{Virtual}$ the virtual correction term and $d\sigma_{Real}$ the real emission part. Equation III.A3 allows contributions of any number of $l = 0, \ldots, k+1$ resolved (or unresolved) jets. Since the tree-level part still diverges if any of the k partons approach the soft and collinear regions, we require that $\int_k \mathcal{O}(\phi_k) d\sigma_{Born}$ always contains exactly k resolved jets, which immediately means having the same requirement in $\int_k \mathcal{O}(\phi_k) d\sigma_{Virtual}$. This then means that $\int_{k+1} \mathcal{O}(\phi_{k+1}) d\sigma_{Real}$ has to be constrained, since otherwise, the NLO calculation could include real-emission corrections to non-existent "underlying" Born configurations with less than k resolved jets. The POWHEG method [17, 18] eliminates this issue by evaluating using one phase space point $\overline{\phi}_n$ for tree-level and virtual parts, and ϕ_{n+1} phase space points that can be projected exactly onto $\overline{\phi}_n$ in real-emission terms. We will assume that in neither of the terms in III.A3, less than k resolved jets are included. Further, the observable $\mathcal{O}$ receives – through real corrections – contributions from $k+1$ (resolved or unresolved) jets. Measurements explicitly depending on the kinematics of $k+1$ resolved jets are only accurate to tree-level approximation, while contributions for an unresolved additional jet are necessary to cancel divergences[13].

[13] In numerical implementations, the singularities of virtual corrections and real-emission con-

In multi-jet merging, $(k+1)-$jet contributions enter through explicitly adding a reweighted $(k+1)-$jet sample. To merge multiple NLO calculations, we also need a clean cut, that makes the classification of the input in terms of jet multiplicities possible. We define that the "NLO part" of an $k-$jet NLO calculation should contain k resolved jets, and at most one unresolved jet, while contributions with $k+1$ resolved jets are regarded leading-order parts

$$\begin{aligned}\langle \mathcal{O} \rangle = &\underbrace{\int d^k\phi\, \mathcal{O}(\phi_k) \left\{ d\sigma_{Born} + d\sigma_{Virtual} + \int^{\rho_{\text{MS}}} d\phi\, d\sigma_{Real} \right\}}_{\text{NLO part}} \\ &+ \underbrace{\int_{\rho_{\text{MS}}} d^{k+1}\phi\, \mathcal{O}(\phi_{k+1})\, d\sigma_{Real}}_{\text{LO part}}\end{aligned} \tag{III.A4}$$

We call the NLO part of such a calculation the *exclusive* NLO cross section.

Merging schemes naturally act on exclusive cross sections. Technically, we assume that all unresolved real emission parts are projected onto n-parton phase space points. In POWHEG, this is facilitated by performing the $d\phi$ integration in the real-emission term explicitly. If an NLO calculation would yield only phase space points with exactly n partons in n resolved jets, and weight these points with[14]

$$\widetilde{\mathrm{B}}_n = d\sigma_{Born} + d\sigma_{Virtual} + \int^{\rho_{\text{MS}}} d\phi\, d\sigma_{Real}\,, \tag{III.A5}$$

then this calculation could be used immediately for NLO merging. However, $\widetilde{\mathrm{B}}_n$ might not be accessible without changing the NLO matrix element generator, since it might not possible to split the calculation into "NLO parts" and "LO parts" as desired. We instead choose to write

$$\widetilde{\mathrm{B}}_n = d\sigma_{Born} + d\sigma_{Virtual} + \int d\phi\, d\sigma_{Real} - \int_{\rho_{\text{MS}}} d\phi\, d\sigma_{Real} \tag{III.A6}$$

and to use the two samples

$$\overline{\mathrm{B}}_n = d\sigma_{Born} + d\sigma_{Virtual} + \int d\phi\, d\sigma_{Real} \tag{III.A7}$$

$$-\int_s \mathrm{B}_{n+1\to n} = -\int_{\rho_{\text{MS}}} d\phi\, d\sigma_{Real} \tag{III.A8}$$

tributions are cancelled separately by regularisation terms.

[14] We give more precise definitions of the notation in the next section.

separately. We call $\overline{\mathrm{B}}_n$ the inclusive NLO cross section, and refer to $\int_s \mathrm{B}_{n+1\to n}$ as phase space subtraction term. Adding the inclusive NLO cross section and the subtraction term, we retrieve the exclusive NLO cross section. It is possible to formulate NLO merging acting on exclusive cross sections, or acting on inclusive cross sections and additional phase space subtraction samples.

We would like to comment on our framework to generate exclusive cross sections from inclusive NLO input. It has already been demonstrated in [6] that extracting integrated states that had been constructed as intermediate states in the parton shower history does indeed give the expected results (see Figure 2 of [6]). However, these comparisons were performed between the shower approximation and the integrated matrix element. To correct for the use of an inclusive NLO cross section, we have to use integrated tree-level events as phase space subtraction for POWHEG-BOX events. Figure III.A1 shows how the exclusive cross section generated through explicitly changing the POWHEG-BOX program code compares to the exclusive cross section produced by a-posteriori phase space subtraction. The differences between the two prescriptions stems from a different phase space mapping in POWHEG-BOX and PYTHIA8. Such effects are beyond the accuracy of the NLO merging methods presented in this article. It should be noted that an a-posteriori phase space subtraction using the PYTHIA8 phase space mapping produces a harder $p_\perp$-spectrum and less forward W-bosons. Ideally, we would like generate the exclusive NLO cross section with an NLO generator which allows for the necessary cuts, so that explicit phase space subtraction become unnecessary. For this publication however, we will use subtractions, since this allows us to perform merging scale variations without continuously having to re-generate LHEF output with the POWHEG-BOX program.

III.A.3 Notation

Formulating NLO merging is unfortunately a fairly notation-heavy task. In this section, we would like to carefully introduce the symbols we will use throughout this article in a tabular style, for easy reference. Let us define the lingo

ϕ_n: Phase space point with n additional resolved jets. This means that ϕ_n can contain p lowest-multiplicity particles (e.g. e^+ and e^- for Drell-Yan production), and n additional partons. Each phase space point has a fixed momentum, flavour and colour configuration.

Underlying configuration: Phase space point ϕ_n which can be to constructed from ϕ_{n+1} by removing one emission, meaning integrating over the one-particle phase space of the emission, and recombining flavours and colours. We will use the terms underlying momentum configuration, underlying flavour configuration and underlying colour configuration when explicitly emphasising one aspect of the underlying configuration.

Φ_{rad} : The radiative phase space, meaning that in

$$\phi_{n+1} \approx \phi_n \Phi_{\text{rad}} \tag{III.A9}$$

Φ_{rad} plays the role of the one-particle phase space of the additional parton, while ϕ_n is the underlying configuration.

Resolved jet: Parton, for which all possible jet separations to other partons in this phase space point are larger than the value ρ_{MS}.

Unresolved jet: Parton, for which at least one jet separations to one other partons in this phase space point is lower than the value ρ_{MS}.

We always assume that matrix elements for n outgoing partons are only integrated over phase space regions with exactly n resolved jets, unless explicitly stated otherwise. In cases where we integrate over emissions, we assume that in the ME input, all partons were resolved jets, and that after the integration, all partons are resolved jets.

Please note that the methods presented in this publication do not rely on a particular regularisation scheme in the NLO calculation, as long as the dependence on the regularisation scheme is cancelled locally, i.e. in the weight of each phase space points separately. We will choose a rather symbolic notation for parts of NLO calculations, and hope that this will

make the formulae in this article more accessible. In the following, we would like to introduce the shorthands:

B_n: Tree-level matrix element with n partons, i.e.

$$\mathrm{B}_n = f_n^+(x_n^+,\mu_F) f_n^-(x_n^-,\mu_F) \left|\mathcal{M}_{n,0}\left(\mu_F,\mu_R\right)\right|^2 , \qquad \text{(III.A10)}$$

where the first subscript on $\left|\mathcal{M}_{n,0}\left(\mu_F,\mu_R\right)\right|^2$ indicates the number of jets, while the second counts loop integrations. Readers more familiar with the notation of [18] should note

$$\mathrm{B}_n \;=\; \left[\, B(\Phi_n) \,\right]_{f_b}$$

For brevity, we always suppress flavour indication on B_n.

$\mathrm{B}_{n+1|n}$: Sum of tree-level configurations with $n+1$ partons, for which the underlying Born configuration is ϕ_n. Loosely, we think of $\mathrm{B}_{n+1|n}$ as the sum of matrix elements B_n, multiplied by splitting kernels (with B_n being evaluated using the underlying momentum, flavour and colour configuration, while the splitting kernels depend on the radiative phase space). Translating to the notation of [18], this means

$$\int d\Phi_{\mathrm{rad}} \mathrm{B}_{n+1|n} \;=\; \sum_{\alpha_r \in \{\alpha_r | f_b\}} \int \left[\, d\Phi_{rad}\; R(\Phi_{n+1}) \,\right]_{\alpha_r}^{\overline{\Phi}_n^{\alpha_r}=\Phi_n}$$

We choose the more symbolic indexing with $n+1|n$, rather than the more rigorous α_r-notation of [18], in order to not obfuscate formulae with details that are not essential for the discussion.

$\int_s \mathrm{B}_{n\to m}$: Sum of tree-level cross sections with n resolved jets in the input ME events, after integration over the phase space of $n-m$ partons. Symbolically:

$$\int_s \mathrm{B}_{n\to m} \;=\; \sum_n \int_s d^{n-m}\phi\; \mathrm{B}_{n|n-m} \qquad \text{(III.A11)}$$

We think of ϕ_n being produced from ϕ_{n-m} by m consecutive splittings. The index s denotes that the integration is accomplished by explicitly removing m partons from the $n-$parton phase space, meaning that we substitute the state S_{+n} by the state S_{+n-m}, as introduced in [6]. The symbol $\int_s \mathrm{B}_{n\to m}$ also indicates that the state S_{+m} only has resolved jets, and that possibly more than one integrations had to be performed in case all of the states $S_{+n-1}, \ldots, S_{+m+1}$ contained unresolved jets.

$\int_s \mathrm{B}^{\uparrow}_{n\to m}$: Sum of tree-level cross sections with n resolved jets in the input ME events, after integration over the phase space of $n-m$ partons. However, in contrast to the symbol $\int_s \mathrm{B}_{n\to m}$, we explicitly require the states S_{+n-1} to contain $n-1$ resolved jets, and still perform this second integration. This is indicated by the upward-pointing arrow. All further integrations only have to be performed because the states $S_{+n-2}, \ldots, S_{+m+1}$ contained unresolved jets. $\int_s \mathrm{B}^{\uparrow}_{3\to 0}$ for example means that we first replace the state S_{+3} by S_{+2} (with two resolved jets), then demand another integration, giving S_{+1}. Then, we find that S_{+1} contains an unresolved jet, so that we integrate once more. The last step would not be necessary for the term $\int_s \mathrm{B}^{\uparrow}_{3\to 1}$.

V_n: Virtual correction matrix element with n partons above ρ_{MS}:

$$\mathrm{V}_n = f_n^+(x_n^+,\mu_F) f_n^-(x_n^-,\mu_F)\, |\mathcal{M}_{n,1}(\mu_F,\mu_R)|^2\,, \qquad \text{(III.A12)}$$

We assume that all ultraviolet divergences have already been removed.

$\mathrm{D}_{n+1|n}$: Sum of infrared regularisation terms with n partons above ρ_{MS}. As above, we indicate these terms can be projected onto underlying Born configurations by the index $n+1|n$. For simplicity, we may think of these regulators as Catani-Seymour dipoles, and *very* symbolically put

$$\mathrm{D}_{n+1|n} \sim \sum_{i'j'k} f_n^+(x_n^+,\mu_F) f_n^-(x_n^-,\mu_F) \left|\mathcal{M}_{n,0}\left(\mu_F,\mu_R,\overline{\phi}_n\right)\right|^2 \otimes D_{ij\to i'j'k}\left(\Phi_{\mathrm{rad}}\right), \tag{III.A13}$$

where i and j are partons of the underlying configuration $\overline{\phi}_n$, while i', j' and k are partons of ϕ_{n+1}. As long as all dependence on the regularisation is contained in the inclusive (exclusive) NLO cross sections, our method will not depend on the actual form of these terms – all numerical NLO subtraction schemes are equally valid. The notation $n+1|n$ is to be understood in the same way as for $\mathrm{B}_{n+1|n}$.

$\mathrm{I}_{n+1|n}$: Sum of integrated infrared regularisation terms with n partons above ρ_{MS}. Remainders due to initial state partons being collinear with identified initial hadrons are included in $\mathrm{I}_{n+1|n}$. As above, we indicate that the terms in $\mathrm{I}_{n+1|n}$ can be projected unto underlying configurations by the index $n+1|n$. Schematically

$$\mathrm{I}_{n+1|n} \sim \int d\Phi_{\mathrm{rad}} \mathrm{D}_{n+1|n} \tag{III.A14}$$

In this case, the one-parton phase space integration is commonly performed analytically. The integration here covers the complete radiative phase space. Integration variables can change for different types of dipoles $D_{ij\to i'j'k}$.

$\overline{\mathrm{B}}_n$: Inclusive NLO weight of $n-$parton phase space points.

$$\begin{aligned}\overline{\mathrm{B}}_n &= \mathrm{B}_n + \mathrm{V}_n + \mathrm{I}_{n+1|n} \\ &\quad + \int d\Phi_{\mathrm{rad}} \left(\mathrm{B}_{n+1|n} - \mathrm{D}_{n+1|n}\right) . \quad \text{(III.A15)}\end{aligned}$$

Note that we will assume that this gives a NLO weight for the phase space point ϕ_n, meaning that we have to evaluate $\mathrm{D}_{n+1|n}$ and $\mathrm{I}_{n+1|n}$ with ϕ_n rather than $\overline{\phi}_n$. This is the standard procedure in the POWHEG and MC@NLO methods. The integration over Φ_{rad} covers the full radiative phase space. Real emission terms can give contributions with an additional resolved jet, which are here included into the weight of n-jet phase space points ϕ_n. As discussed above, the description of an observable at NLO receives n-jet and a $n+1$-jet contributions, so that projecting all $n+1$-jet configurations onto ϕ_n (and leaving no $n+1$ events) seems problematic. However, in matrix-element merging, $n+1$-jet events will be included though the next-higher multiplicity sample. We then need to ensure that the contribution of resolved $n+1$-jet events to the cross section is not double-counted. This is solved by the introduction of exclusive NLO jet cross sections. The inclusive cross section is closely related to the definition of $\bar{B}$ in the POWHEG method. Indeed, if no Sudakov factors are applied in the weight of Born-type phase space points in POWHEG, and all radiative events are projected unto Born configurations, this exactly produces our definition of $\overline{\mathrm{B}}_n$.

$\widetilde{\mathrm{B}}_n$: Exclusive NLO weight of $n-$parton phase space points,

$$\begin{aligned}\widetilde{\mathrm{B}}_n &= \mathrm{B}_n + \mathrm{V}_n + \mathrm{I}_{n+1|n} \\ &\quad + \int^{\rho_{\mathrm{MS}}} d\Phi_{\mathrm{rad}} \left(\mathrm{B}_{n+1|n} - \mathrm{D}_{n+1|n}\right) \\ &= \overline{\mathrm{B}}_n - \int_{\rho_{\mathrm{MS}}} d\Phi_{\mathrm{rad}} \mathrm{B}_{n+1|n} \\ &= \overline{\mathrm{B}}_n - \int_s \mathrm{B}_{n+1\to n} \,. \end{aligned} \tag{III.A16}$$

It is clear from the last equality that an exclusive NLO $n-$jet cross section can be constructed from the inclusive case by explicitly subtracting the phase space points with an additional resolved jet.

$\int_s \overline{\mathrm{B}}_{n\to m}$: Inclusive NLO cross section with n resolved jets in the input ME events, after integration over the phase space of $n-m$ partons. The symbol $\int_s \overline{\mathrm{B}}_{n\to m}$ as always also indicates that more than one integrations had to be performed because all of the states $S_{+n-1}, \ldots, S_{+m+1}$ contained unresolved jets.

$\int_s \widetilde{\mathrm{B}}_{n\to m}$: Exclusive NLO cross sections with n resolved jets in the input ME events, after integration over the phase space of $n-m$ partons. The symbol $\int_s \widetilde{\mathrm{B}}_{n\to m}$ as always also indicates that more than one integrations had to be performed because all of the states $S_{+n-1}, \ldots, S_{+m+1}$ contained unresolved jets.

We will use several different event samples as input for multi-jet merging. An event consists of a phase space point with an associated weight, and can thus be considered completely differential. Only if necessary will we talk about predictions for an observable. We will use "cross section" and "event" interchangeably, and also make little distinction between the terms "(phase space) weight" and "matrix element".

Exclusive cross sections are the basic building blocks needed for multi-jet merging. Tree-level merging uses phase space points weighted with exclusive tree-level matrix elements B_n as input. The NLO multi-jet merging prescriptions advocated in this publication analogously require phase space points weighted by exclusive NLO weights as input. If no exclusive calculation is available, it is possible to extend the algorithm to include the explicit subtraction of eq. (III.A16). To make formulae for NLO merging a bit more transparent, let us introduce the

short-hands

$\widehat{\mathrm{B}}_n$:	UMEPS-reweighted tree-level cross sections with n resolved jets in the input ME events.
$\int_s \widehat{\mathrm{B}}_{n\to m}$:	UMEPS-reweighted tree-level cross sections with n resolved jets in the input ME events, after integration over the phase space of $n-m$ partons. The symbol $\int_s \widehat{\mathrm{B}}_{n\to m}$ also indicates that more than one integrations had to be performed because all of the states $S_{+n-1},\ldots,S_{+m+1}$ contained unresolved jets.
$[A]_{-a,b}$:	Contribution A, with terms of powers α_s^a and α_s^b removed. The resulting terms are calculated with fixed scales μ_R and μ_F.
$[A]_{c,d}$:	Contribution A, with only terms of power α_s^c and α_s^d retained, calculated with fixed scales μ_R and μ_F.

The last two short-hands are particularly useful when trying to summarise terms in the expansion of the tree-level merging weights. For example, the sum of the second and third term in curly brackets in

$$\left[\mathrm{B}_2 w_2\right]_{-2,3} \;=\; \mathrm{B}_2\left\{w_2' - \left[w_2'\right]_0 - \left[w_2'\right]_1\right\}$$

is given by eq. (III.B46) below.

III.A.4 Powheg-Box usage

This section is intended to give guidelines on how to use the POWHEG-BOX program [19] in order to produce the inclusive NLO cross sections [42–45] needed for NLO merging in PYTHIA8. Ideally, this should suffice as tutorial on how to set up the desired POWHEG-BOX outputs. We rely on knowledge on POWHEG-BOX input manipulations. With new versions of POWHEG-BOX, the names of the inputs might change, so that the settings advocated here come without guarantees.

For a given process with n partons in the underlying Born configuration, POWHEG-BOX by default generates output Les Houches events with $n-$ and $(n+1)-$parton kinematics. $n-$parton phase space points

are weighted with the matrix element weights

$$\begin{aligned}
&\overline{\mathrm{B}}_n\,\Delta\left(p_{\perp,min}\right)\\
=&\Big\{\mathrm{B}_n\left(\phi_n\right)+\mathrm{V}_n\left(\phi_n\right)+\mathrm{I}_{n+1|n}\left(\phi_n\right) && \text{(III.A17)}\\
&\quad+\int d\Phi_{\mathrm{rad}}\left[\mathrm{B}_{n+1|n}\left(\phi_n\,\phi_{rad}\right)-\mathrm{D}_{n+1|n}\left(\phi_n\,\phi_{rad}\right)\right]\Big\}\,\Delta\left(p_{\perp,min}\right)\,, && \text{(III.A18)}
\end{aligned}$$

where the integration $\int d\Phi_{\mathrm{rad}}$ contains the complete radiative phase space, and the Sudakov factor is given by

$$\Delta\left(p_\perp\right) \;=\; \exp\left\{-\int_{p_\perp} d\Phi'_{\mathrm{rad}}\frac{\mathrm{B}_{n+1|n}\left(\phi_n,\phi'_{rad}\right)}{\mathrm{B}_n\left(\phi_n\right)}\right\}. \qquad \text{(III.A19)}$$

$(n+1)-$parton phase space points are weighted with

$$\overline{\mathrm{B}}_n\,\Delta\left(p_\perp\right)\,\frac{\mathrm{B}_{n+1|n}\left(\phi_{n+1}\right)}{\mathrm{B}_n\left(\phi_n\right)}\Theta\left(p_\perp-p_{\perp,min}\right). \qquad \text{(III.A20)}$$

The program decides if a radiative (i.e. $(n+1)-$parton) phase space point is generated by comparing the $p_\perp$ of the proposed configuration ϕ_{n+1} against $p_{\perp,min}$. No radiative events are produced if $p_{\perp,min}$ is set to the kinematical limit. Furthermore, we have

$$\left\{\Delta\left(p_{\perp,min}\right)\right\}_{p_{\perp,min}\to\infty}=1\,. \qquad \text{(III.A21)}$$

Thus, using $p_{\perp,min}\to\infty$, we find

$$\begin{aligned}
\left\{\overline{\mathrm{B}}_n\,\Delta\left(p_{\perp,min}\right)\right\}_{p_{\perp,min}\to\infty} \;=\;& \mathrm{B}_n\left(\phi_n\right)+\mathrm{V}_n\left(\phi_n\right)+\mathrm{I}_{n+1|n}\left(\phi_n\right) && \text{(III.A22)}\\
&+\int d\Phi_{\mathrm{rad}}\left[\mathrm{B}_{n+1|n}\left(\phi_n\,\phi_{rad}\right)-\mathrm{D}_{n+1|n}\left(\phi_n\,\phi_{rad}\right)\right]
\end{aligned}$$

This is exactly the inclusive NLO cross section we need to perform NLO merging. The NLO merging prescription will include $(n+1)-$parton configurations in a CKKW-L style.

In the POWHEG-BOX program, the parameter $p_{\perp,min}$ can be set by changing the input variable `ptsqmin`. For example assigning

$$\texttt{ptsqmin} = \texttt{1d15} \qquad \text{(III.A23)}$$

will ensure that for LHC energies, the output events of POWHEG-BOX will contain only $n-$parton kinematics, weighted with the desired inclusive NLO cross section. Setting `ptsqmin` will produce only $n-$parton

kinematics only if every $(n+1)-$parton phase space has an underlying Born configuration. This is for example not true for $c\bar{c} \to u\bar{d}W^-$ scattering via an $s-$channel gluon. Since such processes do not constitute corrections to any lower-order process, we regard these as true leading-order parts, and (internally) neglect these configuration in the POWHEG-BOX output. They will be added by including such configurations with incomplete parton shower histories through the treatment of tree-level matrix elements. Numerically, the treatment of incomplete states does not have any impact.

The desired POWHEG-BOX output should be generated with fixed factorisation- and renormalisation scale. To be completely certain that this is the case, set

```
runningscale  0          (III.A24)
runningscales  0         (III.A25)
btlscalereal  1          (III.A26)
btlscalect  1            (III.A27)
ckkwscalup  0            (III.A28)
```

The POWHEG-BOX program would, upon making the assignment III.A23, attribute a `SCALUP` value of `SCALUP` $= \sqrt{\texttt{ptsqmin}}$ to the output LH events. This number would normally be read by PYTHIA8 and used as factorisation scale in the construction of overestimates for initial state splittings. For our purposes, the true value of μ_F will be an input for PYTHIA8, so that the correct choice can be used internally.

After these settings, the POWHEG-BOX output file can be used for NLO merging in PYTHIA8. We will include a detailed documentation of this procedure, and a manual how the schemes presented in this publication can be used, in the online documentation of an upcoming PYTHIA8 release.

III.B Generation of weights

The aim of this appendix is to provide a complete description of the $\mathcal{O}\left(\alpha_s^1\left(\mu_R\right)\right)-$terms needed to implement the NL^3 and UNLOPS schemes. This task is split into subsections containing the expansion

of factors appearing in the weight w_n

$$w_n = K \cdot \frac{x_n^+ f_n^+(x_n^+,\rho_n)}{x_n^+ f_n^+(x_n^+,\mu_F)} \frac{x_n^- f_n^-(x_n^-,\rho_n)}{x_n^- f_n^-(x_n^-,\mu_F)} \prod_{i=1}^{n} \left[\frac{\alpha_s(b_i\rho_i)}{\alpha_s(\mu_R)} \frac{x_{i-1}^+ f_{i-1}^+(x_{i-1}^+,\rho_{i-1})}{x_{i-1}^+ f_{i-1}^+(x_{i-1}^+,\rho_i)} \frac{x_{i-1}^- f_{i-1}^-(x_{i-1}^-,\rho_{i-1})}{x_{i-1}^- f_{i-1}^-(x_{i-1}^-,\rho_i)} \right.$$
$$\left. \Pi_{S_{+i-1}}(x_{i-1},\rho_{i-1},\rho_i) \right] \Pi_{S_{+n}}(x_n,\rho_n,\rho_{\mathrm{MS}}) \,. \qquad \text{(III.B1)}$$

The weight applied in UMEPS differs in that the last no-emission probability $\Pi_{S_{+n}}(x_n,\rho_n,\rho_{\mathrm{MS}})$ is not included. Note that we have kept the parameter b_i discussed in III.2.3. The generation of the tree-level weights for CKKW-L is discussed in [5], and the UMEPS case is treated in [6]. The K-factor is generated by dividing the (integrated) inclusive NLO zero-jet cross section by the leading-order result

$$K = \frac{\int \overline{\mathrm{B}}_0}{\int \mathrm{B}_0} \qquad \text{(III.B2)}$$

It is in principle possible to rescale the tree-level weights for n partons by K-factors depending on the jet multiplicity. Multiplicity-dependent K-factors will lead to different rescaling of PS higher orders, since the $\mathcal{O}\left(\alpha_s^1(\mu_R)\right)$ −contribution from multiplying K-factors will be removed. This means that different K-factor choices give changes beyond the accuracy of the methods. It is interesting to observe that MC@NLO and POWHEG also differ in the K-factor applied to real-emission events: While the radiative events are not rescaled in MC@NLO, POWHEG includes a phase-space dependent K-factor (see eq. (III.A20)). Though formally sub-leading, this difference can be large, particularly if the NLO result is significantly higher than the Born approximation, e.g. in Higgs-boson production in gluon fusion. An argument against $n-$dependent K-factors is that rescaling every jet multiplicity in CKKW-L by different numbers will result in increased merging scale dependencies. In PYTHIA8, we include the possibility for having $n-$dependent K-factors

$$K_n = \frac{\int_{\rho_{\mathrm{MS}}} \overline{\mathrm{B}}_n}{\int_{\rho_{\mathrm{MS}}} \mathrm{B}_n} \,. \qquad \text{(III.B3)}$$

These will then be calculated by dividing the sums of inclusive NLO and LO cross section weights (with no extra reweighting) of events above the ρ_{MS} cut.

Below, we will give a detailed expansion of all factors in the tree-level weights, which depend on α_s, directly and indirectly through the PDF-ratios. Since we have demanded that the input cross sections be calculated with fixed μ_F and μ_R, we will only keep contributions of powers

α_s^1, and fixed scales. Incoming particles with positive (negative) momentum component p_z will be indicated by a superscript $+$ $(-)$. Final state partons will be enumerated by the superscript k. We will make use of the short-hands

$$\widehat{f}_i^{\pm}(\tfrac{x_i^{\pm}}{y},\rho) = \sum_{j\in\{q,\bar{q},g\}} \widehat{P}_{ij}^{\pm}(y) f_j^{\pm}(\tfrac{x_i^{\pm}}{y},\rho) \tag{III.B4}$$

$$\widetilde{f}_i^{\pm}(\tfrac{x_i^{\pm}}{y},\rho) = \sum_{j\in\{q,\bar{q},g\}} P_{ji}^{\pm}(y) f_j^{\pm}(\tfrac{x_i^{\pm}}{y},\rho) \tag{III.B5}$$

where P_{ji} are the unregularised Altarelli-Parisi splitting kernel for an initial state parton changing from i to j (by backward evolution), and $\widehat{P}_{ij}$ are the plus-prescription-regularised counterparts for forward evolution. For final state splittings, we will write

$$\widetilde{P}_i^k(y,\rho) = \sum_{j\in\{q,\bar{q},g\}} P_{ji}^k(y,\rho) \tag{III.B6}$$

$$P_{ji}^k(y,\rho) = \begin{cases} P_{ji}(y) & \text{If the PS step from } S_{+j} \text{ to } S_{+i} \text{ was final state radiation off leg } k\text{, with a final state recoiler.} \\ P_{ji}(y)\,\min\left\{1, \frac{\frac{x^{\pm}}{y} f_j^{\pm}(\frac{x^{\pm}}{y},\rho)}{x^{\pm} f_i^{\pm}(x^{\pm},\rho)}\right\} & \text{If the PS step from } S_{+j} \text{ to } S_{+i} \text{ was final state radiation off leg } k\text{, and involved the incoming parton } \pm \text{ as recoiler.} \end{cases} \tag{III.B7}$$

The factor $\min\{1, \frac{x^{\pm}}{y} f_j^{\pm}(\frac{x^{\pm}}{y},\rho)/x^{\pm} f_i^{\pm}(x^{\pm},\rho)\}$ is introduced on purely technical grounds, because the overestimate of final state radiation in PYTHIA8 does not include PDF factors, and violations of the overestimate need to be avoided. We split the expansion of eq. (III.B1) into subsections containing detailed expansions of each factor. At the end of each subsection, we will give a description of how the necessary terms are generated in PYTHIA8.

III.B.1 Expansion of K-factors and α_s-ratios

The weight w_n in eq. (III.B1) contains the factors

$$K\prod_{i=1}^{n}\frac{\alpha_s(b_i\rho_i)}{\alpha_s(\mu_R)}$$

Note that we have kept the parameters $b_i \in \{b_I, b_F\}$ stemming from different $\alpha_s(M_Z)-$values in parton shower and fixed-order calculation. The factors have simple α_s-expansions

$$K = 1 + \alpha_s(\mu_R)k_1 + \mathcal{O}(\alpha_s^2(\mu_R)) \quad \text{(III.B8)}$$

$$\alpha_s(b_i\rho_i) = \alpha_s(\mu_R)\left\{1 + \frac{\beta_0}{4\pi}\alpha_s(\mu_R)\ln\left(\frac{\mu_R}{b_i\rho_i}\right)\right\} + \mathcal{O}(\alpha_s^2(\mu_R)) \quad \text{(III.B9)}$$

where $\beta_0 = 11 - \frac{2}{3}n_f$. Multiplying these series, we get the expansion of the product of K-factors and α_s-ratios

$$K\prod_{i=1}^{n}\frac{\alpha_s(b\rho_i)}{\alpha_s(\mu_R)} = 1 + \alpha_s(\mu_R)k_1 + \sum_{i=1}^{n}\alpha_s(\mu_R)\frac{\beta_0}{4\pi}\ln\left(\frac{\mu_R}{b_i\rho_i}\right) + \mathcal{O}(\alpha_s^2(\mu_R)) \quad \text{(III.B10)}$$

We generate the k_1-term by using $k_1 = K - 1$. The sum is generated by stepping through the chosen PS history, and adding, for each nodal state S_{+i}, the logarithmic terms, evaluated at the reconstructed splitting scale ρ_i. This of course means that we have to construct and choose a parton shower history first.

III.B.2 Expansion of ratios of parton distributions

The expansion of the PDF ratios

$$\frac{x_n^+ f_n^+(x_n^+,\rho_n)}{x_n^+ f_n^+(x_n^+,\mu_F)}\frac{x_n^- f_n^-(x_n^-,\rho_n)}{x_n^- f_n^-(x_n^-,\mu_F)}\prod_{i=1}^{n}\frac{x_{i-1}^+ f_{i-1}^+(x_{i-1}^+,\rho_{i-1})}{x_{i-1}^+ f_{i-1}^+(x_{i-1}^+,\rho_i)}\frac{x_{i-1}^- f_{i-1}^-(x_{i-1}^-,\rho_{i-1})}{x_{i-1}^- f_{i-1}^-(x_{i-1}^-,\rho_i)} \quad \text{(III.B11)}$$

is a bit involved. To derive an expansion, we will infer the DGLAP equation

$$\rho\frac{\partial}{\partial\rho}f_i^\pm(x_i^\pm,\rho) = \frac{\alpha_s(\rho)}{2\pi}\int_{x_i^\pm}^1\frac{dy}{y}\widehat{f}_i^\pm(\tfrac{x_i}{y},\rho) \quad \text{(III.B12)}$$

$$\Longrightarrow f_i^\pm(x_i^\pm,\rho_{i-1}) - f_i^\pm(x_i^\pm,\mu) = \int_\mu^{\rho_{i-1}}\frac{d\rho}{\rho}\frac{\alpha_s(\rho)}{2\pi}\int_{x_i^\pm}^1\frac{dy}{y}\widehat{f}_i^\pm(\tfrac{x_i}{y},\rho)$$

$$\Longrightarrow f_i^\pm(x_i^\pm,\rho_{i-1}) = f_i^\pm(x_i^\pm,\rho_{i-1}-\delta\rho) + \int_{\rho_{i-1}-\delta\rho}^{\rho_{i-1}}\frac{d\rho}{\rho}\frac{\alpha_s(\rho)}{2\pi}\int_{x_i^\pm}^1\frac{dy}{y}\widehat{f}_i^\pm(\tfrac{x_i}{y},\rho)\,,$$

where we have used the notation of eq. (III.B4). So far, no approximation to DGLAP scale dependence is made. This equation has contributions from all orders in α_s, and should be regarded as an expansion in the difference of scales $\delta\rho$, rather than an expansion in α_s. Approximating

$\widehat{f}_i(\frac{x_i}{y},\rho)$ as the sum of products of PDFs and leading-order or next-to-leading order splitting kernels (indicated by superscripts (0) and (1) respectively), we find

$$\begin{aligned} f_i^{\pm}(x_i^{\pm},\rho_{i-1}) &= f_i^{\pm}(x_i^{\pm},\mu_F) \\ &\quad + \int_{\mu_F}^{\rho_{i-1}} \frac{d\rho}{\rho} \int_{x_i^{\pm}}^1 \frac{dy}{y} \left\{ \frac{\alpha_s(\rho)}{2\pi} \widehat{f}_i^{\pm,(0)}(\tfrac{x_i}{y},\rho) + \left(\frac{\alpha_s(\rho)}{2\pi}\right)^2 \widehat{f}_i^{\pm,(1)}(\tfrac{x_i}{y},\rho) \right\}. \end{aligned} \tag{III.B13}$$

Shifting the scale in α_s to μ_R, and the scale of parton distributions to μ_F, this gives

$$\begin{aligned} f_i^{\pm}(x_i^{\pm},\rho_{i-1}) &= f_i^{\pm}(x_i^{\pm},\mu_F) \\ &+ \frac{\alpha_s(\mu_R)}{2\pi} \int_{\mu_F}^{\rho_{i-1}} \frac{d\rho}{\rho} \int_{x_i^{\pm}}^1 \frac{dy}{y} \widehat{f}_i^{\pm,(0)}(\tfrac{x_i}{y},\mu_F) \\ &+ \left(\frac{\alpha_s(\mu_R)}{2\pi}\right)^2 \int_{\mu_F}^{\rho_{i-1}} \frac{d\rho}{\rho} \int_{x_i^{\pm}}^1 \frac{dy}{y} \int_{\mu_F}^{\rho} \frac{d\rho'}{\rho'} \int_{x_i^{\pm}/y}^1 \frac{dy'}{y'} \overline{\widehat{f}}_i^{\pm,(0)}(\tfrac{x_i}{yy'},\mu_F) \\ &+ \left(\frac{\alpha_s(\mu_R)}{2\pi}\right)^2 \int_{\mu_F}^{\rho_{i-1}} \frac{d\rho}{\rho} \int_{x_i^{\pm}}^1 \frac{dy}{y} \widehat{f}_i^{\pm,(1)}(\tfrac{x_i}{y},\mu_F) \\ &+ \left(\frac{\alpha_s(\mu_R)}{2\pi}\right)^2 \int_{\mu_F}^{\rho_{i-1}} \frac{d\rho}{\rho} \int_{x_i^{\pm}}^1 \frac{dy}{y} \frac{\beta_0}{2} \ln\left(\frac{\mu_R}{\rho}\right) \widehat{f}_i^{\pm,(0)}(\tfrac{x_i}{y},\mu_F) \\ &+ \mathcal{O}(\alpha_s^3(\mu_R)) \end{aligned} \tag{III.B14}$$

where $\widehat{f}_i^{\pm,(0)}$ is a convolution of parton densities and leading-order DGLAP splitting kernels (see eq. (III.B4)), and $\overline{\widehat{f}}_i^{\pm,(0)}$ a convolution of $\widehat{f}_i^{\pm,(0)}$ and splitting kernels.

The weight w_n contains ratios of parton distributions. Since some of these ratios are the result of rescaling to the lowest-order cross section (see discussion after III.2), it might well be necessary to divide next-to-leading order PDFs. Luckily, eq. (III.B14) ensures that if we are only interested in the expansion up to $\mathcal{O}\left(\alpha_s^1(\mu_R)\right)$, we can safely ignore difficulties relating to NLO splitting kernels. Using

$$\int_{\mu_F}^{\rho_{i-1}} \frac{d\rho}{\rho} = \ln\left(\frac{\rho_{i-1}}{\mu_F}\right), \tag{III.B15}$$

and restricting ourselves to $\mathcal{O}\left(\alpha_s^1(\mu_R)\right)$, we arrive at

$$f_i^{\pm}(x_i^{\pm},\rho_{i-1}) = f_i^{\pm}(x_i^{\pm},\mu_F) + \tfrac{\alpha_s(\mu_R)}{2\pi} \ln\left(\tfrac{\rho_{i-1}}{\mu_F}\right) \int_{x_i^{\pm}}^1 \frac{dy}{y} \widehat{f}_i^{(0)}(\tfrac{x_i}{y},\mu_F) + \mathcal{O}(\alpha_s^2(\mu_R)) \tag{III.B16}$$

From now on, we will drop the superscript (0). With eq. (III.B16), the expansion of a ratio of parton distributions is given by

$$\frac{x_{i-1}^{\pm} f_{i-1}^{\pm}(x_{i-1}^{\pm}, \rho_{i-1})}{x_i^{\pm} f_{i-1}^{\pm}(x_{i-1}^{\pm}, \rho_i)} = 1 + \frac{\alpha_s(\mu_R)}{2\pi} \ln\left\{\frac{\rho_{i-1}}{\rho_i}\right\} \int_{x_{i-1}^{\pm}}^{1} \frac{dy}{y} \frac{x_{i-1}^{\pm} \widehat{f}_{i-1}^{\pm}(\frac{x_{i-1}^{\pm}}{y}, \mu_F)}{x_{i-1}^{\pm} f_{i-1}^{\pm}(x_{i-1}^{\pm}, \mu_F)} + \mathcal{O}(\alpha_s^2(\mu_R)) \tag{III.B17}$$

With this, we can write the expansion of the product of PDF ratios to $\mathcal{O}\left(\alpha_s^1(\mu_R)\right)$ as

$$\begin{aligned}
&\frac{x_n^+ f_n^+(x_n^+, \rho_n)}{x_n^+ f_n^+(x_n^+, \mu_F)} \frac{x_n^- f_n^-(x_n^-, \rho_n)}{x_n^- f_n^-(x_n^-, \mu_F)} \prod_{i=1}^{n} \frac{x_{i-1}^+ f_{i-1}^+(x_{i-1}^+, \rho_{i-1})}{x_{i-1}^+ f_{i-1}^+(x_{i-1}^+, \rho_i)} \frac{x_{i-1}^- f_{i-1}^-(x_{i-1}^-, \rho_{i-1})}{x_{i-1}^- f_{i-1}^-(x_{i-1}^-, \rho_i)} \\
= \quad & 1 + \frac{\alpha_s(\mu_R)}{2\pi} \left\{ \ln\left\{\frac{\rho_n}{\mu_F}\right\} \int_{x_n^+}^{1} \frac{dy}{y} \frac{x_n^+ \widehat{f}_n^+(\frac{x_n^+}{y}, \mu_F)}{x_n^+ f_n^+(x_n^+, \mu_F)} \right. \\
& + \ln\left\{\frac{\rho_n}{\mu_F}\right\} \int_{x_n^-}^{1} \frac{dy}{y} \frac{x_n^- \widehat{f}_n^-(\frac{x_n^-}{y}, \mu_F)}{x_n^- f_n^-(x_n^-, \mu_F)} \\
& + \sum_{i=1}^{n} \ln\left\{\frac{\rho_{i-1}}{\rho_i}\right\} \int_{x_{i-1}^+}^{1} \frac{dy}{y} \frac{x_{i-1}^+ \widehat{f}_{i-1}^+(\frac{x_{i-1}^+}{y}, \mu_F)}{x_{i-1}^+ f_{i-1}^+(x_{i-1}^+, \mu_F)} \\
& + \sum_{i=1}^{n} \ln\left\{\frac{\rho_{i-1}}{\rho_i}\right\} \int_{x_{i-1}^-}^{1} \frac{dy}{y} \frac{x_{i-1}^- \widehat{f}_{i-1}^-(\frac{x_{i-1}^-}{y}, \mu_F)}{x_{i-1}^- f_{i-1}^-(x_{i-1}^-, \mu_F)} \\
& \left. + \mathcal{O}(\alpha_s^2(\mu_R)) \right\}
\end{aligned} \tag{III.B18}$$

These integrals can be calculated by explicit numerical integration. Remember that $\widehat{f}$ has been defined with regularised splitting kernels [49]

$$\widehat{P}_{qq}(z) = C_F \frac{1+z^2}{(1-z)_+} + \frac{3}{2} C_F \delta(1-z) = \widehat{P}_{\bar{q}\bar{q}}(z) \tag{III.B19}$$

$$\widehat{P}_{gq}(z) = C_F \frac{1+(1-z)^2}{z} = \widehat{P}_{qq}(1-z) = \widehat{P}_{g\bar{q}}(z) \tag{III.B20}$$

$$\widehat{P}_{gg}(z) = 2C_A \left[\frac{z}{(1-z)_+} + \frac{1-z}{z} + z(1-z)\right] + \frac{1}{6}\left[11C_A - 4n_f T_R\right] \delta(1-z) \tag{III.B21}$$

$$\widehat{P}_{qg}(z) = T_R \left[z^2 + (1-z)^2\right]. \tag{III.B22}$$

By using these functions explicitly, and inserting

$$\int_0^{x_{i-1}} \frac{dy}{1-y} = -\ln(1-x_{i-1})\,, \tag{III.B23}$$

we find that in the case that $i-1$ is a quark or antiquark, the integral in eq. (III.B17) becomes

$$\begin{aligned}
&\frac{\alpha_s(\mu_R)}{2\pi}\ln\left\{\frac{\rho_{i-1}}{\rho_i}\right\}\int\limits_{x_{i-1}^{\pm}}^{1}\frac{dy}{y}\frac{x_{i-1}^{\pm}\widehat{f}_{i-1}^{\pm}(\frac{x_{i-1}^{\pm}}{y},\mu_F)}{x_{i-1}^{\pm}f_{i-1}^{\pm}(x_{i-1}^{\pm},\mu_F)}\\
&\quad=\frac{\alpha_s(\mu_R)}{2\pi}\ln\left(\frac{\rho_{i-1}}{\rho_i}\right)\left\{\int\limits_{x_{i-1}}^{1}\frac{dy}{1-y}\left[C_F(1+y^2)\frac{\frac{x_{i-1}}{y}f_q\left(\frac{x_{i-1}}{y},\rho_i\right)}{x_{i-1}f_q(x_{i-1},\rho_i)}-2C_F\right]\right.\\
&\qquad+\int\limits_{x_{i-1}}^{1}dy\left[T_R(y^2+(1-y)^2)\frac{\frac{x_{i-1}}{y}f_g\left(\frac{x_{i-1}}{y},\rho_i\right)}{x_{i-1}f_q(x_{i-1},\rho_i)}\right]\\
&\qquad\left.+2C_F\ln(1-x_{i-1})+\frac{3}{2}C_F\right\}\,.
\end{aligned} \tag{III.B24}$$

To arrive at this form, we have used that the sum over all possible flavours in $\widehat{f}_{i-1}$ reduces to two terms, since the antiquark (quark) can only be produced by the evolution of a gluon or an antiquark (quark). If the flavour index $i-1$ indicates a gluon, the integral reads

$$\begin{aligned}
&\frac{\alpha_s(\mu_R)}{2\pi}\ln\left\{\frac{\rho_{i-1}}{\rho_i}\right\}\int\limits_{x_{i-1}^{\pm}}^{1}\frac{dy}{y}\frac{x_{i-1}^{\pm}\widehat{f}_{i-1}^{\pm}(\frac{x_{i-1}^{\pm}}{y},\mu_F)}{x_{i-1}^{\pm}f_{i-1}^{\pm}(x_{i-1}^{\pm},\mu_F)}\\
&\quad=\frac{\alpha_s(\mu_R)}{2\pi}\ln\left(\frac{\rho_{i-1}}{\rho_i}\right)\left\{\int\limits_{x_{i-1}}^{1}\frac{dy}{1-y}\left[2C_A\,y\,\frac{\frac{x_{i-1}}{y}f_g\left(\frac{x_{i-1}}{y},\rho_i\right)}{x_{i-1}f_g(x_{i-1},\rho_i)}-2C_A\right]\right.\\
&\qquad+\int\limits_{x_{i-1}}^{1}dy\,2C_A\left[\frac{1-y}{y}+y(1-y)\right]\left[\frac{\frac{x_{i-1}}{y}f_g\left(\frac{x_{i-1}}{y},\rho_i\right)}{x_{i-1}f_g(x_{i-1},\rho_i)}\right]\\
&\qquad+\int\limits_{x_{i-1}}^{1}dy\,C_F\left[\frac{1+(1-y)^2}{y}\right]\left[\frac{\frac{x_{i-1}}{y}f_q\left(\frac{x_{i-1}}{y},\rho_i\right)}{x_{i-1}f_g(x_{i-1},\rho_i)}+\frac{\frac{x_{i-1}}{y}f_{\bar{q}}\left(\frac{x_{i-1}}{y},\rho_i\right)}{x_{i-1}f_g(x_{i-1},\rho_i)}\right]\\
&\qquad\left.+2C_A\ln(1-x_{i-1})+\frac{1}{6}\left[11C_A-4n_fT_R\right]\right\}
\end{aligned} \tag{III.B25}$$

The sum over all flavours is reduces to three terms – the evolution of a gluon, a quark and an antiquark. Since all remaining integrands in eqs. III.B24 and III.B25 involve PDFs, we need to perform the integrals numerically. This numerical integration will be performed by Monte-Carlo integration, although we have also implemented the Gaussian adaptive quadrature method for this task. We checked that compared to performing a many-point numerical integration, it is sufficient to only pick a single integration point for the Monte-Carlo integral evaluation, already when averaging over a small number of events ($\mathcal{O}(50)$). Thus, we choose the less time-consuming Monte-Carlo method as default. For this, we roll a uniformly distributed random number $r \in [0,1]$, and pick the integration variable as

$$y_{mc} = \begin{cases} x^r & \text{if } i-1 \text{ is a gluon} \\ x + r\cdot(1-x) & \text{otherwise} \end{cases} \tag{III.B26}$$

The full weight in eq. (III.B18) is generated by stepping through the chosen PS history, and adding, for each reconstructed state S_{+i-1} ($i-1 < n$), the $x_{i-1}-$bounded integral for both incoming partons, multiplied by the logarithm of the reconstructed scales ρ_{i-1} and ρ_i. The values x_{i-1}, ρ_{i-1} and ρ_i are easily accessible since the parton shower history contains a complete sequence of fully reconstructed states $S_{+0},\dots,S_{+n}$. For the ME state S_{+n}, we add the x_n-bounded integral, multiplied by the logarithm of ρ_n and μ_F, for both incoming partons.

III.B.3 Expansion of no-emission probabilities

The factors $\Pi_{S_{+i-1}}(x_{i-1},\rho_{i-1},\rho_i)$ in eq. (III.B1) symbolise the probability of a state S_{+i-1} to evolve from scale ρ_{i-1} to ρ_i without resolving emissions. This means that $\Pi_{S_{+i-1}}(x_{i-1},\rho_{i-1},\rho_i)$ is a product of no-emission probabilities for each dipole in the state:

$$\begin{aligned}\Pi_{S_{+i-1}}(x_{i-1},\rho_{i-1},\rho_i) =& \Pi^+_{S_{+i-1}}(x^+_{i-1},\rho_{i-1},\rho_i)\,\Pi^-_{S_{+i-1}}(x^-_{i-1},\rho_{i-1},\rho_i) \\ & \prod_{k\in\{\text{final partons}\}} \Pi^k_{S_{+i-1}}(x^\pm_{i-1},\rho_{i-1},\rho_i)\end{aligned} \tag{III.B27}$$

Using the notation of eq. (III.B5) and eqs. (III.B6), we can write

$$\Pi^\pm_{S_{+i-1}}(x^\pm_{i-1},\rho_{i-1},\rho_i) = \exp\left\{-\int_{\rho_i}^{\rho_{i-1}}\frac{d\rho}{\rho}\int_{\Omega_I}\frac{dy}{y}\frac{\alpha_s(b_I\rho)}{2\pi}\frac{x^\pm_{i-1}\widetilde{f}^\pm_{i-1}(\frac{x^\pm_{i-1}}{y},\rho)}{x^\pm_{i-1}f^\pm_{i-1}(x^\pm_{i-1},\rho)}\right\} \tag{III.B28}$$

and

$$\Pi^k_{S_{+i-1}}(x^\pm_{i-1},\rho_{i-1},\rho_i) = \exp\left\{-\int_{\rho_i}^{\rho_{i-1}}\frac{d\rho}{\rho}\int_{\Omega_F}\frac{dy}{y}\frac{\alpha_s(b_F\rho)}{2\pi}\widetilde{P}^k_{i-1}(y,\rho)\right\}. \tag{III.B29}$$

From eq. (III.B29), we find

$$\Pi^k_{S_{+i-1}}(x^\pm_{i-1},\rho_{i-1},\rho_i) = 1-\int_{\rho_i}^{\rho_{i-1}}\frac{d\rho}{\rho}\int_{\Omega_F}\frac{dy}{y}\frac{\alpha_s(b_F\rho)}{2\pi}\widetilde{P}^k_{i-1}(y,\rho)+\mathcal{O}\left(\alpha_s^2(\rho)\right). \tag{III.B30}$$

All NLO contributions included in NLO merging schemes are generated with fixed scales μ_R and μ_F. For a NLO-accurate description, we need to remove the approximate shower contributions for exactly these scales. Otherwise, e.g. if we choose to remove the second term on the right-hand side of eq. (III.B30), we will remove $\mathcal{O}\left(\alpha_s^2(\mu_R)\right)$ terms as well, thus degrading the description of higher orders. To remove only precisely those parton shower terms that have corresponding contributions in the NLO calculation, we extract an $\mathcal{O}(\alpha_s(\mu_R))$ −expansion from eq. (III.B30):

$$\Pi^k_{S_{+i-1}}(x^\pm_{i-1},\rho_{i-1},\rho_i) = 1-\frac{\alpha_s(\mu_R)}{2\pi}\int_{\rho_i}^{\rho_{i-1}}\frac{d\rho}{\rho}\int_{\Omega_F}\frac{dy}{y}\widetilde{P}^k_{i-1}(y,\mu_F)+\mathcal{O}\left(\alpha_s^2(\mu_R)\right), \tag{III.B31}$$

where we have used that the difference between $\alpha_s(b_F\mu_R)$ and $\alpha_s(\mu_R)$ is of $\mathcal{O}\left(\alpha_s^2(\mu_R)\right)$. The PDFs in appearing in $\widetilde{P}^k_{i-1}(y)$, for final state radiation with an initial state recoiler, should be evaluated at μ_F. Expanding the exponential in eq. (III.B28), we find

$$\Pi^\pm_{S_{+i-1}}(x^\pm_{i-1},\rho_{i-1},\rho_i) = 1-\int_{\rho_i}^{\rho_{i-1}}\frac{d\rho}{\rho}\int_{\Omega_I}\frac{dy}{y}\frac{\alpha_s(b_I\rho)}{2\pi}\frac{x^\pm_{i-1}\widetilde{f}^\pm_{i-1}(\frac{x^\pm_{i-1}}{y},\rho)}{x^\pm_{i-1}f^\pm_{i-1}(x^\pm_{i-1},\rho)}+\mathcal{O}\left(\alpha_s^2(\rho)\right), \tag{III.B32}$$

which can be expanded further to give

$$\Pi^\pm_{S_{+i-1}}(x^\pm_{i-1},\rho_{i-1},\rho_i) = 1-\frac{\alpha_s(\mu_R)}{2\pi}\int_{\rho_i}^{\rho_{i-1}}\frac{d\rho}{\rho}\int_{\Omega_I}\frac{dy}{y}\frac{x^\pm_{i-1}\widetilde{f}^\pm_{i-1}(\frac{x^\pm_{i-1}}{y},\mu_F)}{x^\pm_{i-1}f^\pm_{i-1}(x^\pm_{i-1},\mu_F)}+\mathcal{O}\left(\alpha_s^2(\mu_R)\right). \tag{III.B33}$$

Here, we have used the result eq. (III.B16), i.e. that if we are interested in the $\mathcal{O}\left(\alpha_s^1(\mu_R)\right)$ parts in eq. (III.B33), we can safely evaluate the ratio of parton distributions at μ_F, rather than ρ.

When expanding the CKKW-L weight w_n, we also need to discuss the "last" no-emission probability

$$\Pi_{S_{+n}}(x_n,\rho_n,\rho_{\text{MS}}) = \Pi^+_{S_{+n}}(x_n^+,\rho_n,\rho_{\text{MS}})\,\Pi^-_{S_{+n}}(x_n^-,\rho_n,\rho_{\text{MS}}) \prod_{k\in\{\text{final partons}\}} \Pi^k_{S_{+n}}(x_n^\pm,\rho_n,\rho_{\text{MS}}) \tag{III.B34}$$

with

$$\Pi^\pm_{S_{+n}}(x_n^\pm,\rho_n,\rho_{\text{MS}}) = \exp\left\{-\int_{\rho_{n+1}}^{\rho_n}\frac{d\rho}{\rho}\int_{\Omega_I}\frac{dy}{y}\frac{\alpha_s(b_I\rho)}{2\pi}\frac{x_n^\pm \widetilde{f}_n^\pm(\frac{x_n^\pm}{y},\rho)}{x_n^\pm f_n^\pm(x_n^\pm,\rho)}\Theta\left(t(S_{+n+1},\rho)-\rho_{\text{MS}}\right)\right\} \tag{III.B35}$$

and

$$\Pi^k_{S_{+n}}(x_n^\pm,\rho_n,\rho_{\text{MS}}) = \exp\left\{-\int_{\rho_{n+1}}^{\rho_n}\frac{d\rho}{\rho}\int_{\Omega_F}\frac{dy}{y}\frac{\alpha_s(b_F\rho)}{2\pi}\widetilde{P}_n^k(y,\rho)\Theta\left(t(S_{+n+1},\rho)-\rho_{\text{MS}}\right)\right\} \tag{III.B36}$$

The expansion of these terms carries an additional Θ function

$$\Pi^\pm_{S_{+n}}(x_n^\pm,\rho_n,\rho_{\text{MS}}) = 1 - \frac{\alpha_s(\mu_R)}{2\pi}\int_{\rho_{n+1}}^{\rho_n}\frac{d\rho}{\rho}\int_{\Omega_I}\frac{dy}{y}\frac{x_n^\pm \widetilde{f}_n^\pm(\frac{x_n^\pm}{y},\mu_F)}{x_n^\pm f_n^\pm(x_n^\pm,\mu_F)}\Theta\left(t(S_{+n+1},\rho)-\rho_{\text{MS}}\right) + \dots \tag{III.B37}$$

and

$$\Pi^k_{S_{+n}}(x_n^\pm,\rho_n,\rho_{\text{MS}}) = 1 - \frac{\alpha_s(\mu_R)}{2\pi}\int_{\rho_{n+1}}^{\rho_n}\frac{d\rho}{\rho}\int_{\Omega_F}\frac{dy}{y}\widetilde{P}_n^k(y,\mu_F)\Theta\left(t(S_{+n+1},\rho)-\rho_{\text{MS}}\right) + \dots \tag{III.B38}$$

The definition of t is given in appendix III.A.1. Collecting all terms, we find that the expansion of the product of no-emission probabilities in

the CKKW-L weight w_n is given by

$$
\begin{aligned}
&\Pi_{S_{+n}}(x_n,\rho_n,\rho_{\text{MS}})\prod_{i=1}^{n}\Pi_{S_{+i-1}}(x_{i-1},\rho_{i-1},\rho_i) \qquad \text{(III.B39)}\\
=&1-\sum_{i=1}^{n}\Bigg\{\sum_{\pm}\frac{\alpha_{\text{s}}(\mu_R)}{2\pi}\int_{\rho_i}^{\rho_{i-1}}\frac{d\rho}{\rho}\int_{\Omega_I}\frac{dy}{y}\frac{x_{i-1}^{\pm}\widetilde{f}_{i-1}^{\pm}(\frac{x_{i-1}^{\pm}}{y},\mu_F)}{x_{i-1}^{\pm}f_{i-1}^{\pm}(x_{i-1}^{\pm},\mu_F)}\\
&\qquad+\quad\sum_{k}\frac{\alpha_{\text{s}}(\mu_R)}{2\pi}\int_{\rho_i}^{\rho_{i-1}}\frac{d\rho}{\rho}\int_{\Omega_F}\frac{dy}{y}\widetilde{P}_{i-1}^{k}(y,\mu_F)\Bigg\}\\
&-\sum_{\pm}\frac{\alpha_{\text{s}}(\mu_R)}{2\pi}\int_{\rho_{n+1}}^{\rho_n}\frac{d\rho}{\rho}\int_{\Omega_I}\frac{dy}{y}\frac{x_n^{\pm}\widetilde{f}_n^{\pm}(\frac{x_n^{\pm}}{y},\mu_F)}{x_n^{\pm}f_n^{\pm}(x_n^{\pm},\mu_F)}\Theta\left(t(S_{+n+1},\rho)-\rho_{\text{MS}}\right)\\
&-\sum_{k}\frac{\alpha_{\text{s}}(\mu_R)}{2\pi}\int_{\rho_{n+1}}^{\rho_n}\frac{d\rho}{\rho}\int_{\Omega_F}\frac{dy}{y}\widetilde{P}_n^{k}(y,\mu_F)\Theta\left(t(S_{+n+1},\rho)-\rho_{\text{MS}}\right)\;+\;\mathcal{O}\left(\alpha_{\text{s}}^2\left(\mu_R\right)\right).
\end{aligned}
$$

Although this looks fairly complicated, it is in fact easily generated. It is useful to remember that if the probability for n incidents (e.g. nuclear decays) is given by

$$P_n=\frac{1}{n!}x^n e^{-x}\,, \qquad \text{(III.B40)}$$

then the average number of incidents is

$$\langle n\rangle=\sum_{n=0}^{\infty}nP_n=\sum_{n=1}^{\infty}nP_n=e^{-x}\sum_{n=1}^{\infty}\frac{1}{(n-1)!}x^n=xe^{-x}\sum_{n=1}^{\infty}\frac{1}{(n-1)!}x^{n-1}=x\,. \qquad \text{(III.B41)}$$

The probability P_n has the same form as the probability for n emissions in a parton shower, and the $\mathcal{O}\left(\alpha_{\text{s}}^1\left(\mu_R\right)\right)$ −terms in eq. (III.B39) can be identified with the exponents x. That means we can calculate the $\mathcal{O}\left(\alpha_{\text{s}}^1\left(\mu_R\right)\right)$ −terms by generating, with fixed μ_R and μ_F, an average number of emissions. In final state radiation off final parton k for

example had been generated with fixed scales, we can write

$$\begin{aligned}
&\langle n_{\text{FSR emissions between } \rho_{i-1} \text{ and } \rho_i} \rangle \\
&= \sum_{n=0}^{\infty} n \frac{1}{n!} \left(\int_{\rho_i}^{\rho_{i-1}} \frac{d\rho}{\rho} \int_{\Omega_F} \frac{dy}{y} \widetilde{P}^k_{i-1}(y, \mu_F) \right)^n \exp\left\{ -\int_{\rho_i}^{\rho_{i-1}} \frac{d\rho}{\rho} \int_{\Omega_F} \frac{dy}{y} \widetilde{P}^k_{i-1}(y, \mu_F) \right\} \\
&= \int_{\rho_i}^{\rho_{i-1}} \frac{d\rho}{\rho} \int_{\Omega_F} \frac{dy}{y} \widetilde{P}^k_{i-1}(y, \mu_F)
\end{aligned} \tag{III.B42}$$

The average number of emissions is additive. This means that instead of averaging over emissions from each leg separately, we can directly average *all* emissions: We can simply start the shower off state S_{+i-1} at ρ_{i-1}, count any emission above ρ_i, restart the shower (off S_{+i-1} from ρ_{i-1}) N times, and average. This will give the sum of all contributions to one i in eq. (III.B39) [15].

For the $\mathcal{O}\left(\alpha_s^1(\mu_R)\right)$ −terms of the expansion of the last no-emission probability (i.e. the last two lines of eq. (III.B39)), the Θ function is included by only increasing the number of counted emissions for a trial emissions is above the merging scale.

In our implementation, we will generate all trial emissions with running scales, and count relevant trial emissions with the weight

$$g_e = \frac{\alpha_s(\mu_R)}{\alpha_s(\rho_e)} g_{\text{pdf},e} \tag{III.B43}$$

$$g_{\text{pdf},e} = \begin{cases} \dfrac{x_{i-1} f_{i-1}(x_{i-1}, \rho_e)}{x_{i-1} f_{i-1}(x_{i-1}, \mu_F)} \dfrac{x_{i-1} \widehat{f}_e\left(\frac{x_{i-1}}{y_e}, \mu_F\right)}{x_{i-1} \widehat{f}_e\left(\frac{x_{i-1}}{y_e}, \rho_e\right)} & \text{if the trial emission was produced in ISR,} \\ 1 & \text{if the trial emission was produced in FSR,} \\ & \text{with final state recoiler,} \\ \dfrac{x_{i-1} f_{i-1}(x_{i-1}, \rho_e)}{x_{i-1} f_{i-1}(x_{i-1}, \mu_F)} \dfrac{x_{i-1} \widehat{f}_e\left(\frac{x_{i-1}}{y_e}, \mu_F\right)}{x_{i-1} \widehat{f}_e\left(\frac{x_{i-1}}{y_e}, \rho_e\right)} & \text{if the trial emission was produced in FSR,} \\ & \text{with initial state recoiler,} \end{cases} \tag{III.B44}$$

where ρ_e is the evolution scale of the trial emission, y_e the energy splitting, and e the flavour of the initial line after the trial emission. This

[15] Even if we had an analytic way of generating the integrals, implementing the average number of emissions is superior, since using trial emissions will capture correlations between potentially radiating dipoles, and automatically include phase space constraints.

weight will give trial emissions generated with fixed scales, as can e.g. be verified for initial state splittings by using

$$\int_{\rho_i}^{\rho_{i-1}} \frac{d\rho}{\rho} \int_{\Omega_I} \frac{dy}{y} \frac{\alpha_s(\rho)}{2\pi} \frac{x_{i-1}^{\pm} \widetilde{f}_{i-1}^{\pm}\left(\frac{x_{i-1}^{\pm}}{y}, \rho\right)}{x_{i-1}^{\pm} f_{i-1}^{\pm}(x_{i-1}^{\pm}, \rho)} = V \frac{1}{N} \sum_{l}^{N} \frac{\alpha_s(\rho_l)}{2\pi} \frac{x_{i-1}^{\pm} \widetilde{f}_{l}^{\pm}\left(\frac{x_{i-1}^{\pm}}{y_l}, \rho_l\right)}{x_{i-1}^{\pm} f_{i-1}^{\pm}(x_{i-1}^{\pm}, \rho_l)} \tag{III.B45}$$

$$= V \frac{1}{N} \sum_{l}^{N} \frac{\alpha_s(\mu_R)}{2\pi} \frac{x_{i-1}^{\pm} \widetilde{f}_{l}^{\pm}\left(\frac{x_{i-1}^{\pm}}{y_l}, \mu_F\right)}{x_{i-1}^{\pm} f_{i-1}^{\pm}(x_{i-1}^{\pm}, \mu_F)} \times g_l^{-1} \qquad \left(\text{where } V = \int_{\rho_i}^{\rho_{i-1}} \frac{d\rho}{\rho} \int_{\Omega_I} \frac{dy}{y}\right).$$

Weighting every trial emission with g_l will exactly cancel the g_l^{-1} factor in the sum, thus producing the desired fixed-scale terms.

In conclusion, the algorithm to generate all $\mathcal{O}\left(\alpha_s^1(\mu_R)\right)$ −terms in one multiplicity i is

1. Start a trial shower off state S_{+i-1} at scale ρ_{i-1}.
2. If the trial shower yields an emission, and
   a) $i-1 < n$, count the emissions with weight g_e if $\rho_e > \rho_i$
   b) $i-1 = n$, count the emissions with weight g_e if $t(S_e, \rho_e) > \rho_{\text{MS}}$.
3. If the trial emission has been counted, restart the trial shower off state S_{+i-1}, with a starting scale ρ_e. Repeat steps 2 and 3.
   If $\rho_e < \rho_i$, or $\rho_e < \rho_{\text{MS}}$, or no trial emission has been constructed, set the number of emissions to the sum of weights, and exit.

The average is generated by restarting this algorithm N times, and dividing the sum of the N results by N. To generate the sum of all $\mathcal{O}\left(\alpha_s^1(\mu_R)\right)$ −terms in eq. (III.B39), we step through the reconstructed PS history, and subtract, for each reconstructed state S_{+i-1} $(i-1 < n)$, the average number of emissions between ρ_{i-1} and ρ_i, as generated by the above algorithm.

III.B.4 Summary of weight generation

This section is intended to collect the results of appendices III.B.1, III.B.2 and III.B.3, and to summarise how the necessary weights are generated. In NL^3 and UNLOPS, tree-level samples $\mathbb{T}'_m$ ($\mathbb{B}_m$) are, respectively, defined as

$$\mathbb{T}'_m = \mathrm{B}_m \left\{ w_m - [w_m]_0 - [w_m]_1 \right\}, \qquad \mathbb{B}_m = \mathrm{B}_m \left\{ w'_m - [w'_m]_0 - [w'_m]_1 \right\}$$

The weights w_n and w'_n differ in that w'_n does not contain the "last" no-emission probability ($\Pi_{S_{+n}}$) present in w_n. Once all approximate $\mathcal{O}\left(\alpha_s^0(\mu_R)\right)$ and $\mathcal{O}\left(\alpha_s^1(\mu_R)\right)$ terms in the weight of tree-level samples are removed, we can add NLO events, and still retain NLO accuracy. Collecting all $\mathcal{O}\left(\alpha_s^0(\mu_R)\right)$ and $\mathcal{O}\left(\alpha_s^1(\mu_R)\right)$ terms of appendices III.B.1, III.B.2 and III.B.3, we find

$$
\begin{aligned}
\left[w_m\right]_0 + \left[w_m\right]_1 \quad = \quad & 1 + \alpha_s(\mu_R) k_1 + \sum_{i=1}^{n} \alpha_s(\mu_R) \frac{\beta_0}{4\pi} \ln\left(\frac{\mu_R}{b_i \rho_i}\right) \\
& + \frac{\alpha_s(\mu_R)}{2\pi} \sum_{i=1}^{n} \Bigg\{ \sum_{\pm} \Bigg[\ln\left\{\frac{\rho_{i-1}}{\rho_i}\right\} \int_{x_{i-1}^{\pm}}^{1} \frac{dy}{y} \frac{x_{i-1}^{\pm} \widehat{f}_{i-1}^{\pm}(\frac{x_{i-1}^{\pm}}{y}, \mu_F)}{x_{i-1}^{\pm} f_{i-1}^{\pm}(x_{i-1}^{\pm}, \mu_F)} \\
& \qquad - \int_{\rho_i}^{\rho_{i-1}} \frac{d\rho}{\rho} \int_{\Omega_I} \frac{dy}{y} \frac{x_{i-1}^{\pm} \widetilde{f}_{i-1}^{\pm}(\frac{x_{i-1}^{\pm}}{y}, \mu_F)}{x_{i-1}^{\pm} f_{i-1}^{\pm}(x_{i-1}^{\pm}, \mu_F)} \Bigg] \\
& \qquad - \sum_k \int_{\rho_i}^{\rho_{i-1}} \frac{d\rho}{\rho} \int_{\Omega_F} \frac{dy}{y} \widetilde{P}_{i-1}^k(y, \mu_F) \Bigg\} \\
& + \frac{\alpha_s(\mu_R)}{2\pi} \sum_{\pm} \Bigg[\ln\left\{\frac{\rho_n}{\mu_F}\right\} \int_{x_n^{\pm}}^{1} \frac{dy}{y} \frac{x_n^{\pm} \widehat{f}_n^{\pm}(\frac{x_n^{\pm}}{y}, \mu_F)}{x_n^{\pm} f_n^{\pm}(x_n^{\pm}, \mu_F)} \\
& \qquad - \int_{\rho_{n+1}}^{\rho_n} \frac{d\rho}{\rho} \int_{\Omega_I} \frac{dy}{y} \frac{x_n^{\pm} \widetilde{f}_n^{\pm}(\frac{x_n^{\pm}}{y}, \mu_F)}{x_n^{\pm} f_n^{\pm}(x_n^{\pm}, \mu_F)} \Theta\left(t(S_{+n+1}, \rho) - \rho_{\text{MS}}\right) \Bigg] \\
& - \frac{\alpha_s(\mu_R)}{2\pi} \sum_k \int_{\rho_{n+1}}^{\rho_n} \frac{d\rho}{\rho} \int_{\Omega_F} \frac{dy}{y} \widetilde{P}_n^k(y, \mu_F) \Theta\left(t(S_{+n+1}, \rho) - \rho_{\text{MS}}\right) . \qquad \text{(III.B46)}
\end{aligned}
$$

The first terms in the expansion of the UNLOPS weight $\left(\left[w'_m\right]_0 + \left[w'_m\right]_1\right)$ do not contain terms proportional to Θ, but are otherwise identical. The complete expression can be generated by using the reconstructed parton shower history of the matrix element input event S_{+n}. Each step in the parton shower history corresponds to a fully reconstructed state S_{+i}, and an associated production scale ρ_i. Thus, we have enough information at step i to generate all $\mathcal{O}\left(\alpha_s^1(\mu_R)\right)$ −terms depending on the index i in III.B46. Without specifying details, the method to generate the right-hand side of III.B46 is

1. Construct all PS histories for S_{+n}, select one history. Set $v = 1 + \alpha_s(\mu_R)k_1$, and start stepping through the history at the lowest-multiplicity state S_{+0}. Steps will be counted as $i-1$, starting from $i = 1$.
2. For each step $i-1$,
   a) If $i-1 < n$, increase v by the term due to the expansion of α_s-ratios, calculated with scale ρ_i.
   b) Increase v by the term due to the expansion of PDF-ratios containing the index $i-1$. This means adding, at each step $i-1$, two numerically integrated terms.
   c) Decrease v by the term due to the expansion of no-emission probabilities containing the index $i-1$. This means subtracting, at each step $i-1$, the average number of emissions between the scales ρ_{i-1} and ρ_i. In UNLOPS, only subtract until step $i-1 = n-1$.
4. To arrive at $\mathbb{T}'_n$ ($\mathbb{B}_n$) samples, subtract v from the weight w_n (w'_n). Use the weight

$$w_n - v \qquad \left(\text{ or } \; w'_n - v\right)$$

   to fill histograms.

In UNLOPS, there is an additional complication in that the contributions

$$\left[\int_s \widehat{\mathrm{B}}_{n\to n-1}\right]_{-n,n+1} = \int \mathrm{B}_{n\to n-1}\left\{w'_n - \left[w'_n\right]_0 - \left[w'_n\right]_1\right\}$$
$$\left[\int_s \widehat{\mathrm{B}}_{n\to n-1}\right]_{-n} = \int \mathrm{B}_{n\to n-1}\left\{w'_n - \left[w'_n\right]_0\right\} = \int \mathrm{B}_{n\to n-1}\left\{w'_n - 1\right\}$$

have to be generated. For this, we generate the weights w'_n and the necessary subtractions, and afterwards integrate over the phase space of the n'th jet, as outlined in the generation of class C in section III.3.2. Having the weights w_n, w'_n, and the first terms in their expansions ($[w_n]_0, [w_n]_1, [w'_n]_0, [w'_n]_1$), at our disposal, we can produce NL^3 or UNLOPS predictions for merging multiple NLO calculations by following the steps in III.3.1 and III.3.2.

III.C Derivation of NL^3

The aim of this section is to give a motivated derivation of the NL^3 method. Since this derivation will explicitly require NLO-correctness as condition, the following can also be seen as a proof of the validity of the scheme. We will use the notation of sections III.3 and III.A.3.

To include the parton shower resummation in a CKKW-L style, corrective weights will have to be applied to events. When deriving a NLO merging method, the aim must be that the scheme

(a) Is correct to next-to-leading order for all exclusive $n-$jet observables;

(b) Keeps the parton shower (i.e. CKKW-L) approximation for all higher orders.

(c) Shows small dependence on the separation between matrix element and parton shower region, especially in the inclusive cross section.

To handle both inclusive and exclusive NLO cross sections at the same time, let us introduce the symbols

$$\mathrm{L}_n = \begin{cases} \overline{\mathrm{B}}_n & \text{if inclusive NLO cross sections are used,} \\ \widetilde{\mathrm{B}}_n & \text{if exclusive NLO cross sections are used.} \end{cases} \tag{III.C1}$$

$$\mathrm{S}_n = \begin{cases} -\int_s \mathrm{B}_{n+1\to n} & \text{if inclusive NLO cross sections are used,} \\ 0 & \text{if exclusive NLO cross sections are used,} \end{cases} \tag{III.C2}$$

where B_n are the tree-level cross sections. If all the corresponding event samples are multiplied with corrective weights, conditions (a) and (b) read

$$\mathrm{B}_n w_B \;+\; \mathrm{L}_n w_L \;-\; \mathrm{S}_n w_S \tag{III.C3}$$

$$= \mathrm{B}_n + \mathrm{V}_n + \mathrm{I}_{n+1|n} + \int^{\rho_{\mathrm{MS}}} d\Phi_{\mathrm{rad}} \left(\mathrm{B}_{n+1|n} - \mathrm{D}_{n+1|n}\right) \;+\; \mathrm{B}_n \sum_{i=2}^{\infty} \left[w_n\right]_i \tag{III.C4}$$

and

$$\mathrm{B}_{n+1} w_n = \mathrm{B}_{n+1} \sum_{i=0}^{\infty} \left[w_n\right]_i . \tag{III.C5}$$

The last equation is trivially fulfilled if we choose to reweight higher-multiplicity tree-level matrix elements as in CKKW-L. If we do not have control over the NLO calculation, we cannot assume that tree-level, virtual and real emission samples are evaluated at identical n-jet phase

space points. Thus, without having the actual functional form of the matrix element weights, the merging conditions for B_n, L_n and S_n have to decouple, since we cannot allow w_B, w_L and w_S to be functions of the matrix elements[16]. To accommodate the merging constraint eq. (III.C3), we make an ansatz

$$\begin{aligned} w_B &= a_{B,0} + \sum_{i=1}^{\infty} b_{B,i}\alpha_s^i + \sum_{i=1}^{\infty} c_{B,i}\left(\frac{1}{\alpha_s}\right)^i \qquad \text{(III.C6)} \\ w_L &= a_{L,0} + \sum_{i=1}^{\infty} b_{L,i}\alpha_s^i + \sum_{i=1}^{\infty} c_{L,i}\left(\frac{1}{\alpha_s}\right)^i \\ w_S &= a_{S,0} + \sum_{i=1}^{\infty} b_{S,i}\alpha_s^i + \sum_{i=1}^{\infty} c_{S,i}\left(\frac{1}{\alpha_s}\right)^i \end{aligned}$$

We choose this form to allow for complete generality. Negative powers of α_s are included to allow for a simple visualisation of weights stemming e.g. from division by an all-order expression, if such factors should be desirable.

If we insert eq. (III.C6) into eq. (III.C3), remember that B_n is of $\mathcal{O}(\alpha_s^n)$, that L_n contains a Born term of $\mathcal{O}(\alpha_s^n)$ and corrections of $\mathcal{O}(\alpha_s^{n+1})$, and that S_n is of $\mathcal{O}(\alpha_s^{n+1})$, we can read off constraints on the coefficients order by order. This leads to weights of the form[17]

$$w_B = w_n - [w_n]_0 - [w_n]_1 + \sum_{i=1}^{\infty} c_{B,i}\left(\frac{1}{\alpha_s}\right)^i \qquad \text{(III.C7)}$$

$$w_L = 1 + \sum_{i=2}^{\infty} c_{L,i}\left(\frac{1}{\alpha_s}\right)^i \qquad \text{(III.C8)}$$

$$w_S = 1 + \sum_{i=2}^{\infty} c_{S,i}\left(\frac{1}{\alpha_s}\right)^i \qquad \text{(III.C9)}$$

So far, we have allowed the coefficients c to be non-vanishing. If we naively do so, we allow changes of $\mathcal{O}(\alpha_s^{n-i})$ to the $n-$jet cross section. Since the exact result (in $\mathcal{O}(\alpha_s^n)$ and $\mathcal{O}(\alpha_s^{n+1})$) should not be changed by numerically large terms, we are bound to enforce the conditions

$$c_{B,1} = 0 \qquad \text{(III.C10)}$$

$$c_{B,i} + c_{L,i} + c_{S,i} = 0 \qquad (i \geq 2) \qquad \text{(III.C11)}$$

[16] This is not the case for MEPS@NLO in SHERPA, where full control of the matrix element functions is available, thus opening other avenues for NLO merging [26, 27].

[17] If L_n does not contain an additional Born term, we would not have to subtract the term $[w_n]_0$ in w_B, which would have the benefit of fewer negative weights.

One way to include this condition is by replacing $c_{B,i}$ in the tree-level weight, which gives allowed weights of the form

$$w_B = w_n - \left[w_n\right]_0 - \left[w_n\right]_1 - \sum_{i=2}^{\infty} \left[c_{V,i} + c_{R,i}\right] \left(\frac{1}{\alpha_s}\right)^i \qquad \text{(III.C12)}$$

Finally, if we choose to use inclusive NLO cross sections for L_n, there are non-trivial cancellations between L_n and S_n, since S_n was introduced as an explicit phase space subtraction. If we choose w_L and w_S differently, these cancellations are jeopardised in higher orders. We thus think it reasonable to only allow the weights

$$w_B = w_n - \left[w_n\right]_0 - \left[w_n\right]_1 - \sum_{i=2}^{\infty} 2c_{L,i} \left(\frac{1}{\alpha_s}\right)^i \qquad \text{(III.C13)}$$

$$w_L = w_S = 1 + \sum_{i=2}^{\infty} c_{L,i} \left(\frac{1}{\alpha_s}\right)^i \qquad \text{(III.C14)}$$

This still allows for some arbitrariness, since $c_{L,i}$ is not fixed. We choose a pragmatic approach, and exclude weights that are not easily generated by the PYTHIA8 shower[18]. An example for such are weights with negative α_s order. Thus, we set

$$w_B = w_n - \left[w_n\right]_0 - \left[w_n\right]_1 \qquad \text{(III.C15)}$$

$$w_L = w_S = 1 \qquad \text{(III.C16)}$$

We will not reweight any $\mathcal{O}(\alpha_s^{n+1})-$terms. This immediately implies that the merging scale should be defined in the parton shower evolution variable, since otherwise, Sudakov factors would have to be multiplied in regions of t_{MS}-unordered splittings [25]. Sudakov factors can be represented by a power series in positive powers of α_s, so that even in eq. (III.C14), we could not easily accommodate such factors. The main constraint on w_L and w_S is condition (b), which can also be interpreted as the statement that only tree-level samples are allowed "seeds" for higher order contributions.

So far, we have only been concerned with conditions (a) and (b). Condition (c) becomes important when combining different jet multiplicities. In NL^3, this combination is constructed by simply summing

[18] We would like to point out that the approach of Plätzer [32] does indeed use a smart choice to generate different weights, which contain Sudakov-form-factor denominators.

all reweighted $n-$jet samples. Let M be number of additional jets in the highest-multiplicity NLO calculation, and let us use

$$\mathbb{T}_n = \begin{cases} \mathrm{B}_n w_B & (n \leq M) \\ \mathrm{B}_n w_n & (n > M) \end{cases} \tag{III.C17}$$

$$\mathbb{V}_n = \mathrm{L}_n = \overline{\mathrm{B}}_n \qquad (n \leq M) \tag{III.C18}$$

$$\mathbb{S}_n = \mathrm{S}_n = -\int_s \mathrm{B}_{n+1\to n} \qquad (n \leq M) \tag{III.C19}$$

The NL^3 method then sums reweighted event samples:

- ◇ If $n \leq M$, include the samples B_n, L_n and S_n, reweighted according to eq. (III.C15) or eq. (III.C16). Remember that S_n has a negative sign. This will produce $\mathbb{T}'_n$, $\mathbb{V}_n$ and $\mathbb{S}_n$.
- ◇ If $n > M$, reweight B_n as in CKKW-L. This will produce $\mathbb{T}_n$.

For an observable $\mathcal{O}$, this produces the prediction

$$\begin{aligned} \langle \mathcal{O} \rangle &= \sum_{m=0}^{M} \int d\phi_0 \int \cdots \int \mathcal{O}(S_{+mj}) \left\{ \mathbb{T}'_m + \mathbb{V}_m + \mathbb{S}_m \right\} \\ &+ \sum_{n=M+1}^{N} \int d\phi_0 \int \cdots \int \mathcal{O}(S_{+nj}) \mathbb{T}_n \\ &= \sum_{m=0}^{M} \int d\phi_0 \int \cdots \int \mathcal{O}(S_{+mj}) \Bigg\{ \\ &\qquad \mathrm{B}_m \left\{ w_m - [w_m]_0 - [w_m]_1 \right\} + \mathrm{B}_m + \mathrm{V}_m + \mathrm{I}_{m+1|m} \\ &\qquad + \int d\Phi_{\mathrm{rad}} \left(\mathrm{B}_{m+1|m} - \mathrm{D}_{m+1|m} \right) - \int_s \mathrm{B}_{m+1\to m} \Bigg\} \\ &+ \sum_{n=M+1}^{N} \int d\phi_0 \int \cdots \int \mathcal{O}(S_{+nj})\, \mathrm{B}_n w_n \end{aligned} \tag{III.C20}$$

Let us briefly investigate how this method changes the inclusive cross section in the special case of merging zero- and one-jet NLO calculations. At $\mathcal{O}\left(\alpha_s^1(\mu_R)\right)$, the cross section is given by the full NLO result by construction, while at $\mathcal{O}\left(\alpha_s^2(\mu_R)\right)$, we find

$$\begin{aligned} [\langle \mathcal{O} \rangle]_2 = &\int d\phi_0 \mathcal{O}(S_{+0j})\, \mathrm{B}_0\, [w_0]_2 \\ &+ \int d\phi_0 \int \mathcal{O}(S_{+1j}) \left\{ \mathrm{V}_1 + \mathrm{I}_{1|0} + \int d\Phi_{\mathrm{rad}} \left(\mathrm{B}_{1|0} - \mathrm{D}_{1|0} \right) - \int_s \mathrm{B}_{2\to 1} \right\} \\ &+ \int d\phi_0 \iint \mathcal{O}(S_{+2j})\, \mathrm{B}_2 \end{aligned} \tag{III.C21}$$

It is useful to compare this to the result of CKKW-L

$$\begin{aligned}\left[\langle\mathcal{O}\rangle\right]_2 &= \int d\phi_0 \mathcal{O}(S_{+0j})\, \mathrm{B}_0 \left[w_0\right]_2 \\ &\quad + \int d\phi_0 \int \mathcal{O}(S_{+1j})\, \mathrm{B}_1 \left[w_1\right]_1 \\ &\quad + \int d\phi_0 \iint \mathcal{O}(S_{+2j})\, \mathrm{B}_2 \,. \end{aligned} \tag{III.C22}$$

For very low merging scales, logarithmic contributions of a single jet in B_2 approaching the soft/collinear limit should be cancelled to better accuracy in NL^3, since the one-jet NLO results should contain the complete logarithmic structure. However, since the zero-jet description is given by the CKKW-L result, enhancements for the one-jet NLO contributions approaching the phase space boundary are not fully cancelled. For W$-$boson production, this means that NL^3 does not fully compensate contributions of $\mathcal{O}\left(\alpha_s^2 \ln^2\left\{\frac{\mu_F}{\rho_{MS}}\right\}\right)$. Enhancements due to both jets in B_2 stretching into the infrared are unchecked in CKKW-L, but should cancel some of the one-jet NLO terms in NL^3.

We find it difficult to assess if CKKW-L or NL^3 is more problematic. The merging scale value is chosen to separate the parton shower phase space from the hard matrix element region. Seeing that multiparton interactions at the LHC certainly play a role already at scales of $\mathcal{O}(10\ \mathrm{GeV})$, it is common practise to set the merging scale to a slightly higher value. In the particular case of W$-$boson production, with a merging scale of $\rho_{MS} \gtrsim 10$ GeV, double logarithms are considerably smaller than the next higher order in α_s, so that it is difficult to isolate the questionable terms. We think these important issues nevertheless, and address them, in the context of the UNLOPS method, in section III.3.2.

For completeness, we add the NL^3 result for exclusive NLO input, which simply does not contain phase space subtraction samples:

$$\begin{aligned}\langle\mathcal{O}\rangle &= \sum_{m=0}^{M} \int d\phi_0 \int\cdots\int \mathcal{O}(S_{+mj}) \left\{ \mathbb{T}'_m + \mathbb{V}_m \right\} + \sum_{n=M+1}^{N} \int d\phi_0 \int\cdots\int \mathcal{O}(S_{+nj}) \mathbb{T}_n \\ &= \sum_{m=0}^{M} \int d\phi_0 \int\cdots\int \mathcal{O}(S_{+mj}) \left\{ \mathrm{B}_m \left\{ w_m - \left[w_m\right]_0 - \left[w_m\right]_1 \right\} + \mathrm{B}_m + \mathrm{V}_m + \mathrm{I}_{m+1|m} \right. \\ &\qquad \left. + \int d\Phi_{\mathrm{rad}} \left(\mathrm{B}_{m+1|m} - \mathrm{D}_{m+1|m} \right) \right\} \\ &\quad + \sum_{n=M+1}^{N} \int d\phi_0 \int\cdots\int \mathcal{O}(S_{+nj})\, \mathrm{B}_n w_n \end{aligned} \tag{III.C23}$$

This ends the derivation and discussion of the NL^3 method. The main conclusion of this section is that the allowed weights for samples in NLO merging are restricted by merging conditions. The constraints apply to other CKKW-L inspired NLO merging schemes as well. If, for example, NLO accuracy has to be safeguarded, it is mandatory to remove the $\mathcal{O}\left(\alpha_s^0\left(\mu_R\right)\right)$- and $\mathcal{O}\left(\alpha_s^1\left(\mu_R\right)\right)$-parts of the weight of tree-level events.

III.D Derivation of UNLOPS

In this part, we aim to give a step-by-step derivation of the UNLOPS method. We will use the notation defined in section III.3, and start with the UMEPS prediction for incorporating up to three additional jets: $\mathcal{O}$ as

$$\begin{aligned}\langle\mathcal{O}\rangle \;=\; \int d\phi_0 \Bigg\{ & \mathcal{O}(S_{+0j}) \left(\widehat{\mathrm{B}}_0 \;-\; \int_s \widehat{\mathrm{B}}_{1\to 0} \;-\; \int_s \widehat{\mathrm{B}}_{2\to 0} \;-\; \int_s \widehat{\mathrm{B}}_{3\to 0} \right) \\ & + \int \mathcal{O}(S_{+1j}) \left(\widehat{\mathrm{B}}_1 \;-\; \int_s \widehat{\mathrm{B}}_{2\to 1} \;-\; \int_s \widehat{\mathrm{B}}_{3\to 1} \right) \\ & + \iint \mathcal{O}(S_{+2j}) \left(\widehat{\mathrm{B}}_2 \;-\; \int_s \widehat{\mathrm{B}}_{3\to 2} \right) \\ & + \iiint \mathcal{O}(S_{+3j})\, \widehat{\mathrm{B}}_3 \Bigg\} \end{aligned} \tag{III.D1}$$

Our method will be to identify which prediction for an exclusive n-jet observable we want, replace the UMEPS approximation by these terms, find the difference between the improved result and the UMEPS prediction, and remove this difference from the next-lower jet multiplicity.

As a warm-up exercise, let us include a NLO calculation for zero-jet observables. We then want zero-jet observables to be described by the sum of Born, virtual and unresolved real terms, and also include the PS resummation. Keeping in mind that we do not want to introduce approximate $\mathcal{O}(\alpha_s^0)$- or $\mathcal{O}(\alpha_s^1)$-terms[19], the zero-jet exclusive cross section

[19] We use the intuitive result in eq. (III.C15): If we want to include the n-jet NLO result, we have to subtract the $\mathcal{O}(\alpha_s^0)$- and $\mathcal{O}(\alpha_s^1)$-terms of the weight for n-jet tree-level events to ensure NLO accuracy.

should read

$$\widetilde{\mathrm{B}}_0 + \left[\widehat{\mathrm{B}}_0\right]_{-0,1} - \left[\int_s \widehat{\mathrm{B}}_{1\to 0}\right]_{-1} - \int_s \widehat{\mathrm{B}}_{2\to 0} - \int_s \widehat{\mathrm{B}}_{3\to 0}$$
$$= \widetilde{\mathrm{B}}_0 - \left[\int_s \widehat{\mathrm{B}}_{1\to 0}\right]_{-1} - \int_s \widehat{\mathrm{B}}_{2\to 0} - \int_s \widehat{\mathrm{B}}_{3\to 0}\,. \qquad \text{(III.D2)}$$

We would thus need to remove the terms

$$\int \widetilde{\mathrm{B}}_0 + \int \widehat{\mathrm{B}}_0 \qquad \text{(III.D3)}$$

from the next-lower multiplicity. Since there is no next-lower multiplicity, we simply get

$$\begin{aligned}\langle \mathcal{O} \rangle \;=\; \int d\phi_0 \Bigg\{ & \mathcal{O}(S_{+0j}) \left(\widetilde{\mathrm{B}}_0 - \left[\int_s \widehat{\mathrm{B}}_{1\to 0}\right]_{-1} - \int_s \widehat{\mathrm{B}}_{2\to 0} - \int_s \widehat{\mathrm{B}}_{3\to 0} \right) \\ & + \int \mathcal{O}(S_{+1j}) \left(\widehat{\mathrm{B}}_1 - \int_s \widehat{\mathrm{B}}_{2\to 1} - \int_s \widehat{\mathrm{B}}_{3\to 1} \right) \\ & + \iint \mathcal{O}(S_{+2j}) \left(\widehat{\mathrm{B}}_2 - \int_s \widehat{\mathrm{B}}_{3\to 2} \right) \\ & + \iiint \mathcal{O}(S_{+3j})\, \widehat{\mathrm{B}}_3 \Bigg\} \end{aligned} \qquad \text{(III.D4)}$$

or, in terms of the inclusive NLO cross section

$$\begin{aligned}\langle \mathcal{O} \rangle \;=\; \int d\phi_0 \Bigg\{ & \mathcal{O}(S_{+0j}) \left(\overline{\mathrm{B}}_0 - \int_s \widehat{\mathrm{B}}_{1\to 0} - \int_s \widehat{\mathrm{B}}_{2\to 0} - \int_s \widehat{\mathrm{B}}_{3\to 0} \right) \\ & + \int \mathcal{O}(S_{+1j}) \left(\widehat{\mathrm{B}}_1 - \int_s \widehat{\mathrm{B}}_{2\to 1} - \int_s \widehat{\mathrm{B}}_{3\to 1} \right) \\ & + \iint \mathcal{O}(S_{+2j}) \left(\widehat{\mathrm{B}}_2 - \int_s \widehat{\mathrm{B}}_{3\to 2} \right) \\ & + \iiint \mathcal{O}(S_{+3j})\, \widehat{\mathrm{B}}_3 \Bigg\} \end{aligned} \qquad \text{(III.D5)}$$

Thus, we can promote UMEPS to a tree-level multi-jet merged, lowest-multiplicity NLO corrected calculation by simply replacing the zero-jet Born cross section with the inclusive zero-jet NLO cross section. Such a scheme is often called MENLOPS [39–41]. Note that the the total cross

section is conserved, because we started from the UMEPS prediction, rescaled with a factor $K = \int \overline{\mathrm{B}}_0 \,/\, \int \mathrm{B}_0$.

The derivation of a multi-jet merging scheme with NLO accuracy for any $n-$jet observable is organised as follows. First, we will extend the MENLOPS result eq. (III.D5) to simultaneously include a one-jet NLO calculation. Then, we add the two jet NLO result. After a short discussion, we present the general case.

To including one-jet NLO predictions, we need to replace the UMEPS one-jet result by

$$\widetilde{\mathrm{B}}_1 + \left[\widehat{\mathrm{B}}_1\right]_{-1,2} - \left[\int_s \widehat{\mathrm{B}}_{2\to 1}\right]_{-2} - \int_s \widehat{\mathrm{B}}_{3\to 1} \tag{III.D6}$$

Further we have to subtract the difference of the new one-jet prediction and the UMEPS case from the zero-jet part. The difference is given by

$$- \left(- \widetilde{\mathrm{B}}_1 + \left[\widehat{\mathrm{B}}_1\right]_{1,2} - \left[\int_s \widehat{\mathrm{B}}_{2\to 1}\right]_2 \right) , \tag{III.D7}$$

so that the zero-jet contribution becomes

$$\begin{aligned}
\langle \mathcal{O} \rangle_0 &= \int d\phi_0 \mathcal{O}(S_{+0j}) \Bigg\{ \widetilde{\mathrm{B}}_0 - \left[\int_s \widehat{\mathrm{B}}_{1\to 0}\right]_{-1} - \int_s \widehat{\mathrm{B}}_{2\to 0} - \int_s \widehat{\mathrm{B}}_{3\to 0} \\
&\quad - \int_s \widetilde{\mathrm{B}}_{1\to 0} + \left[\int_s \widehat{\mathrm{B}}_{1\to 0}\right]_{1,2} - \left[\int_s \widehat{\mathrm{B}}^{\uparrow}_{2\to 0}\right]_2 \Bigg\} \\
&= \int d\phi_0 \mathcal{O}(S_{+0j}) \Bigg\{ \widetilde{\mathrm{B}}_0 - \int_s \widetilde{\mathrm{B}}_{1\to 0} + \int_s \mathrm{B}_{1\to 0} - \left[\int_s \widehat{\mathrm{B}}_{1\to 0}\right]_{-1,2} \\
&\quad - \int_s \mathrm{B}^{\uparrow}_{2\to 0} - \int_s \widehat{\mathrm{B}}_{2\to 0} - \int_s \widehat{\mathrm{B}}_{3\to 0} \Bigg\}
\end{aligned} \tag{III.D8}$$

Note that the integrated two-jet contribution

$$\left[\int_s \widehat{\mathrm{B}}^{\uparrow}_{2\to 0}\right]_2 = \int_s \mathrm{B}^{\uparrow}_{2\to 0} \tag{III.D9}$$

is integrated twice, even though the result of the first integration (S_{+1})

contains only resolved jets. Putting the pieces together, we arrive at

$$\begin{aligned}\langle\mathcal{O}\rangle = \int d\phi_0 \Bigg\{ & \mathcal{O}(S_{+0j}) \left(\widetilde{\mathrm{B}}_0 - \int_s \widetilde{\mathrm{B}}_{1\to 0} + \int_s \mathrm{B}_{1\to 0} - \left[\int_s \widehat{\mathrm{B}}_{1\to 0} \right]_{-1,2} \right. \\ & \left. - \int_s \mathrm{B}^{\uparrow}_{2\to 0} - \int_s \widehat{\mathrm{B}}_{2\to 0} - \int_s \widehat{\mathrm{B}}_{3\to 0} \right) \\ & + \int \mathcal{O}(S_{+1j}) \left(\widetilde{\mathrm{B}}_1 + \left[\widehat{\mathrm{B}}_1 \right]_{-1,2} - \left[\int_s \widehat{\mathrm{B}}_{2\to 1} \right]_{-2} - \int_s \widehat{\mathrm{B}}_{3\to 1} \right) \\ & + \iint \mathcal{O}(S_{+2j}) \left(\widehat{\mathrm{B}}_2 - \int_s \widehat{\mathrm{B}}_{3\to 2} \right) \\ & + \iiint \mathcal{O}(S_{+3j}) \, \widehat{\mathrm{B}}_3 \Bigg\} \end{aligned} \tag{III.D10}$$

Let us rewrite this in terms of inclusive NLO calculations:

$$\begin{aligned}\langle\mathcal{O}\rangle = \int d\phi_0 \Bigg\{ & \mathcal{O}(S_{+0j}) \left(\overline{\mathrm{B}}_0 - \int_s \overline{\mathrm{B}}_{1\to 0} - \left[\int_s \widehat{\mathrm{B}}_{1\to 0} \right]_{-1,2} - \int_s \widehat{\mathrm{B}}_{2\to 0} - \int_s \widehat{\mathrm{B}}_{3\to 0} \right) \\ & + \int \mathcal{O}(S_{+1j}) \left(\overline{\mathrm{B}}_1 + \left[\widehat{\mathrm{B}}_1 \right]_{-1,2} - \int_s \widehat{\mathrm{B}}_{2\to 1} - \int_s \widehat{\mathrm{B}}_{3\to 1} \right) \\ & + \iint \mathcal{O}(S_{+2j}) \left(\widehat{\mathrm{B}}_2 - \int_s \widehat{\mathrm{B}}_{3\to 2} \right) \\ & + \iiint \mathcal{O}(S_{+3j}) \, \widehat{\mathrm{B}}_3 \Bigg\} \end{aligned} \tag{III.D11}$$

This result will be used in section III.3.2, and is discussed there.

Before presenting a general master formula, we will take yet another intermediate step, and generalise eq. (III.D11) to further include two-jet NLO predictions. Two-jet observables should be described by

$$\widetilde{\mathrm{B}}_2 + \left[\widehat{\mathrm{B}}_2 \right]_{-2,3} - \left[\int_s \widehat{\mathrm{B}}_{3\to 2} \right]_{-3} . \tag{III.D12}$$

To conserve unitarity, we then have to subtract the difference of the new result and the UMEPS contributions, i.e.

$$- \left(- \widetilde{\mathrm{B}}_2 + \left[\widehat{\mathrm{B}}_2 \right]_{2,3} - \int_s \mathrm{B}_{3\to 2} \right) , \tag{III.D13}$$

from the one-jet case. This gives the new one-jet contributions

$$\widetilde{\mathrm{B}}_1 - \int_s \widetilde{\mathrm{B}}_{2\to 1} + \left[\widehat{\mathrm{B}}_1 \right]_{-12} - \left[\int_s \widehat{\mathrm{B}}_{2\to 1} \right]_{-2,3} + \int_s \mathrm{B}_{2\to 1} - \int_s \mathrm{B}^{\uparrow}_{3\to 1} - \int_s \widehat{\mathrm{B}}_{3\to 1} . \tag{III.D14}$$

In the case that $\widetilde{\mathrm{B}}_{2\to 1}$, $\int_s \mathrm{B}^{\uparrow}_{3\to 1}$ or $\left[\int_s \widehat{\mathrm{B}}_{2\to 1} \right]_{2,3}$ does not result in a state with one jet above the merging scale, we choose to integrate twice, as in

the case of UMEPS. Thus, the UNLOPS prediction for simultaneously merging zero, one and two jets at next-to-leading order is given by

$$\begin{aligned}\langle\mathcal{O}\rangle = \int d\phi_0 \Bigg\{ & \mathcal{O}(S_{+0j}) \left(\widetilde{\mathrm{B}}_0 - \int_s \widetilde{\mathrm{B}}_{1\to 0} - \int_s \widetilde{\mathrm{B}}_{2\to 0} + \int_s \mathrm{B}_{1\to 0} - \left[\int_s \widehat{\mathrm{B}}_{1\to 0} \right]_{-1,2} \right. \\ & \left. - \int_s \mathrm{B}^{\uparrow}_{2\to 0} - \int_s \mathrm{B}^{\uparrow}_{3\to 0} - \left[\int_s \widehat{\mathrm{B}}_{2\to 0} \right]_{-2,3} - \int_s \widehat{\mathrm{B}}_{3\to 0} \right) \\ & + \int \mathcal{O}(S_{+1j}) \left(\widetilde{\mathrm{B}}_1 - \int_s \widetilde{\mathrm{B}}_{2\to 1} + \left[\widehat{\mathrm{B}}_1 \right]_{-1,2} - \left[\int_s \widehat{\mathrm{B}}_{2\to 1} \right]_{-2,3} \right. \\ & \left. + \int_s \mathrm{B}_{2\to 1} - \int_s \mathrm{B}^{\uparrow}_{3\to 1} - \int_s \widehat{\mathrm{B}}_{3\to 1} \right) \\ & + \iint \mathcal{O}(S_{+2j}) \left(\widetilde{\mathrm{B}}_2 + \left[\widehat{\mathrm{B}}_2 \right]_{-2,3} - \left[\int_s \widehat{\mathrm{B}}_{3\to 2} \right]_{-3} \right) \\ & + \iiint \mathcal{O}(S_{+3j}) \, \widehat{\mathrm{B}}_3 \Bigg\} \end{aligned} \tag{III.D15}$$

Again expressing this in terms of NLO inclusive cross sections, we find

$$\begin{aligned}\langle\mathcal{O}\rangle = \int d\phi_0 \Bigg\{ & \mathcal{O}(S_{+0j}) \left(\overline{\mathrm{B}}_0 - \int_s \overline{\mathrm{B}}_{1\to 0} - \int_s \overline{\mathrm{B}}_{2\to 0} - \left[\int_s \widehat{\mathrm{B}}_{1\to 0} \right]_{-1,2} \right. \\ & \left. - \left[\int_s \widehat{\mathrm{B}}_{2\to 0} \right]_{-2,3} - \int_s \widehat{\mathrm{B}}_{3\to 0} \right) \\ & + \int \mathcal{O}(S_{+1j}) \left(\overline{\mathrm{B}}_1 - \int_s \overline{\mathrm{B}}_{2\to 1} + \left[\widehat{\mathrm{B}}_1 \right]_{-1,2} - \left[\int_s \widehat{\mathrm{B}}_{2\to 1} \right]_{-2,3} - \int_s \widehat{\mathrm{B}}_{3\to 1} \right) \\ & + \iint \mathcal{O}(S_{+2j}) \left(\overline{\mathrm{B}}_2 + \left[\widehat{\mathrm{B}}_2 \right]_{-23} - \int_s \widehat{\mathrm{B}}_{3\to 2} \right) \\ & + \iiint \mathcal{O}(S_{+3j}) \, \widehat{\mathrm{B}}_3 \Bigg\} \end{aligned} \tag{III.D16}$$

Let us have a closer look at eq. (III.D15), and in particular how the $\mathcal{O}\left(\alpha_s^3(\mu_R)\right)$ −term of the one-jet descriptions:

$$\left[\langle\mathcal{O}\rangle_1\right]_3 = \left[\widehat{\mathrm{B}}_1\right]_3 - \left[\int_s \widetilde{\mathrm{B}}_{2\to 1}\right]_3 - \left[\int_s \mathrm{B}^{\uparrow}_{3\to 1}\right]_3 - \left[\int_s \widehat{\mathrm{B}}_{3\to 1}\right]_3 \tag{III.D17}$$

The first term is the parton shower approximation of unresolved emissions in the underlying zero-jet configurations. The second and third terms give an approximation of unresolved contributions in one-jet states. Compared to the UMEPS result $\left(\int_s \mathrm{B}_{2\to 1}\left[w_2'\right]_1\right)$, this should give an improved description. The last term in eq. (III.D17) is unchanged compared to UMEPS, and should not induce logarithmic terms in ρ_{MS}.

Coming back to the first term in eq. (III.D17), it is natural to ask if reweighting the $\mathcal{O}(\alpha_s^2)-$part of $\widetilde{\mathrm{B}}_1$ would not give a better description. Since reweighting exclusive NLO events (which contain both $\mathcal{O}(\alpha_s^n)$ and $\mathcal{O}(\alpha_s^{n+1})$ parts) will mix higher-order terms in a difficult way, this interesting possibility is not examined here. We hope to come back to this issue for comparisons between different NLO merging prescriptions[20].

We hope it is clear that the UNLOPS method preserves NLO accuracy by construction, and improves the higher-order description of UMEPS further. The formal accuracy of exclusive $n-$jet observables, however, is not better than next-to-leading order combined with PS resummation. Only for a limited set of observables do parton showers capture more than leading logarithmic enhancements. We have presented UNLOPS both for exclusive and inclusive NLO cross sections. This is motivated by trying to accommodate NLO calculations while requiring only minor – or ideally no – changes to the actual NLO implementation.

After explicitly deriving the UNLOPS scheme for describing up to two jet observables next-to-leading order accuracy, we now give the UNLOPS master formula, when using exclusive NLO samples

$$\begin{aligned}
\langle\mathcal{O}\rangle = &\sum_{m=0}^{M-1}\int d\phi_0\int\cdots\int\mathcal{O}(S_{+mj})\left\{\widetilde{\mathrm{B}}_m+\left[\widehat{\mathrm{B}}_m\right]_{-m,m+1}+\int_s \mathrm{B}_{m+1\to m}\right.\\
&\qquad -\sum_{i=m+1}^{M}\int_s\widetilde{\mathrm{B}}_{i\to m}-\sum_{i=m+1}^{M}\left[\int_s\widehat{\mathrm{B}}_{i\to m}\right]_{-i,i+1}-\sum_{i=m+1}^{M}\int_s\mathrm{B}^{\uparrow}_{i+1\to m}\\
&\qquad \left.-\sum_{i=M+1}^{N}\int_s\widehat{\mathrm{B}}_{i\to m}\right\}\\
&+\int d\phi_0\int\cdots\int\mathcal{O}(S_{+Mj})\left\{\widetilde{\mathrm{B}}_M+\left[\widehat{\mathrm{B}}_M\right]_{-M,M+1}-\left[\int_s\widehat{\mathrm{B}}_{M+1\to M}\right]_{-M}\right.\\
&\qquad \left.-\sum_{i=M+1}^{N}\int_s\widehat{\mathrm{B}}_{i+1\to M}\right\}\\
&+\sum_{n=M+1}^{N}\int d\phi_0\int\cdots\int\mathcal{O}(S_{+nj})\left\{\widehat{\mathrm{B}}_n-\sum_{i=n+1}^{N}\int_s\widehat{\mathrm{B}}_{i\to n}\right\}
\end{aligned}\qquad\text{(III.D18)}$$

Furthermore, since most results in this publication are produced using inclusive NLO samples, we also give the UNLOPS prediction for inclu-

[20] We in particular think about comparisons with MEPS@NLO, were $\widetilde{\mathrm{B}}-$events are reweighted.

sive input

$$\begin{aligned}\langle\mathcal{O}\rangle = &\sum_{m=0}^{M-1}\int d\phi_0\int\cdots\int\mathcal{O}(S_{+mj})\left\{\overline{\mathrm{B}}_m+\left[\widehat{\mathrm{B}}_m\right]_{-m,m+1}\right.\\ &\left.-\sum_{i=m+1}^{M}\int_s\overline{\mathrm{B}}_{i\to m}-\sum_{i=m+1}^{M}\left[\int_s\widehat{\mathrm{B}}_{i\to m}\right]_{-i,i+1}-\sum_{i=M+1}^{N}\int_s\widehat{\mathrm{B}}_{i\to m}\right\}\\ &+\int d\phi_0\int\cdots\int\mathcal{O}(S_{+Mj})\left\{\overline{\mathrm{B}}_M+\left[\widehat{\mathrm{B}}_M\right]_{-M,M+1}-\sum_{i=M+1}^{N}\int_s\widehat{\mathrm{B}}_{i\to M}\right\}\\ &+\sum_{n=M+1}^{N}\int d\phi_0\int\cdots\int\mathcal{O}(S_{+nj})\left\{\widehat{\mathrm{B}}_n-\sum_{i=n+1}^{N}\int_s\widehat{\mathrm{B}}_{i\to n}\right\}\end{aligned}\tag{III.D19}$$

Although the number of contributions in UNLOPS becomes somewhat unwieldy, we still only require $M+N$ input event files, since some files can be reused – as in NL^3. The procedure (including processing some input events multiple times) has been implemented in PYTHIA8, and will become available in the near future.

III.D.1 Upgrading one-jet UNLOPS to a NNLO matching scheme

The UNLOPS scheme has the advantage that the lowest-multiplicity cross section is not reweighted. This makes replacements of this term with more accurate calculations relatively easy. Here, we would like to hint at how UNLOPS could be shaped into a NNLO matching scheme. The starting point is again UMEPS, but instead of multiplying every UMEPS contribution with a NLO K-factor, we rescale with a NNLO K-factor K'. Apart from this change, we directly move to the UNLOPS prescription including zero- and one-jet NLO calculations. Then, we assume that an exclusive zero-jet NNLO calculation is available, producing phase space points with the weight $\widetilde{\widetilde{\mathrm{B}}}_0$. The weight $\widetilde{\widetilde{\mathrm{B}}}_0$ should be the sum of the Born approximation, one-loop corrections, unresolved single real corrections, two-loop corrections, one-loop corrections with an additional unresolved jet, and double unresolved double real radiation contributions.

We replace $\widetilde{\mathrm{B}}_0$ in eq. (III.21) by $\widetilde{\widetilde{\mathrm{B}}}_0$, and remove all other $\mathcal{O}\left(\alpha_s^2(\mu_R)\right)$ −terms in the zero-jet part:

$$\langle\mathcal{O}\rangle = \int d\phi_0\left\{\mathcal{O}(S_{+0j})\left(\widetilde{\widetilde{\mathrm{B}}}_0-\left[\int_s\widehat{\mathrm{B}}_{1\to0}\right]_{-1,2}-\left[\int_s\widehat{\mathrm{B}}_{2\to0}\right]_{-2}\right)\right.$$

$$+\int \mathcal{O}(S_{+1j})\left(\widetilde{\mathrm{B}}_1+\left[\widehat{\mathrm{B}}_1\right]_{-1,2}-\left[\int_s \widehat{\mathrm{B}}_{2\to 1}\right]_{-2}\right)$$
$$+\iint \mathcal{O}(S_{+2j})\,\widehat{\mathrm{B}}_2\Bigg\} \qquad \text{(III.D20)}$$

We see that the inclusive cross section is given by

$$\int d\phi_0 \mathcal{O}(S_{+0j})\widetilde{\widetilde{\mathrm{B}}}_0 \;+\; \int d\phi_0 \int \mathcal{O}(S_{+1j})\,\widetilde{\mathrm{B}}_1 \qquad \text{(III.D21)}$$

Zero-jet observables are correct to $\mathcal{O}\left(\alpha_s^2\left(\mu_R\right)\right)$, as is the description of one- and two-jet observables. It is of course possible to improve higher orders by including additional matrix elements in UMEPS-fashion. The major obstacle for implementing this method is the lack of available ME generators generating phase space points according to $\widetilde{\widetilde{\mathrm{B}}}_0$.

III.E NLO merging and multiparton interactions

Observable jets at hadron colliders are not only produced in a single energetic interactions, but also emerge from additional scatterings of other proton constituents. Multiparton interactions (MPI) models are essential in describing hadron collider data which include these "underlying events" [50–52]. When trying to describe the underlying event at the LHC, one is in practise still largely forced to use phenomenological models, although efforts are under way to construct more solid theoretical foundations (see [53] for a recent review). Due to continuous development, it is valid to say that current phenomenological models offer a good description of a wide range of experimental data.

A sophisticated MPI machinery has always been a cornerstone of PYTHIA8 [54–57]. Multiparton interactions in PYTHIA8 are modelled by including QCD $2 \to 2$ scatterings in addition to the hard process. It is reasonable to assume that energetic secondary scatterings induce constraints on how much beam energy would be left for further initial state radiation. PYTHIA8 incorporates such phase space constraints by interleaving MPI with parton showering: An energetic secondary scattering is produced *before* soft radiation. This is achieved by generating initial state radiation, final state radiation, and MPI in one decreasing sequence of evolution scales. One benefit of this method is that for a high shower starting scale, more jet-like MPI are produced, which increases the underlying event activity for increasing hardness of the core scattering – a phenomenon called pedestal effect.

From the point of precision QCD, we have to recognise that for observables which are influenced by multiple interactions, the formal accuracy of any merging method will be governed by MPI. Only if the influence of MPI is negligible are statements about the formal accuracy of the result reasonable. However, suppressing hard multiparton interactions leads to an inferior data description. Following the philosophy of [5] and [6], we will sacrifice the formal accuracy label of the NLO merging method in regions where MPI are important. This does not mean that we undo any improvements of our method, but only that we can no longer claim a particular accuracy, even in the presence of improvements.

We include MPI in NL^3 and UNLOPS in the same way as was previously done for UMEPS in [6] and we refer to that publication and [5] for more background. First we amend the normal PS no-emission probabilities with no-MPI factors, $\Pi^{\text{MPI}}_{S_{+n}}$. This means that all event samples with n partons ($\mathbb{B}_n$, $\mathbb{V}_n$, $\mathbb{I}_n$, and $\mathbb{L}_n$) are multiplied with the no-MPI probabilities

$$\prod_{i=0}^{m-1} \Pi^{\text{MPI}}_{S_{+i}}(\rho_i, \rho_{i+1}), \tag{III.E1}$$

which are easily incorporated in the trial showers. Note, however, that MPI emissions are not taken into account when calculating the $\mathcal{O}(\alpha_s^1)-$term of no-emission probabilities (which is natural since MPI's are of $\mathcal{O}(\alpha_s^2)$). Then, when the shower is started from the reweighted (and possibly reclustered) states, using ρ_n as starting scale, MPI's are included. As before, for $n < N$, any parton emission above ρ_{MS} are vetoed, but if a MPI is generated, it is always accepted, and no emissions are vetoed in the subsequent showering.

As in the UMEPS and CKKW-L methods, this means that any event where the $n \leq N$ hardest jets are bove the merging scale and are from the primary interaction a, these will be described by the corresponding tree-level ME. In addition if $n \leq M$ these jets will be described by the corresponding NLO ME. In both cases, the higher order α_s-terms will be resummed to the precision of the shower. Again we note that the NLO-prediction will be modified by the inclusion of MPI. The modification is beyond the "leading twist" approximation of the NLO calculation, but may nevertheless be large, especially for jets with low transverse momenta.

Before concluding, we would also point out that in this article, we have used `CTEQ6M` PDFs in the generation of secondary scatterings. This is not advisable, since the dominant contribution to the underlying

event stem from soft secondary scatterings. For such scatterings, PDFs are evaluated at low scales $\mathcal{O}(1\,\text{GeV})$, and very small $x-$values, i.e. in a region where NLO PDFs are poorly constrained and need not even be positive definite, which clearly is problematic in the probabilistic MPI picture. When developing a future tune to be used together with NLO merged predictions, we will utilise NLO parton distributions for the hard interaction, while employing leading-order PDFs in the multiple interactions and parton showers.

III References

[1] S. Catani, F. Krauss, R. Kuhn, and B. R. Webber, "QCD matrix elements + parton showers," *JHEP* **11** (2001) 063, arXiv:hep-ph/0109231.

[2] L. Lönnblad, "Correcting the colour-dipole cascade model with fixed order matrix elements," *JHEP* **05** (2002) 046, arXiv:hep-ph/0112284.

[3] N. Lavesson and L. Lönnblad, "W + jets matrix elements and the dipole cascade," *JHEP* **07** (2005) 054, arXiv:hep-ph/0503293.

[4] S. Höche, F. Krauss, S. Schumann, and F. Siegert, "QCD matrix elements and truncated showers," *JHEP* **05** (2009) 053, arXiv:0903.1219 [hep-ph].

[5] L. Lönnblad, and S. Prestel, "Matching Tree-Level Matrix Elements with Interleaved Showers," *JHEP* **1203** (2012) 019, arXiv:1109.4829 [hep-ph].

[6] L. Lönnblad and S. Prestel, "Unitarising Matrix Element + Parton Shower merging," arXiv:1211.4827 [hep-ph].

[7] Z. Bern, L. J. Dixon, D. C. Dunbar, and D. A. Kosower, "One loop n point gauge theory amplitudes, unitarity and collinear limits," *Nucl.Phys.* **B425** (1994) 217–260, arXiv:hep-ph/9403226 [hep-ph].

[8] R. Britto, F. Cachazo, and B. Feng, "Generalized unitarity and one-loop amplitudes in N=4 super-Yang-Mills," *Nucl.Phys.* **B725** (2005) 275–305, arXiv:hep-th/0412103 [hep-th].

[9] A. Denner and S. Dittmaier, "Reduction schemes for one-loop tensor integrals," *Nucl.Phys.* **B734** (2006) 62–115, arXiv:hep-ph/0509141 [hep-ph].

[10] G. Ossola, C. G. Papadopoulos, and R. Pittau, "Reducing full one-loop amplitudes to scalar integrals at the integrand level," *Nucl.Phys.* **B763** (2007) 147–169, arXiv:hep-ph/0609007 [hep-ph].

[11] R. K. Ellis, W. Giele, and Z. Kunszt, "A Numerical Unitarity Formalism for Evaluating One-Loop Amplitudes," *JHEP* **0803** (2008) 003, arXiv:0708.2398 [hep-ph].

[12] G. Ossola, C. G. Papadopoulos, and R. Pittau, "On the Rational Terms of the one-loop amplitudes," *JHEP* **0805** (2008) 004, arXiv:0802.1876 [hep-ph].

[13] R. K. Ellis, W. T. Giele, Z. Kunszt, and K. Melnikov, "Masses, fermions and generalized D-dimensional unitarity," *Nucl.Phys.* **B822** (2009) 270–282, arXiv:0806.3467 [hep-ph].

[14] C. Berger, Z. Bern, L. Dixon, F. Febres Cordero, D. Forde, *et al.*, "An Automated Implementation of On-Shell Methods for One-Loop Amplitudes," *Phys.Rev.* **D78** (2008) 036003, arXiv:0803.4180 [hep-ph].

[15] S. Becker, C. Reuschle, and S. Weinzierl, "Numerical NLO QCD calculations," *JHEP* **1012** (2010) 013, arXiv:1010.4187 [hep-ph].

[16] F. Cascioli, P. Maierhofer, and S. Pozzorini, "Scattering Amplitudes with Open Loops," *Phys.Rev.Lett.* **108** (2012) 111601, arXiv:1111.5206 [hep-ph].

[17] P. Nason, "A new method for combining NLO QCD with shower Monte Carlo algorithms," *JHEP* **11** (2004) 040, arXiv:hep-ph/0409146.

[18] S. Frixione, P. Nason, and C. Oleari, "Matching NLO QCD computations with Parton Shower simulations: the POWHEG method," *JHEP* **11** (2007) 070, arXiv:0709.2092 [hep-ph].

[19] S. Alioli, P. Nason, C. Oleari, and E. Re, "A general framework for implementing NLO calculations in shower Monte Carlo programs: the POWHEG BOX," *JHEP* **1006** (2010) 043, arXiv:1002.2581 [hep-ph].

[20] S. Platzer and S. Gieseke, "Dipole Showers and Automated NLO Matching in Herwig++," *Eur.Phys.J.* **C72** (2012) 2187, arXiv:1109.6256 [hep-ph].

[21] S. Frixione and B. R. Webber, "Matching NLO QCD computations and parton shower simulations," *JHEP* **06** (2002) 029, arXiv:hep-ph/0204244.

[22] S. Höche, F. Krauss, M. Schönherr, and F. Siegert, "A critical appraisal of NLO+PS matching methods," *JHEP* **1209** (2012) 049, arXiv:1111.1220 [hep-ph].

[23] S. Höche, F. Krauss, M. Schönherr, and F. Siegert, "W+n-jet predictions with MC@NLO in Sherpa," *Physical Review Letters* (2012) , arXiv:1201.5882 [hep-ph].

[24] V. Hirschi, R. Frederix, S. Frixione, M. V. Garzelli, F. Maltoni, *et al.*, "Automation of one-loop QCD corrections," *JHEP* **1105** (2011) 044, arXiv:1103.0621 [hep-ph].

[25] N. Lavesson and L. Lönnblad, "Extending CKKW-merging to One-Loop Matrix Elements," *JHEP* **12** (2008) 070, arXiv:0811.2912 [hep-ph].

[26] T. Gehrmann, S. Höche, F. Krauss, M. Schönherr, and F. Siegert, "NLO QCD matrix elements + parton showers in e+e- $\to$ hadrons," arXiv:1207.5031 [hep-ph].

[27] S. Höche, F. Krauss, M. Schönherr, and F. Siegert, "QCD matrix elements + parton showers: The NLO case," arXiv:1207.5030 [hep-ph].

[28] R. Frederix and S. Frixione, "Merging meets matching in MC@NLO," arXiv:1209.6215 [hep-ph].

[29] Z. Nagy and D. E. Soper, "Matching parton showers to NLO computations," *JHEP* **10** (2005) 024, hep-ph/0503053.

[30] K. Hamilton, P. Nason, and G. Zanderighi, "MINLO: Multi-Scale Improved NLO," *JHEP* **1210** (2012) 155, arXiv:1206.3572 [hep-ph].

[31] T. Sjöstrand, S. Mrenna, and P. Skands, "A Brief Introduction to PYTHIA 8.1," *Comput. Phys. Commun.* **178** (2008) 852–867, arXiv:0710.3820 [hep-ph].

[32] S. Plätzer, "Controlling inclusive cross sections in parton shower + matrix element merging," arXiv:1211.5467 [hep-ph].

[33] J. Alwall *et al.*, "A standard format for Les Houches Event Files," *Comput. Phys. Commun.* **176** (2007) 300–304, hep-ph/0609017.

[34] C. W. Bauer, F. J. Tackmann, and J. Thaler, "GenEvA. I. A New framework for event generation," *JHEP* **0812** (2008) 010, arXiv:0801.4026 [hep-ph].

[35] C. W. Bauer, F. J. Tackmann, and J. Thaler, "GenEvA. II. A Phase space generator from a reweighted parton shower," *JHEP* **0812** (2008) 011, arXiv:0801.4028 [hep-ph].

[36] S. Alioli, C. W. Bauer, C. J. Berggren, A. Hornig, F. J. Tackmann, *et al.*, "Combining Higher-Order Resummation with Multiple NLO Calculations and Parton Showers in GENEVA," arXiv:1211.7049 [hep-ph].

[37] M. Rubin, G. P. Salam, and S. Sapeta, "Giant QCD K-factors beyond NLO," *JHEP* **1009** (2010) 084, arXiv:1006.2144 [hep-ph].

[38] F. Campanario and S. Sapeta, "WZ production beyond NLO for high-pT observables," *Phys.Lett.* **B718** (2012) 100–104, arXiv:1209.4595 [hep-ph].

[39] K. Hamilton and P. Nason, "Improving NLO-parton shower matched simulations with higher order matrix elements," *JHEP* **1006** (2010) 039, arXiv:1004.1764 [hep-ph].

[40] S. Höche, F. Krauss, M. Schönherr, and F. Siegert, "NLO matrix elements and truncated showers," arXiv:1009.1127 [hep-ph].

[41] S. Alioli, K. Hamilton, and E. Re, "Practical improvements and merging of POWHEG simulations for vector boson production," *JHEP* **1109** (2011) 104, arXiv:1108.0909 [hep-ph].

[42] S. Alioli, P. Nason, C. Oleari, and E. Re, "NLO vector-boson production matched with shower in POWHEG," *JHEP* **0807** (2008) 060, arXiv:0805.4802 [hep-ph].

[43] S. Alioli, P. Nason, C. Oleari, and E. Re, "Vector boson plus one jet production in POWHEG," *JHEP* **1101** (2011) 095, arXiv:1009.5594 [hep-ph].

[44] S. Alioli, P. Nason, C. Oleari, and E. Re, "NLO Higgs boson production via gluon fusion matched with shower in POWHEG," *JHEP* **0904** (2009) 002, arXiv:0812.0578 [hep-ph].

[45] J. M. Campbell, R. K. Ellis, R. Frederix, P. Nason, C. Oleari, *et al.*, "NLO Higgs Boson Production Plus One and Two Jets Using the POWHEG BOX, MadGraph4 and MCFM," *JHEP* **1207** (2012) 092, arXiv:1202.5475 [hep-ph].

[46] M. Cacciari, G. P. Salam, and G. Soyez, "FastJet User Manual," *Eur.Phys.J.* **C72** (2012) 1896, arXiv:1111.6097 [hep-ph].

[47] **ATLAS Collaboration** Collaboration, G. Aad *et al.*, "Study of jets produced in association with a W boson in pp collisions at $\sqrt{s} = 7$ TeV with the ATLAS detector," *Phys.Rev.* **D85** (2012) 092002, arXiv:1201.1276 [hep-ex].

[48] T. Sjostrand and P. Z. Skands, "Transverse-momentum-ordered showers and interleaved multiple interactions," *Eur.Phys.J.* **C39** (2005) 129–154, arXiv:hep-ph/0408302 [hep-ph].

[49] R. K. Ellis, W. J. Stirling, and B. Webber, "QCD and collider physics," *Camb.Monogr.Part.Phys.Nucl.Phys.Cosmol.* **8** (1996) 1–435.

[50] **Axial Field Spectrometer Collaboration** Collaboration, T. Akesson *et al.*, "DOUBLE PARTON SCATTERING IN p p COLLISIONS AT S**(1/2) = 63-GeV," *Z.Phys.* **C34** (1987) 163.

[51] **CDF Collaboration** Collaboration, F. Abe *et al.*, "Measurement of double parton scattering in $\bar{p}p$ collisions at $\sqrt{s} = 1.8$ TeV," *Phys.Rev.Lett.* **79** (1997) 584–589.

[52] **Atlas Collaboration** Collaboration, G. Aad *et al.*, "Measurement of underlying event characteristics using charged particles in pp collisions at $\sqrt{s} = 900GeV$ and 7 TeV with the ATLAS detector," *Phys.Rev.* **D83** (2011) 112001, arXiv:1012.0791 [hep-ex].

[53] P. Bartalini, E. Berger, B. Blok, G. Calucci, R. Corke, *et al.*, "Multi-Parton Interactions at the LHC," arXiv:1111.0469 [hep-ph].

[54] T. Sjöstrand, S. Mrenna, and P. Skands, "PYTHIA 6.4 physics and manual," *JHEP* **05** (2006) 026, arXiv:hep-ph/0603175.

[55] R. Corke, "Multiple Interactions in Pythia 8," arXiv:0901.2852 [hep-ph].

[56] R. Corke and T. Sjostrand, "Multiparton Interactions and Rescattering," *JHEP* **1001** (2010) 035, arXiv:0911.1909 [hep-ph].

[57] R. Corke and T. Sjostrand, "Multiparton Interactions with an x-dependent Proton Size," *JHEP* **1105** (2011) 009, arXiv:1101.5953 [hep-ph].

. . . mühsam ernährt sich das Eichhörnchen.